Detection of Biological Pathogens Using Multiple Wireless Magnetoelastic Biosensors

by

Wen Shen

A dissertation submitted to the Graduate Faculty of
Auburn University
in partial fulfillment of the
requirements for the Degree of
Doctor of Philosophy

Auburn, Alabama
May 9, 2011

Keywords: magnetoelastic, pathogen detection, multiple biosensors

Approved by

Bryan A. Chin, Chair, Professor of Materials Engineering
Valery A. Petrenko, Professor of Pathobiology
ZhongYang (Z.-Y.) Cheng, Professor of Materials Engineering
Dong-Joo (Daniel) Kim, Associate Professor of Materials Engineering
Barton C. Prorok, Associate Professor of Materials Engineering

Abstract

A number of recent, high-profile incidences of food-borne illness spreading through the food supply and the use of anthrax by terrorists after the September 11, 2001 attacks have demonstrated the need for new technologies that can rapidly detect the presence of biological pathogens. A bevy of biosensors show excellent detection sensitivity and specificity. However, false positive and false negative signals remain one of the primary reasons that many of these newly developed biosensors have not found application in the marketplace.

The research described in this dissertation focuses on developing a free-standing magnetoelastic based bio-sensing system using a pulse method. This method allows fast detection, eliminates the bias magnetic field that is necessary in current methods, makes the system more simply and suitable for in-field detection. This system has two pairs of transformer coils, where a measurement sensor and a control sensor can be put in each pair of coils. The control sensor is used to compensate for environmental variables. The effect of pulse power on the performance of the magnetoelastic sensors in the pulse system is studied. The system is found to have excellent stability, good detection repeatability when used with multiple sensors.

This research has investigated and demonstrated a multiple sensors approach. Because it will involve the simultaneous measurement of many sensors, it will significantly reduce problems encountered with false positive indications. The positioning and interference of sensors are investigated. By adding a multi-channel structure to the pulse detection system, the effect of sensor interference is minimized. The result of the repeatability test shows that the standard deviation when measuring three 1 mm magnetoelastic sensors is around 500 Hz, which is smaller than the minimum requirement for actual spores/bacteria detection.

Magnetoelastic sensors immobilized with JRB7 phages and E2 phages have been used to specifically detect *Bacillus anthracis* spores and *Salmonella typhimurium* bacteria. The real-time monitoring of the detection of *B. anthracis* spores in a flowing system was performed using 2 mm sensors and 1 mm sensors. The detection of *S. typhimurium* in air has been performed using the pulse based system with both single and grouped sensors. Because grouped sensor detection involves the simultaneous measurement of many sensors, statistical evaluation shows that it can significantly reduce problems encountered with false positive indications. This method has been implemented in an investigation of a method that allows direct detection of *S. typhimurium* on cantaloupe surfaces. It has been demonstrated that multiple E2 phage based magnetoelastic sensors are able to detect *Salmonella* directly on fresh cantaloupe surfaces. Confirmation of the spore or bacteria binding to the sensor surfaces was achieved through SEM study of the sensor surfaces.

Acknowledgments

The author would like to thank her parents, Huiqi Shen and Lanli Wu, and her grandmother, Mingmei Qu, for their sacrifices, patience and encouragement to prepare me for advanced studies in the United States and their encouragement and guidance as I continued my studies and research. I am deeply indebted to my advisor, Dr. Bryan Chin for his guidance in my research, for showing me how to be a good research engineer and his many anecdotes to prepare me for a future career. I am also very indebted to my professors, Dr. ZhongYang (Z.-Y.) Cheng, Dr. Barton C. Prorok, Dr. Valery A. Petrenko and Dr. Dong-Joo (Daniel) Kim for their help with research questions and procedures. Dr. ZhongYang Cheng has been especially helpful in instructing me on the value of the research of my present and previous colleagues in relation to my own research and career. I wish to thank I-hsuan Chen for her help in understanding the characteristics of phages and for helping me when things did not go as planned.

I especially with to thank Mr. Leslie (L.C.) Mathison for helping with the electrical design of the pulse system and for helping me to understand the magnetic and electrical properties that make this system possible and for his assistance and support during the writing of this document.

I want to add my appreciation for the help received from my colleagues and group members, and especially Dr. Suiqiong Li and Shin Horikawa for their help with experiments and research efforts.

I am also very indebted to Dr. Billor of the math department for teaching me the statistical methods that make this research possible.

Table of Contents

Abstract ii

Acknowledgments iv

List of Figures viii

List of Tables xv

List of Abbreviations xvii

1 Introduction 1

1.1 Motivation for the Research 1

1.2 Objectives of the Research 2

1.3 Dissertation Organization 4

2 Literature Review 6

2.1 Introduction to the Target Pathogens 6

2.1.1 Introduction to *B. Anthracis* Spores 6

2.1.2 *Salmonella* and Food Safety 7

2.2 Conventional Biological Detection Techniques 8

2.2.1 Bacterial Culture Technique 9

2.2.2 Enzyme-Linked Immunosorbent Assay (ELISA) 9

2.2.3 Polymerase Chain Reaction (PCR) 10

2.2.4 Flow Cytometry (FCM) 10

2.3 Biosensor Techniques 11

2.3.1 Biological Recognition Elements 13

2.3.2 Transduction Mechanisms 17

3 Materials and Experiments 25

3.1 Design and Fabrication of Sensor Platform 25

3.2 Phage Coating 28
3.3 Bacteria Cultures and Spore Solutions 28
3.4 Scanning Electron Microscopy Imaging 29
4 Detection Techniques for Magnetoelastic Sensors 31
4.1 Review of Currently Existing Methods 31
4.1.1 Time Domain Method 31
4.1.2 Frequency Domain Method 32
4.2 Frequency Domain Method in This Research 32
4.3 Development of the Pulse Detection Method 35
4.3.1 Principle of Pulse Detection 35
4.3.2 Electronic Implementation 38
4.3.3 Sensor Behavior in Pulse System 43
5 Characterization of Magnetoelastic Platform for Sensing Applications 47
5.1 Resonance Behavior of Free-standing Magnetoelastic Sensors 47
5.2 Principle of Sensor Detection 53
5.3 Mass Sensitivity 54
5.4 Magnetic Field Tuning 56
5.5 Damping Effect 66
5.6 Effect of Sensor Position in the Coil 69
5.7 Effect of Pulse power 72
5.8 Stability of the Sensor in Pulse System 76
5.9 Multiple Sensors 78
5.9.1 Multiple Sensor Detection using Frequency Domain Method 79
5.9.2 Multiple Sensor Detection using Pulse Method 83
6 Real-Time Detection of *B. Anthracis* in Flowing System 88
6.1 Real-Time Detection Curve 90
6.2 The Time Factor 93

6.3 Specificity 95
6.4 Microscopic Observation 95
6.5 Detection Limit and Sensitivity 98
6.6 Hill Plot and K_d 100
6.7 Conclusions and Discussion 103
7 Detection of *S. Typhimurium* using Pulse System 104
7.1 Detection using one Measurement Sensor and one Control Sensor 104
7.2 Detection using Grouped Sensors 109
7.3 Conclusions and Discussion 118
8 Optimization of Blocking on E2 Phage Based Magnetoelastic Biosensors 119
9 Detection of *S. Typhimurium* on Cantaloupe Surface Using Multiple Magnetoelastic Sensors 138
9.1 Detection of *S. typhimurium* on Cantaloupe Surface 138
9.2 Conclusions and Discussion 157
10 Conclusions 158
11 Recommendations for Future Works 161
Bibliography 162

List of Figures

2.1 Schematic of biosensors. 12

2.2 Basic antibody structure. 14

2.3 Structure of a filamentous bacteriophage. 16

2.4 Principle of SPR based biosensing. 20

2.5 Typical disc TMS sensor. 22

3.1 Schematic illustration of the magnetoelastic sensor platform. 27

3.2 SEM picture of a magnetoelastic sensor platform. Dimentions: $2000 \times 400 \times 15\mu m$. 27

4.1 Schematic of sensor measurement set up. 33

4.2 Network analyzer signal of a magnetoelastic sensor. Sensor dimensions: 2000 $\times$ 400 $\times$ 15 μm. 34

4.3 Matlab simulation of (a) a rectangular pulse with (b) its Fourier transform spectrum along with (c) its phase of spectrum ($A = 0.5$, $T = 80s$ and $t_0 = -4.9s$). 37

4.4 Block diagram of the pulse system. 40

4.5 Photograph of the pulse system showing power supplies, function generator, final amplifier and prototype boards with timing circuits and small board with the transformer coils. 41

4.6 Oscilloscope waveforms of (top to bottom) 1) Function Generator, 2) Sensor "ringdown", 3) Power Pulse, 4) Delayed Gate pulse. 42

4.7 Matlab simulated showing the time-domain response of a single free-standing magnetoelastic sensor to a rectangular pulse. The resonant frequency of the sensor is set to be 2.326 MHz and the damping constant ξ used is 0.0035. . . 45

4.8 Measured signal from a single free-standing magnetoelastic sensor in pulse system. The resonant frequency of the sensor is measured as 2.326 MHz. . . 45

4.9 Matlab simulation showing the time-domain response of two independent free-standing magnetoelastic sensors to a same rectangular pulse. The resonance frequencies of the two sensors are set to be 2.193 Mhz and 2.281 MHz. The damping constant ξ used is 0.0035. 46

4.10 Measured signal from two free-standing magnetoelastic sensors separated in the two transformers in pulse system. The resonance frequencies of the two sensors are measured as 2.193 Mhz and 2.281 MHz. 46

5.1 Coventor simulation of the first mode oscillation of a magnetoelastic sensor. Length to width ratio is 5. 49

5.2 Coventor simulation of the second mode oscillation of a magnetoelastic sensor. Length to width ratio is 5. 50

5.3 Coventor simulation of the third mode oscillation of a magnetoelastic sensor. Length to width ratio is 5. 51

5.4 Calibration of resonant frequency as a function of sensor length (Blue: From [1]). 53

5.5 Plot of mass sensitivity for various lengths of the sensor platform (Red: From [2]; Blue: From [1]). 55

5.6 Typical magnetization versus magnetic field curve for 1 mm and 2mm sensors. 58

5.7 Resonance specrtrum of a 2 mm sensor under different bias magnetic field strengths. 60

5.8 Experimental measurements and theoretical model showing the resonant frequency of a 1 mm sensor under different DC magnetic field strengths. 61

5.9 Experimental measurements and theoretical model showing the resonant frequency of a 2 mm sensor under different DC magnetic field strengths. 62

5.10 Amplitude and Q-factor of the resonance peak of a 1 mm sensor as a function of magnetic field strength. 63

5.11 Amplitude and Q-factor of the resonance peak of a 2 mm sensor as a function of magnetic field strength. 64

5.12 Difference in resonant frequencies of 1 mm magnetoelastic sensors before and after coating a uniform layer of mass under different DC magnetic field strengths. 65

5.13 Resonant frequency of magnetoelastic sensor in air and water for a 1 mm ($1000 \times 200 \times 15$ μm) sensor. 68

5.14 Resonant frequency of magnetoelastic sensor in air and water for a 2 mm (2000 × 400 × 15 μm) sensor. 68

5.15 Measured sensor oscillation under various pulse power voltages.Measured sensor oscillation under various pulse power voltages. 73

5.16 Resonant frequency under various pulse magnetic fields. 74

5.17 Amplitude of FFT signal and Q value of resonant peak under various pulse magnetic fields. 75

5.18 A typical received data of (a) resonant frequency and (b) signal amplitude of a magnetoelastic sensor in pulse system during a time period of 5.4 hours. . 77

5.19 Frequency spectrum of ten 2 mm magnetoelastic sensors measured separately and simultaneously using frequency domain method. 80

5.20 Frequency spectrum of ten 500 μm magnetoelastic sensors measured separately and simultaneously using frequency domain method. 81

5.21 Multi-access channel illustration. 84

5.22 Frequency spectrum after FFT: (a) Simultaneous detection of Sensor 1 and Sensor 2 (Sensor 1 was inside Transformer 1 and Sensor 2 was inside Transformer 2); (b) Single sensor detection of Sensor 1 placed inside Transformer 1 and Sensor 2 placed inside Transformer 2. 85

6.1 Schematic of the flowing system. 89

6.2 Typical magnetoelastic sensor response for 5 × 10^8 spores/ml *B. anthracis* spore suspension by a 1 mm (1000 × 200 × 15 μm) sensor. 91

6.3 Typical magnetoelastic sensor response for 5 × 10^8 spores/ml *B. anthracis* spore suspension by a 2 mm (2000 × 400 × 15μm) sensor. 92

6.4 Kinetic analysis for the binding of *B. anthracis* spores suspension (5 × 10^8 spores/ml) using a 1 mm magnetoelastic sensor at a flow rate of 40 μl/min. The attachment rate constant was determined from the slope of the curve. . 94

6.5 Control sensor surface after exposure to 5 × 10^8 spore/ml *B. anthracis* suspended in distilled water in a flowing system. 96

6.6 Measurement sensor surface after exposure to 5 × 10^8 spore/ml *B. anthracis* suspensed in distilled water in a flowing system. 97

6.7 Illustration of a sensor calibration curve showing the lower detection limit (LOD). 98

6.8 Resonant frequency shift as a function of concentration of *B. anthracis* spore (5×10^1 to 5×10^8 spores/ml). The frequency shifts of control sensors are extracted from those of the measurement sensors. The smooth lines are the sigmoid fit for the experimental data (1 mm sensor: $R^2 = 0.9976$, $\chi^2 = 0.1753$; 2 mm sensor: $R^2 = 0.9956$, $\chi^2 = 0.09359$). 99

6.9 Hill Plot of the sensor responses to *B. anthracis* spore suspensions (5×10^1 to 5×10^8 spores/ml) in a flowing system . The smooth lines are the linear least square fit to the data. 102

7.1 Magnetoelastic sensor response as a function of concentrations of *S. typhimurium* suspentions (5×10^1 to 5×10^8 cfu/ml). The frequency shifts of control sensors are extracted from those of the measurement sensors. The smooth line is the sigmoid fit for the experimental data ($R^2 = 0.9968$; $\chi^2 = 0.1810$). 105

7.2 Hill plot showing the *S. typhimurium* binding to 1 mm magnetoelastic biosensors. The squares represent experimental data. The line represents the least square fit of the data (slope $= 0.39 \pm 0.04$, $R = 0.9780$, $P < 0.0001$). 106

7.3 Typical SEM picture of the measurement sensor surface after exposure to 5×10^8 cfu/ml *S. typhimurium* suspension in distilled water. 107

7.4 Typical SEM picture of the control sensor surface after exposure to 5×10^8 cfu/ml *S. typhimurium* suspension in distilled water. 108

7.5 Typical response of a group of three magnetoelastic sensors (a) before and (b) after exposure to *S. typhimurium* suspension at a concentration of 5×10^7 cfu/ml. 110

7.6 Typical response of a group of three magnetoelastic sensors (a) before and (b) after exposure to *S. typhimurium* suspension at a concentration of 5×10^5 cfu/ml. 111

7.7 Multiple sensor response to concentrations of *S. typhimurium* suspensions (5×10^1 to 5×10^8 cfu/ml). The frequency shifts of control sensors are extracted from those of the measurement sensors. The smooth lines are the sigmoid fit for the experimental data ($R^2 = 0.9994$, $\chi^2 = 0.0043$; 113

7.8 Hill plot showing the *S. typhimurium* binding to groups of 2 mm magnetoelastic biosensors. The frequency shifts of control sensors are extracted from those of the measurement sensors. The squares represent experimental data. The line represents the least square fit of the data ($R^2 = 0.9994$, $\chi^2 = 0.0043$). 114

7.9 Typical SEM picture of the magnetoelastic biosensor surface after exposure to *S. typhimurium* suspension at a concentration of 5×10^6 cfu/ml. 115

7.10 Typical SEM picture of the magnetoelastic biosensor surface after exposure to *S. typhimurium* suspension at a concentration of 5×10^7 cfu/ml. 116

7.11 Typical SEM picture of the magnetoelastic biosensor surface after exposure to *S. typhimurium* suspension at a concentration of 5×10^8 cfu/ml. 117

8.1 Typical SEM picture of the magnetoelastic biosensors blocked with 0.5 mg/ml BSA after exposure to 5×10^8 cfu/ml *S. typhimurium* suspension. 121

8.2 Typical SEM picture of the magnetoelastic biosensors blocked with 1 mg/ml BSA after exposure to 5×10^8 cfu/ml *S. typhimurium* suspension. 122

8.3 Typical SEM picture of the magnetoelastic biosensors blocked with 3 mg/ml BSA after exposure to 5×10^8 cfu/ml *S. typhimurium* suspension. 123

8.4 Typical SEM picture of the magnetoelastic biosensors blocked with 5 mg/ml BSA after exposure to 5×10^8 cfu/ml *S. typhimurium* suspension. 124

8.5 Typical SEM picture of the magnetoelastic biosensors blocked with 0.1 mg/ml milk after exposure to 5×10^8 cfu/ml *S. typhimurium* suspension. 125

8.6 Typical SEM picture of the magnetoelastic biosensors blocked with 0.5 mg/ml milk after exposure to 5×10^8 cfu/ml *S. typhimurium* suspension. 126

8.7 Typical SEM picture of the magnetoelastic biosensors blocked with 3 mg/ml milk after exposure to 5×10^8 cfu/ml *S. typhimurium* suspension. 127

8.8 Typical SEM picture of the magnetoelastic biosensors blocked with 5 mg/ml milk after exposure to 5×10^8 cfu/ml *S. typhimurium* suspension. 128

8.9 Typical SEM picture of the magnetoelastic biosensors blocked with 0.5 mg/ml casein after exposure to 5×10^8 cfu/ml *S. typhimurium* suspension. 129

8.10 Typical SEM picture of the magnetoelastic biosensors blocked with 1 mg/ml casein after exposure to 5×10^8 cfu/ml *S. typhimurium* suspension. 130

8.11 Typical SEM picture of the magnetoelastic biosensors blocked with 5 mg/ml casein after exposure to 5×10^8 cfu/ml *S. typhimurium* suspension. 131

8.12 Average of bound *Salmonella* cell coverage on magnetoelastic biosensor surfaces that were blocked with different concentrations of BSA after exposure to 5×10^8 cfu/ml *S. typhimurium* suspension. 132

8.13 Average of bound *Salmonella* cell coverage on magnetoelastic biosensor surfaces that were blocked with different concentrations of milk after exposure to 5×10^8 cfu/ml *S. typhimurium* suspension. 133

8.14 Average of bound *Salmonella* cell coverage on magnetoelastic biosensor surfaces that were blocked with different concentrations of casein after exposure to 5×10^8 cfu/ml *S. typhimurium* suspension. 134

8.15 Frequency shifts of magnetoelastic biosensors that were blocked with different concentrations of BSA after exposure to 5×10^8 cfu/ml *S. typhimurium* suspension. 135

8.16 Frequency shifts of magnetoelastic biosensors that were blocked with different concentrations of milk after exposure to 5×10^8 cfu/ml *S. typhimurium* suspension. 136

8.17 Frequency shifts of magnetoelastic biosensors that were blocked with different concentrations of casein after exposure to 5×10^8 cfu/ml *S. typhimurium* suspension. 137

9.1 Three magnetoelastic sensors for simultaneously detecting *S. typhimurium* directly on the cantaloupe surface. Sensor Dimensions: $2000 \times 400 \times 15$ μm. 139

9.2 Typical response of a group of three measurement sensors before and after the detection of *S. typhimurium* suspensions (5×10^8 cfu/ml) on cantaloupe surface. 141

9.3 Typical response of a group of three control sensors before and after the detection of *S. typhimurium* suspensions (5×10^8 cfu/ml) on cantaloupe surface. 141

9.4 Typical SEM picture of the measurement biosensors after binding with *S. typhimurium* suspension at concentration of 5×10^8 cfu/ml spiked on cantaloupe surface. 142

9.5 Typical SEM picture of the control biosensors after exposed to *S. typhimurium* suspension at concentration of 5×10^8 cfu/ml spiked on cantaloupe surface. . 143

9.6 Typical SEM picture ($\times$1000) showing the cantaloupe surface spiked with 5×10^8 cfu/ml *S. typhimurium* suspension. 144

9.7 Typical SEM picture ($\times$1000) showing the cantaloupe surface spiked with 5×10^6 cfu/ml *S. typhimurium* suspension. 145

9.8 Typical SEM picture ($\times$1000) showing the cantaloupe surface spiked with 5×10^4 cfu/ml *S. typhimurium* suspension. 146

9.9 Typical SEM picture ($\times$1000) showing the cantaloupe surface spiked with 5×10^1 cfu/ml *S. typhimurium* suspension. 147

9.10 Multiple sensor response to concentrations of *S. typhimurium* suspensions (5×10^1 to 5×10^8 cfu/ml) on cantaloupe surfaces. 149

9.11 Result of second test using multiple sensor to detect concentrations of *S. typhimurium* suspensions (5×10^1 to 5×10^8 cfu/ml) spiked on cantaloupe surfaces. 151

9.12 Typical SEM picture of the measurement biosensors after binding with *S. typhimurium* suspension at a concentration of 5×10^8 cfu/ml spiked on cantaloupe surface. 152

9.13 Typical SEM picture of the measurement biosensors after binding with *S. typhimurium* suspension at a concentration of 5×10^7 cfu/ml spiked on the cantaloupe surface. 153

9.14 Typical SEM picture of the measurement biosensors after binding with *S. typhimurium* suspension at concentration of 5×10^6 cfu/ml spiked on the cantaloupe surface. 154

9.15 Typical SEM picture of the measurement biosensors after binding with *S. typhimurium* suspension at concentration of 5×10^4 cfu/ml spiked on the cantaloupe surface. 155

9.16 Typical SEM picture of the control biosensors after exposure to *S. typhimurium* suspension at concentration of 5×10^4 cfu/ml spiked on the cantaloupe surface. 156

List of Tables

3.1 General properties of MetGlas® 2826MB [3]. 25

5.1 Coventor simulation of the oscillation of a $2000 \times 800 \times 15 \mu m$ magnetoelastic sensor. 48

5.2 Resonance behavior of magnetoelastic sensors in media. 67

5.3 Summary of the resonant frequencies of a single sensor when placed at three positions of the coil (Unit: kHz). 70

5.4 One-way ANOVA result of resonant frequencies of a sensor when placed at three positions of the coil. 70

5.5 Tukey's Studentized Range (HSD) test for resonant frequencies of a sensor when placed at three positions of the coil (significance level is set to 0.10). . 70

5.6 Summary of resonant frequencies of two sensors when placed differently in the coil (Unit: kHz). 71

5.7 Two-way ANOVA result of resonant frequencies of two sensors when placed differently in the coil. 71

5.8 Summary of resonant frequencies of two sensors when placed in distilled water (Unit: kHz). 72

5.9 Summary of stability test results in pulse system. 76

5.10 Summary of the probability of failure of detection when using various numbers of sensors. 78

5.11 Peak parameters of frequency spectrum of ten 2 mm magnetoelastic sensors. 79

5.12 Peak parameters of frequency spectrum of ten 500 μm magnetoelastic sensors. 82

5.13 Summary of a repeated test of three magnetoelastic sensors measured simultaneously in pulse system (Unit: MHz). 87

6.1 Specificity of a 500 μm magnetoelastic sensor over a range of *Bacillus* species. 95

6.2 Performance characteristics of 1 mm and 2 mm JRB7 phage coated magnetoelstic biosensors for the detection of *B. anthracis* spores in the flowing system. 101

7.1 Performance characteristics of 2 mm E2 phage coated magnetoelastic biosensors for the detection of *S. typhimurium*. 112

9.1 P values associated with one-sided student's t-test for detection of *Salmonella* for all concentrations (5×10^1 cfu/ml to 5×10^8 cfu/ml) after comparing measurement sensors and control sensors. 150

9.2 P values associated with two-sided student's t-test for measurement sensors (clear area) and control sensors (shaded area) after comparing detection of *Salmonella* for all concentrations (5×10^1 cfu/ml to 5×10^8 cfu/ml). 150

List of Abbreviations

Bacillus anthracis *B. anthracis*

CDC Centers for Disease Control and Prevention

ELISA Enzyme-Linked Immunosorbent Assay

FCM Flow Cytometry

FET Field Effect Transistors

FFT Fast Fourier Transformation

PCR Polymerase Chain Reaction

QCM Quartz Crystal Microbalance

SAW Surface Acoustic Wave Resonator

S. typhimurium *Salmonella typhimurium*

SEM Scanning Electron Microscopy

U.S. United States

TEM Transmission electron microscopy

TSM Thickness Shear Mode Resonator

U.S. United States and Prevention

Chapter 1

Introduction

1.1 Motivation for the Research

The use of anthrax by terrorists after the September 11, 2001 attacks brought about a concern for security threats in nearly every county and has inspired new research into sensors for early and rapid detection of such threats. Along with this threat has been a new emphasis on food safety and ways to monitor and detect pathogens in the food chain from the agricultural field to the family food table. Each year, foodborne pathogens account for 76 million illnesses in the U.S., more than 300,000 people are hospitalized and 5,000 die from foodborne illness [4] . Each year in the U.S., the cost of lost productivity associated with foodborne bacteria is more than $ 30 billion.

In 2008 and 2009, the CDCs reported that the outbreak of *Salmonella typhimurium* infections from peanut butter caused 714 illnesses from 46 states of the U.S. [5]. Recently, it was reported that from May to August of 2010, approximately 1,469 illnesses are thought to be caused by a multistate outbreak of *Salmonella enteritidis* infections from shell eggs [6]. These events demonstrate the need for advanced devices and technologies that can rapidly detect the presence of biological pathogens to guard against this threat. A bevy of biosensors based upon acoustic wave devices such as the quartz crystal microbalance [7], flexure plate wave device [8] [9], surface acoustic wave devices [10] [11] and micro-fabricated cantilever [12] show excellent detection sensitivity. However, since most of these devices require complex wiring for power and measurement of the transducer, they are relatively difficult and costly to fabricate, and require care to avoid contamination of the test equipment. In addition, conventional methods of detection use antibodies and peptides as bio-molecular

recognition elements [13] [14]. These methods tend to be very expensive, may not be selective enough, and most importantly, antibodies and peptides can not survive very long under harsh environmental conditions. This limits the application of these biosensors to laboratory conditions. Moreover, because most of these devices are single-sensor devices, false positive and false negative signals remain one of the main reasons that many of these newly developed biosensors have not found application in the marketplace.

1.2 Objectives of the Research

The primary objectives of this research are to study phage coated magnetoelastic biosensors for the detection of anthrax and foodborne pathogens, to develop a new detection system that eliminates the bias field necessary for magnetic field tuning to allow fast and accurate detection, and to investigate multiple magnetoelastic biosensor technology for providing more reliable detection.

To accomplish the above objectives, this research was divided into five sections:

1. Development of a pulse detection system to allow accurate detection of multiple magnetoelastic sensors and differentiate between resonant frequencies of sensors that are close in frequency.

Present detection methods for magnetoelastic sensors have limitations due to magnetic tuning methods and background noise, especially when the noise rides on top of the peak and gives an erroneous measurement of peak frequency. A similar problem is that the present system cannot differentiate between resonant frequencies that are close in frequency. In this research, we proposed and developed the first detection system of this type that does not use a bias magnet for magnetoelastic sensors. This new pulse based system uses Fast Fourier Transformation (FFT) to separate the signals from the noise, can provide good signal to noise ratio, is able to differentiate between sensors that are close in resonant frequencies, has provisions for a control sensor, is very stable versus time and has the capability to work with multiple sensors simultaneously.

2. Characterization of the performance of phage-coated magnetoelastic biosensors for the applications of detecting target pathogens.

In this work, the characterizations of the magnetoelastic sensors for the sensing applications, such as the resonance behavior in air and in liquid, mass sensitivity and magnetic field tuning, are studied. Meanwhile, the performance of the magnetoelastic sensors in the pulse system, such as the resonance behavior and the effect of pulse power are studied. Furthermore, the performance of multiple magnetoelastic sensors has been investigated and evaluated in both the frequency domain detection system and the pulse detection system. A multi-channel built-in pulse detection system is developed and used to allow reliable detection using multiple magnetoelastic sensors simultaneously.

3. Characterization of the performance of JRB7 phage based magnetoelastic biosensors in a liquid flowing system using a frequency domain method for real-time detection of *B. anthracis* spores.

Because *B. anthracis* spores can infect humans via inhalation, it is very dangerous and extreme care must be used in handling spores in air. In our lab, the detection of *B. anthracis* spores is in liquid. Previous research has verified the detection of *B. anthracis* spores in static liquid using magnetoelastic sensors coated with JRB7 phage as probes. To reliably detect low concentrations, we have designed and used a flowing system that can bring the spores to the sensor, and used a micro-scale, freestanding, magnetoelastic biosensor coated with phage as probes for the real-time in-vitro detection of *B. anthracis* spores. The biosensors are exposed to graded concentrations of *B. anthracis* spores and the sensor responses and kinetics are studied.

4. Characterization of the performance of E2 phage based magnetoelastic biosensors using the pulse-detection system for the detection of *S. typhimurium* for single sensors and for multiple sensors.

Here, we used the pulse system to detect *S. typhimurium* using E2 phage-coated magnetoelastic biosensors. Moreover, we utilized a design of grouped-sensor-detection that includes

simultaneous detection of multiple magnetoelastic biosensors. This method effectively solved the problem of erroneous signals caused by defective sensors and greatly increased the reliability of the magnetoelastic biosensor detection.

5. Direct detection of *S. typhimurium* on real food produce using multiple E2 phage based magnetoelastic biosensors compared with multiple control sensors.

The current bacterial detection methods require many sampling processes and tedious laboratory assays, which include both time and labor consuming steps. In this research work, we have shown that the E2 phage coated magnetoelastic biosensors are able to detect *S. typhimurium* with excellent specificity and sensitivity, and this detection is able to occur not only in liquid, but also in humid air. Based on these results, we used the aforementioned multi-sensor detection system and developed a detection method to allow direct placement of the sensors on fresh produce for *Salmonella* detection. The experimental results from using fresh produce such as cantaloupes and tomatoes confirmed that this magnetoelastic bio-sensing method is able to detect *Salmonella* directly on fresh produce.

1.3 Dissertation Organization

This dissertation consists of ten chapters. The first chapter is an introduction to the dissertation. The second chapter gives a general overview of current techniques for the detection of biological pathogens, including conventional biotechnologies and advanced biosensor techniques. This chapter discusses details of antibodies and bacteriophages as bio-recognition elements and the magnetoelastic platform as a transducer.

The third chapter introduces the details of the experimental procedures included in this work. The forth chapter discusses the detection methods for magnetoelastic sensors, including currently existing detection methods and the new pulse detection method introduced here. Chapter five is a more detailed discussion of fundamentals and characterizations of the magnetoelastic platform for sensing applications and includes the fundamentals of the

resonance behavior of single and multiple sensors, the principle of detection, mass sensitivity, magnetic field tuning and the effect of variations in pulse power.

Chapters six through nine are the application of the magnetoelastic biosensors to the real-time detection of biological pathogens. Chapter six gives the real-time detection of *B. anthracis* spores in flowing liquid. Chapter seven includes the detection of *S. typhimurium* using the pulse system with single and multiple magnetoelastic sensors. Chapter eight is the optimization of the blocking condition for E2 based magnetoelastic sensors, and Chapter nine is the direct detection of *S. typhimurium* on real food produce.

The last two chapters, Chapters ten and eleven are the overall conclusions and recommendations for future works.

Chapter 2

Literature Review

2.1 Introduction to the Target Pathogens

2.1.1 Introduction to *B. Anthracis* Spores

B. anthracis is the causative bacterium of anthrax. It was first observed by a French physician, Casimir Davaine, in the 1850s and 1860s [15], and was isolated and further studied by a famous German physician, Robert Koch, in 1870s [16]. The anthracis is named after a Greek work, anthracis, which means coal and refers to large black skin lesions formed in cutaneous anthrax, the most common form of the anthrax disease.

B. anthracis is a Gram-positive, rod-shaped bacterium, with a width of around 2 μm and a length of 3-5 μm [17][18]. It is able to synthesize a protein capsule (D-Glutamate) and is the only pathogenic bacterium known to have this capability. Also, it is able to carry its own adenylyl cyclase virulence factor, known as the edema factor. It is highly resilient and can be grown in an ordinary nutrient medium under either aerobic or anaerobic conditions. Although *B. anthracis* cannot survive outside a host for long in its bacterium form, when a suitable host is not available, *B. anthracis* forms endospores, which are oval spores located centrally in a non-swollen sporangium. This endospore form of *B. anthracis* is highly resistant to extreme temperature, low-nutrient environments, and harsh chemical treatments [19], and can survive for a long time in these conditions.

Infections of *B. anthracis* can occur in three ways, cutaneous, inhalation and gastrointestinal [20]. The cutaneous anthrax infection is the most common form of anthrax infection and accounts for 95% of anthrax diseases. It causes a localized inflammatory black necrotic lesion called "eschar" on the skin. The anthrax infection caused by inhalation of spores is

called pulmonary anthrax. This is the most serious form of the disease as its death rate is nearly 100%. An infectious dose is about 8,000 to 50,000 organisms. Intestinal anthrax is cased by ingestion of meat from infected animals. And this form of anthrax disease causes a fatality rate of about 20% to 60%. The most common forms of infection for human beings is through handling diseased animals or inhaling spores.

Because of their ability to cause mortality in humans and because they are extremely resilient and may remain naturally viable in anaerobic conditions, *B. anthracis* spores have become well-known biological warfare agents [21]. Perhaps the most widely publicized event was the terrorist threat in October 2001 [22], when several letters containing *B. anthracis* spores were intentionally sent through the U.S. Postal Service and caused 23 inhalational or cutaneous anthrax infections, five of which were fatal. To guard against this threat, scientists and researchers have been trying to develop a method of anthrax detection that is very rapid, very sensitive, and small enough that it can be taken to the site of possible contamination and give results without requiring extensive training of operating personnel.

2.1.2 *Salmonella* and Food Safety

Salmonella is a genus of Gram-negative, rod-shaped bacterium, with a width of around 0.7 to 1.5 μm and a length of 2-5 μm. It was discovered by Theobald Smith and Daniel Elmer Salmon in 1885. Since then, over 2,200 serovars of *Salmonella* have been found, most belonging to species *S. enterica* [23] [24]. So far, *S. enterica* includes six sub-species: *enterica*, *salame*, *arizonae*, *diarizonae*, *houtenae*, and *indica* [25] [23]. An important serovar of *Salmonella* is *S. typhimurium*. It can penetrate into intestinal epithelium and causes a wide range of gastroenteritis in humans and other mammals [26], including *Salmonella enteritis*, called "food poisoning."

In general, *Salmonella* bacteria cause Salmonellosis, one of the major foodborne illnesses in most countries. The infection occurs through ingestion of contaminated food or water containing high concentrations of *Salmonella*. The incubation time is a few hours to a few

days, and the main symptoms are diarrhea, typhoid fever or paratyphoid fever [25] [27] and most healthy people generally recover after a few days. However, when these infections occur in young children or as a complication in weakened elderly patients, they can be fatal.

Salmonella normally exists in high protein foods such as eggs, meat, poultry, seafood and dairy products. However, it can contaminate any food and cause Salmonellosis when ingested by humans. Undercooked foods and un-refrigerated foods are good hosts for *Salmonella* and can result in localized or individual cases of food poisoning.

Recent *Salmonella* outbreaks have been associated with lettuce, spinach, tomatoes [28] [28], cantaloupe[29], watermelon, meat, eggs [6], and even peanut butter [5], resulting in sickness and even death, but also resulting in recalls of products and time consuming investigation to find and correct the source of the contamination.

An outbreak of *Salmonella* constitutes a major public health burden and a significant economic cost. According to the CDC, about 40,000 cases of *Salmonella* infection are reported each year in the U.S.. Worldwide, over 16 million cases of *Salmonella* infection are recorded in the form of typhoid fever with some 500,000 to 600,000 cases resulting in death.

Salmonella can survive for weeks outside a host, and is not destroyed by freezing [30] [31]. Therefore, even proper refrigeration cannot guarantee food safety. Early detection of the source of a *Salmonella* outbreak has become a growing concern. This need, coupled with the high incidences of *Salmonella* infection worldwide has driven the research and development of advanced devices for fast and efficient detection and the ability to trace *Salmonella* bacteria in the food product chain.

2.2 Conventional Biological Detection Techniques

Conventional methods for the detection of biological pathogens include cell culturing, Enzyme-Linked Immunosorbent Assay (ELISA), Polymerase Chain Reaction (PCR), Flow Cytometry, etc. Although they are limited in either specificity or selectivity and although most of them are time and labor consuming and can only work in laboratory conditions,

they are the basis for the more advanced technologies. Some of these methods are still quite common and often indispensable techniques in scientific and commercial interests as the official method to detect and confirm the existence of pathogens.

2.2.1 Bacterial Culture Technique

The culturing technique has historically been a foundational and primary diagnostic and research tool in molecular biology. It is a complex process by which microbial organisms are grown and multiplied under controlled conditions. Usually, the cells or organisms are grown on a gelatinous medium, such as agar, or in a nutrient broth under controlled laboratory conditions. This method is often used to isolate a pure culture of microorganisms and to determine the type of the organism. However, since cultures that cannot grow under provided conditions but still might be infective are usually ignored, this method is not able to determine the concentration of the organisms analyzed [32].

2.2.2 Enzyme-Linked Immunosorbent Assay (ELISA)

ELISA, enzyme-linked immunosorbent assay, or EIA, enzyme immunoassay, is a technique used to detect the presence of an antibody or antigen in a biological sample [33]. There are many variations of this test, but the most basic is to attach an unknown amount of antigen to a solid surface, and then apply a specific antibody which is linked to an enzyme so that it can bind to the antigen. Finally, a substance that the enzyme acts on is added so that the amount of product can be measured in some way, such as the magnitude of the fluorescence or a change in color of the solution. This technique is very common and is used by most regulatory agencies for the assessment of the quality of foods or for detecting potential pathogens in foods such as milk, peanuts, walnuts, almonds, and eggs [34] or the presence of certain bacteria in water or other agricultural areas (soil, fertilizers, etc.). They are also used in the medical field to determine the sterility and quality of medicines and laboratory conditions. Additionally, industry has needs for quality control that make use

of these techniques. However, this method can only identify a group of organisms having known components, and is normally time consuming.

2.2.3 Polymerase Chain Reaction (PCR)

Polymerase chain reaction, known as PCR, was developed by Kary Mullis in 1983 [35] and is a technique in molecular biology to amplify a specific region of a DNA strand, sizes ranging from a few kilo base pairs (kb) to 40 kb [36]. This technique uses a DNA polymerase to replicate a piece of DNA, and then the newly generated DNA becomes a template itself to produce new DNA pieces. As this process, known as "chain reaction," continues, the DNA template is exponentially amplified through this action. This technique is widely used in medical and biological labs for a variety of applications [35] [37] [38], including DNA cloning for sequencing, functional analysis of genes, identification of genetic fingerprints and detection and identification of infectious diseases or existence of bacteria. However, this technique can only detect the existence of a DNA strand and identify the DNA or bacteria associated with it. It can not determine the concentration or other information. Moreover, to perform this experiment requires trained personnel and often takes several days.

2.2.4 Flow Cytometry (FCM)

Flow cytometry is a technique in which cells are passed through a concentrated light beam. The cells may be detected by observing and analyzing fluctuations in brightness of scattered and fluorescent light. The lights are originated from a high intensity and very small light source such as a laser beam (as in laser flow cytometry) or an arc lamp (arc-lamp-based cytometry).

Flow cytometry is used for counting particles such as cells or chromosomes that are suspended in a liquid. The system can process thousands of particles per second and algorithms can be applied for various kinds of parametric or physical analysis.

One of the main applications of flow cytometry is in the medical field where detection and counting of blood cancer (Leukemia) cells is necessary. It is also used in pathology, immunology, plant biology, marine biology and molecular biology. However, medical is still one of the primary areas where it is used for applications in tumor immunology, chemotherapy, genetics, hematology and other similar functions.

Flow cytometry suffers from a few disadvantages that limit its usage. It requires that cells be suspended in a liquid, thus requiring solid tissue to undergo a separate process in which the cells are disaggregated by treatment with an enzyme to release individual cells. Although the system is faster than many techniques, it still has a relatively slow count rate and can only process a few thousand cells per second. Moreover, operation of the flow cytometer is not simple. The machinery is complex and can only be operated by skilled personnel in order to get best performance. Equipment cost and the ongoing maintenance cost is also a major disadvantage. With prices ranging to $100,000 for a laser flow cytometer and to about $75,000 for an arc-lamp based unit, the cost is prohibitive except for large hospitals and some research organizations.

2.3 Biosensor Techniques

Biosensors are a compact analytical device aimed at providing fast and selective identification of biological targets. This technique incorporates conventional biological detection methods integrated with the modern physio-chemical transducer techniques to convert the complex biological interaction into measurable signals. A biosensor consists of three parts as shown in Figure 2.1. The bio-recognition elements play a central role in biosensing because of their ability to genetically "recognize" and "capture" the target analyte from a biological sample. These sensitive biological elements, including enzymes, antibodies, nucleic acids, tissue, cells, etc., have a great impact on the sensitivity and selectivity of the detection technique. The transducers constitute another important area in biosensing. They use physiochemical techniques, such as optical, electrochemical, acoustic, etc., to convert the signals

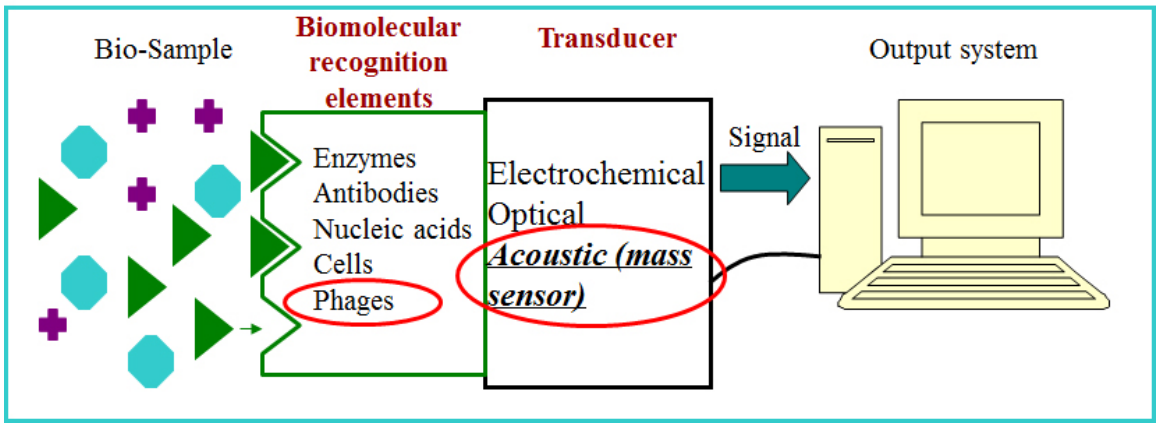

Figure 2.1: Schematic of biosensors.

resulting from the interaction between analyte and receptor into measurable and quantified signals. These signals are received, processed and finally displayed using signal processors [39].

Compared to traditional biological analytical methods, the most distinct advantage of biosensors is their fast response. The detection using biosensors normally occurs in minutes or tens of minutes. Moreover, the biosensors are easy to operate and handle and they do not need complicated preparation steps as used in conventional analytical methods. Now, with the advent of micro- or nano- techniques and the development of transducer and interface materials, a new generation of biosensors are being developed that are adaptable to miniaturization and high sensitivity. The applications of biosensors are not limited to biomedical diagnosis, but they are also used in chemical samples, environmental samples (e.g. air, water and soil) and biological samples. Although conventional analytical methods such as PCR and ELISA are still the primary methods, biosensors are considered to be one of the most promising techniques for pathogen detection. Extensive research, both in academia and in industrial labs, is being conducted in applying biosensor techniques to detect foodborne pathogens and for monitoring food quality.

2.3.1 Biological Recognition Elements

2.3.1.1 Antibodies

Antibodies, also known as immunoglobulins [40] or Igs, are gamma globulin proteins that are produced by plasma cells when foreign objects, known as "antigens", such as bacteria and viruses, enter and are recognized by the immune system [41]. The typical structure of an Ig monomer is a "Y"-shaped molecule that consists of two large heavy chains and two small light chains as shown in Figure 2.2. The large chains come in several different types that define the isotype of an antibody. There are five types of mammalian immunoglobulin heavy chains found in IgG, IgD, IgA, IgM and IgE antibodies [42], differing in their biological properties, functions and ability to deal with different antigens in the immune system [43]. Two types of immunoglobulin light chains, κ or λ, are found in mammals [44]. Only one type of light chain is present in each antibody in mammals. Although all antibodies are very similar in their general structures, some regions of antibodies are extremely different in their functions. For example, each antibody is characterized by a hypervariable region that can bind to its unique epitope of the antigen [45] in a highly specific fashion, thus allowing antibodies to recognize and bind to only their target antigens in a mixture of a wide variety of antigens. This allows millions of different types of antigen binding sites, which can recognize and bind to specific foreign objects. The antigen binding site, located at the amino terminal end of the Fab (fragment, antigen binding) region, is comprised of a set of highly variable loops, referred to as the complementarity-determining regions (CDRs) and is the most important region for determining the binding specificity of the antibody to an antigen. The Fc (Fragment, crystallizable) region, which is the base of the "Y", modulates the immune activity.

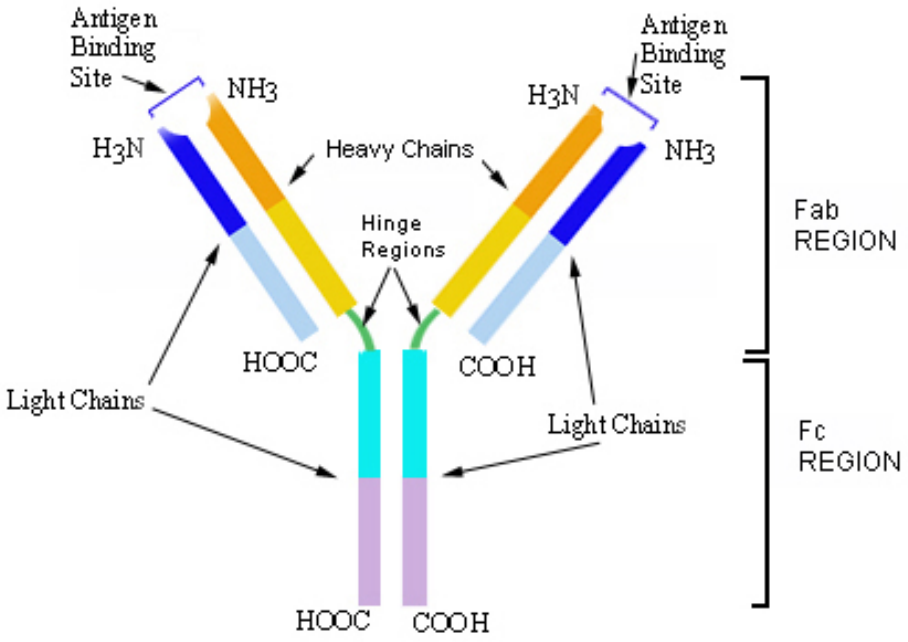

Figure 2.2: Basic antibody structure.

Antibodies have been extensively used as bio-recognition elements in biosensors, especially after the monoclonal antibody (mAb or moAb) technique was developed by Kohler, Milstein and Jerne [46]. With this technique, monoclonal antibodies that specifically bind to target cells can now be produced in laboratories and used for reorganization, identification and binding of target analytes. Currently, the majority of biosensor detection systems use antibodies as the biological recognition elements. These monoclonal antibody based biosensors have high specificity and sensitivity, and more importantly, do not require the target analyte to be purified prior to detection.

Antibody based bio-sensing and detection uses the immunoreactions between antibody and its antigens. In general, a variety of assays can be employed with antibody based biomolecular recognition and biodetection. In direct assays, analyte bound to the antibody is detected directly by measuring fluorescence [47], change in refractive index such as used in surface plasmon resonance [48], change in impedance [49], and so on. The signal increases

with the increase of analyte concentration. In a competitive indirect assay, both the analyte and the labeled competitor antigen compete for limited numbers of antibody binding sites. Therefore, the signal is weaker with a higher analyte concentration in the sample. In a sandwich assay, a labeled secondary antibody is added to bind to the target analyte while the analyte binds to the immobilized antibody. The label can be fluorescent, electrochemical, magnetic, and so on. Also, an ingenious combination of PCR technique and immunodetection method was developed [50] and used for amplification of biosensor signals. This technique has been successfully used in detection of clinically relevant tumor markers, pathogens and toxins [51].

Although the antibody-antigen immuno-reaction is fast, highly specific, and is easy to incorporate into a sensor, there are limits to its usage. The monoclonal antibodies, which are highly specific to target antigens, are expensive to produce and the production is time and labor consuming. The other type of antibody, the polyclonal antibodies, although cheap and easy to culture, has poor specificity for target antigens and thus are not as useful.

2.3.1.2 Bacteriophages

Bacteriophages ("phages", for short) are viruses that infect bacteria. They are typically composed of genetic material, such as DNA or RNA, and an outer proterin capsid. The replication and infection of bacteriophages may be a lytic cycle, which results in lysing of the host cell, or a lysogenic cycle, in which host cells are not destroyed after the replication of the phage. A few viruses have the ability of both types of replication. Based on the fact that each type of bateriophage can only infect a certain host because they can only bind to specific receptors on those bacteria surfaces, bacteriophages can become good biomolecular recognition elements.

Previous work has shown great success in producing and using phages selected from a landscape library to specifically bind with target antigens [52]. These phages are filamentous bacteriophages Ff and have a rod filament shape with sizes of approximately 800-900 nm long

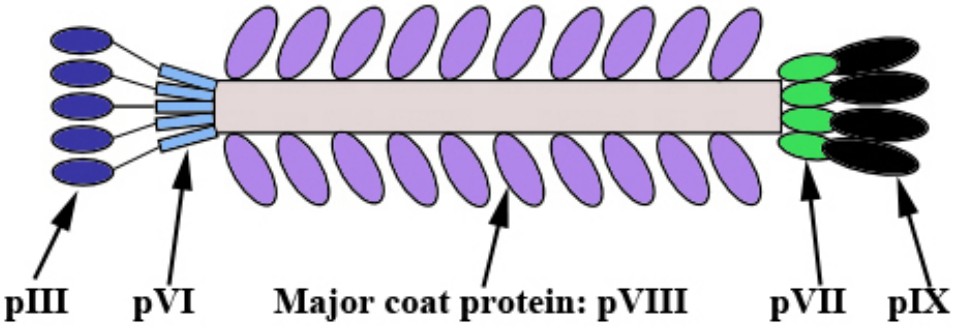

Figure 2.3: Structure of a filamentous bacteriophage.

by 6.5 nm in diameter (Figure 2.3). Each filament contains a single stranded DNA packed in a capsid composed of the major coat protein pVIII and minor coat proteins pIII, pVI, pVII and pIX [53] [54]. This unique feature allows displaying thousands of copies of random peptides by fusing them to the N-terminus of the each major phage coat protein, allowing the display of large amounts and high densities of epitopes, thus having a high potential to greatly increase the sensitivity of the immunoassay. The random peptides on the surface of the phage subtend an organic "landscape", therefore, this phage is called a landscape phage and a large mixture of such phages is called landscape library.

As new types of bio-recognition elements, the phage probes derived from the landscape phage library have a few distinct advantages. They have been proven to be good substitutes for antibodies with high affinity and specificity to the target agents. Moreover, the phages are resilient to harsh environments. They can survive at high heat (up to 70 ° Celsius), in many organic solvents, such as acetonitrile [55], urea (up to 6 M), acid, alkali, and are also resistant to low humidity and other environmental stresses. These unique characteristics are favorable for the usage of phage based biosensors in extreme environmental conditions.

2.3.2 Transduction Mechanisms

2.3.2.1 Optical

After immobilizing the biomolecular recognition elements on the surface of an optical transducer surface, the target analyte can be detected by measuring the intensity or refractive index of the light. This transduction method allows immediate detection upon the reaction between the bio-recognition elements and the target analyte. Moreover, the interference that can limit and even hinder the measurement in other forms of transduction, such as voltage surges, harmonic induction and radio frequency interference, is not a problem for optical transduction. The disadvantages of using the optical transduction method is the high cost of some detection system components and the challenges when detecting in turbid samples.

At present, a wide variety of optical transducer have been employed in the biosensing area. These transducers include fluorescence based transducers, surface plasmon resonance, resonant mirror, interferometry, etc.

Fluorescence Fluorescence-based transduction is the most fundamental form of optical transduction. In most cases, the bio-recognition elements are labeled with fluorescent reporters and the intensity represents the presence and concentration of the target analytes. In addition, by monitoring the time dependence in the wavelength or energy transfer of the fluorophore reporter, we can also monitor the binding interaction occurring in the assay employed. This technique, coupled with techniques such as flow cytometry, microfluidics and biological imaging array systems, has been widely used in biomolecular recognition and detection. Biological imaging array systems are systems which utilize biological recognition elements (biochips) in an ordered array to screen targets.

Interferometry Interferometers are instruments used to cause interference of two or more waves that are created by their superposition [56]. Typically, two identical waves travel through different paths and are combined upon reaching the detector. A disturbance in one

path will result in a detectable change at the detector. The interference pattern introduced by the phase difference of the two waves can be used to diagnose the change in the refractive index along the path. This technique is able to measure biomolecular interactions that take place at a surface within an evanescent field, causing a refractive index change and thus the phase change of the propagating waves.

Current interferometers use waveguides to define a reference and a "sensing" wave. The "sensing" wave experiences refractive index changes at the surface where the target analyte reacts with the bio-molecular recognition elements while the reference wave does not go through this change. Superposition of the "sensing" and the reference waves creates an interference pattern, which is used to diagnose the presence of the target analyte. One such example is dual polarization interferometry (DPI) [57] [58]. The DPI focuses the evanescent wave of a laser beam into the reference and the sensing waveguides and is able to rotate rapidly between two polarization modes of the waveguides. This technique is typically used to measure the conformational information about biochemical interactions taking place as the biomolecules function. Like the other optical transducers, DPI allows real time measurements of the biochemical reaction on the surface. Moreover, it also allows detection of not only the refractive index change but also the thickness of the biomolecular layer on the surface. A highly sensitive DPI measurement reported by Boudjemline et. al. was able to distinguish the guided light during the protein crystallization. This was used to monitor the early stage of protein crystal nucleation in real time [59]. Recent development of DPI has allowed the study of the kinetics of lipid bilayer formation [60] and the interaction between membrane and proteins [61] [62]. Other configurations of interferometers include Mach Zehnder interferometer [63] [64], Fabry Perotot interferometer [65], etc. The primary problem of this technique is the lack of robustness due to the complex instrumentation required for the measurement. Another problem that limits the usage of this technique in practical applications is the high number of false-positives.

Surface Plasmon Resonance Many optical transducers for biosensors are based on the phenomenon of surface plasmon resonance (SPR). This occurs at a planar interface between any two materials, e.g., a metal-dielectric interface. Upon illuminating the metal surface, surface electromagnetic waves (surface plasmons, or "SPs") are produced [66]. Due to the high sensitivity of these waves to the change on this interface, the SPR can be harnessed to measure biomolecular interactions [67].

A schematic diagram illustrating the principles of SPR biosensing is shown in Figure 2.4 [68]. A typical SPR chip consists of a prism, which is made of high refractive index glass, on top of which is coated a thin layer of gold. Light of a certain wavelength from the light source is totally reflected from the prism surface coated with gold and the reflected light is detected by an optical detection apparatus. At a specific incident angle, θ, surface plasmons are produced, resulting in a decrease in reflected light. This angle θ changes when the refractive index at the interface changes. When target analytes bind onto the biological recognition elements on the other side of the gold surface, the local refractive index changes. Thus, by measuring the change in the resonance excitation of surface plasmons, the target analytes can be detected [69].

Although SPR is easy to use and allows very rapid detection, its sensitivity is limited due to reflected light. To solve this problem, researchers have developed a resonant mirror design [70], [71], where a series of polarizing filters are added to the SPR to block the internally reflected light.

Another a major problem with SPR-based sensing is that the refractive index is affected by many things other than the detection of target analyte, such change in density, chemical component of the solution, etc. Therefore, this method is limited to detection in homogeneous solutions.

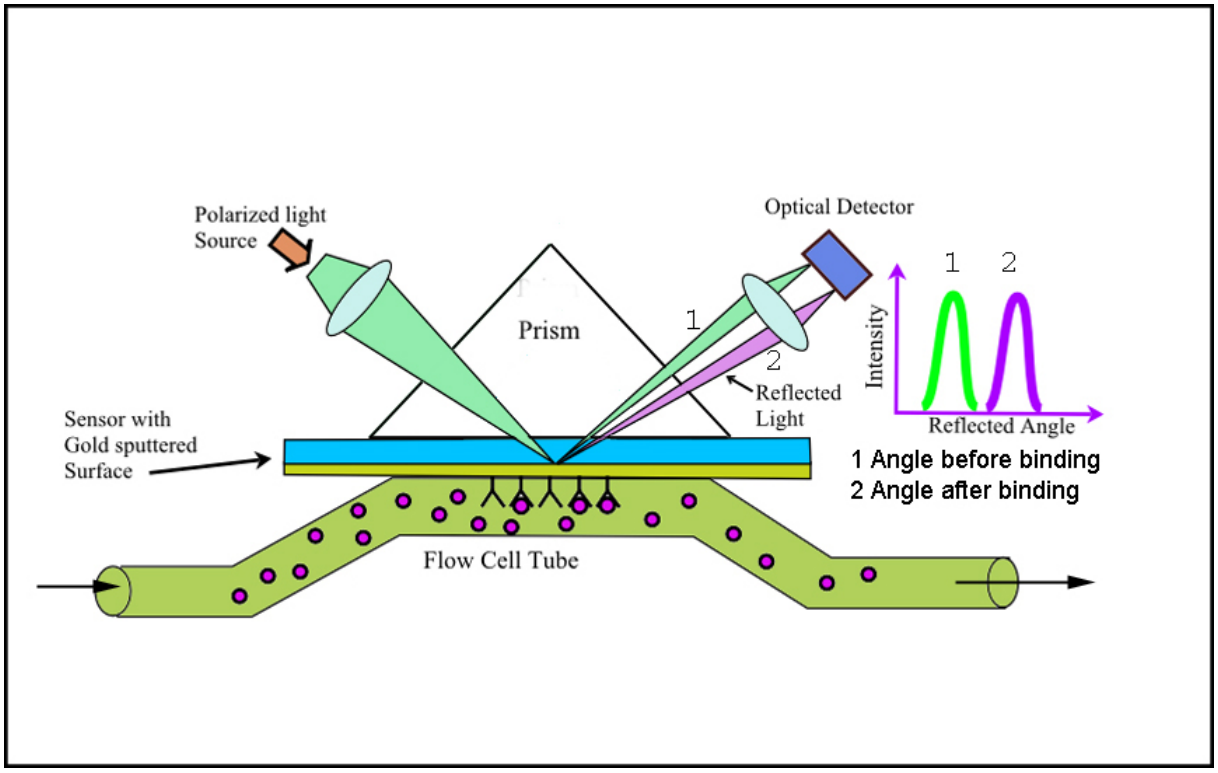

Figure 2.4: Principle of SPR based biosensing.

2.3.2.2 Electrochemical

Electrochemical transductions are normally based on redox reactions that generate or consume electrons. These reactions usually involve the use of enzymes to catalyze oxidation or reduction of the working electrode. This transduction method has been widely used in the biosensing area due to its several distinct advantages. First, unlike a lot of the optical transduction methods that require homogeneous sampling solutions, the electrochemical transduction is effective in complex or turbid solutions. Second, the electrochemical based sensing devices are normally low cost and reusable. Third, these devices can be miniaturized to be portable and to detect a small amount of sample.

In general, the electrochemical transduction can be amperometric, potentiometric or conductometric. The amperometric transduction mornitors directly the change in current and this current is normally proportional to the analyte concentration. The potentiometric

transduction measures the change in potential, which is attributed to the change in ionic strength or pH at an ion-selective electrode. Conductometric transduction is based on the variation of the resistance of the device. Although this type of device generally has low sensitivity, by using an array of several electrodes, each with a different coating to provide different resistive responses, it can be used for detection in very complex samples. For example, Marrakchi et. al. used a conductometric biosensor based on lucose oxidase and beta-galactosidase to detect the amount of lactose in milk [72]. Zhang et. al. developed a conductometric biosensor using various cytochrome c nitrite reductase composite membranes immobilized on a planar interdigitated electrode to detect nitride in water solutions [73]. Furthermore, the field effect transistors (FETs) are considered to be a variation of potentiometric sensors with miniaturized structure and improved sensitivity [74]. One such FET biosensor was reported by Villamizar et. al. for the selective detection of *Salmonella* Infantis. The detection limit of this sensor for S. Infantis was 100 cfu/ml [75].

2.3.2.3 Acoustic

The detection mechanism of acoustic transduction in biosensing is based on the change of mechanical or acoustic waves due to the detection of analyte. These transducers predominately rely on piezoelectricity. Piezoelectricity is the phenomenon where electrical charges are produced on piezoelectric materials when a mechanical stress is applied [76]. This process is reversible. Applying an electrical field to the piezoelectric material creates a mechanical stress inside the material. Piezoelectric sensors generate mechanical waves upon application of an oscillating electric field. When biomolecular recognition occurs and target analytes bind onto the sensor surface, this wave is changed accordingly due to the increase of mass on the sensor. These sensors have fast response, are low priced and reliable, and are widely used for sensing and monitoring of a wide variety biological ligands. However, they must have wire connections which limits their usage in many applications. In addition to piezoelectric sensors, some magnetic acoustic sensors have recently been developed for biosensing

applications, such as magnetoelastic micro-biosensors. Compared with piezoelectric sensors, these sensors are wireless, have higher Q-values and higher mass sensitivity [77].

Bulk Wave Acoustic Resonator Thickness Shear Mode Resonator (TSM), one of the most commonly employed transducers, relies on the transmission of bulk waves. The schematic of a typical disc TSM, often referred to as a quartz crystal microbalance (QCM), is shown in Figure 2.5. A typical disc TSM may consist of a thin disk of AT-cut quartz with circular electrodes plated on both sides. Upon application of an AC voltage between the electrodes, an oscillating electric field is formed in the quartz. This oscillating field causes a shear deformation across the crystal, generating a mechanical wave across the device. When target analytes bind to the bio-recognition elements on the surface of the device, the associated mass increase on the TSM surface causes a decrease in the resonant frequency of the wave.

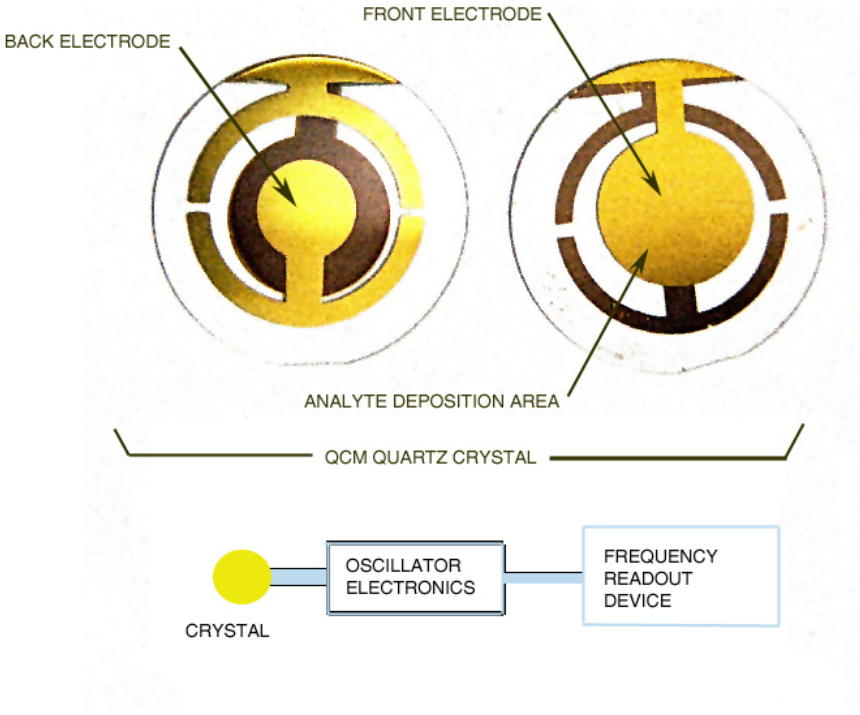

Figure 2.5: Typical disc TMS sensor.

A quantitative relationship between the change in resonant frequency and the added mass was first derived by Sauerbrey in 1959 [78]. In Sauerbreys equation, by assuming that a small amount of mass is uniformly added onto the TSM surface, the change in the resonant frequency is proportional to the amount of added mass. Therefore, by measuring the shift in resonant frequency, the amount of target analyte bound to the sensor can be estimated.

Biosensors based on TSM transducers have been developed for the affinity detection and monitoring of a variety of bacteria [79] [80], nucleic acids [81], cells [82] [83], etc.

Surface Acoustic Wave Resonator Surface acoustic wave (SAW) transduction is based on the transmission of surface acoustic waves, or Rayleigh waves, discovered by Lord Rayleigh in 1885 [84] and named after their discoverer. These waves, traveling along the surface of a material, are strongly affected by the coupling with the medium in contact with the surface. This feature enables SAW sensors to directly sense the change in mass on the surface of the SAW devices due to the biomolecular recognition of target analytes and the bioreceptors. Because nearly all Rayleigh waves are confined within one wavelength from the surface, SAW sensors exhibit significantly high sensitivity compared with all the other acoustic sensors. However, the Rayleigh wave is severely dampened in liquid biological solutions, limiting its utility for biosensing applications.

Magnetoelastic Micro-Resonator Magnetoelastic materials have been investigated by many researchers for sensor applications due to their unique characteristic of magnetoelastic interactions. Under an external magnetic field, the direction of magnetization in the magnetoelastic material will reorient along the external magnetic field direction, generating a magnetoelastic stress. In a bulk material, this magnetoelastic stress causes the material to change dimensions as the direction of magnetization is changed under the external field. Under the influence of an alternating magnetic field these devices will vibrate at the applied frequency, and will have maximum vibration amplitude at a frequency the same as their natural resonant frequency, where the natural resonant frequency is determined by the physical

properties of the material, i.e., length, width, thickness and mass. Since natural resonant frequency is affected by mass, a change in mass and its associated change in resonant frequency can be the basis of a mass sensor. Like other surface acoustic wave devices, where a wave propagates along the surface and is affected by mass these devices can be used to directly measure the effects of a change in mass.

Magnotoelastic materials are typically amorphous ferromagnetic alloys that have high tensile strength (1000-1700 MPa), high magnetoelastic coupling coefficient (up to 0.98) and high magnetostriction (10^{-5} ppm) [3]. The high magnetostriction and magnetoelastic coupling coefficient allows the characteristic resonant frequency of the material to be easily observed and energy conversion between magnetic energy and elastic energy is being highly efficient.

Compared with other acoustic sensors being reviewed, magnetoelastic sensors have exclusively high Q-values and sensitivity, high mechanical stiffness, simple construction and are capable of wireless and remote detection.

Previous research has demonstrated the use of magnetoelastic cantilevers [85] [12] or free-beams [86] [87] [88] [89] [90] for the detection of biological pathogens such as *S. typhimurium* and *B. anthracis* with high sensitivity. The disadvantage is that these devices require some type of holding fixture.

The research reported here has adopted the free-standing magnetoelastic sensor structure, which can be easily adapted to the detection of pathogens by using many sensors simultaneously.

Chapter 3

Materials and Experiments

3.1 Design and Fabrication of Sensor Platform

The sensor platform is made from Metglas® 2826MB, a magnetoelastic film obtained from Honeywell International. This film is an amorphous alloy with an average composition of $Fe_{40}Ni_{38}Mo_4B_{18}$ with a saturation magnetostriction (λ_s) of 12 ppm [3]. The basic physical and magnetic properties of Metglas® 2826MB alloy are shown in Table 3.1.

Table 3.1: General properties of MetGlas® 2826MB [3].

Electromagnetic	Saturation Induction (T)	0.88
	Maximum DC Permeability (μ): Annealed (High Freq.)	800000
	Maximum DC Permeability (μ): As Cast	>50,000
	Saturation Magnetostriction (ppm)	12
	Electrical Resistivity ($\mu\Omega$-cm)	138
	Curie Temperature (°C)	353
	Thickness (mils)	1.15
Physical	Density (g/cm^3)	7.9
	Vicker's Hardness (50g Load)	740
	Tensile Strength (GPa)	1-2
	Elastic Modulus (GPa)	100-110
	Lamination Factor (%)	>75
	Thermal Expansion (ppm/°C)	11.7
	Crystallization Temperature (°C)	410
	Continuous Service Temp. (°C)	125

The sensor platform consists of a magnetoelastic film covered with a chromium inner layer and a gold outer layer as shown in Figure 3.1. The chromium inner layer is used to improve the adhesion between the gold layer and the magnetoelastic resonator platform.

The gold layer is used to protect the magnetoelastic material from corrosion and at the same time to provide a bioactive surface to which the bio-recognition element may be easily attached. The length to width ratio of the sensor platform is kept to be 5. This length to width ratio is chosen so that the sensor is long enough that its first mode vibration can be approximated as a pure longitudinal vibration, and at the same time, is wide enough that a large surface area can be obtained for the attachment of bacteria and spores. Sensors of various dimensions were fabricated to evaluate parametric effects, including: lengths (500 μm to 5 mm) and thicknesses (15 μm and 30 μm). The chromium layer and the gold layer are both around 100 nm thick.

The magnetoelastic sensors were fabricated from an as-received film. This film is an amorphous ribbon with one side smooth and one side slightly rough. In order to have consistency, both sides were polished using standard metallographic preparation techniques until a desired thickness was achieved. After polishing, the material was diced into rectangular pieces with sizes ranging from 500 μm to 5 mm long. These pieces were ultrasonically cleaned in a bath of acetone and then ethanol and afterwards were annealed at 220 °C in a vacuum of 10^{-3} Torr for 2 hours to reduce residual stresses [91]. After the annealing, the pieces were sputter coated in an argon atmosphere using a Denton Vacuum Discovery-18$^{\text{TM}}$ magnetron sputtering system at a pressure of 5 milli-Torr. First a layer of chromium was sputtered at a power of 200 watts DC followed by a gold layer sputtered at a power of 100 watts RF. The chromium is used to improve the adhesion of gold to the metglas film. The magnetoelastic sensor platforms were then cleaned and stored in a controlled temperature and humidity chamber. Figure 3.2 is a SEM picture of a magnetoelastic sensor platform.

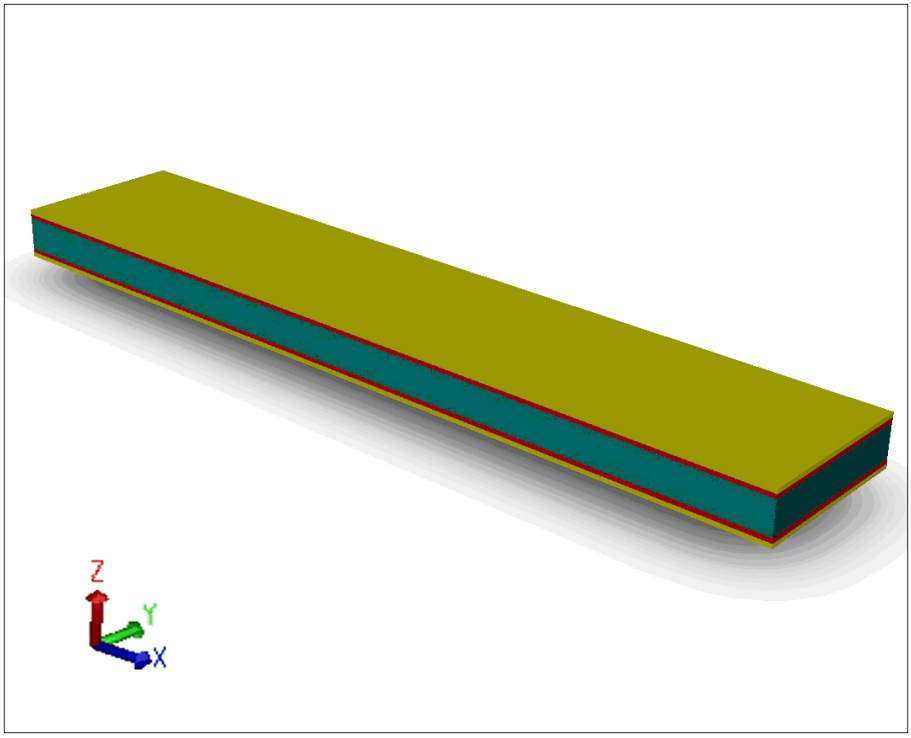

Figure 3.1: Schematic illustration of the magnetoelastic sensor platform.

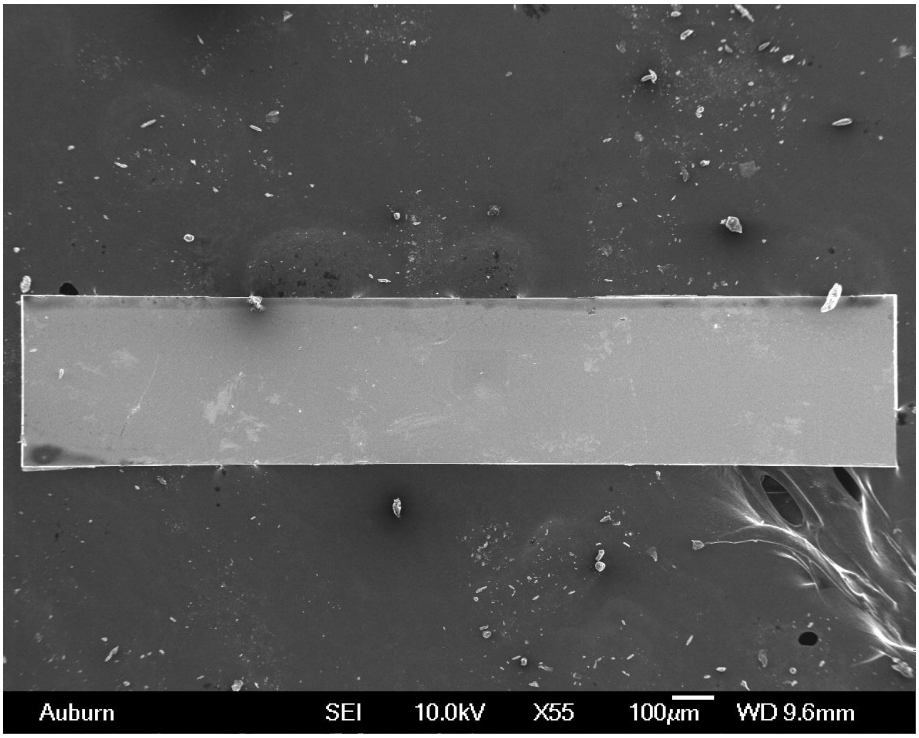

Figure 3.2: SEM picture of a magnetoelastic sensor platform. Dimentions: $2000 \times 400 \times 15 \mu m$.

3.2 Phage Coating

In this work, JRB7 phage is used as the biomolecular recognition element for specifically binding with *B. anthracis* spores, and E2 phage is used as a specific binding probe for *S. typhimurium*. JRB7 phage and E2 phage are both filamentous phages and are selected from a landscape phage library. Previous research has illustrated the ability of these phages to serve as substitutes of antibodies for the detection of *B. anthracis* spores and *S. typhimurium* bacterium on various sensor platforms [52] [14] [92]. The original JRB7 phage and E2 phage were prepared in Dr. Valery Petrenko's lab in the Department of Pathobiology and in Dr. James Barbaree's lab in the Department of Biological Sciences at Auburn University in Auburn Alabama, USA. The phages received from their labs were at a concentration of 1×10^{12} vir/ml and were suspended in 1X TBS (Tris Buffered Saline) solution. The as-received solutions were diluted with 1X TBS to a concentration of 5×10^{11} vir/ml for immobilizing onto the sensor platforms. The immobilization takes place by immersing the magnetoelastic platform in a tube of 0.3 ml prepared phage solution (JRB7 phage or E2 phage with a concentration of 5×10^{11} vir/ml) and rotating on a rotor at a speed of 10 RPM for 1 hour. In this process, phages bind to the gold on the surface of the sensor via physical adsorption. The sensors are then washed by 1X TBS solution for three times to remove the unbound or loosely bound phages and finally dried in air. Concentration of the phage is checked by spectrophotometer.

3.3 Bacteria Cultures and Spore Solutions

B. anthracis Sterne spores were provided from Dr. James Barbaree's lab in the Department of Biological Science at Auburn University. After obtaining *B. anthracis* Sterne spore production, the spores were then washed in sterilized water and purified by Renografin gradient. The spores were maintained in sterilized water and checked regularly in Dr. Barbaree's lab before using to conduct experiments. The *B. anthracis* spores delivered from Dr.

Barbaree's lab were suspended in distilled water at the concentration of 5×10^8 spore/ml. For my biosensor testing, this suspension was further diluted in distilled water to a series of concentrations ranging from 5×10^1 spore/ml to 5×10^8 spore/ml. These spore solutions were stored at 4°C and brought to room temperature in a water bath prior to the biosensor tests.

S. typhimurium ATCC 13311 was obtained from American Type Culture Collection (Rockvill, MD) and propagated in Dr. Barbaree's lab. The *S. typhimurium* ATCC 13311 was inoculated from BDS plate LB broth and then suspended in distilled water for experimental usage. The *S. typhimurium* obtained from Dr. Barbaree's lab was at a concentration of 5×10^8 cfu/ml. This concentration was determined using spectrophotometer and confirmed by viable plate count. The *S. typhimurium* ATCC 13311 strain suspension was then diluted in distilled water to a series of concentrations ranging from 5×10^1 cfu/ml to 5×10^8 cfu/ml for the experiments and prepared on the same day as the biosensor testing.

S. typhimurium 29631 AMES is a wildtype strain obtained from Dr. Staurt Price's lab in the Department of Pathobiology, School of Veterinary Medicine, Auburn University. This strain was further grown and prepared in Dr. James Barbaree'a lab at the Department of Biological Science, Auburn University. The preparation of steps included growing the strain in LB broth for overnight culture, washing the culture with 1X PBS twice by centrifugation, and diluting the final bacterial solution to a count of 5×10^8 cfu/ml. This *S. typhimurium* AMES strain suspension was then stored at 4°C and as described previously, diluted with distilled water to a series of concentrations ranging from 5×10^1 cfu/ml to 5×10^8 cfu/ml before biosensor testing.

3.4 Scanning Electron Microscopy Imaging

A scanning electron microscope was used to confirm the binding of spores to the sensor surface. To prepare for the SEM, the biosensors were exposed to an Osmium Tetroxide (OsO_4) vapor for 30 minutes to kill the spores and bacterim cells and protect the outer cell

layers from damage during the examination process. The sensors were then mounted onto aluminum stages and sputter coated with a 30 nm gold layer in an argon atmosphere of 0.8 mBar vacuum. A JEOL-7000 SEM, operated at 15 keV, was used to examine the sensor surface for binding.

Chapter 4

Detection Techniques for Magnetoelastic Sensors

4.1 Review of Currently Existing Methods

4.1.1 Time Domain Method

In the early 2000s, Zeng et. al. proposed a method of time domain characterization of magnetoelastic sensors [93] [94] [95]. In their work, a burst of AC pulses was used to excite a 30mm sensor into vibration and then a processor counted the zero crossings from the sensor coil. When the input frequency and the counted frequency are the same, the resonant frequency is known. This technique uses a microprocessor to generate a low frequency burst and a zero-crossing detector to give a digital pulse for each crossing of the decaying sinusoidal waveform. A microprocessor then determines the number of pulses during a time period or determines the time between pulses to determine if the zero-crossing signal is the same frequency as the applied frequency. If not, the input frequency is incremented and the counting is repeated. When the two are almost the same, the processor can adjust the applied frequency by smaller increments until the applied and counted frequencies are almost the same. This method works well when signal levels are large compared to baseline noise so that the zero crossing detector (an analog circuit) can give good accuracy. For very low-level signals from small sensors, the noise may give zero crossing errors and make the technique unreliable or unusable. For this system, an external bias magnet must be used to bias the sensor to its most sensitive condition where the change in length is greatest for a small change in magnetic field.

4.1.2 Frequency Domain Method

The detection method used most frequently is a frequency domain method, in which the sensor is continuously excited by sweeping an excitation signal over a frequency range that includes the sensor's resonant frequency and where maximum vibration occurs [96], [97], [77]. This method allows wireless, almost real-time detection. For maximum vibration amplitude, a DC bias magnetic field is needed to bias the sensor to the point of maximum magnetostriction. Small sensors need a well-controlled bias field and are very sensitive to field changes since they cause changes in the resonant frequency.

4.2 Frequency Domain Method in This Research

Researchers at Auburn University have characterized sensors as small as 200 microns in length [88], but best response has been obtained with sensors with a length of 0.4 to 2.0 mm. The technique used for characterizing these sensors uses a network analyzer with an S-parameter adapter to sweep the excitation frequency over a fixed range and monitor the output for maximum signal amplitude [96]. The analyzer uses a very accurate oscillator to give the frequency of maximum amplitude. If the sweep rate is set very low, the accuracy is limited by the noise level combined with the signal. This noise error can be reduced by averaging over a number of sweeps, but this increases the detection time. For small and unknown sensors, the rate of frequency change must be very slow to allow the system to "see" the sensor output. As before, a bias magnet is needed. Like the previous system, this technique is fastest when the signal is relatively large and when the resonant frequency is known within a small window.

In this research, sensors of length 2mm and 1 mm were used. The basic procedure is the same as outlined above where an analyzer with S-parameter adapter is used to sweep a frequency over a range that includes the sensor's resonant frequency and simultaneously shows the peak resonant frequency that it detects.

The basic structure of the detection system for our magnetoelastic sensors is presented in Figure 4.1. The signal processing section is used for measuring resonant frequency of the sensors. Coils are used for applying a magnetic field to the sensor and for receiving signals from the sensor. By measuring the signal amplitude at each applied frequency, maximum amplitude is measured at the resonant frequency. In our case we monitor the difference between the applied signal and the sensed signal to give a negative going peak as shown Figure 4.2.

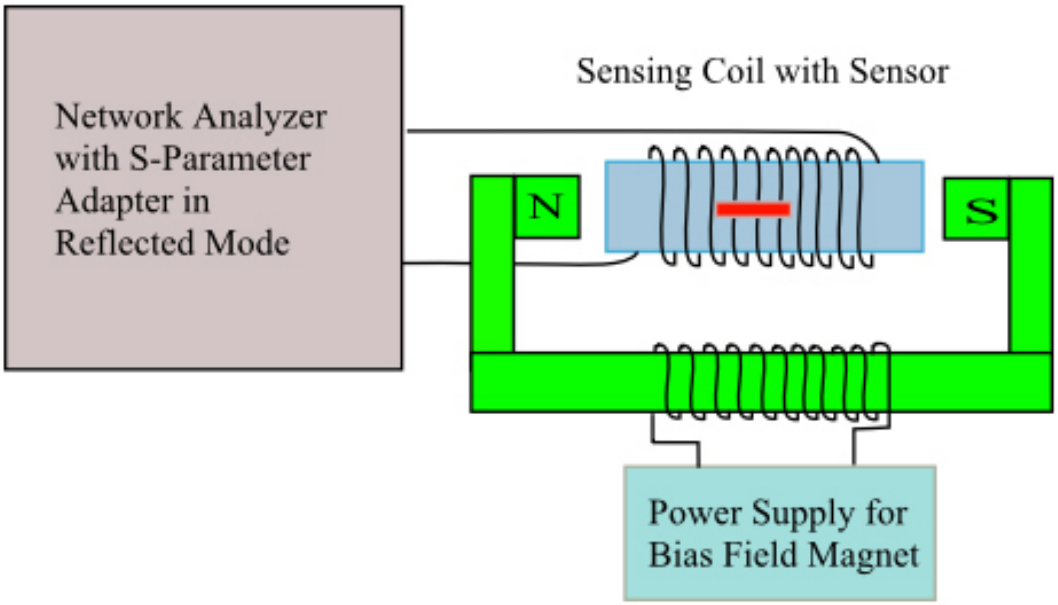

Figure 4.1: Schematic of sensor measurement set up.

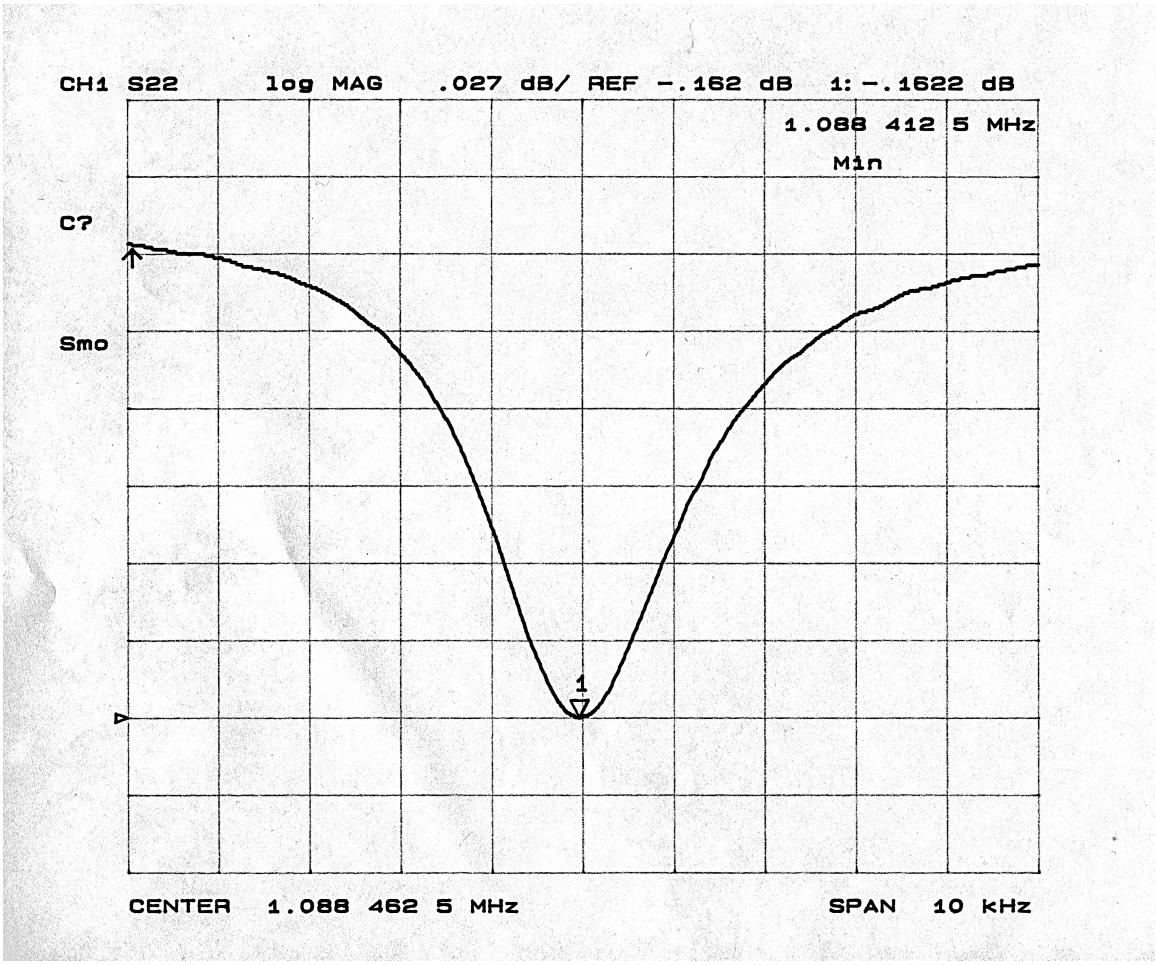

Figure 4.2: Network analyzer signal of a magnetoelastic sensor. Sensor dimensions: 2000 × 400 × 15 μm.

4.3 Development of the Pulse Detection Method

For the above methods, there is sensitivity to bias the magnetic fields, which may result in detection errors, especially if the sensor moves within the magnetic field and changes resonant frequency. There is also sensitivity to noise contained within the signal of interest, which may cause variation of the detected resonant frequency.

To solve the bias field problem and improve the accuracy of detection, we have developed a time-domain detection method that does not use a bias magnet and gives very stable and accurate detection. In this method, we apply a magnetic field as a short magnetic excitation pulse that acts as a mechanical striking force to "shock" the magnetoelastic sensor into vibrating at its characteristic resonant frequency. The change in length due to this vibration modulates the magnetic field in a sensing coil to give a detectable signal. This signal is connected to a spectrum analyzer where it is transformed into a frequency spectrum using FFT [98].

4.3.1 Principle of Pulse Detection

This method uses a magnetic excitation pulse to "shock" the magnetoelastic sensor into vibration, causing it to vibrate at its natural characteristic resonant frequency. In this system, the magnetoelastic sensor is placed inside a coil of wire. A pulse of current is applied to the coil, the magnetic field suddenly increases, and the magnetoelastic sensor is set into a condition of damped sinusoidal vibration as it settles back into its "quiescent" state.

A rectangular pulse is determined by three parameters: its height A, width T and center t_0. Mathematically, a rectangular pulse is defined by the following equation (Equation 4.1),

$$g(t-t_0) = A\ rect\left(\frac{t-t_0}{T}\right) = \begin{cases} A\left(\frac{t-t_0}{T}\right) \leq \frac{1}{2} \\ 0 \text{ otherwise} \end{cases} \tag{4.1}$$

the fast Fourier transform (FFT) spectrum of this rectangular pulse is defined as:

$$G(f) = ATsinc(\pi fT)exp(-i2\pi ft_0) \tag{4.2}$$

Figure 4.2 (a) displays an example of a rectangular pulse with amplitude A being 0.5, width T being 80 s and center t_0 being -5.1. Its Fourier transform spectrum along with its phase are shown in Figure 4.2 (b) and (c).

As indicated in Equation 4.2 and Figure 4.3, the frequency spectrum generated from the square pulse contains a DC component and an AC component that includes a broad range of frequencies. The DC component may contribute to the fact that no extra DC magnetic field is required in this system. The AC component includes a broad range of frequencies. By setting the Spectrum Analyzer to monitor a range of frequencies between a low to high frequency setting that includes the resonant frequency of the sensor, its resonant frequency range can be detected and displayed by a spectrum analyzer. Therefore, this method avoids the time consuming frequency scan that is required by the before mentioned methods.

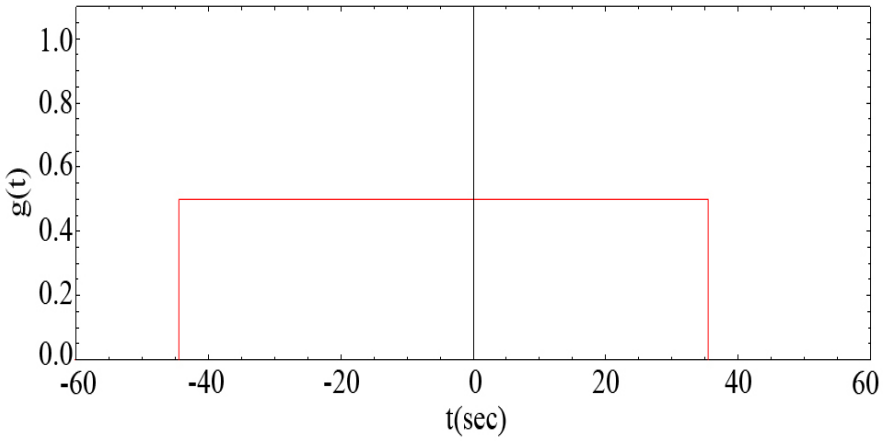

(a) $Arect(\frac{t-t_0}{T})$

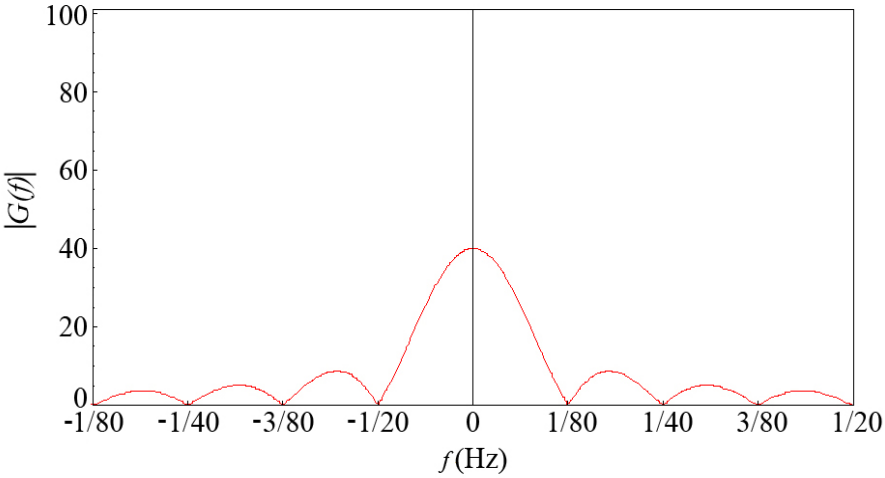

(b) magnitude of Fourier transform spectrum

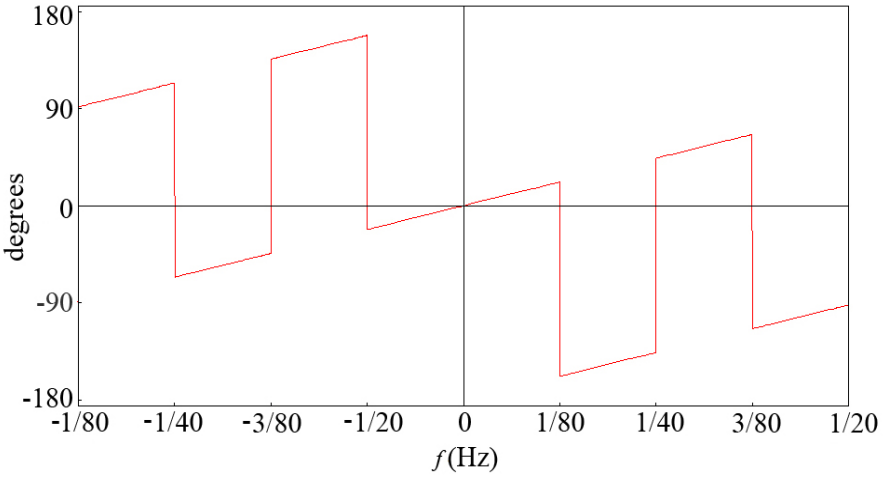

(c) phase of Fourier transform spectrum

Figure 4.3: Matlab simulation of (a) a rectangular pulse with (b) its Fourier transform spectrum along with (c) its phase of spectrum ($A = 0.5$, $T = 80s$ and $t_0 = -4.9s$).

4.3.2 Electronic Implementation

Figure 4.4 [99] is a block diagram of the complete system used for the pulse detection method and Figure 4.5 shows the laboratory components used for testing, excluding the spectrum analyzer. The function generator sets the basic pulse repetition rate of the system. Its output is a square wave at the pulse repetition rate. The rising edge of this signal is used to start the power pulse and is also used to initiate the delay for the gate used by the spectrum analyzer. For each rising edge of the function generator waveform, the excitation timer generates a 5 volt logic level pulse of a time duration set by the timer circuit. The pulse time is adjusted to allow sufficient ring-down of the sensor oscillation. This pulse is then fed to a power amplifier sub-circuit that converts the 5 volt level to a higher level power pulse of magnitude determined by the power supply that feeds the power amplifier. The delay and gate timer are used to insure the spectrum can trigger on the signal of interest and not on the transient noise at the leading edge of the power pulse. The spectrum analyzer is set to "see" only the signal within a window time. After a delay time generated in the delay sub circuit and long enough for the transient noise from the power pulse to subside, a gate pulse is generated and used to start a timing window in the spectrum analyzer. This window time is set to encompass most of the ring-down signal. The spectrum analyzer performs an FFT on signals that are present within the window time. Figure 4.6 shows the timing pulses used in the system. An oscilloscope is used to see the timing signal relationships so that the timing parameters can be set.

The two transformers with opposing windings are used to implement a differential, balanced bridge transformer setup. The primary side of each transformer is an excitation coil and the secondary serves as a sensor coil. With no signal present the output is zero. When the magnetoelastic sensor is put inside one transformer the bridge becomes unbalanced and gives an output signal. Similarly, a control sensor may be placed in the other transformer to provide an independent reference signal from the main sensor.

The signal from the transformer bridge is fed to a 26 dB amplifier by HP to increase the signal for the spectrum analyzer. The spectrum analyzer performs an FFT on this signal and generates the FFT data which is displayed and sent to a computer for analysis of the sensor response versus time.

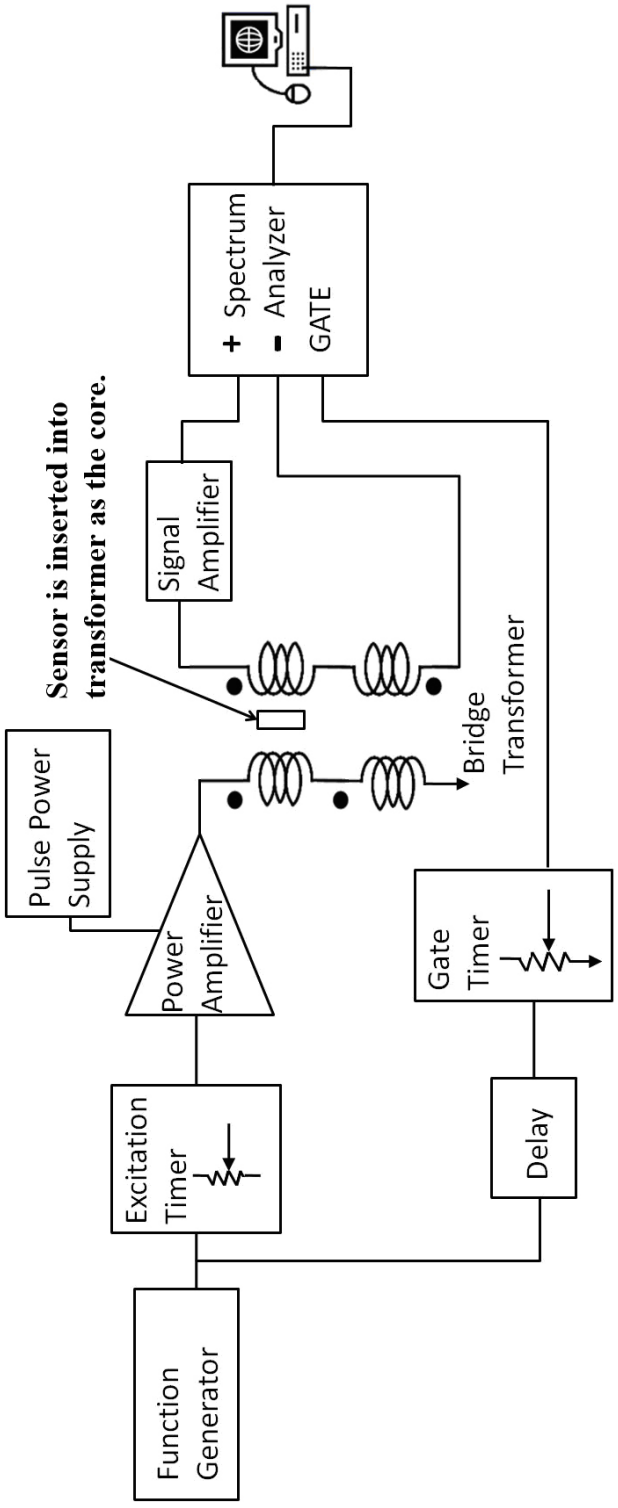

Figure 4.4: Block diagram of the pulse system.

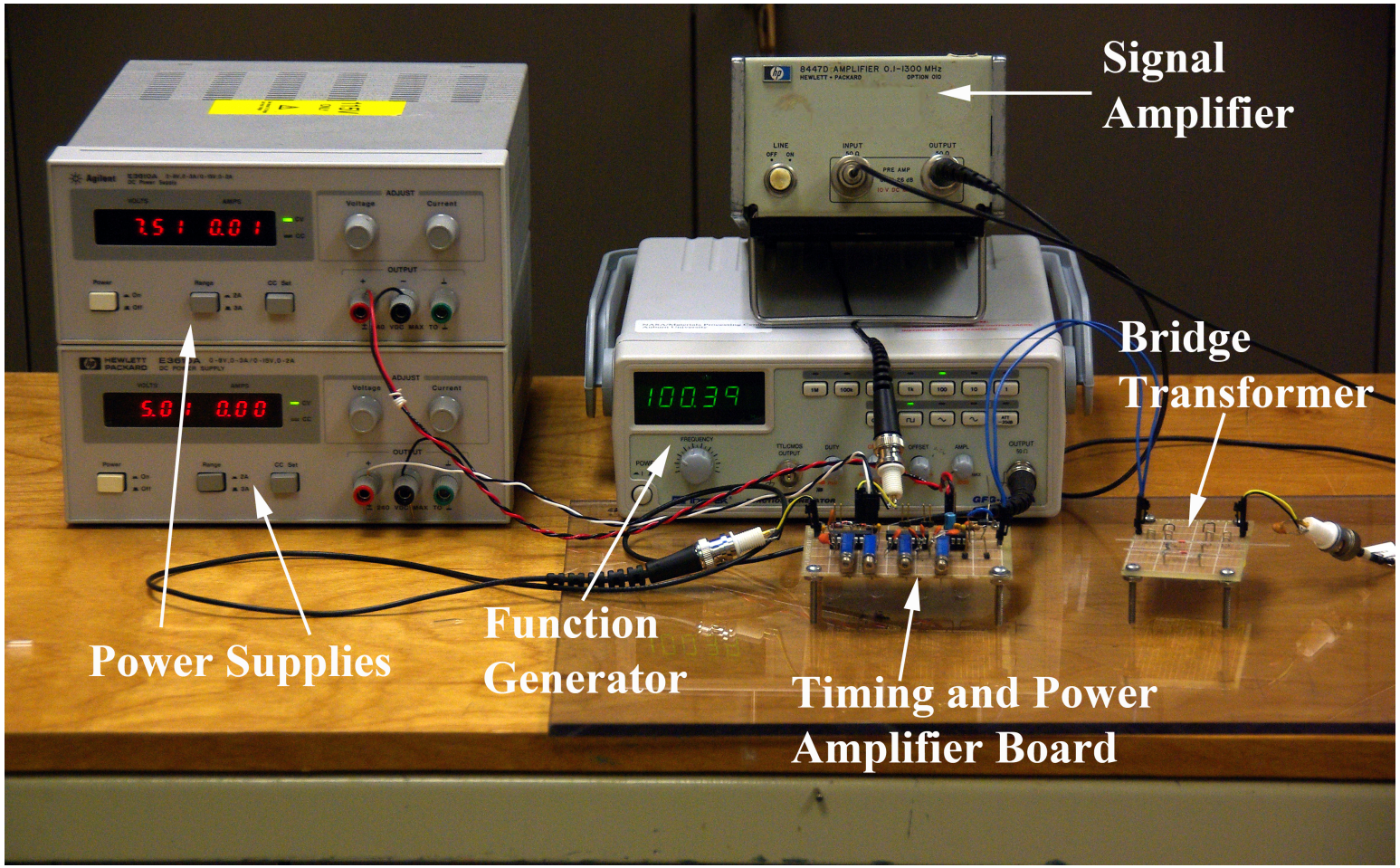

Figure 4.5: Photograph of the pulse system showing power supplies, function generator, final amplifier and prototype boards with timing circuits and small board with the transformer coils.

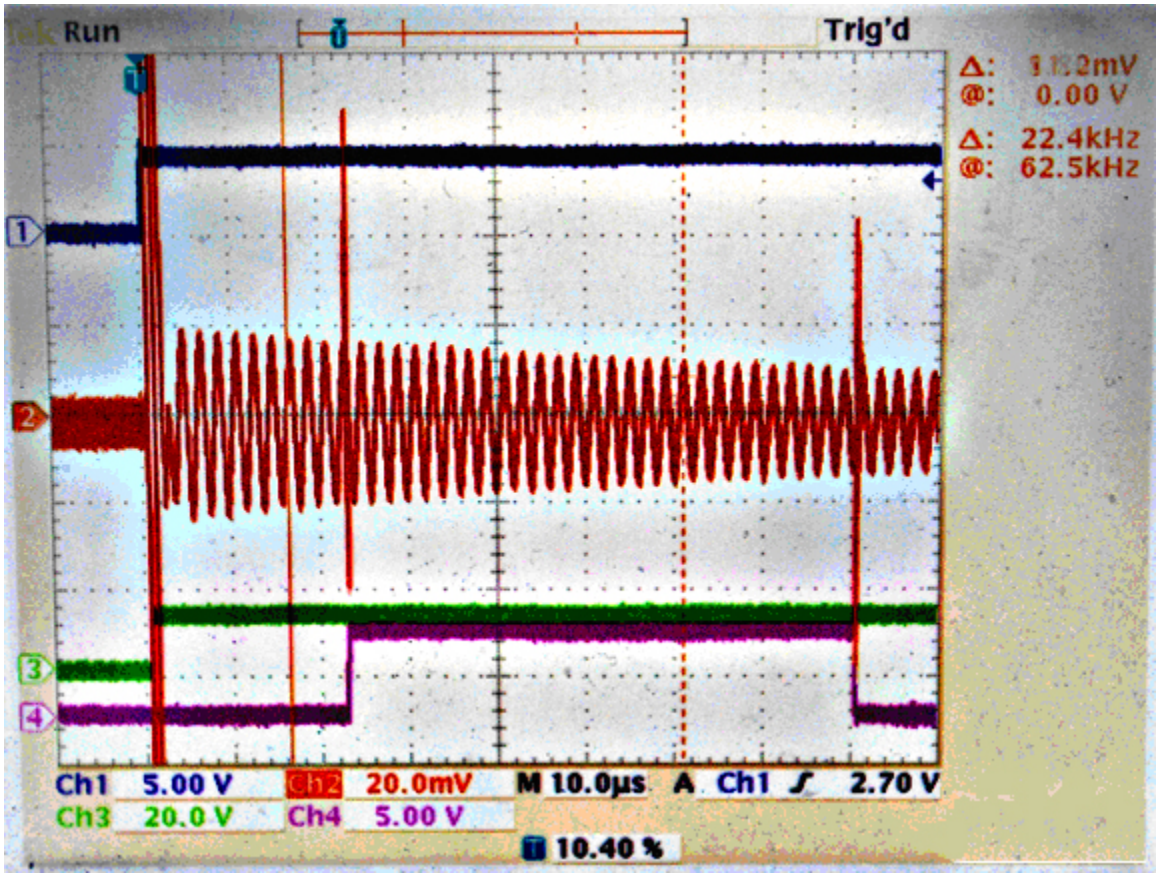

Figure 4.6: Oscilloscope waveforms of (top to bottom) 1) Function Generator, 2) Sensor "ringdown", 3) Power Pulse, 4) Delayed Gate pulse.

4.3.3 Sensor Behavior in Pulse System

Ringdown signal and FFT The oscillation of a sensor under the application of a step pulse is described by [93] [100]

$$y''(t) + 2\xi\omega_n y'(t) + \omega_n^2 y(t) = \frac{1}{k}\omega_n^2 f(t) \tag{4.3}$$

where $f(t) = \begin{cases} a, & t_1 \leq t \\ 0, & t \leq t_1 \end{cases}$ is the driving force, t is time and is always positive, $y(t)$ is the displacement, k is the spring constant, ω_n is the radian resonant frequency of the sensor and ξ is the damping factor of the media.

The Laplace transforms of $y(t - t_1)$ is

$$Y(s) = \frac{\omega_n^2}{kas(s^2 + 2\xi\omega_n s + \omega_n^2)} + \frac{y'(0) + (s + 2\xi\omega_n)y(0)}{s^2 + 2\xi\omega_n s + \omega_n^2} \tag{4.4}$$

By solving Equation 4.4 at the initial conditions when $t = 0$, $y(0) = 0$ and $y'(0) = 0$, we can than obtain the response of the sensor under a pulse as

$$y(t) = \frac{1}{k}f(t) + A\exp\left(-\xi\omega_n(t - t_1)\right)\sin\left(\omega_d t + \phi\right) \tag{4.5}$$

where $A = -\frac{f(t)}{k\sqrt{1-\xi^2}}$, $\arctan\phi = \tanh\frac{\xi}{\sqrt{1-\xi^2}}$ and $\omega_d = \sqrt{1-\xi^2}\omega_n$ is the sensor radian frequency under the effect of damping.

The above equation describes the oscillation of a sensor in a single transformer under the application of a step pulse. This result is consistant with the result in [100]. To avoid the problem of large transients when a pulse is applied to the coil ($V_{coil} = Ld_i/d_t$), we use a second transformer connected in opposing series so that $V_{out} = coil1 + V_{coil2} = 0$ (L is inductance, d_i/d_t is instantaneous rate of current change in the coil). A sensor in one transformer will unbalance the outputs so that V_{out} from the transformers is the sensor signal. An added advantage of two transformers is that a reference sensor can be installed inside the

second transformer. Therefore, the final time domain signal of the two series transformers is a damped sinusoid given by the following equation:

$$y(t) = 2\frac{f(t)}{k\sqrt{1-\xi^2}} \exp\left(-\xi\omega_n t\right) \sin\left(\sqrt{1-\xi^2}\omega_n t + \tanh\frac{\sqrt{1-\xi^2}}{\xi}\right) \tag{4.6}$$

This equation is plotted using Matlab and fitted with measured data to show the same decay rate. Figure 4.7 is a plot of Equation 4.6 and Figure 4.8 is an oscilloscope trace of an actual sensor response to a step pulse. The amplitude of the pulse is set to be 1×10^{13}. The radian resonant frequency ω_n, where $\omega_n = 2\pi f$ and f is 2.326 MHz is set to be the same as the resonant frequency obtained from the actual measurement shown in Figure 4.8. This simulation does not attempt to describe the transient conditions that occur at the start of the pulse. The gate pulse allows the transients to decay before the signal is processed by the spectrum analyzer. The damping factor ξ, determined as 0.0035, was chosen experimentally by substituting values into the equation and then comparing the simulation and real results until the difference between the decay rates of the two are minimized. Figure 4.9 and Figure 4.10 show the Matlab simulated and actual measured responses of two independent sensors in the two transformers. The resonance frequencies of the two sensors are 2.193 MHz and 2.281 MHz and again, the damping constant ξ used in the simulation is determined to be 0.0035.

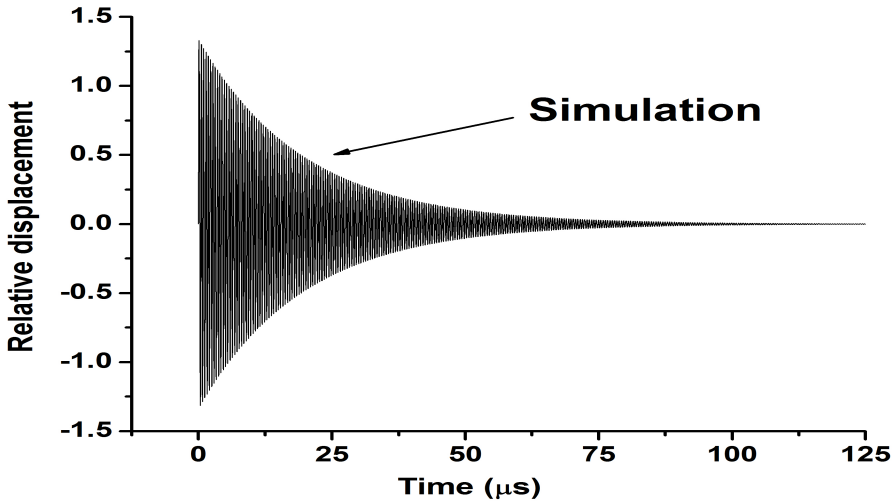

Figure 4.7: Matlab simulated showing the time-domain response of a single free-standing magnetoelastic sensor to a rectangular pulse. The resonant frequency of the sensor is set to be 2.326 MHz and the damping constant ξ used is 0.0035.

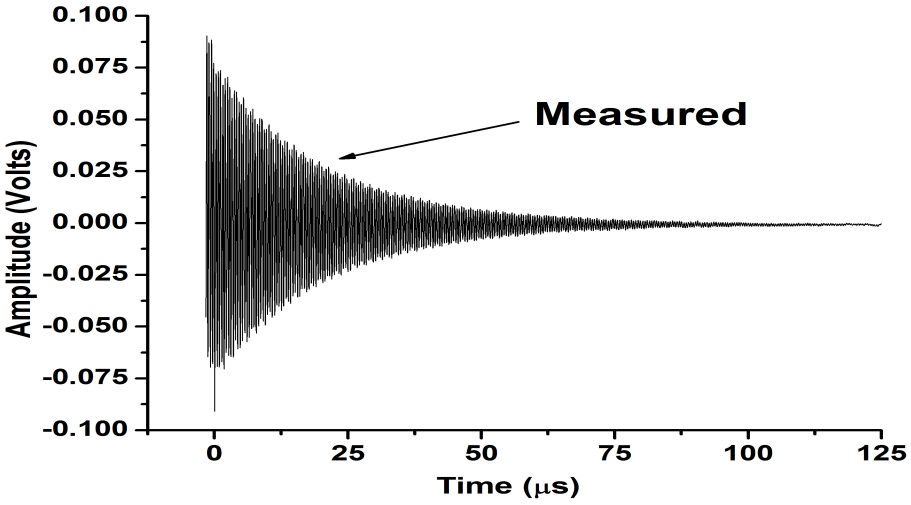

Figure 4.8: Measured signal from a single free-standing magnetoelastic sensor in pulse system. The resonant frequency of the sensor is measured as 2.326 MHz.

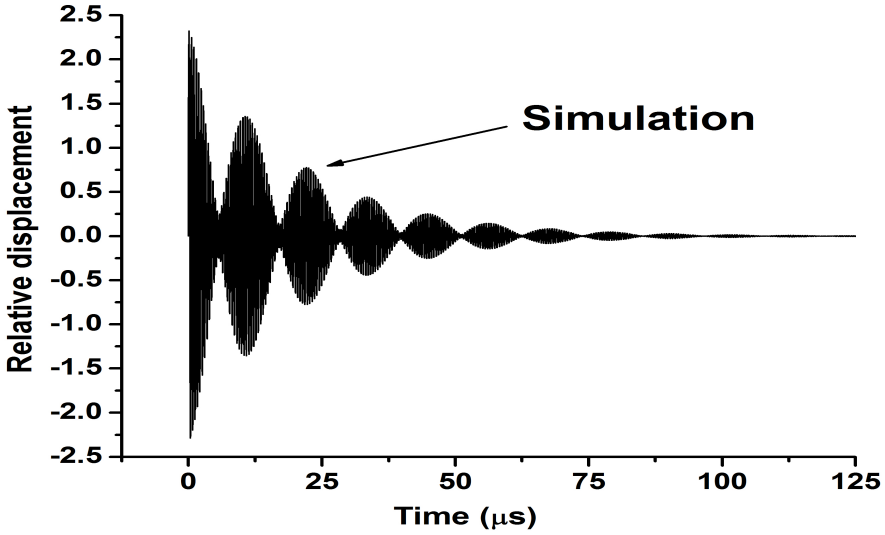

Figure 4.9: Matlab simulation showing the time-domain response of two independent free-standing magnetoelastic sensors to a same rectangular pulse. The resonance frequencies of the two sensors are set to be 2.193 Mhz and 2.281 MHz. The damping constant ξ used is 0.0035.

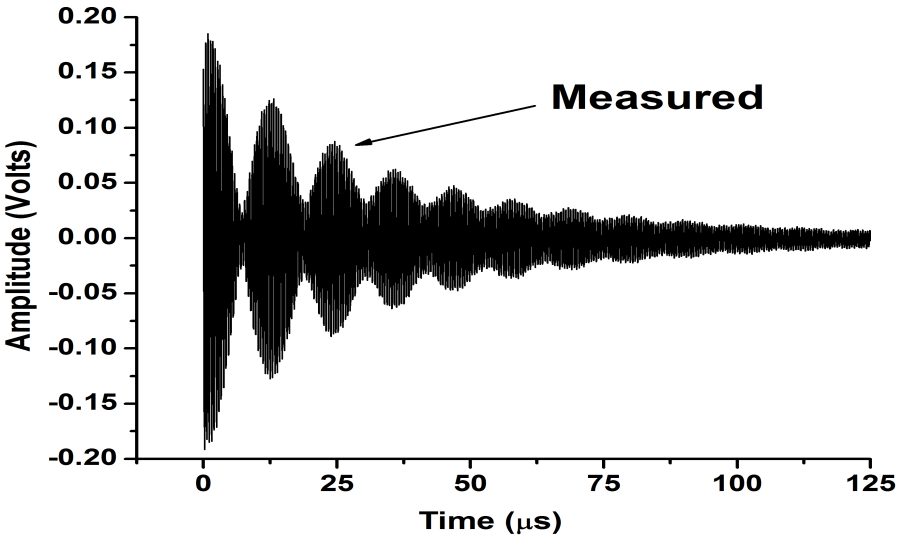

Figure 4.10: Measured signal from two free-standing magnetoelastic sensors separated in the two transformers in pulse system. The resonance frequencies of the two sensors are measured as 2.193 Mhz and 2.281 MHz.

Chapter 5

Characterization of Magnetoelastic Platform for Sensing Applications

5.1 Resonance Behavior of Free-standing Magnetoelastic Sensors

According to its boundary condition, a magnetoelastic sensor as illustrated in Figure 3.1 can be constructed into four types: (1) end suspension as in a cantilever; (2) central suspension as in a dual beam structured sensor; (3) both end suspension; and (4) no suspension as in a free beam structured sensor.

The cantilever is a beam that is supported at one end. This structure has been applied to magnetoelastic sensors to detect biological pathogens. A magnetoelastic cantilever sensor consists of a magnetoelastic layer and a non-magnetoelastic layer [85]. Because of the difference in magnetoelastic coupling effect, the deformation of the magnetoelastic material along the longitudinal direction is restricted by the non-magnetoelastic layer, thus the sensor bends under an alternating magnetic field.

The central suspension structure is supported at the center of the beam. A magnetoelastic sensor with this structure deforms very similarly to the free beam magnetoelastic sensors at the first mode, where the sensor deforms along the longitudinal direction with minimum deformation at the center of the beam and maximum deformation at the two ends.

Currently, no sensor uses both-end suspension structure because of the damping effect.

For all the end suspension and center suspension structures, the sensors need support and the support needs to be fixed, thus these structures are difficult to apply in real fields. Moreover, when sensor sizes are reduced to the micrometer or even the nanometer region, the fabrication of these structures becomes very difficult. Due to the above reasons, in this research where we intend to eventually use very small sensors to detect pathogens directly on real food, we chose to use the free-standing bream structure. This structure does not

require any external support for the sensor, and the fabrication is relatively easy for very small sensors.

Under an alternating magnetic field along the longitudinal direction of the sensor, the magnetoelastic sensors change shape and vibrate in the longitudinal direction due to magnetoelastic interaction. A simulation of the free-standing magnetoelastic sensor oscillation was performed using Coventor. Figure 5.1 shows a Conventor simulation result for the first mode oscillation of a magnetoelastic sensor. In this mode, the sensor changes shape only in the longitudinal direction. The center has no change in length with magnitude of the length change increasing to a maximum at both ends. Figure 5.2 and Figure 5.3 are the Coventor simulation of the second and third mode oscillation of the freestanding magnetoelastic sensors. Table 5.1 is a summary of a Coventor simulation result of the oscillation of a $2000 \times 800 \times 15\mu m$ magnetoelastic sensor. In reality, the resonance signal of the first mode oscillation is the strongest while the signal of the second and the latter modes are normally extremely week. Due to the damping in liquid, the resonance signals are greatly weakened in liquid compared with the signals in air. In order to obtain strong signals both in air and in liquid, the first mode longitudinal oscillation was used in this research.

Table 5.1: Coventor simulation of the oscillation of a $2000 \times 800 \times 15\mu m$ magnetoelastic sensor.

Mode Domain	Resonance Frequency (MHz)	Generalized Mass	Damping Coefficient
1	1.08E+06	4.74E-08	0
2	2.17E+06	4.74E-08	0
3	2.54E+06	1.94E-08	0
4	2.55E+06	1.81E-08	0
5	2.86E+06	1.90E-08	0

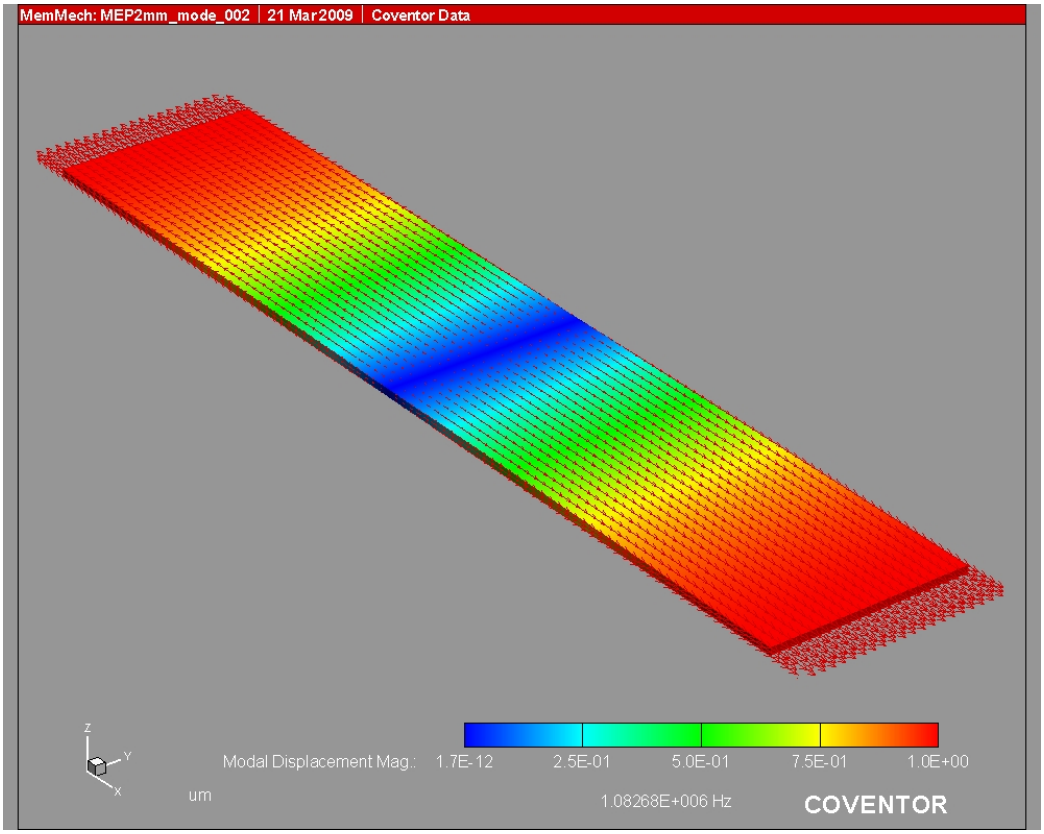

Figure 5.1: Coventor simulation of the first mode oscillation of a magnetoelastic sensor. Length to width ratio is 5.

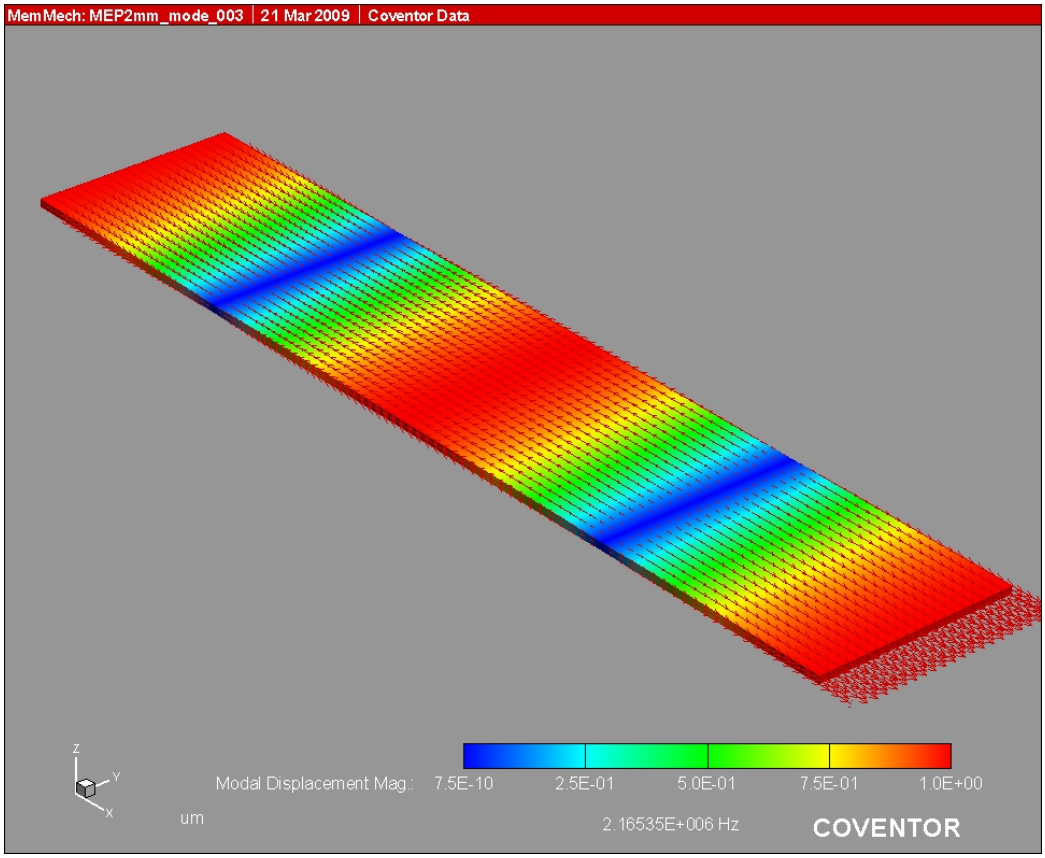

Figure 5.2: Coventor simulation of the second mode oscillation of a magnetoelastic sensor. Length to width ratio is 5.

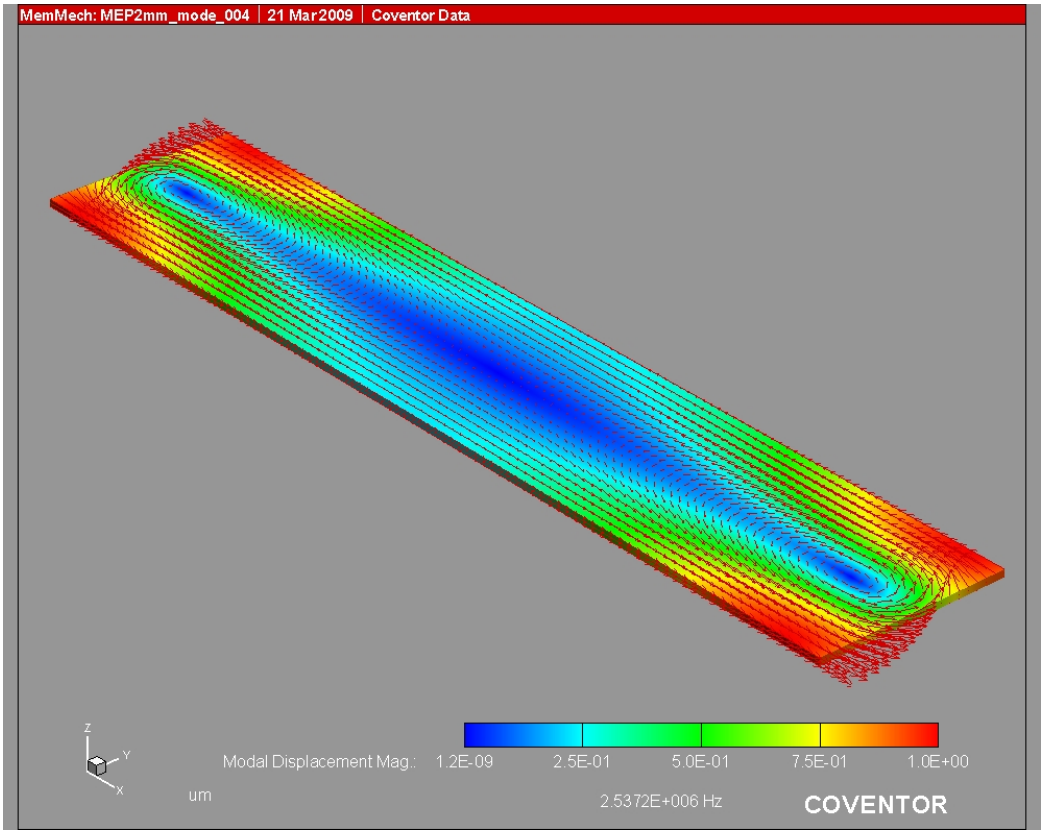

Figure 5.3: Coventor simulation of the third mode oscillation of a magnetoelastic sensor. Length to width ratio is 5.

The characteristic resonant frequency of the sensor in vacuum depends on the sensor material properties and dimensions. However, when the sensor is in media, the external DC magnetic field and the density of the media are able to alter the sensor's characteristic resonant frequency and at the same time change the Q factor of the resonance peak signal.

J. Wan's results showed that the measured resonant freqencies of magneotoelastic sensors followed the trend of the following equation closely [101] [102]:

$$f_1 = \frac{1}{2L}\sqrt{\frac{E}{\rho^2(1-\upsilon)}} \tag{5.1}$$

C. Liang [103] showed that a freestanding magnetoelastic beam with length to width ratio of 5 is better described as being in a plane-stress or biaxial state. He modified the above equation to reflect this ratio and showed that the resonant frequency of the sensor corresponding to the first mode longitudinal vibration (in short, "resonant frequency") is described as:

$$f_1 = \frac{1}{2L}\sqrt{\frac{E}{\rho(1-\upsilon)}} \tag{5.2}$$

where L, E, ρ and υ are the length, Young's modulus, density and the Poisson's ratio of the magnetoelastic material. Since all the sensing tests were conducted at room temperature and one atmosphere, ρ and υ were considered to be constant. Theoretically, E is a constant at zero applied magnetic field, i.e., $H = 0$. Hence, the theoretical calculated resonant frequency of the as-fabricated sensor at $H = 0$ is proportional to the reciprocal of the sensor length.

Figure 5.4 shows the resonant frequency of magnetoelastic sensors with lengths ranging from 500 μm to 5 mm, and as explained in the sensor design section, the length to width ratio was kept 5. Ten sensors were measured for each size selected. The theoretical prediction was calculated from Equation 5.2 by using a density of 7.9 g/cm^3, Young's modulus of 105 GPa [3] and Poisson's ratio of 0.33 [103]. By comparing the theoretical prediction line and

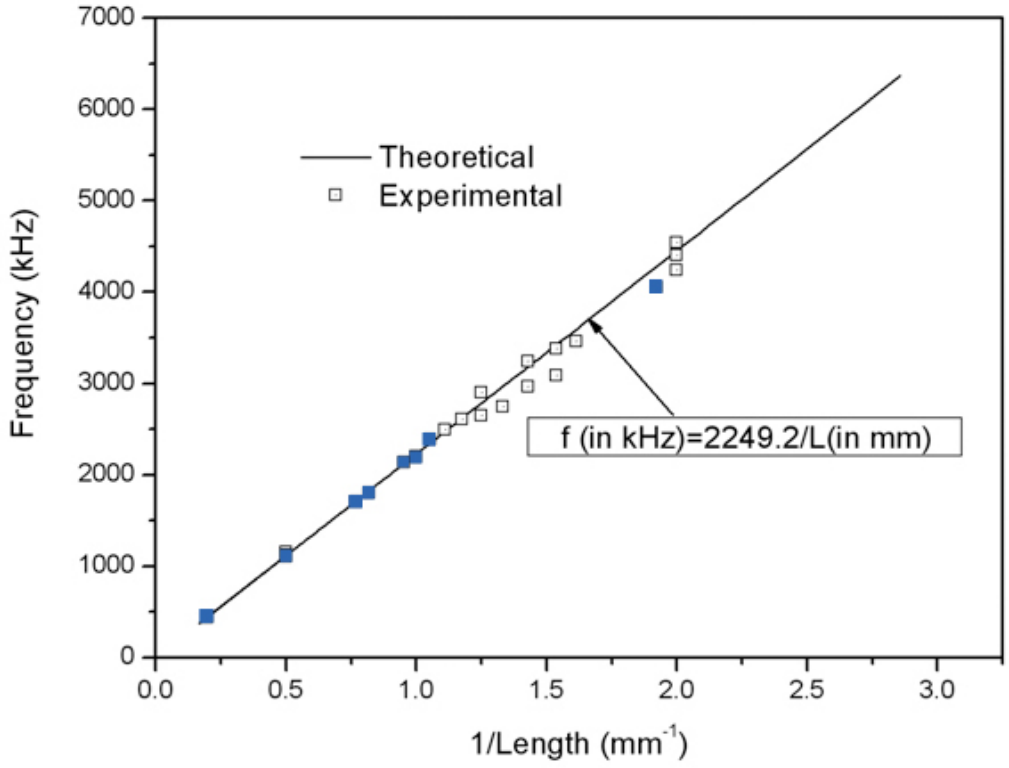

Figure 5.4: Calibration of resonant frequency as a function of sensor length (Blue: From [1]).

experimental results, it was proved that the experimental values were very close to this theoretical prediction.

5.2 Principle of Sensor Detection

The magnetoelastic material has a characteristic resonant frequency that is a function of its material properties [104], shape, physical dimensions [105] [103], mass of the material [106] and temperature. For small changes in mass ($\Delta m << M$) the change in frequency Δf is given by [106]

$$\triangle f = -\frac{f}{2}\frac{\triangle m}{M} \tag{5.3}$$

where M is initial mass, $\triangle m$ is the change in mass and f is the initial resonant frequency.

This is the basis for spore detection using magnetoelastic sensors. The biomolecular recognition layer of the sensor captures spores in analyte solutions and the captured spores add a small mass to the sensor and cause a corresponding decrease in the resonant frequency of the sensor.

5.3 Mass Sensitivity

The biosensor accumulates mass as the spores or bacteria become bound to the sensor. The frequency change associated with this mass increase is determined by the mass sensitivity of the sensor (S_m), which is defined as the change in frequency caused by a unit of mass change [106]:

$$S_m = -\frac{df}{dm} \tag{5.4}$$

Substituting Equation 5.2 and Equation 5.3 into Equation 5.4, the mass sensitivity becomes:

$$S_m = -\frac{1}{2\rho L^2 W t}\sqrt{\frac{E}{\rho(1-\upsilon)}} \tag{5.5}$$

For a sensor with length to width ratio of 5,

$$S_m = -\frac{5}{2\rho L^3 t}\sqrt{\frac{E}{\rho(1-\upsilon)}} \tag{5.6}$$

where L is length, t is thickness, and E, ρ and υ are material constants. Thus, mass sensitivity is determined only by the length and thickness of the sensor. By making the sensor shorter and thinner, a higher mass sensitivity can be achieved.

To verify the theoretical equation, J. Wan and R. Lakshmanan did some preliminary work with a few sensors [102] [87] [2]. To further varify and determine the mass sensitivity, I have performed a series of experiments to add to his data. Sensors with a thickness of 30 μm were used. The sensors were tagged and the frequency change before and after mass

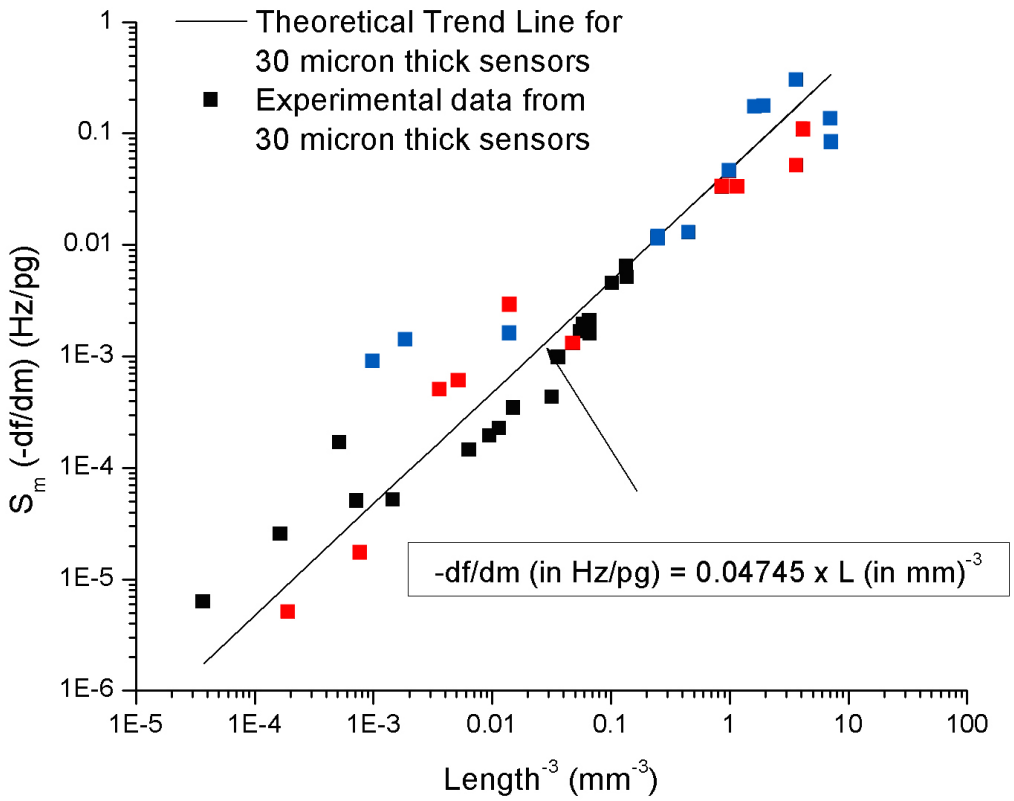

Figure 5.5: Plot of mass sensitivity for various lengths of the sensor platform (Red: From [2]; Blue: From [1]).

addition of each individual sensor was measured. The results of these tests are shown in Figure 5.5 along with the theoretical line determined by Equation 5.6. The experimental results are close to the theoretical trend line. As the sensor become smaller, the mass sensitivity increases. By decreasing the sensor length to 500 μm, a high mass sensitivity of up to 3.75 Hz/pg can be reached. This allows the sensor's applications in accurate sensing such as a very low concentrations of bacteria or spores. Based on this, one single spore with mass of 2 pg can cause a 500 μm long sensor to have a 7.5 Hz frequency decrease.

5.4 Magnetic Field Tuning

It has been found that the amplitude and phase of the resonant behavior of amorphous, magnetoelastic resonators depends on the external DC magnetic field [107] [101] [108]. The external magnetic field changes the coupling of magnetization and elasticity of the sensor material [107], causing the internal magnetization of the magnetoelastic material to change from its original stable state, a state with no external magnetic field, to a state under external magnetic field (H) [108]. This change in magnetization alters Young's Modulus of the magnetoelastic sensor as described by [109]

$$\frac{1}{E_H} = \frac{1}{E_M} + \frac{9\lambda_s^2 H^2}{M_s H_{A\sigma}^3} \tag{5.7}$$

where E_H is Young's Modulus of the magnetoelastic sensor under an magnetic field H, E_M is Young's Modulus without the effect of an external magnetic field (for example, at saturation magnetization), $H_{A\sigma}$ is the reduced anisotropy field, λ_s is the saturation magnetostriction and M_s is the saturation magnetization.

The magnetic susceptibility (χ) of the material is [110]

$$\chi = \frac{M}{H} \tag{5.8}$$

The relationship between $H_{A\sigma}$ and H is described by [109]

$$M = M_s \frac{H}{H_{A\sigma}} \tag{5.9}$$

Substituting Equation 5.8 and Equation 5.9 into Equation 5.7 yields

$$\frac{1}{E_H} = \frac{1}{E_M} + \frac{9\lambda_s^2 H^2 \chi^3}{M_s^3} \tag{5.10}$$

and substituting E_H from Equation 5.10 into Equation 5.2 gives the resonant frequency of the sensor under magnetic field H:

$$f_H = \frac{1}{2L}\sqrt{\frac{E_M}{\rho(1-\upsilon)}\left(1+\frac{9E_M\lambda_s^2H^2\chi^3}{M_s^4}\right)^{-1}}$$
$$= \left(1+\frac{9E_M\lambda_s^2H^2\chi^3}{M_s^4}\right)^{-1/2} f_1 \tag{5.11}$$

Equation 5.11 shows that the resonance behavior of the magnetoelastic sensor varies as a function of different magnetic fields. This equation is similar to the equation developed by Mungle, Grimes and Dreschel [108]. The relation between f_H (resonant frequency of the sensor under magnetic field H) and f_1 (resonant frequency of the sensor without the effect of the external magnetic field) is a function of magnetic field strength (H) and magnetic susceptibility (χ) of the sensor material.

The magnetization (M) curves of the 1 mm and 2 mm sensor platforms were measured using a Princeton Measurements Corp. MicroMag Model 3900 VSM system. Figure 5.6 shows a typical result for each size of the sensor. The susceptibility (χ) was calculated from the slope of the M-H curve. The saturation magnetization (M_s) is 668 emu/cm^3 and 587 emu/cm^3 respectively for the 1 mm and 2 mm sensors. This difference is due to the effect of the demagnetizing factor, N.

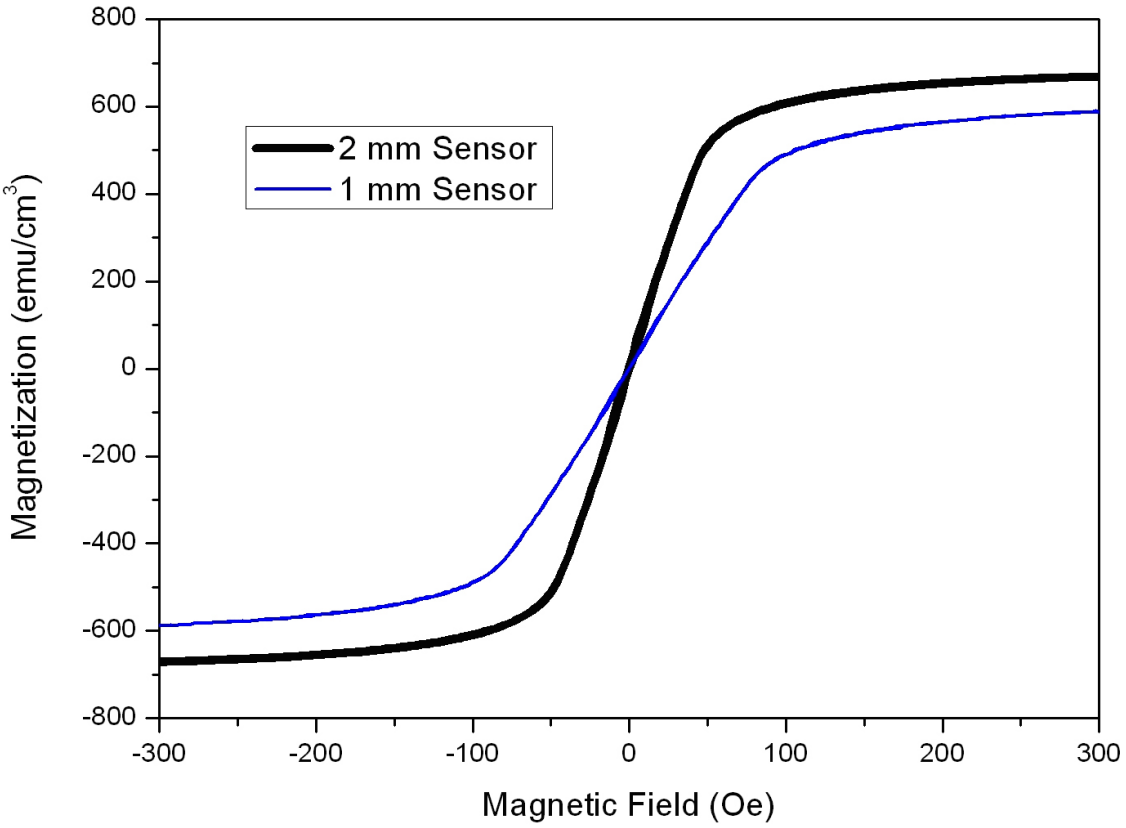

Figure 5.6: Typical magnetization versus magnetic field curve for 1 mm and 2mm sensors.

To determine the effect of magnetic field strength on the magnetoelastic sensors experimentally, the resonance behavior of 1 mm ($1000 \times 200 \times 15 \mu m$) and 2 mm ($2000 \times 400 \times 15 \mu m$) sensors in air was investigated under various DC magnetic field strengths. Figure 5.7 shows a typical result of the resonance spectrum of a 2 mm sensor under various DC magnetic fields. Figure 5.8 and Figure 5.9 show the summary of the resonance frequencies of the 1 mm and 2 mm sensors under various DC fields compared with the theoretical prediction computed using Equation 5.11.

In Figure 5.8 and Figure 5.9, the measured resonance frequencies under various DC magnetic fields are shown to be close to the theoretical model calculated from Equation 5.11 for both sized sensors. For the experimental data, only the DC field was measured. The AC field was very small compared with the DC magnetic field, though it does affect the resonant frequency.

A high Q-factor improves resonant frequency resolution, resulting in high sensitivity to mass changes. From Figure 5.10 and Figure 5.11, it was found that the Q-factor is lowest when amplitude is maximum. However, since a large amplitude is necessary for good signal-to-noise ratio, especially when using the sensor in liquid with a high damping factor, the optimum DC magnetic fields for 1 mm and 2 mm sensors were determined to be 75 Oe and 38 Oe respectively to give maximum amplitude.

To verify the effect of a DC magnetic field on the mass sensitivity of the magnetoelastic sensors, a layer of the same amount of mass was sputtered on five 2 mm sensors. The resonance frequencies of these five sensors were measured before and after the addition of mass under various DC magnetic fields. The difference in resonant frequency before and after the addition of mass are plotted versus various DC fields as shown in Figure 5.12. No significant differences are found for the resonant frequency shifts under various DC fields. Therefore, the DC magnetic field does not have a significant effect on mass sensitivity of magnetoelastic sensors.

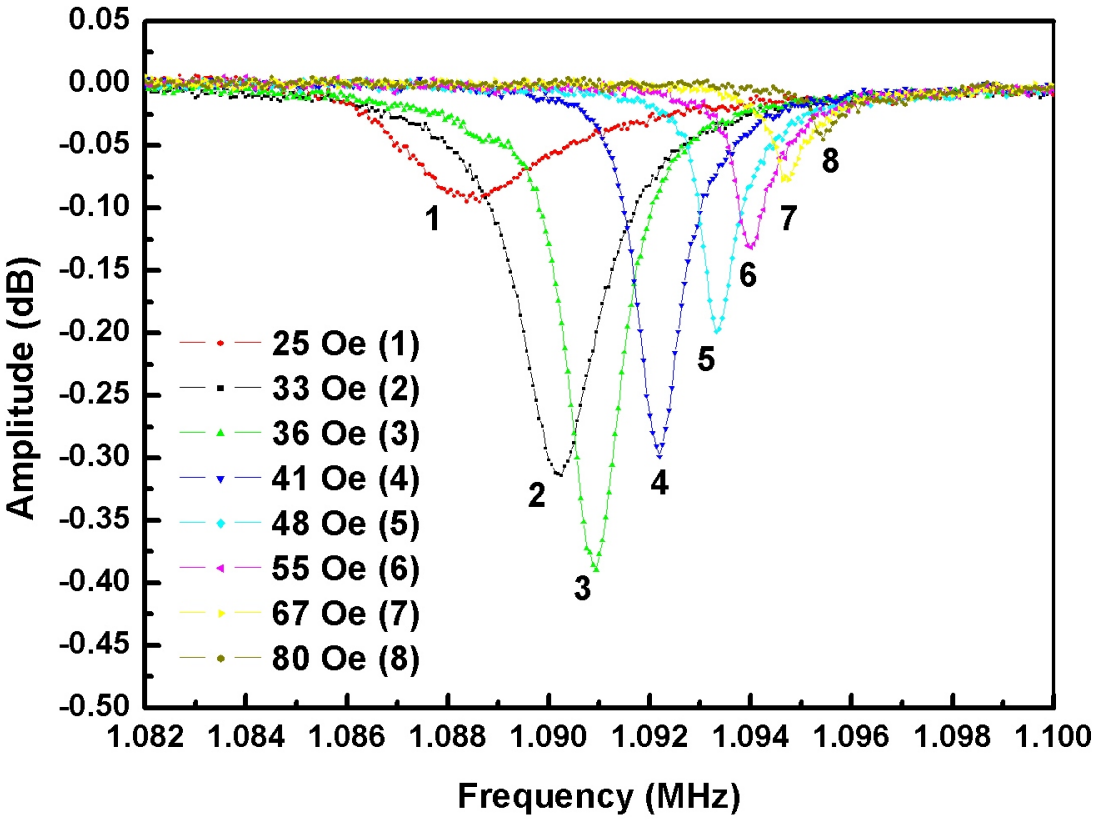

Figure 5.7: Resonance specrtrum of a 2 mm sensor under different bias magnetic field strengths.

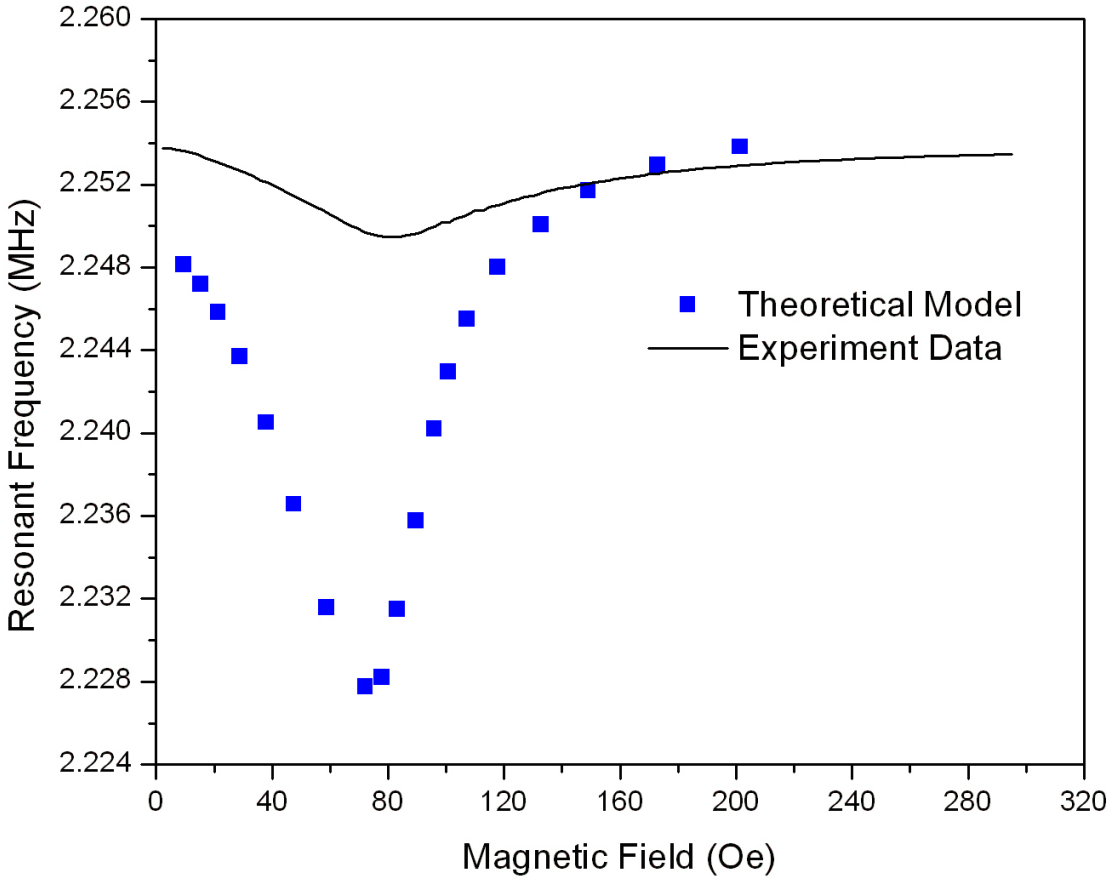

Figure 5.8: Experimental measurements and theoretical model showing the resonant frequency of a 1 mm sensor under different DC magnetic field strengths.

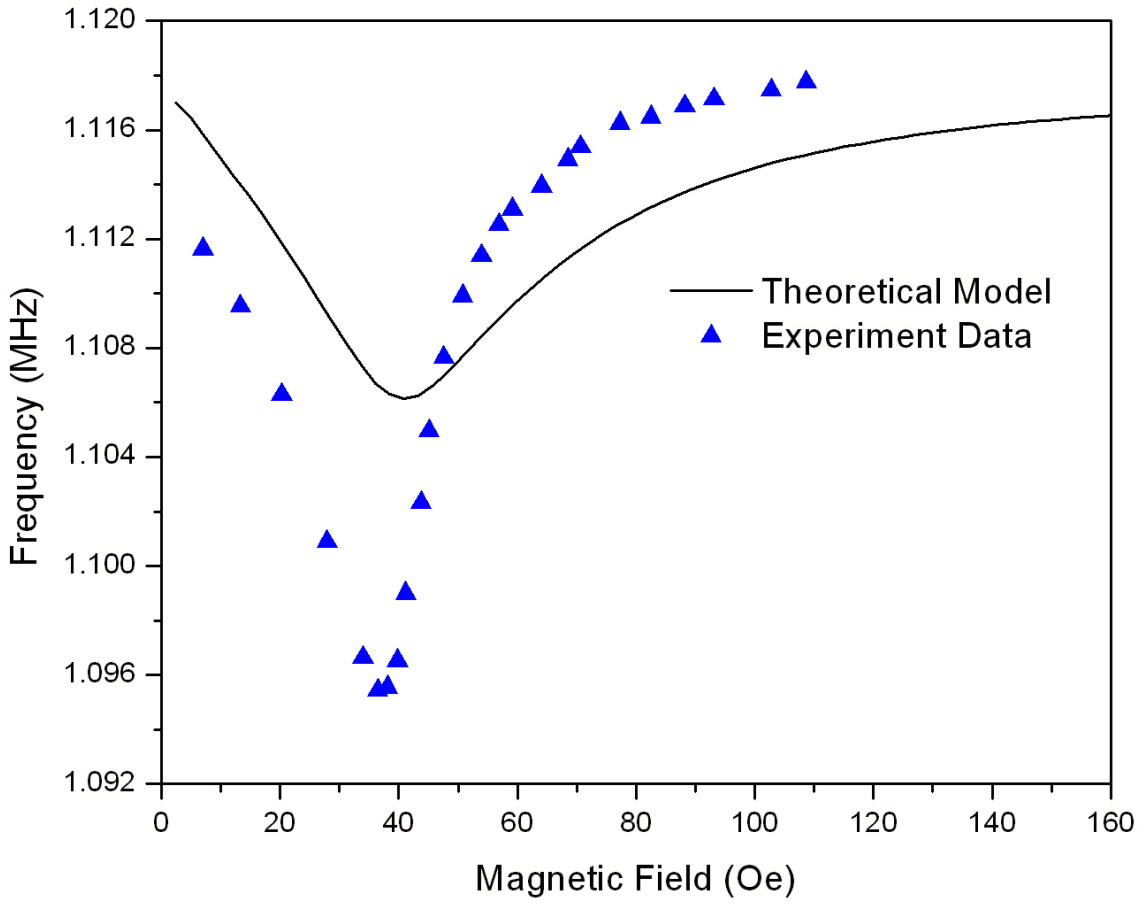

Figure 5.9: Experimental measurements and theoretical model showing the resonant frequency of a 2 mm sensor under different DC magnetic field strengths.

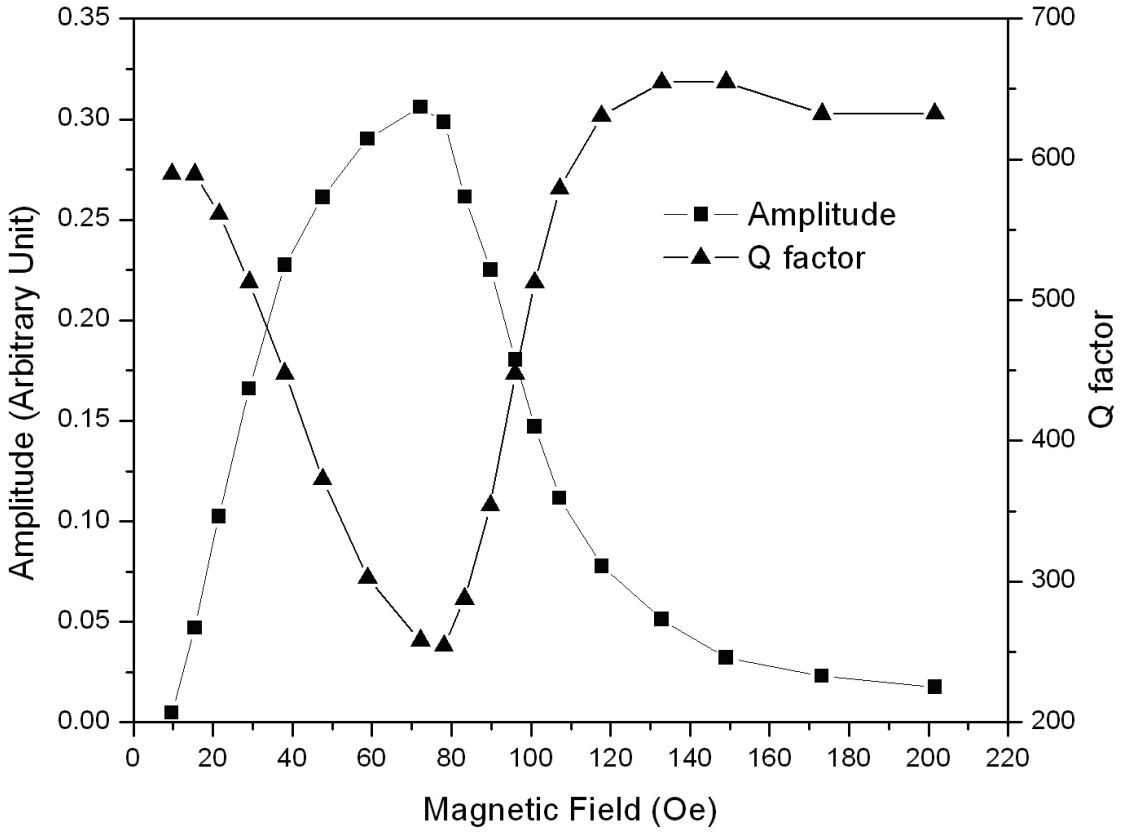

Figure 5.10: Amplitude and Q-factor of the resonance peak of a 1 mm sensor as a function of magnetic field strength.

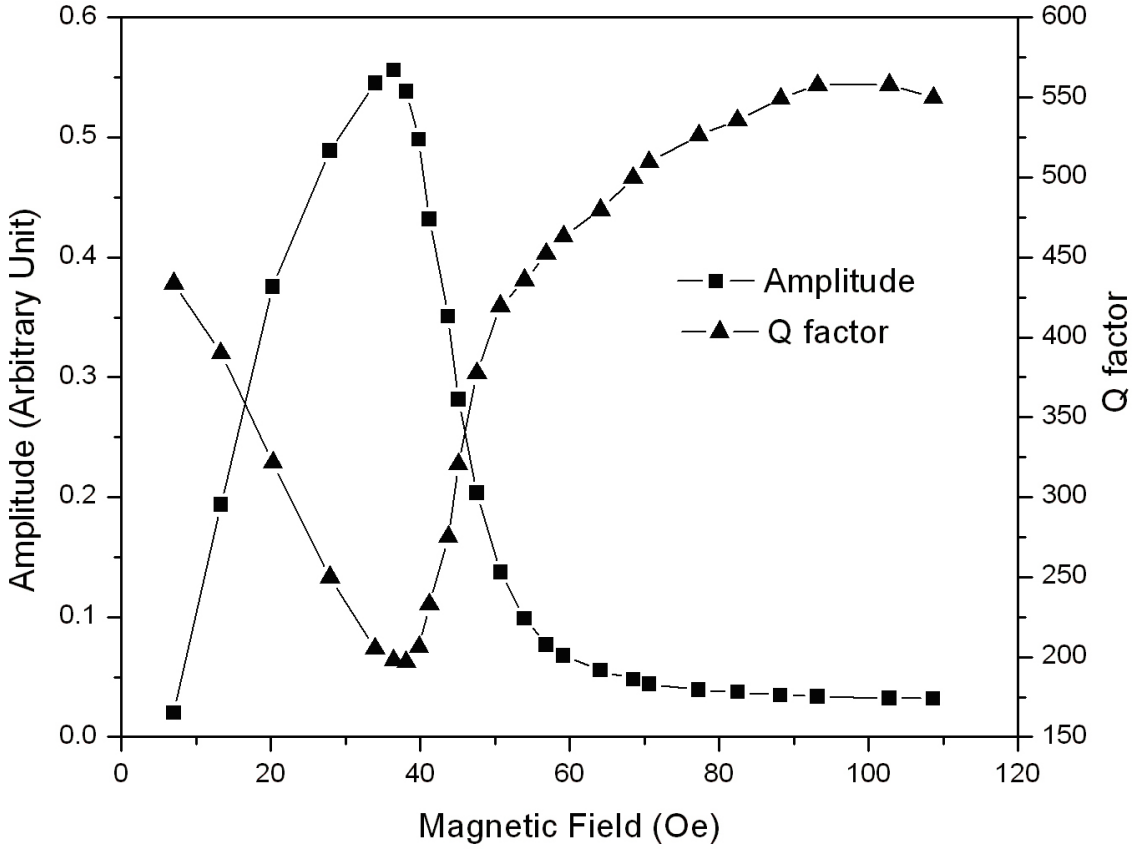

Figure 5.11: Amplitude and Q-factor of the resonance peak of a 2 mm sensor as a function of magnetic field strength.

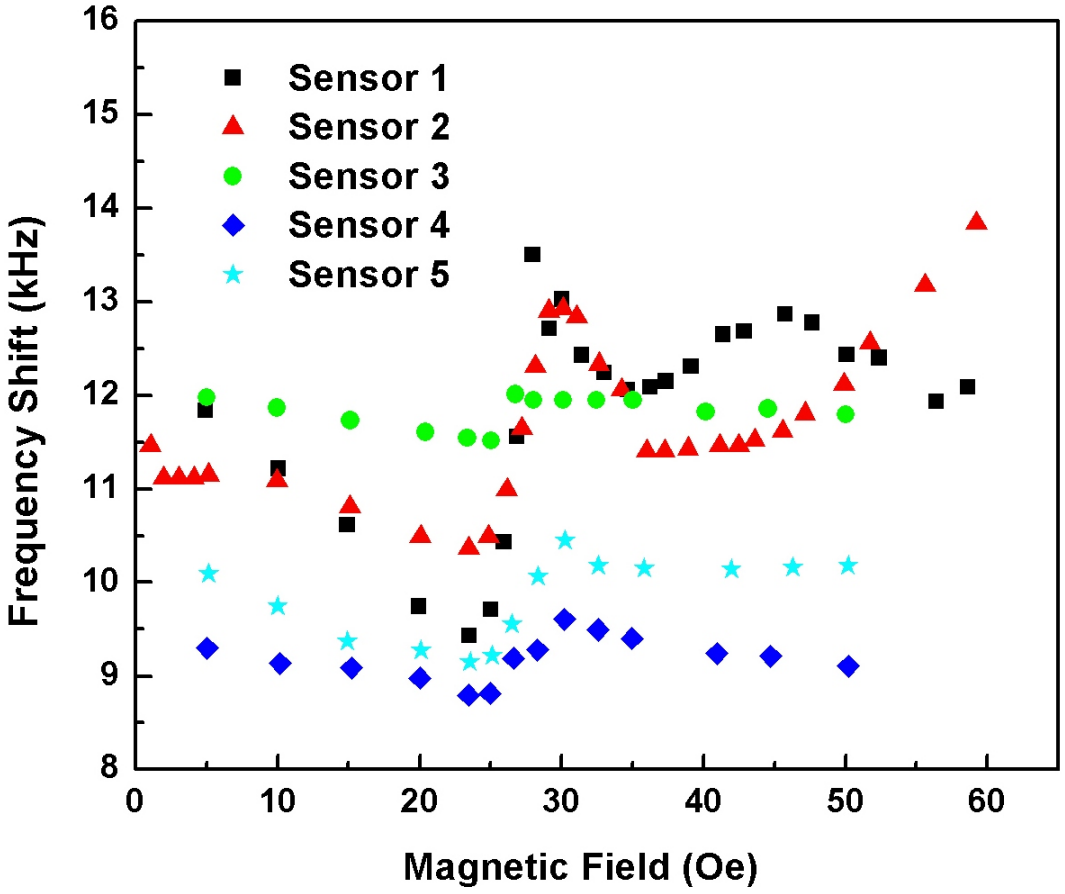

Figure 5.12: Difference in resonant frequencies of 1 mm magnetoelastic sensors before and after coating a uniform layer of mass under different DC magnetic field strengths.

5.5 Damping Effect

Since most bacteria or spores will be found in liquid media, it is necessary to determine how the sensor response changes when it is submerged in a liquid. From vibration theory, the resonant frequency of damped oscillation (ξ) of a freestanding beam in a specific media can be represented as [111]:

$$f_d = f_1\sqrt{1-\xi^2} \tag{5.12}$$

where f_1 is the resonant frequency in air as defined in equation 2 and ξ is the damping ratio. In liquid media, interaction between the media and sensor causes damping of the sensor oscillation. In this case, $\xi < 1$, thus $f_d < f_1$, and there is an amplitude decrease.

The damping ratio of the sensor in air was determined from Equation 4.6 in Chapter 4.

The *B. anthracis* spores and *S. typhimurium* were suspended in distilled water for our detection so it was necessary to know the damping effect in distilled water before the spores or bacterium were introduced to the sensor. This gave us a baseline for monitoring the frequency change as the sensor captures the spores.

To observe the damping in distilled water, the resonant frequency of 1 mm long sensors and 2 mm long sensors were measured in air and distilled water and the results are shown in Figure 5.13 and Figure 5.14. The optimum magnetic field from Figure 5 for each sensor size was used in all media to bias the sensor for maximum sensitivity. The resonance behavior of these sensors in the relevant media are listed in Table 5.2. Notice that the resonant frequency, amplitude and Q-factor of the sensors are smaller in distilled water than in air for both sizes. The damping ratio (ξ) is 0.12 and 0.11 for the 1 mm sensor and 2 mm sensor respectively. Q-factor is measured by taking the frequency at maximum amplitude (peak minimum) and dividing by the difference of the two frequencies at 50 percent amplitude. The amplitude in water is only 37% of the amplitude in air for the 1 mm sensor and 66% for the 2 mm sensor. A Q-factor of 99 was obtained in water compared with a Q-factor of

286 in air for the 1 mm sensor, while a Q-factor was 107 in water compared with a Q-factor of 187 in air for the 2 mm sensor. Comparing the results of the two sized sensors, it was observed that the damping in water has a greater effect on the 1 mm sensor than on the 2 mm sensor.

Table 5.2: Resonance behavior of magnetoelastic sensors in media.

Size (μm)	1000×200×15		2000×400×15	
Media	Air	Water	Air	Water
Resonance (MHz)	2.09	2.07	1.07	1.06
Amplitude (a.u.)	0.29	0.11	0.55	0.38
Percent Amplitude	100	37	100	66
Q	286	99	187	107
Magnetic Field (Oe)	75	75	38	38
Damping Ratio, ξ	0.0035	0.12	0.0035	0.11

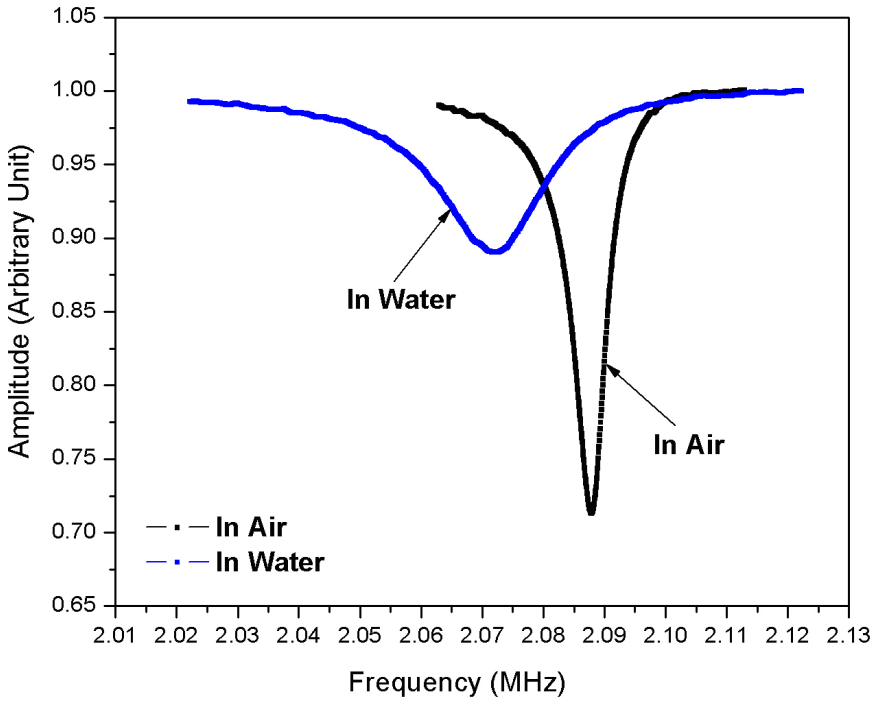

Figure 5.13: Resonant frequency of magnetoelastic sensor in air and water for a 1 mm (1000 $\times$ 200 $\times$ 15 μm) sensor.

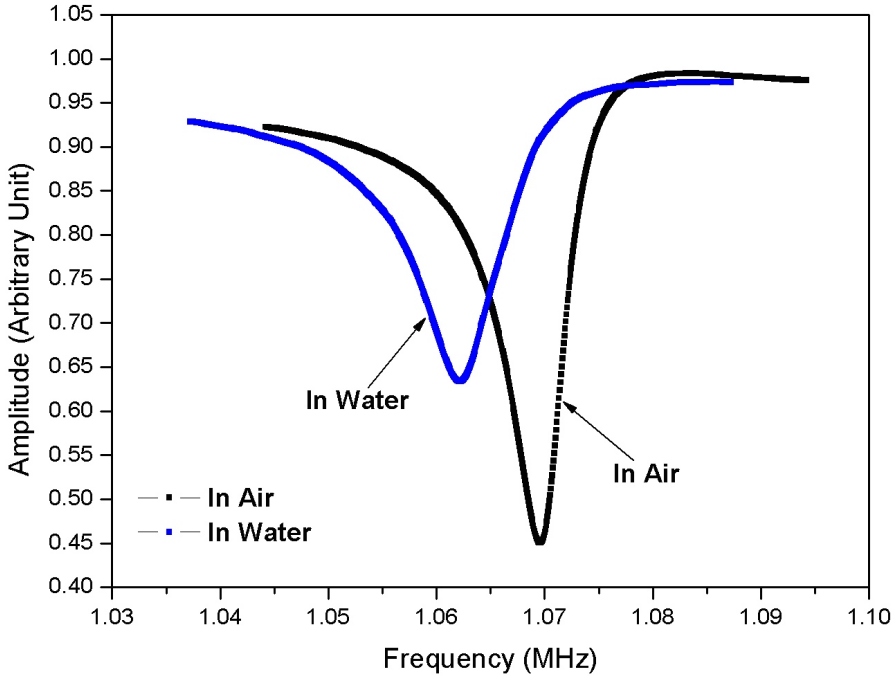

Figure 5.14: Resonant frequency of magnetoelastic sensor in air and water for a 2 mm (2000 $\times$ 400 $\times$ 15 μm) sensor.

5.6 Effect of Sensor Position in the Coil

A study was done to show the effect on resonant frequency when the sensor position in the coil changes. Sensors of 4 mm long length (4000 $\times$ 800 $\times$ 30 μm) were used in order to have control over the sensor position. Each coil has an inner diameter of 2 mm and length of 10 mm. Tests were performed with single sensors half-out of the left side of the coil, in the center of the coil and half-out on the right side of the coil. Tests were also performed with two sensors in the middle of the coil to show the effect of positional relationships of the sensors, including end-to-end touching and side-by-side (full overlapping). Finally tests were done with two sensors in liquid (distilled water) to show the effects of two sensors overlapping in the middle of the coil.

Table 5.3 shows a summery of repeated tests on a single sensor's resonant frequency; half-out of the coil left side, in the coil middle, and half-out of the right side. The standard deviations of the sensor resonant frequency at these three positions are 0.24, 0.22 and 0.28 kHz respectively. A one-way ANOVA (analysis of variance) was performed to compare the resonant frequencies of the sensor at these three positions and the results are shown in Table 5.4. From the ANOVA result, we found that the resonant frequency of the sensor is different when it is placed at different positions of the coil. The detailed differences between each two positions were examined using a Tukey's studentized range (HSD) test. The results of this test (Table 5.5) show that the resonant frequencies of the sensor when placed in the middle of the coil and when half out of the coil are different, while no significant difference was found between sensor resonant frequencies when it is half out of the either left or right side of the coil.

The interferences between two magnetoelastic sensors are examined by placing two sensors close together in different ways. Repeated tests were performed to measure the resonant frequencies of the two sensors when they are placed end to end and side by side in the middle of the coil. The results show that the standard deviations of the two sensors are 0.32 kHz and 1.23 kHz when they are placed end to end in the coil, whereas when

Table 5.3: Summary of the resonant frequencies of a single sensor when placed at three positions of the coil (Unit: kHz).

Sensor Position	Mean	Standard Deviation	Minimum	Maximum
Half out from left	558.51	0.24	558.28	558.96
In the middle	558.27	0.22	558.07	558.87
Half out from right	558.61	0.28	558.28	558.98

Table 5.4: One-way ANOVA result of resonant frequencies of a sensor when placed at three positions of the coil.

	DF	Sum of Squares	Mean Square	F Value	$Pr > F$
Sensor Position	2	0.76492840	0.38246420	6.38	0.0048
Model	31	1.85756571	0.05992147		
Error	33	2.62249412			

R-Square	Coeff Var	Rood MSE	freq Mean
0.2917	0.0438	0.2448	558.4418

Table 5.5: Tukey's Studentized Range (HSD) test for resonant frequencies of a sensor when placed at three positions of the coil (significance level is set to 0.10).

Position Comparison	Difference Between Means	Simultaneous 90% Confidence Limits		Different
		Lower Limits	Upper Limits	
right - left	0.95000	-0.13827	0.32827	No
right - middle	0.34314	0.12718	0.55910	Yes
left - middle	0.24814	0.03218	0.46410	Yes

they are placed side by side, the standard deviations, which are 22.25 kHz and 1.88 kHz for the two sensors, become significantly increased compared with those of single sensors (Table 5.6). This large deviation prohibits the application of the sensors for accurate sensing and for detecting very small amounts of target mass. Moreover, it was found from a two-way ANOVA (Table 5.7) and a Tukey's studentized range test that the positioning of the sensor, i.e., whether they are placed end to end or side by side, has a significant effect of the resonance frequencies of the sensor.

Table 5.6: Summary of resonant frequencies of two sensors when placed differently in the coil (Unit: kHz).

Sensor Position	Sensor No.	Mean	Standard Deviation	Minimum	Maximum
End to End	1	495.04	0.32	494.72	495.31
	2	528.82	1.23	527.51	529.95
Side by Side	1	507.69	22.25	494.72	533.38
(Full Overlaping)	2	531.76	1.88	529.59	533.01

Table 5.7: Two-way ANOVA result of resonant frequencies of two sensors when placed differently in the coil.

	DF	Sum of Squares	Mean Square	F Value	$Pr > F$
Source	2	3211.738763	1605.869382	16.88	0.0006
Sensor Position	1	336.631572	336.631572	3.54	0.0893
Sensor No.	1	2875.107191	2875.107191	30.22	0.0003
Model	10	951.245914	95.124591		
Error	12	4162.984677			

R-Square	Coeff Var	Rood MSE	freq Mean
0.2921	0.0417	0.2329	558.4203

Since the interference of the sensors causes a large variance when the sensors are close to or touching each other, it was presumed that flowing water in the coil might help to separate the sensors and thus reduce the variance in the resonant frequency. To verify this hypothesis and trying to solve the sensor interference problem, a test was performed where two sensors were placed side by side floating in a tube filled with distilled water. The results

displayed in Table 5.8 show that the standard deviations, which are 0.67 kHz and 2.76 kHz for the two sensors, are greatly decreased compared with those measured in air. However, this deviation is still beyond the range that is acceptable for biological pathogen detection. Further improvement on separating the sensors and avoiding interference is required to allow accurate detection of low concentrations of pathogens.

Table 5.8: Summary of resonant frequencies of two sensors when placed in distilled water (Unit: kHz).

Sensor Position	Sensor No.	Mean	Standard Deviation	Minimum	Maximum
Side by Side	1	551.18	0.67	550.52	552.42
	2	556.00	2.76	551.17	558.32

5.7 Effect of Pulse power

The strength of the magnetic field applied to the sensor is determined by the magnitude of the voltage pulse applied to the transformer, altering the Young's modulus and hence the resonant frequency of the sensor [77]. As the applied voltage pulse increases from 7 to 13.5 volts (Figure 5.15), the amplitude of the maximum ringdown signal recorded increases by 56% and the amplitude of resonant peak and the resonant frequency both decrease. Figure 5.15 plots the magnitude of the resonant peak and the maximum ringdowm signal recorded versus pulse power voltage. To ensure that neither the ringdown signal nor the resonant peak will be too small, a pulse power of 10.5 volts is chosen for this system.

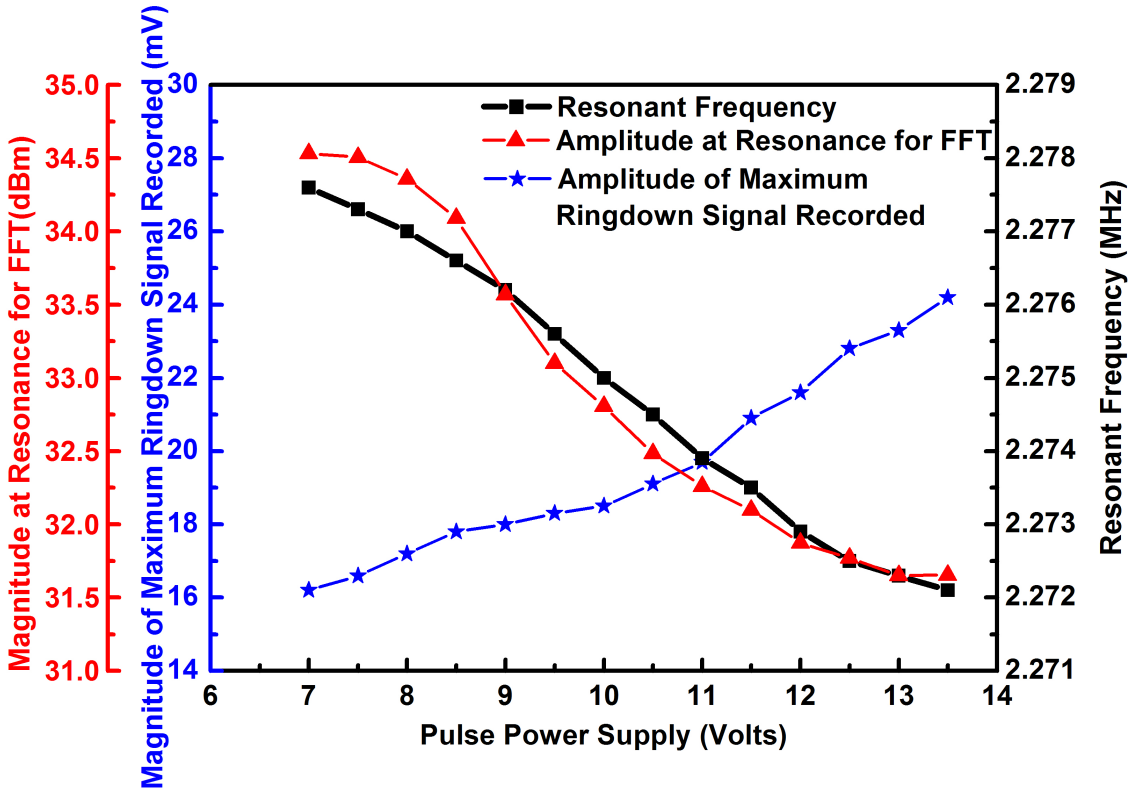

Figure 5.15: Measured sensor oscillation under various pulse power voltages.Measured sensor oscillation under various pulse power voltages.

The power pulse voltage was varied over a range of 7 to 14 volts to determine any sensitivity versus pulse power. The magnetic field generated in the solenoid field was calculated by the following equation:

$$B = \frac{\mu_0 N I}{l} \tag{5.13}$$

where B is the magnetic field in the coil, N is the number of turns, l is the length of the coil and I is the current in the coil. The coils used in the system are 3.3 mm long and have 36 turns. The current through the coil is measured by measuring the voltage across a small resistance connected in series with the coil. As shown in Figure 5.16 and Figure 5.17, for the particular sensor measured, the magnitude of the spectrum signal, measured from the noise baseline to the signal peak varied from 65 to 50 dBm above the noise floor. Although the

amplitude change is relatively insignificant, the resonant frequency changes nearly 12 kHz as the pulse amplitude is varied. This is because of the change in magnetic field [77] caused by the change in pulse voltage. Although the actual pulse voltage is not so significant, the importance of a stable power source for the pulse amplifier is obvious. The Q-value becomes important when signals are small and noise can mask the actual sensor frequency. Again, a stable power supply avoids significant changes in Q value.

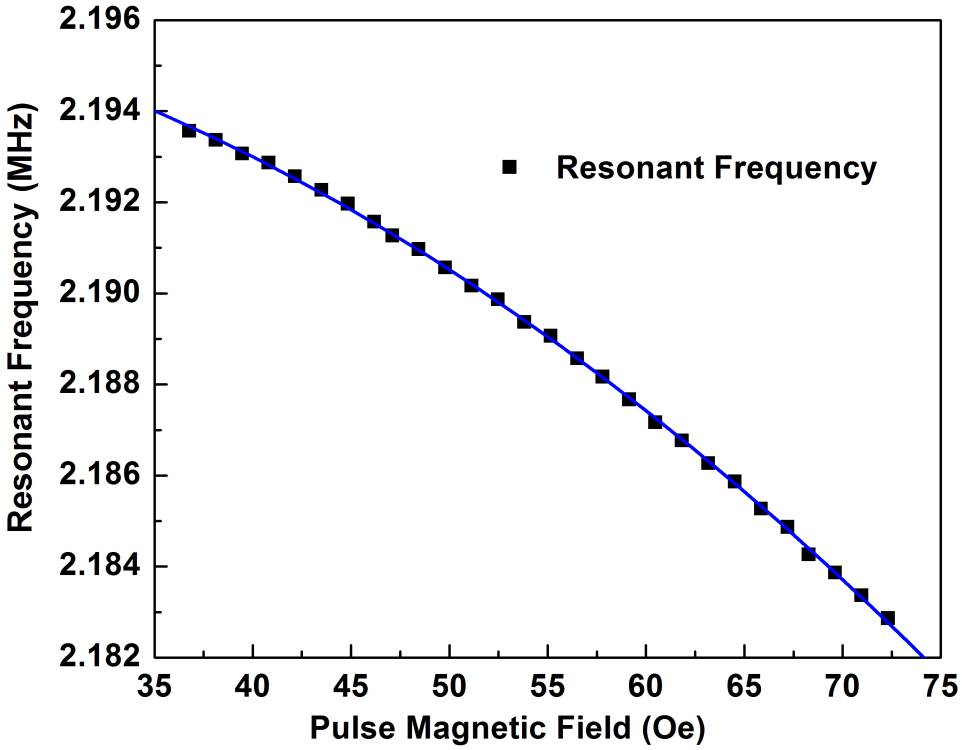

Figure 5.16: Resonant frequency under various pulse magnetic fields.

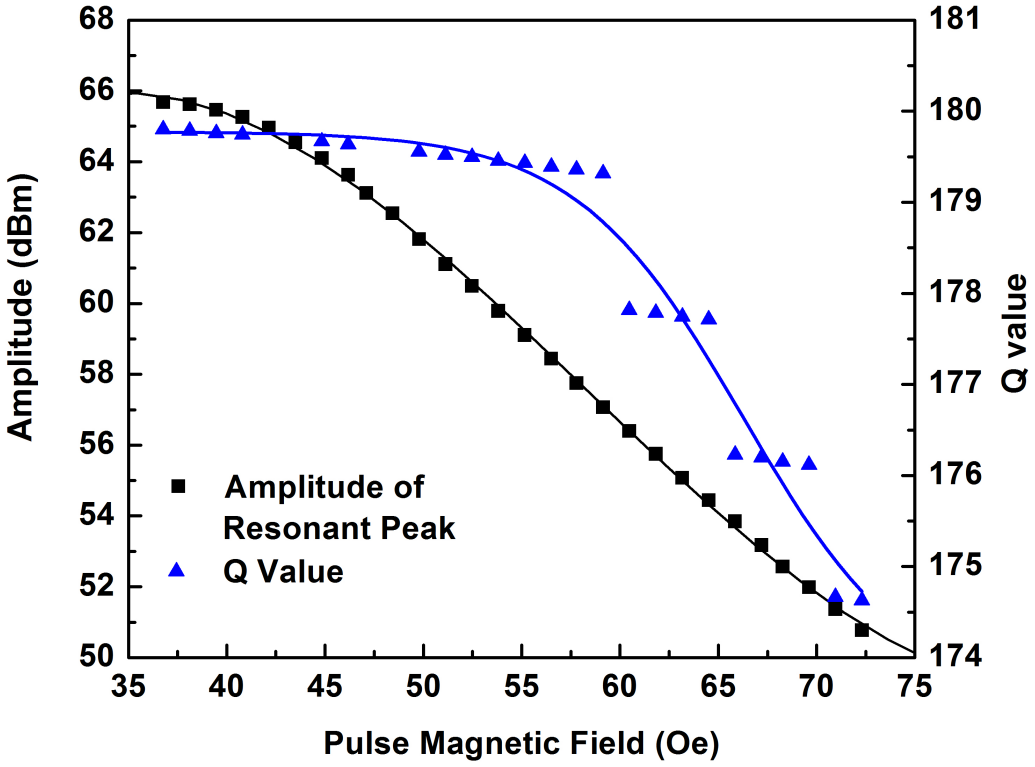

Figure 5.17: Amplitude of FFT signal and Q value of resonant peak under various pulse magnetic fields.

5.8 Stability of the Sensor in Pulse System

Another factor in a detection system is the stability over time. Table 5.9 summarizes the results of eight sensors that were tested for stability over periods ranging from 4.5 to 22.5 hours. Tests were conducted in a lab with well controlled ambient temperature, which was 23 ± 1 °C. The average deviation of the resonant frequency of the sensors is 129 Hz and the average drift per hour for the sensors is only 10.4 Hz. Figure 5.18 also shows typical stability data for a 1mm sensor over a period of 14 hours in air. During this time the frequency varies over a range of ± 100 Hz, and the magnitude variation is an insignificant 0.5 dBm. This stability, which represents an actual measurement condition in flowing liquid, is similar to the stability data of the reference sensor used in the flowing system test.

Table 5.9: Summary of stability test results in pulse system.

Sensor No.	Test Time (hours)	Mean (MHz)	Standard Deviation (Hz)	Drift / Hour (Hz/hr)
1	17	2.49	220	-71
2	22.5	2.21	56	7
3	5	2.18	161	70
4	16	2.28	62	-9
5	15	2.29	54	7
6	14	2.21	30	-7
7	4.5	2.22	44	29
8	5.5	2.15	403	-109
Average		2.25	129	-10.4

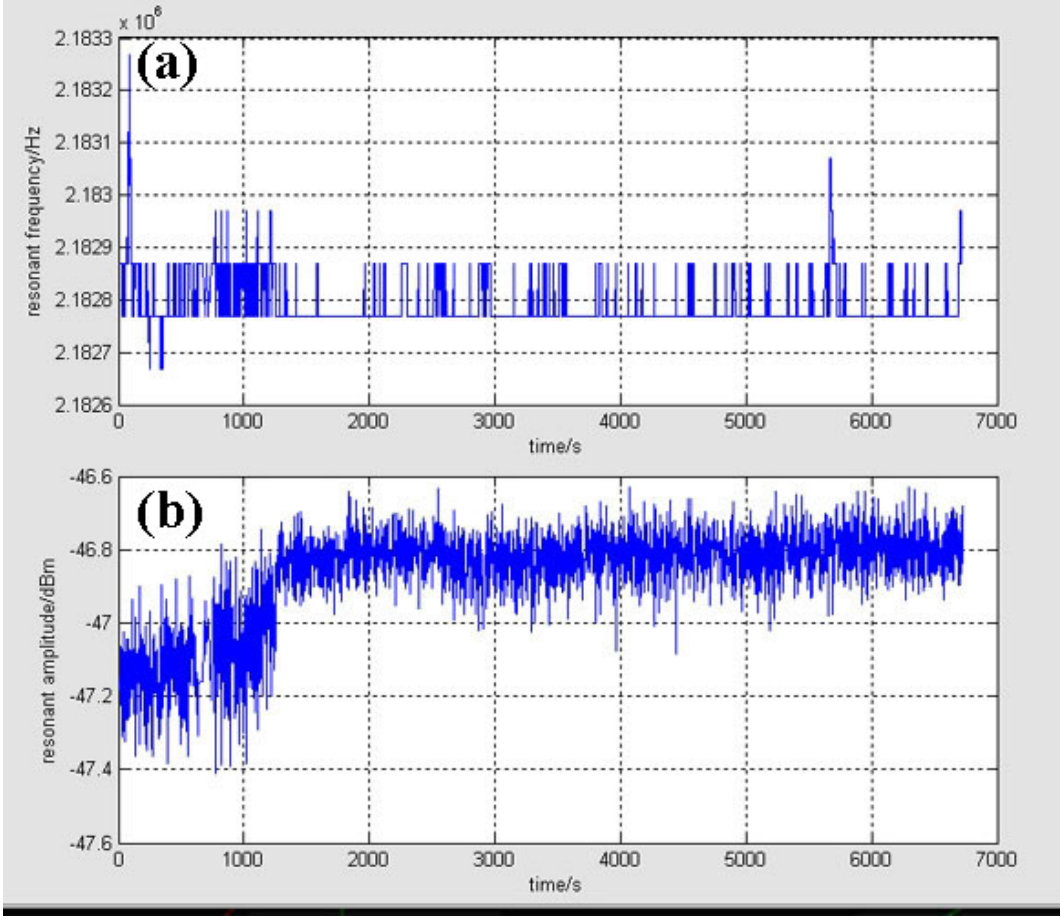

Figure 5.18: A typical received data of (a) resonant frequency and (b) signal amplitude of a magnetoelastic sensor in pulse system during a time period of 5.4 hours.

5.9 Multiple Sensors

As explained in Section 5.3, the smaller magnetoelastic sensor provides higher mass sensitivity. Current microfabrication techniques allows the fabrication of micrometer or even nanometer sized sensors. However, these sensors are very difficult to manipulate and are easy to lose. Moreover, the magnetoelastic sensors are fragile and easy to break. Often, a single magnetoelastic sensor will not give useable or reliable results. By using a group of sensors, the effects of a single defective sensor is eliminated and we get the benefit of averaging many sensors to give a much more reliable result. Assuming that all sensors are identical and the probability of failing is identically 50% for each sensor, and also assuming that no interference exists among the sensors, the the probability of a failure of detection when using various numbers of sensors ranging from 1 to 10 is listed in Table 5.10. One can see from Table 5.10 that if a single sensor has a probability of failure of 50%, by using 3 sensors together, the probability of failure is reduced to 12.5%. Therefore, sensor failure is greatly reduced by using multiple sensors.

Table 5.10: Summary of the probability of failure of detection when using various numbers of sensors.

Number of Sensors	Probability of Failing
1	50.000 %
2	25.000 %
3	12.500 %
4	6.250 %
5	3.125 %
6	1.563 %
7	0.781 %
8	0.391 %
9	0.195 %
10	0.098 %

5.9.1 Multiple Sensor Detection using Frequency Domain Method

The multiple sensor approach using frequency domain method has been demonstrated by S. Li [101]. In her work, using $12500 \times 2000 \times 30\mu m$, she has demonstrated that in a group of ten sensors, a very large mass change of one sensor may be detected. Moreover, she has also demonstrated that by using two groups of sensors with slightly different sizes, a large mass change can be detected in each of the sizes.

In this section, the characteristics of resonant peak of multiple sensors has been investigated using frequency domain method. A group of ten sensors of size $2000 \times 400 \times 30\mu m$ were measured individually and then together in the same coil simultaneously. The resonant peaks of these sensors were investigated. Similarly, a second group of ten sensors of size $500 \times 100 \times 4\mu m$ was investigated.

Figure 5.19 is the frequency response curve of ten 2 mm samples both as a group and as individuals, and Table 5.11 is a summary of the resonant frequency peaks of these ten samples. The peak of the ten 2 mm magnetoelastic sensors as a group covered frequencies of all the ten individual response peaks. The standard deviation of the resonant frequencies of the ten sensors measured individually is 4.91 kHz.

Table 5.11: Peak parameters of frequency spectrum of ten 2 mm magnetoelastic sensors.

			f_0(MHz)	FWHM(kHz)	Relative Intensity
Individual Sensors	Sensor 01		1.10700	3.33	10.76
	Sensor 02		1.10700	3.51	10.76
	Sensor 03		1.10025	7.01	31.32
	Sensor 04		1.10775	2.27	10.24
	Sensor 05		1.09950	5.67	32.67
	Sensor 06		1.10475	3.27	28.22
	Sensor 07		1.11525	2.27	3.38
	Sensor 08		1.10325	2.27	14.84
	Sensor 09		1.10475	5.67	28.18
	Sensor 10		1.09688	1.14	27.51
	Average		1.10464	3.64100	
	Standard Deviation		0.00491	1.78127	
Group Sensors	Sensor 01 through 10	Peak 1	1.10138	5.68	100
		Peak 2	1.11825	13.48	

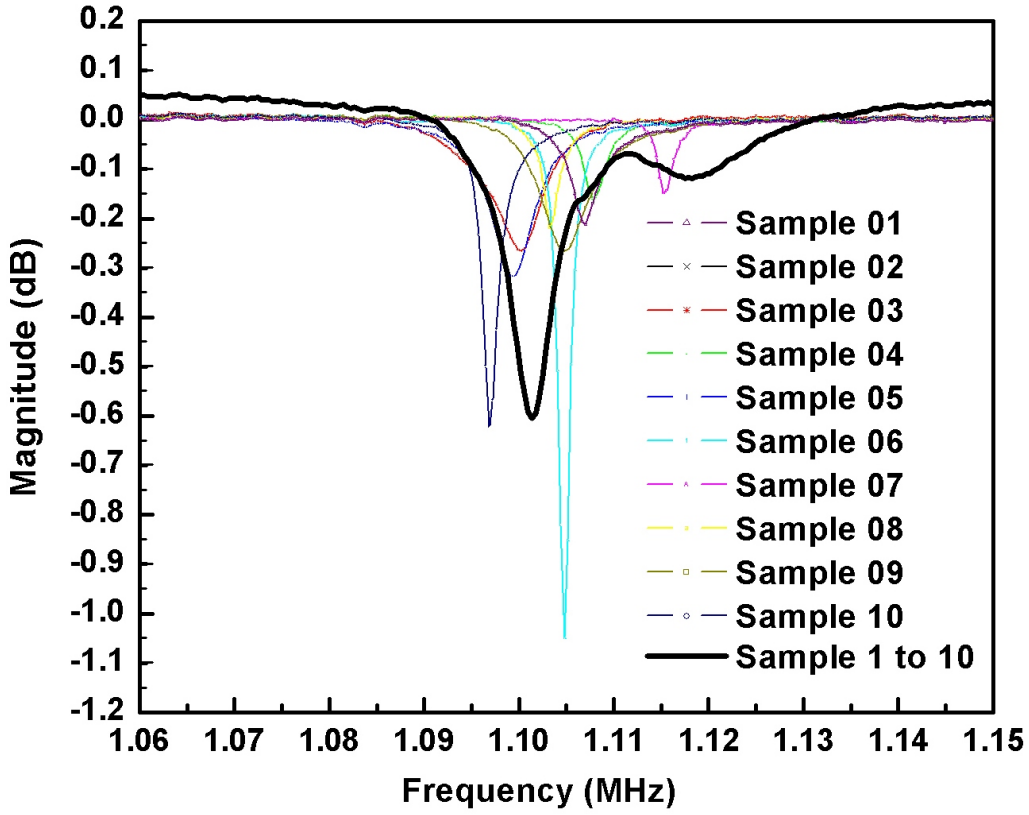

Figure 5.19: Frequency spectrum of ten 2 mm magnetoelastic sensors measured separately and simultaneously using frequency domain method.

Figure 5.20 shows the frequency spectrum of ten $500 \times 100 \times 4 \mu m$ magnetoelastic sensors measured both individually and together as a group. The resonant frequency and peak intensity of each individual sensor and of the ten sensors as a group are shown in Table 5.12. Due to the limitation of current microfabrication techniques, a broad resonant peak was observed when using multiple sensors.

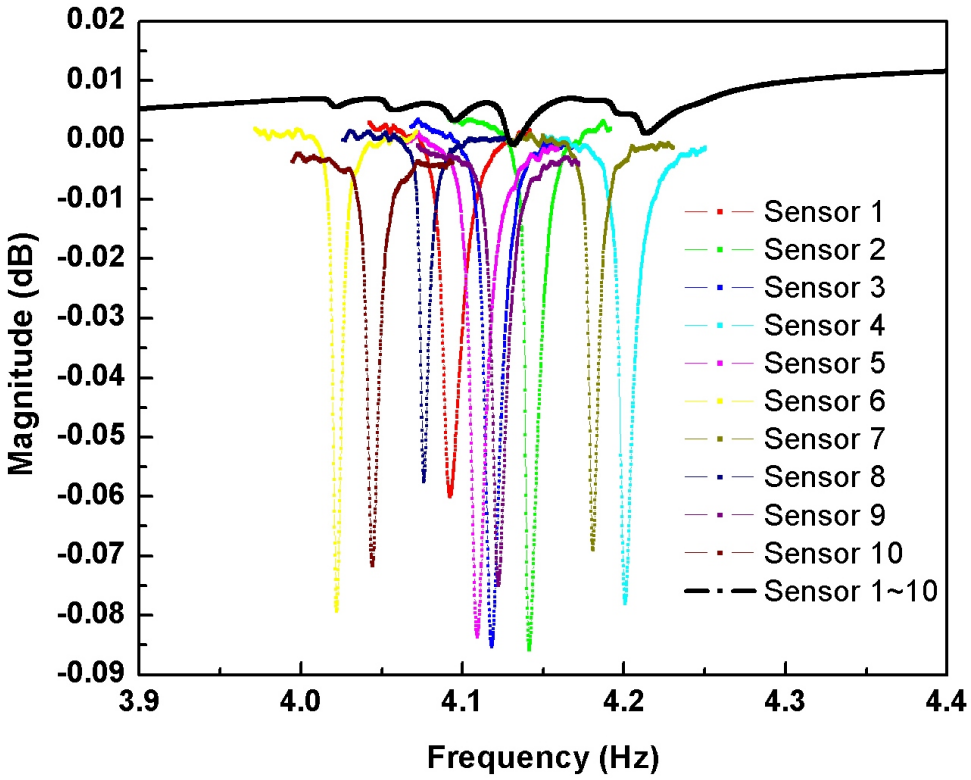

Figure 5.20: Frequency spectrum of ten 500 μm magnetoelastic sensors measured separately and simultaneously using frequency domain method.

Table 5.12: Peak parameters of frequency spectrum of ten 500 μm magnetoelastic sensors.

			f_0(MHz)	FWHM(kHz)	Relative Intensity
Individual Sensors	Sensor 01		4.09219	13.38	129.46
	Sensor 02		4.14131	9.45	135.63
	Sensor 03		4.11819	10.54	154.12
	Sensor 04		4.20094	9.17	125.76
	Sensor 05		4.10919	10.54	151.66
	Sensor 06		4.02219	5.81	74.54
	Sensor 07		4.18088	6.9	77.26
	Sensor 08		4.07625	5.9	70.9
	Sensor 09		4.12237	10.6	119.66
	Sensor 10		4.04437	7.87	91.11
	Average		4.11079	9.01600	
	Standard Deviation		0.05288	2.28450	
Group Sensors	Sensor 01 through 10	Peak 1	4.02288		100
		Peak 2	4.05912		
		Peak 3	4.09537		
		Peak 4	4.13162		
		Peak 6	4.21475		

According to the data listed in Table 5.11 and Table 5.12, we realize that the intensities of the peaks do not add when the ten sensors are measured together. The intensity of the resonant peak of the whole group of the 2 mm sensors shown in Figure 5.19 is about 60% of the addition of the intensity of each single sensor response curve, while the intensity of the resonant peak of the group of the 500 μm sensors is about 16% of the addition of the intensity of each single sensor response curve. This differnece in amplitude is believed to be caused by the interferences between ajacent sensors. Therefore, in the next section in multiple sensors approach using pulse method, the sensors are seperated to minimize their interferences.

5.9.2 Multiple Sensor Detection using Pulse Method

Since the pulse detection method eliminated the bias magnetic field, positioning and slight movement of the sensors inside the coil does not cause a DC bias change and result in a resonant frequency change. The only difference that may be caused by different positioning of the sensors in the coil is the slight AC magnetic field change due to the non-uniformity of the coil and the interferance between two adjacent sensors. The effect of different positioning of a single sensor on its resonant frequency due to the non-uniformity of the coil is discussed in Section 5.6. The interference between two adjacent sensors is eliminated by using a structure as shown in Figure 5.21, where three small separate tubes are included inside a larger tube that is wound with the coils. The dimensions of the tubes are shown in Figure 5.21(a). The large tube has an inner diameter (I.D.) of 2 mm and an outer diameter (O.D.) of 3.2 mm; each of the small tubes has an I.D. of 0.56 mm (0.0219 inches) and an O.D. of 0.80 mm (0.0315 inches). The three small tubes are glued together as a triangle. This multi-tube setup allows simultaneous detection of sensors in each coil. Although multiple sensors are put inside the coil, they are separated from each other, thus avoiding the touching and interference between adjacent sensors.

Since there are two pairs of coil in the pulse system, there are three choices for performing the multiple sensor detection:

(1) Two sensors: In this design, only one tube of the multi-channel structure is used, and one magnetoelastic sensor is put in each of the two transformer coils. Normally one sensor is used as a measurement sensor and the other as control sensor to calibrate the detection system and environmental effects.

To verify the operation of the pulse system with one or two sensors, we first subjected two individual sensors, one at a time, into its respective transformer coil and recorded the resonant frequency of each sensor. Then the two sensors were again put into the respective

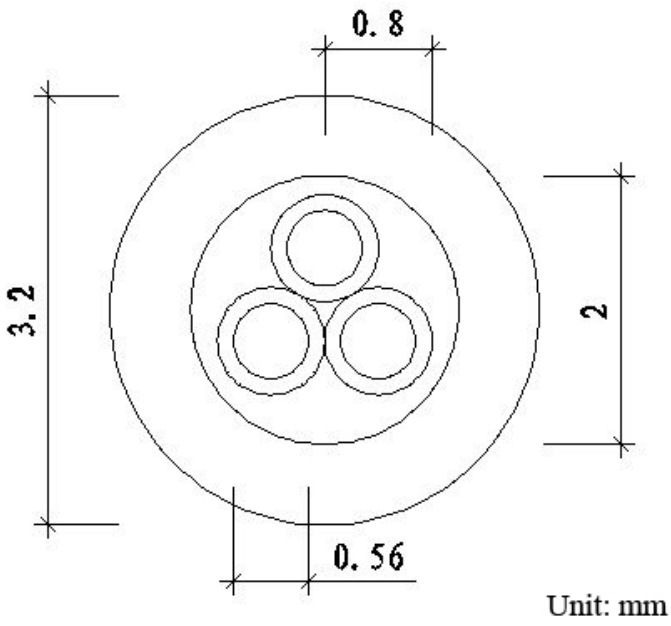

(a) Cross section view

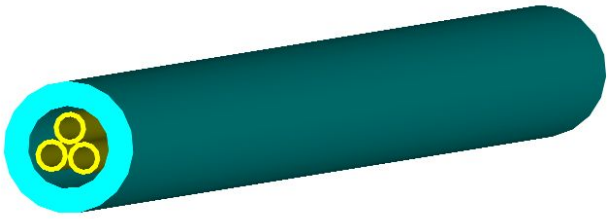

(b) 3-D view

Figure 5.21: Multi-access channel illustration.

coils at the same time and the resonant frequencies were recorded. As shown in Figure 5.22, the resonant frequency was not affected when tested separately or together.

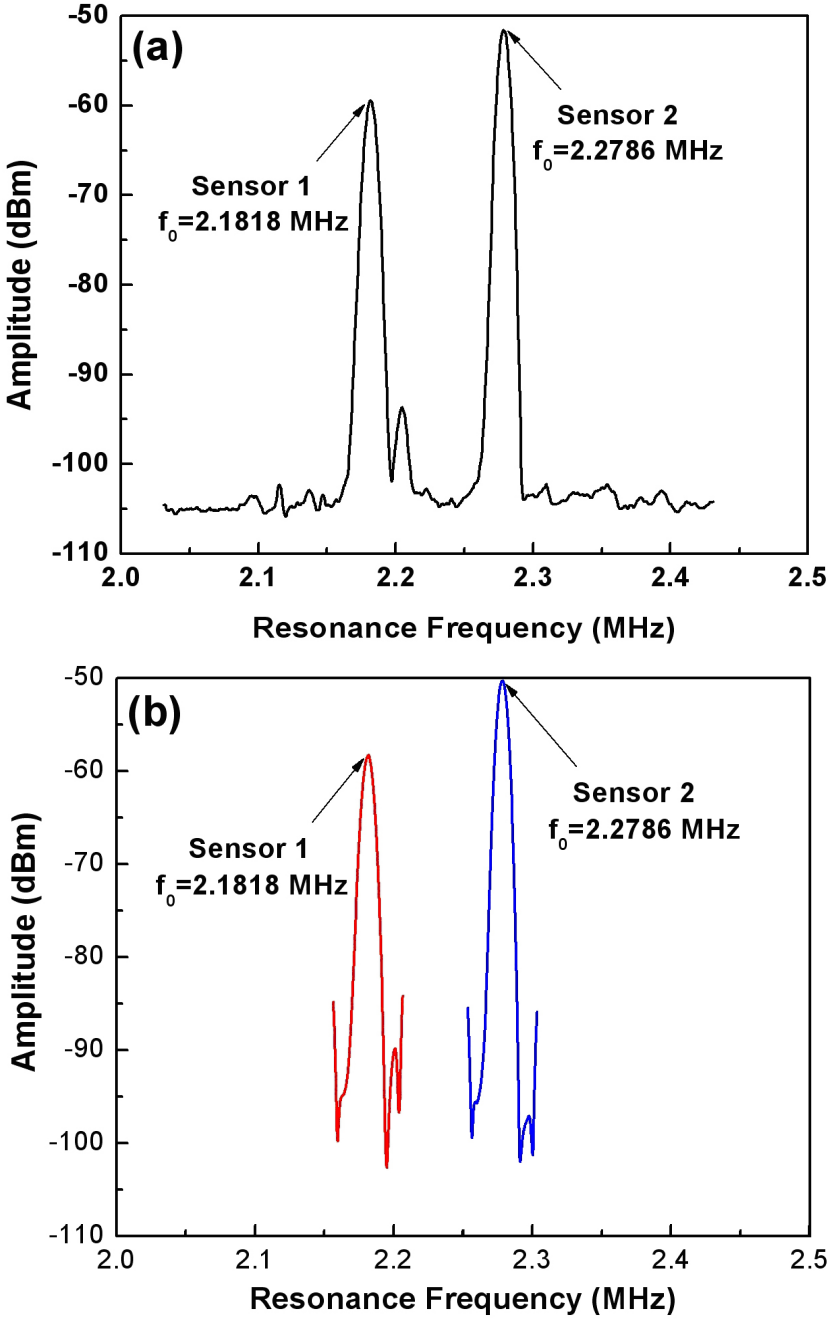

Figure 5.22: Frequency spectrum after FFT: (a) Simultaneous detection of Sensor 1 and Sensor 2 (Sensor 1 was inside Transformer 1 and Sensor 2 was inside Transformer 2); (b) Single sensor detection of Sensor 1 placed inside Transformer 1 and Sensor 2 placed inside Transformer 2.

(2) Four sensors: In this design, three tubes are used in the multi-channel structure. Then three sensors are put in the tubes of one coil and one sensor is put in one of the tubes of the other coil. The three sensors put in the multi-access channel are used as measurement sensors, and the single sensor put in the other coil is used as the control.

(2) Six sensors: In this design, three tubes are used in the multi-channel structures. In this way, three sensors can be put in each of the coils and a total of six sensors can be measured simultaneously. The three sensors in one of the coils are used as the measurement sensors and the three sensors in the other coil are used as the control sensors.

To verify the repeatability of the three sensor simultaneous detection system, we put three 1 mm magnetoelastic sensors ino the three tubes of the multi-channel structure and measured the resonance frequencies of the sensors. Then, we removed the sensors from the tubes, replaced them, and re-measured the resonance frequencies. This was repeated nine times. The resonance frequencies of the three sensors from the nine independent tests are summarized in Table 5.13. The results show that the standard deviations of the resonant frequency measurements for the three 1 mm sensors are 435.9 Hz, 447.2 Hz and 550.0 Hz. This deviation in measurement is much less than the maximum resonant frequency shift that can be achieved by a 1 mm sensor when detecting spores/bacteria. Also, based on the later experiment, this deviation is comparative to the frequency shift at limit of detection (LOD). This indicates that the bacteria detection results are valid at a 69% confidence level.

Table 5.13: Summary of a repeated test of three magnetoelastic sensors measured simultaneously in pulse system (Unit: MHz).

Test No.	Sensor 1	Sensor 2	Sensor 3
1	2.1374	2.1632	2.1764
2	2.1374	2.1632	2.1750
3	2.1376	2.1628	2.1750
4	2.1374	2.1632	2.1752
5	2.1370	2.1630	2.1750
6	2.1376	2.1626	2.1754
7	2.1378	2.1630	2.1746
8	2.1386	2.1620	2.1750
9	2.1376	2.1622	2.1752
Average	2.1376	2.1628	2.1752
Standard Deviation	435.9E-6	447.2E-6	500.0E-6

Moreover, since the FFT is a math function based on the digital sampling of the analog signal frequencies, it is able to separate frequencies that are very near to each other. This is quite different from the frequency/magnitude function where a signal is applied and the resonance is based on the magnitude of the signal as it exhibits sympathetic vibration. Therefore, the pulse method is able to separate and recognize resonant frequencies that are very close together.

Chapter 6

Real-Time Detection of *B. Anthracis* in Flowing System

The real test of the biosensor is to subject it to a "real world" application. The magnetoelastic biosensors were used to detect *B. anthracis* spores in flowing water. A bias magnetic field of 38 Oe was used for the 2mm sensor and 75 Oe was used for the 1mm sensor to adjust for maximum amplitude.

This real-time detection was performed in a flowing system (Figure 6.1), which consists of two parts: 1) an excitation/measurement part and 2) a fluid handling part. The former was explained in detail in the Chapter 4. The fluid handling section consists of a reservoir to hold the analyte test solution (spores) and a second reservoir to hold the waste solution. A peristaltic pump provides a controlled flow rate for the system with flexible tubes to complete the path from start to finish.

The detection of *B. anthracis* in a flowing system has been charicterized using 2 mm magnetoelastic sensors by S. Huang [112]. In this work, this detection was repeated by using 2 mm sensors and 1 mm sensors.

For each test, the JRB7 phage coated magnetoelastic sensor is moved into a testing chamber in the system and positioned within the magnetic field of the measurement coil. The sensor is initially exposed to distilled water for about 10 minutes before the introduction of a 10^8 spores/ml suspension of *B. anthracis* sterne strain spores. The flow rate was adjusted to be 40 μl/min, providing continuous exposure to the test solution. To determine the resonant frequency change caused by different concentration levels of *B. anthracis* suspension exposure to the sensor, the sensor was exposed to increasing concentrations (5×10^1 to 5×10^8 spores/ml) of *B. anthracis* spores suspensions in water at a flow rate of 40 μl/min. The exposure time to each concentration was 20 minutes.

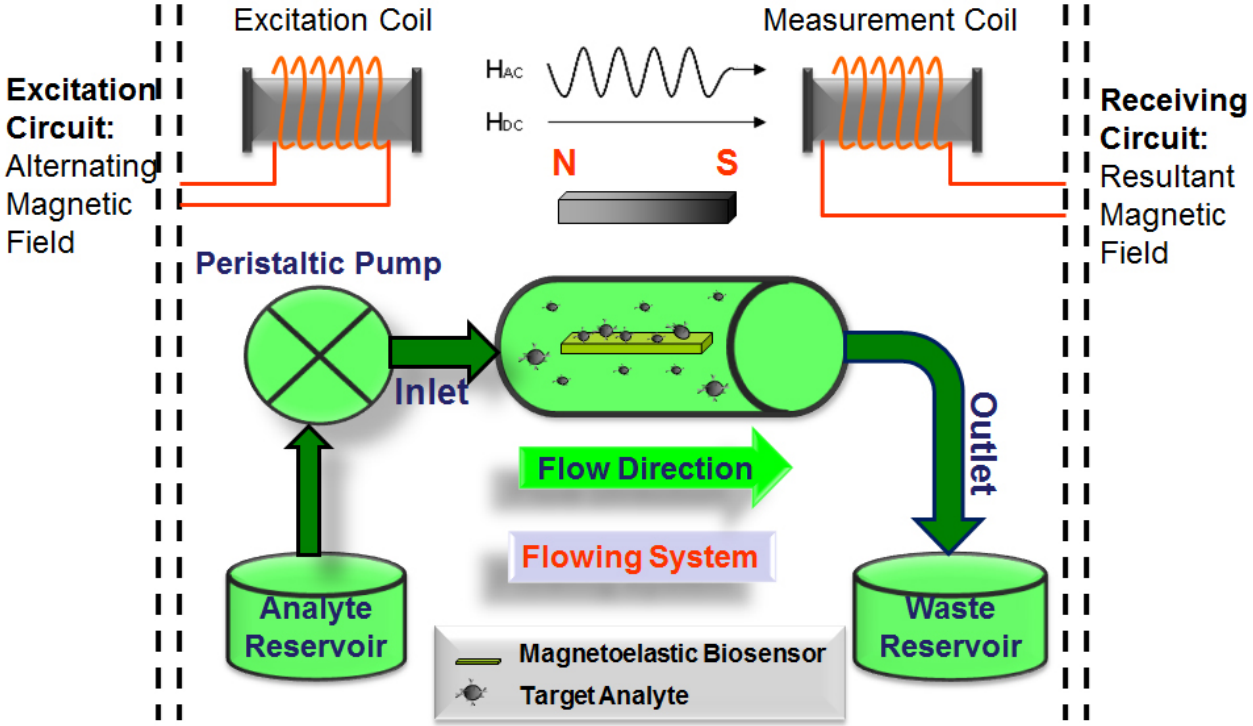

Figure 6.1: Schematic of the flowing system.

6.1 Real-Time Detection Curve

Figure 6.2 and Figure 6.3 shows the actual response of tests using a 1 mm sensor and using a 2 mm sensor. The test began with exposure of the biosensor to distilled water to generate a baseline and then the spore solution of 5×10^8 spores/ml was introduced and the resonant frequency measured continuously until saturation of the spore binding occurred. The response of the 1 mm sensor is shown in Figure 6.2. A baseline was established using distilled water for nearly 20 minutes, after which the spore solution of 5×10^8 spores/ml was introduced. Saturation of spore binding occurred within 55 minutes. The frequency change of 1.80 kHz was observed, corresponding to 9.9×10^3 spores according to Equation 5.3.

The response of the 2 mm sensor is shown in Figure 6.3. Again a baseline was established using distilled water for 20 minutes, after which the spore solution of 5×10^8 spores/ml was introduced. Once the spore solution was applied to the 2 mm sensor, about 35 minutes of reaction time elapsed before saturation occurred (Figure 6.3). A total frequency change of 823 Hz was observed, corresponding to a binding of to 3.7×10^4 spores according to Equation 5.3.

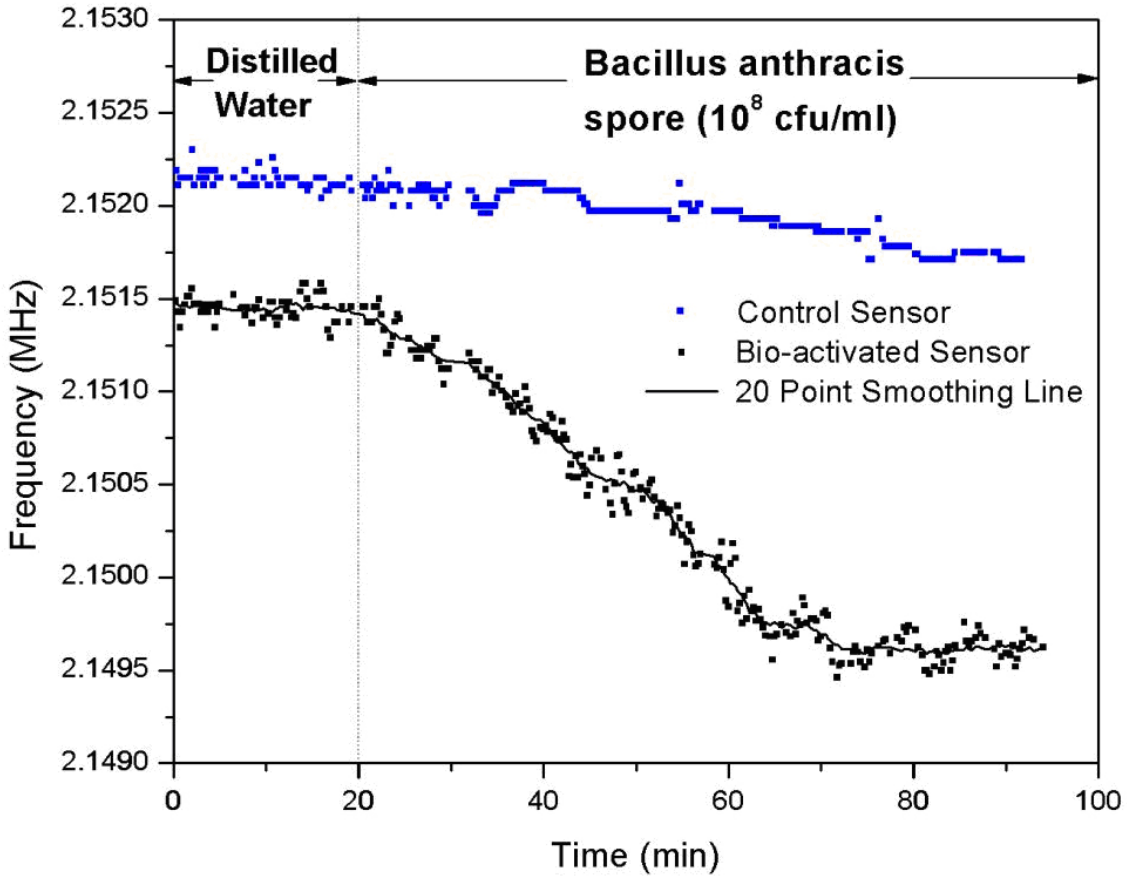

Figure 6.2: Typical magnetoelastic sensor response for 5×10^8 spores/ml *B. anthracis* spore suspension by a 1 mm ($1000 \times 200 \times 15$ μm) sensor.

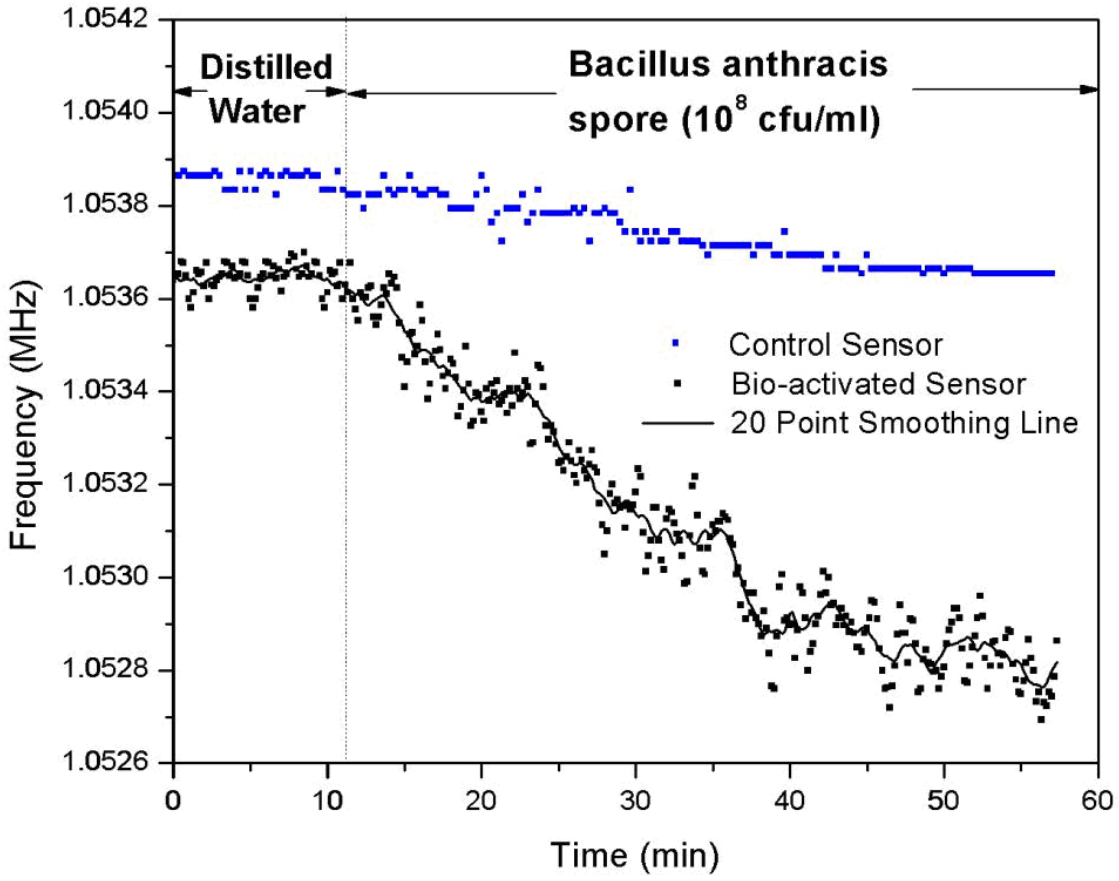

Figure 6.3: Typical magnetoelastic sensor response for 5×10^8 spores/ml *B. anthracis* spore suspension by a 2 mm ($2000 \times 400 \times 15\mu$m) sensor.

6.2 The Time Factor

The rate of spore/bacterium attachment to the sensor was quantitatively determined by a first order kinetic model [113] for antibody and antigen reaction as:

$$-kC_0t = \ln \frac{\triangle f_\propto - \triangle f}{\triangle f_\propto} \tag{6.1}$$

where $\triangle f$ is the change in frequency, $\triangle f_\propto$ is the change in frequency when all the attachment sites are filled, k is the attachment rate constant, C_0 is the initial spore/bacterial concentration and t is the time spent when the frequency change is $\triangle f$.

The attachment rate of the *B. anthracis* spores to the magnetoelastic sensors is very similar to the above case. But unlike the antibody-antigen reaction (each antibody site captures only one antigen), each spore can be bound with more than one phage. Theoretically, the upper boundary of the number of spore binding would occur when all of the (phage) binding sites are occupied, that is, the entire sensor surface was covered with spores. However, this condition does not exist in reality, because the phages are normally positively charged and form a certain distribution on the sensor surface. The theoretical determination of the actual amount of binding sites on the sensor surface was extremely difficult. However, it was observed from each detection curve (e.g. Figure 6.2) that the sensor reaches saturation after a certain period of time. It is believed that this saturation was reached when all the active binding sites were occupied by the spores. The $\triangle f_\propto$ should be the frequency change between the sensor's resonant frequency before spore binding and after saturation. The attachment constant determined based on this $\triangle f_\propto$ is $3.47 \times 10^{-}10$ min^{-1} $(\text{spores/ml})^{-1}$ as shown in Figure 6.4.

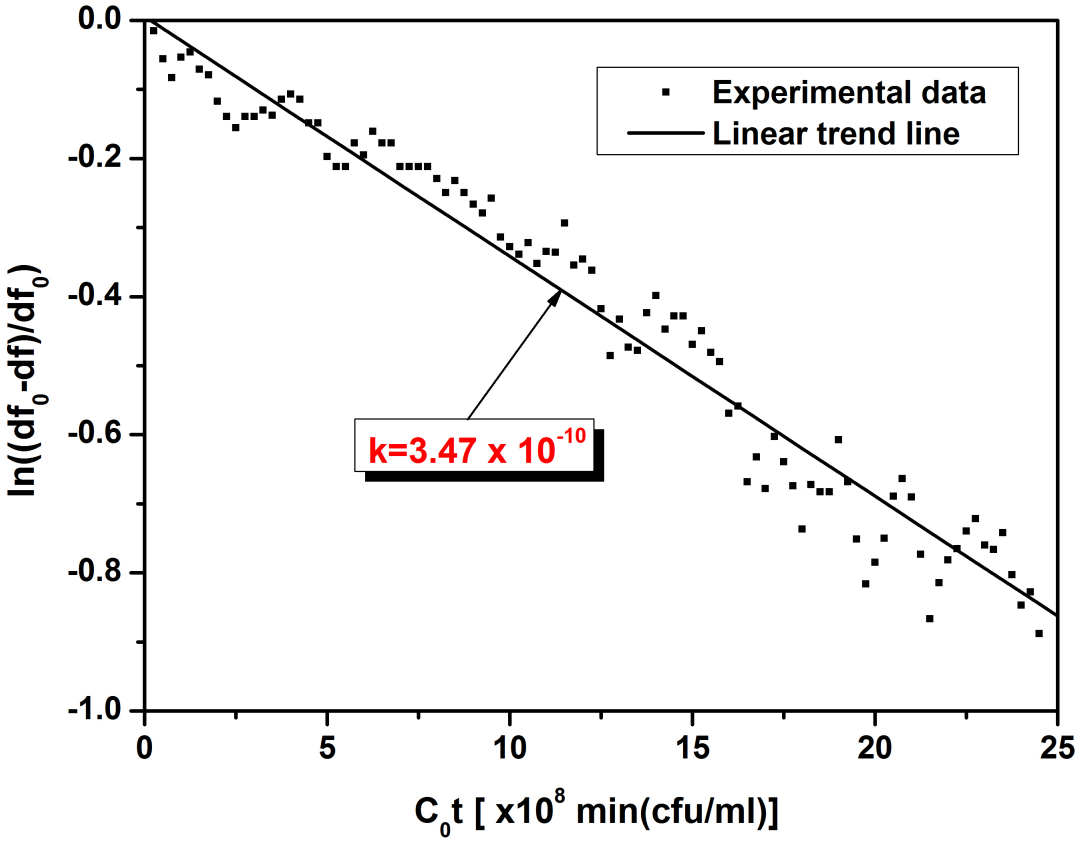

Figure 6.4: Kinetic analysis for the binding of *B. anthracis* spores suspension (5×10^8 spores/ml) using a 1 mm magnetoelastic sensor at a flow rate of 40 μl/min. The attachment rate constant was determined from the slope of the curve.

6.3 Specificity

In order to verify the effectiveness of the bio-probe, it was necessary to verify the ability of the sensor to detect *B. anthracis* but reject similar strains of *Bacillus*. To do this, we obtained a set of similar spores from Dr. Barbaree's Lab in the Department of Biological Science at Auburn University. The Sterne strain spores of *B. anthracis* alone with *B. megaterium*, *B. paratyphosus*, *B. cereus*, *B. subtilis* and *B. licheniformis* were tested. Concentrated spore suspensions were stored in sterile distilled water at about 5°C. Suspensions of the each of the different strains were tested under nearly identical conditions and the analyzer results were compared with the actual spore count using SEM photographs of the sensor surface. Table 6.1 below shows the results of this test. Note that the spore count of *B. anthracis* is many times greater than that of any of the other *Bacillus* strains, with the next nearest being only about 2.5 percent in comparison.

Table 6.1: Specificity of a 500 μm magnetoelastic sensor over a range of *Bacillus* species.

Bacillus Species	**Resonance Frequency Change (Hz)**	**Spore capture (vir)**
B. anthracis	5250	6980
B. megaterium	54	72
B. paratyphosus	57	76
B. cereus	132	175
B. subtilis	37	49
B. licheniformis	89	118

6.4 Microscopic Observation

SEM pictures of the control and measurement sensor surfaces after detection of *B. anthracis* spore in the flowing system are shown in Figure 6.6 and Figure 6.5. The spores were found to be uniformly distributed over most of the sensor surface. The actual spore count from the SEM picture showed that there was a close correlation between the actual count and the spore number calculated from the measured frequency change. For example,

for the 1 mm sensor detection shown above, the attached spore number counted from SEM photomicrographs is 1.80×10^4 bound spores. This number (within 12%) is very close to the spore number calculated from Equation (1), 2.02×10^4 spores.

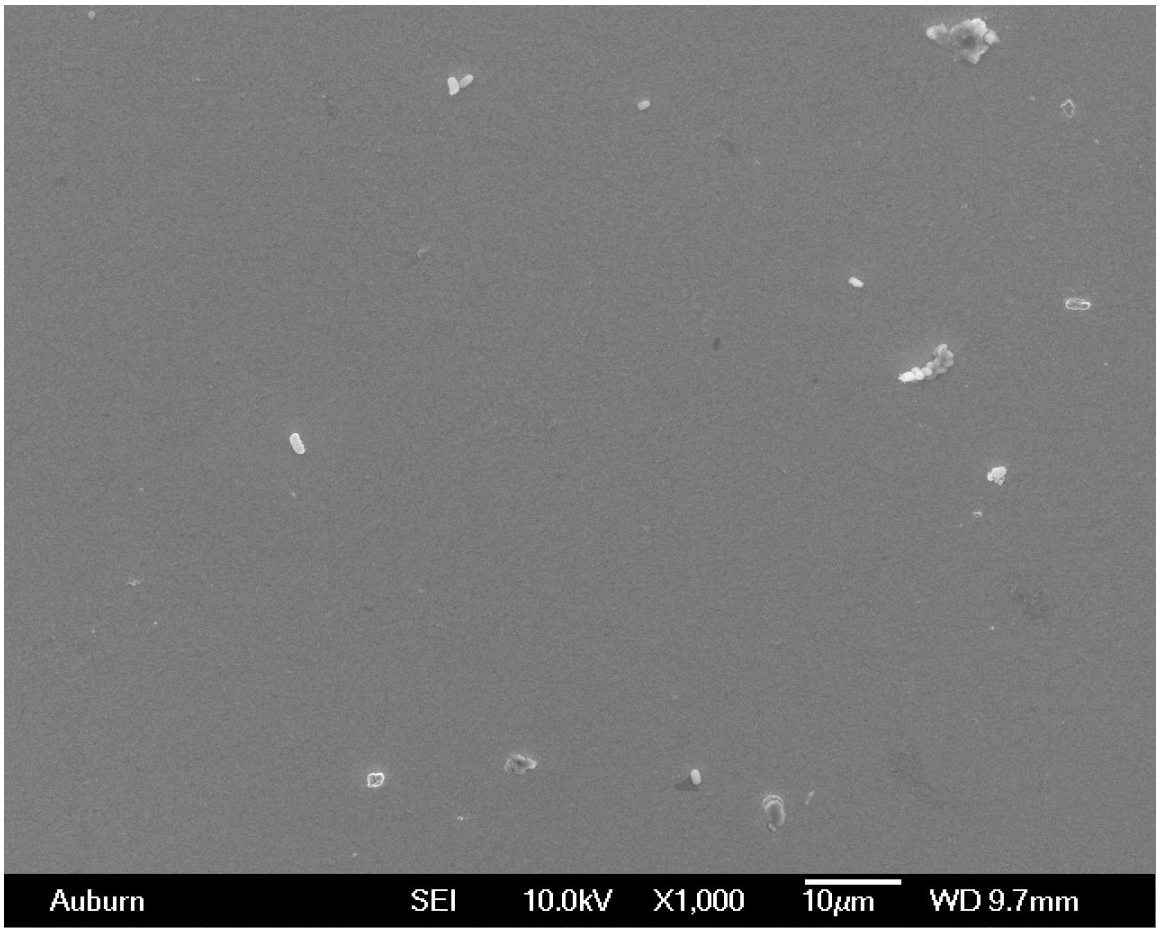

Figure 6.5: Control sensor surface after exposure to 5×10^8 spore/ml *B. anthracis* suspended in distilled water in a flowing system.

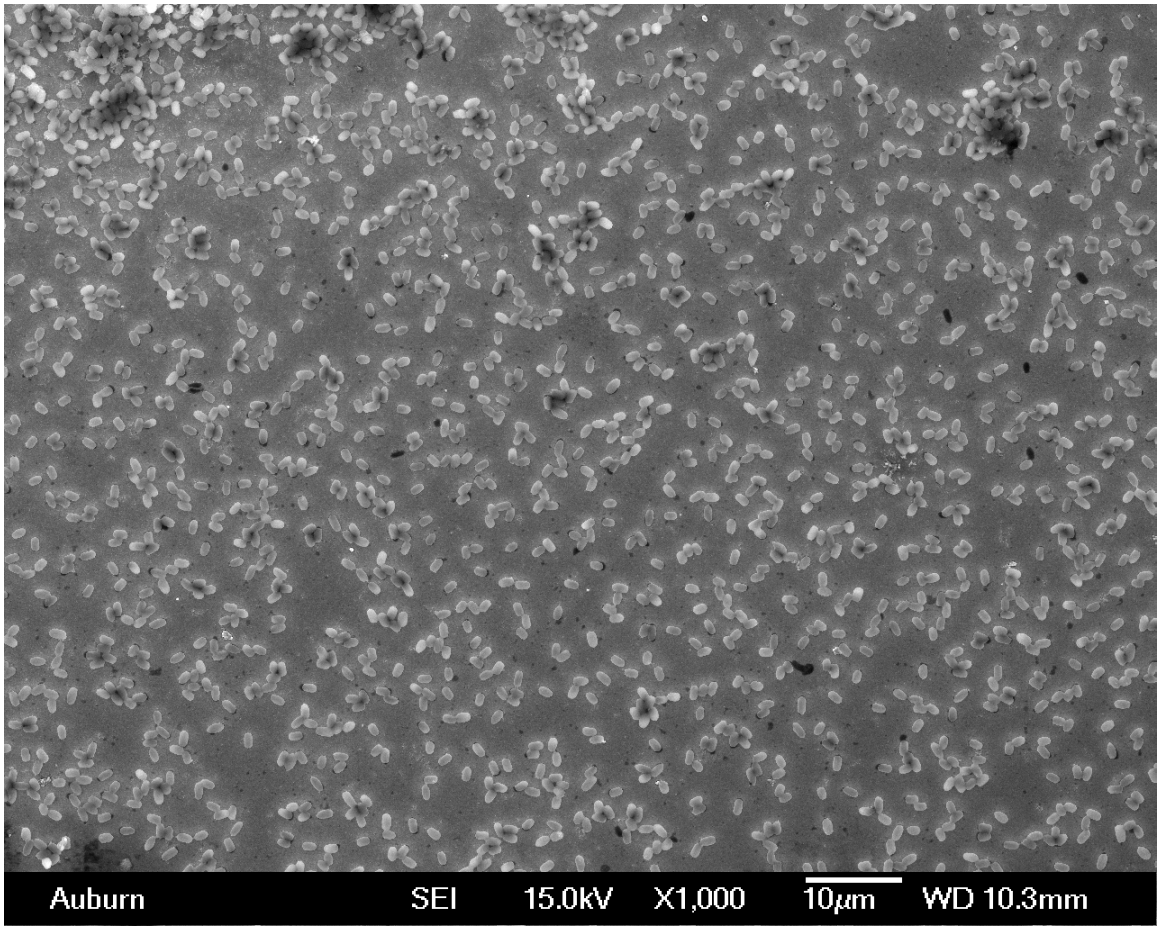

Figure 6.6: Measurement sensor surface after exposure to 5×10^8 spore/ml *B. anthracis* suspensed in distilled water in a flowing system.

6.5 Detection Limit and Sensitivity

From an analytical view point, it is important to know over what concentration range the sensor response is linear. The limit of detection (LOD or detection limit) is defined as the concentration level at the knee of the curve. The knee point is determined as the intersection of a straight line drawn through the linear portion of the response curve and another line drawn parallel to the baseline at the zero point of the calibration curve (Figure 6.7). The sensitivity is defined as the slope of the calibration curve.

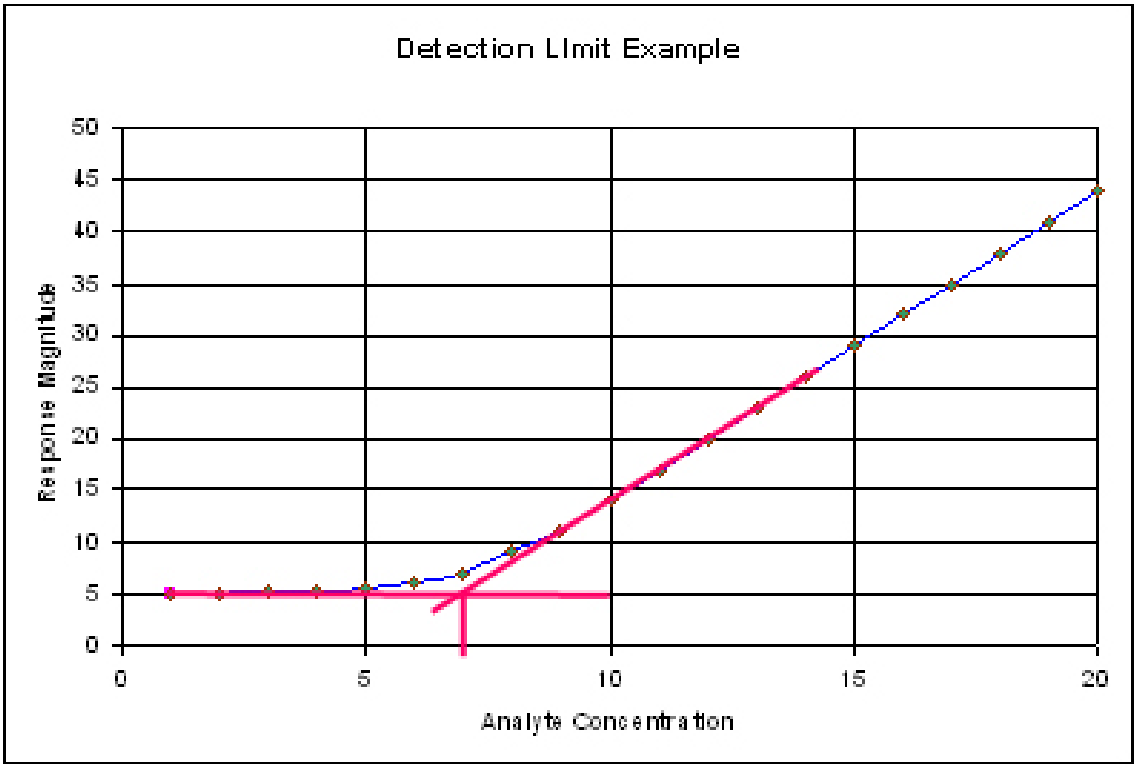

Figure 6.7: Illustration of a sensor calibration curve showing the lower detection limit (LOD).

The accumulated dose response of the biosensors were determined by measuring the frequency changes during exposure to increasing concentrations (5×10^1 to 5×10^8 spores/ml) of *B. anthracis* spore suspensions in water for a certain time period (20 minutes for each concentration). Figure 10 shows the dose response curves for 2 mm and 1 mm sensors. The detection limit for the 2 mm sensor is determined to be 10^5 spores/ml and is 3.3×10^4

spores/ml for the 1 mm sensor. A linear response was found between the concentrations of 5×10^5 to 5×10^8 spores/ml for 2 mm sensors and 5×10^4 to 5×10^8 spores/ml for 1 mm sensors. The sensitivities of the 1 mm and 2 mm sensors are determined to be 333.11 Hz/decade and 138.17 Hz/decade respectively.

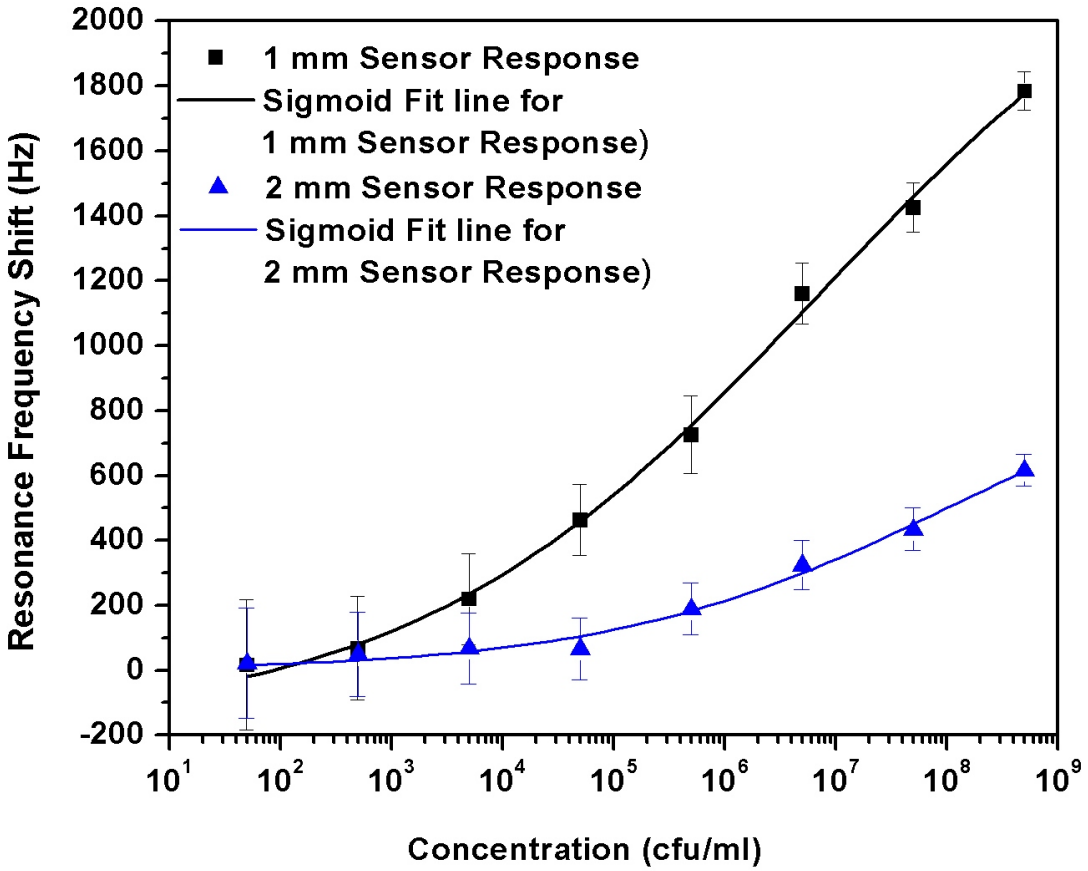

Figure 6.8: Resonant frequency shift as a function of concentration of *B. anthracis* spore (5×10^1 to 5×10^8 spores/ml). The frequency shifts of control sensors are extracted from those of the measurement sensors. The smooth lines are the sigmoid fit for the experimental data (1 mm sensor: $R^2 = 0.9976$, $\chi^2 = 0.1753$; 2 mm sensor: $R^2 = 0.9956$, $\chi^2 = 0.09359$).

6.6 Hill Plot and K_d

The binding of phage with target antigen (e.g., spores, bacterium) can be described by the following reaction.

$$nAg + P \rightleftharpoons_{k_d}^{k_a} PAg_n \tag{6.2}$$

where Ag represent the target antigen, such as *B. anthracis* spore or *S. typhimurium* and P represents the phage that binds with the target antigen, such as JRB7 phage or E2 phage. k_a AND k_d are the association and dissociation rate constants respectively. The equilibrium constant (or the affinity, K) is given by

$$K = \frac{k_a}{k_d} = \frac{[PAg_n]}{[P][Ag]^n} \tag{6.3}$$

$$K_d = \frac{1}{K} = \frac{[P][Ag]^n}{[PAg_n]} \tag{6.4}$$

The Hill equation defines Y being the fraction of the phage binding site occupied by the analyte:

$$Y = \frac{[Ag]^n}{K_d + [Ag]^n} = \frac{[Ag]^n}{K^n + [Ag]^n} \tag{6.5}$$

where n is the Hill coefficient and $N = 1/n$ is an estimate of binding valency.

Taking the logarithm on both sides, we can obtain

$$\log\left(\frac{Y}{1-Y}\right) = \log\frac{1}{K_d} + \left(\frac{1}{N}\right)\log\left[Ag\right] \tag{6.6}$$

By ploting Equation 6.6 in a logarithm scale, we can obtain the Hill constant n and $K_d$are the slope and intercept of the plot. Table 6.2 is a summary of the sensor performance characteristics in the flowing system. The Hill plots of the *B. anthracis* spore detection in

the flowing system using 1 mm sensors and 2 mm sensors are shown in Figure 6.9. From this plot, K_d is determined to be 366.70 spore/ml and 132.59 spore/ml for the 1 mm and 2 mm sensors respectively, the Hill coefficient is determined to be 0.32 and 0.16 for 1 mm and 2mm sensors respectively, and N is determined as 3.12 and 3.85 for 1 mm and 2 mm sensors respectively.

Table 6.2: Performance characteristics of 1 mm and 2 mm JRB7 phage coated magnetoelstic biosensors for the detection of *B. anthracis* spores in the flowing system.

Characteristics	$2000 \times 400 \times 15\mu m$ biosensors	$1000 \times 200 \times 15\mu m$ biosensors
Detection Limit (spores/ml)	10^5	3.3×10^4
Sensitivity (Hz/decade)	138.17	333.11
Kd (spores/ml)	132.59	366.70
Hill coefficient	0.26	0.32
N	3.85	3.12

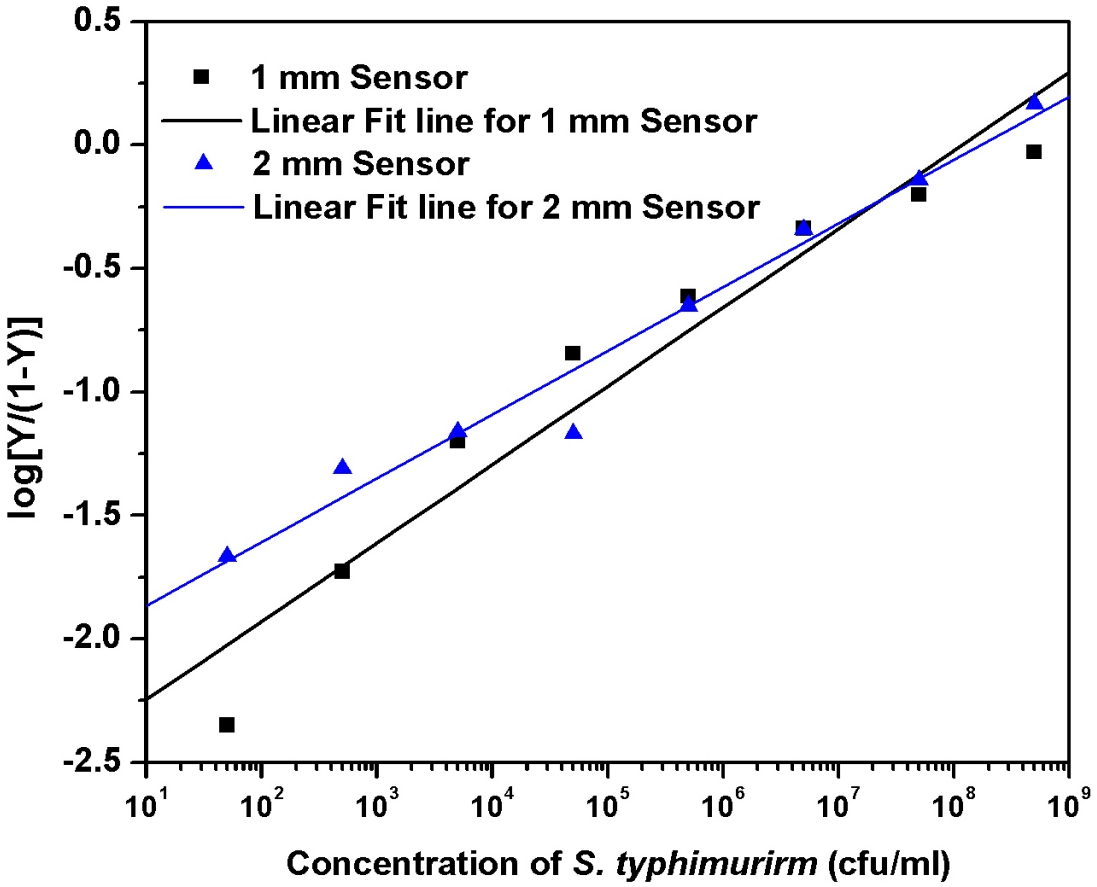

Figure 6.9: Hill Plot of the sensor responses to *B. anthracis* spore suspensions (5×10^1 to 5×10^8 spores/ml) in a flowing system . The smooth lines are the linear least square fit to the data.

6.7 Conclusions and Discussion

This research was conducted to demonstrate and study the application of a magneto-elastic sensor coated with JRB7 phage for the real-time in-vitro detection of *B. anthracis* spores in a flowing system. The free-standing and wireless nature of the sensor allows it to be easily used in flowing liquid without the demands of a complex circuit structure.

The real-time detection of *B. anthracis* spore in a water suspension at a flow rate of 40 μl/min using 1 mm and 2 mm sensors showed that the resonant frequency of the sensor decreased continuously until the saturation of the binding occurs. The SEM pictures of the sensor surfaces were taken after the detection of *B. anthracis* spores and the results show that the number of bound spores counted from SEM pictures are consistent with the results calculated from the frequency shifts. The binding kinetics were analyzed using a first order kinetic model. The attachment constant of a 1 mm sensor at a flow rate of 40 μl/min is 3.47×10^{-10} $\text{min}^{-1}(\text{spores/ml})^{-1}$. The sensor was shown to be highly specific to *B. anthracis* spores compared with other *Bacillus* species. The sensor was characterized to show frequency response as a function of concentration levels of spore solutions (5×10^1 to 5×10^8 spores/ml). The 1 mm and 2 mm sensors were found to have a detection limit of 10^5 spores/ml and 3.3×10^4 spores/ml respectively. A linear response was found between the concentrations of 5×10^5 to 5×10^8 spores/ml for 2 mm sensors and the sensitivity of these sensors was determined to be 138.17 Hz/decade. For 1 mm sensors, a linear response was found between the concentrations of 5×10^4 to 5×10^8 spores/ml and the sensitivity was determined to be 333.11 Hz/decade. The 1 mm sensor has a K_d of 366.70 spore/ml and the 2 mm has a K_d of 132.59 spore/ml for the 1 mm and 2 mm sensors based on the flowing system detection results. The Hill coefficient was determined to be 0.32 and 0.26 for 1 mm and 2mm sensors respectively, and an estimated binding valency was determined as 3.12 and 3.85 for 1 mm and 2 mm sensors respectively.

Following this study, J. Wan has later on demonstrated the detection of *B. anthracis* spores in flowing system using 500 μm and 200 μm sensors [1] [114].

Chapter 7

Detection of *S. Typhimurium* using Pulse System

7.1 Detection using one Measurement Sensor and one Control Sensor

The detection of *S. typhimurium* in liquid utilized a dynamic binding procedure. An untreated sensor (devoid of E2 phage) was used as a control sensor and a sensor coated with E2 phage was used as a measurement sensor for specific detection of *S. typhimurium*. For each of the 10 tests performed, one control sensor and one measurement sensor were immersed in a 0.3 ml tube filled with *S. typhimurium* suspension. This test tube was rotated at a speed of 10 rpm on a rotor to allow maximum and uniform contact of the sensor with *Salmonella* cells in the solution. After one hour, the two sensors were taken out of the tube and washed one time with distilled water, and then allowed to day in air. These sensors are then tested for their resonant frequencies and then observed for surface bacteria binding using the SEM. Ten control sensors and ten measurement sensors were used for each *S. typhimurium* concentration and concentrations of 5×10^1 cfu/ml through 5×10^8 cfu/ml were tested.

Figure 7.1 shows a summary of the test results. The detection limit determined from the calibration curve is 1.8×10^4 cfu/ml. To determine the LOD statistically, we tested 10 measurement sensors in distilled water using the same procedure that was used for detecting *S. typhimurium*. The mean frequency change of these ten tests ("blank" response) was 384 Hz. Assuming the tested results at each concentration are normally distributed, at a confidence level of 99%, the detection limit should be the "point" (concentration) where the difference between the mean response to *S. typhimurium* and the "blank" response being equal or greater than 2.8 times of the standard deviation at this point, since t-values is 2.8 for a 99% confidence level with nine degrees of freedom. For our experiment, the det ection

limit of *S. typhimurium* using the pulse system is determined to be 5×10^3 cfu/ml (between 10^3 and 10^4 cfu/ml). The sensitivity of the sensor is determined was 615.75 Hz/decade.

The Hill plot showng sensor binding with concentrations of 5×10^1 to 5×10^8 cfu/ml concentrations of *S. typhimurium* suspensions is shown in Figure 7.2. K_d is determined to be 450 cfu/ml, the Hill coefficient is determined as 0.39 and N as 2.57.

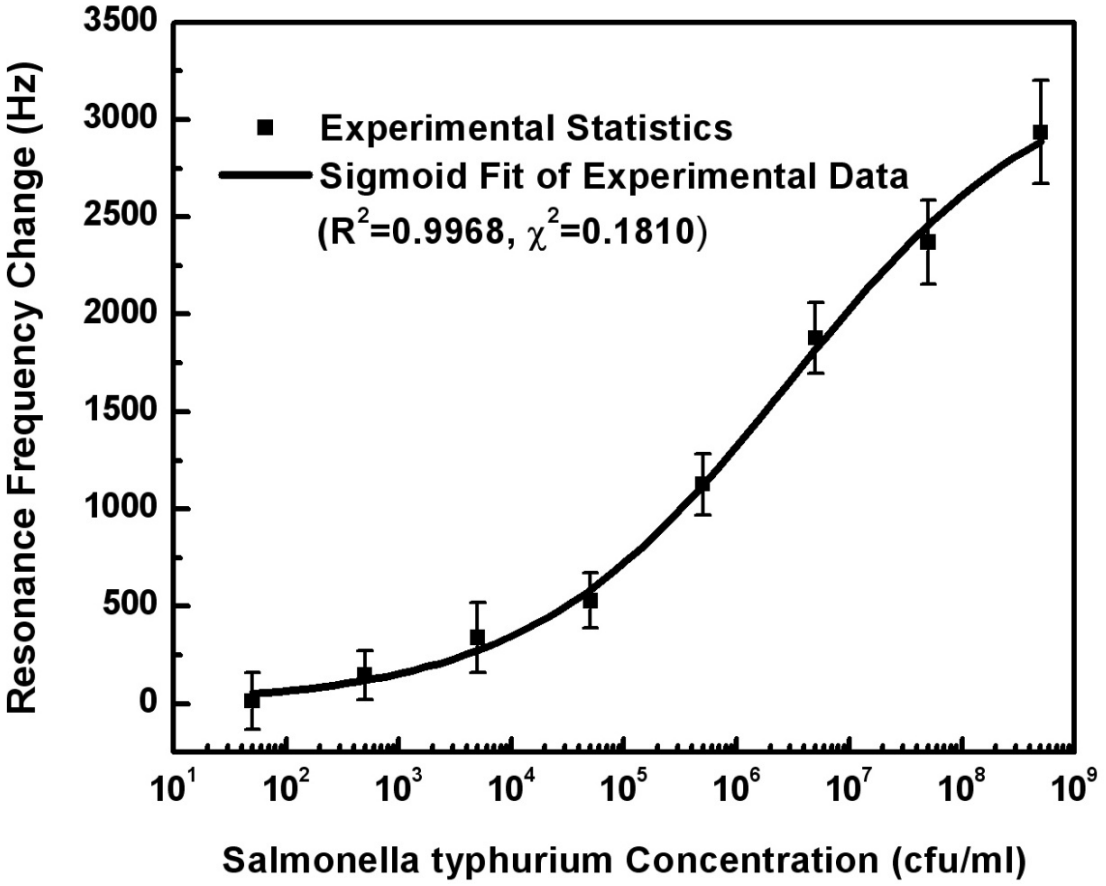

Figure 7.1: Magnetoelastic sensor response as a function of concentrations of *S. typhimurium* suspentions (5×10^1 to 5×10^8 cfu/ml). The frequency shifts of control sensors are extracted from those of the measurement sensors. The smooth line is the sigmoid fit for the experimental data ($R^2 = 0.9968$; $\chi^2 = 0.1810$).

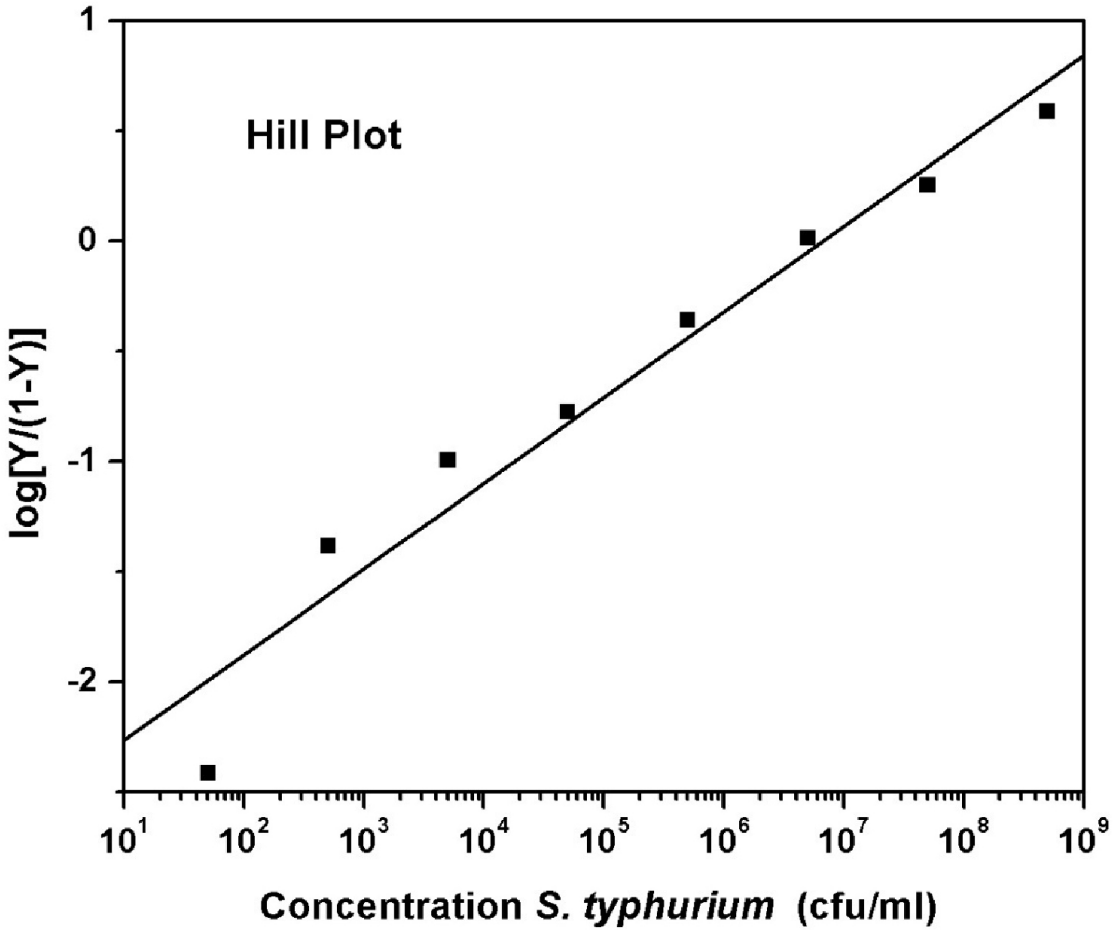

Figure 7.2: Hill plot showing the *S. typhimurium* binding to 1 mm magnetoelastic biosensors. The squares represent experimental data. The line represents the least square fit of the data (slope $= 0.39 \pm 0.04$, $R = 0.9780$, $P < 0.0001$).

After the tests, the SEM was used to observe the binding of *S. typhimurium* cells on the sensor surface (Figures 7.3 and 7.4).

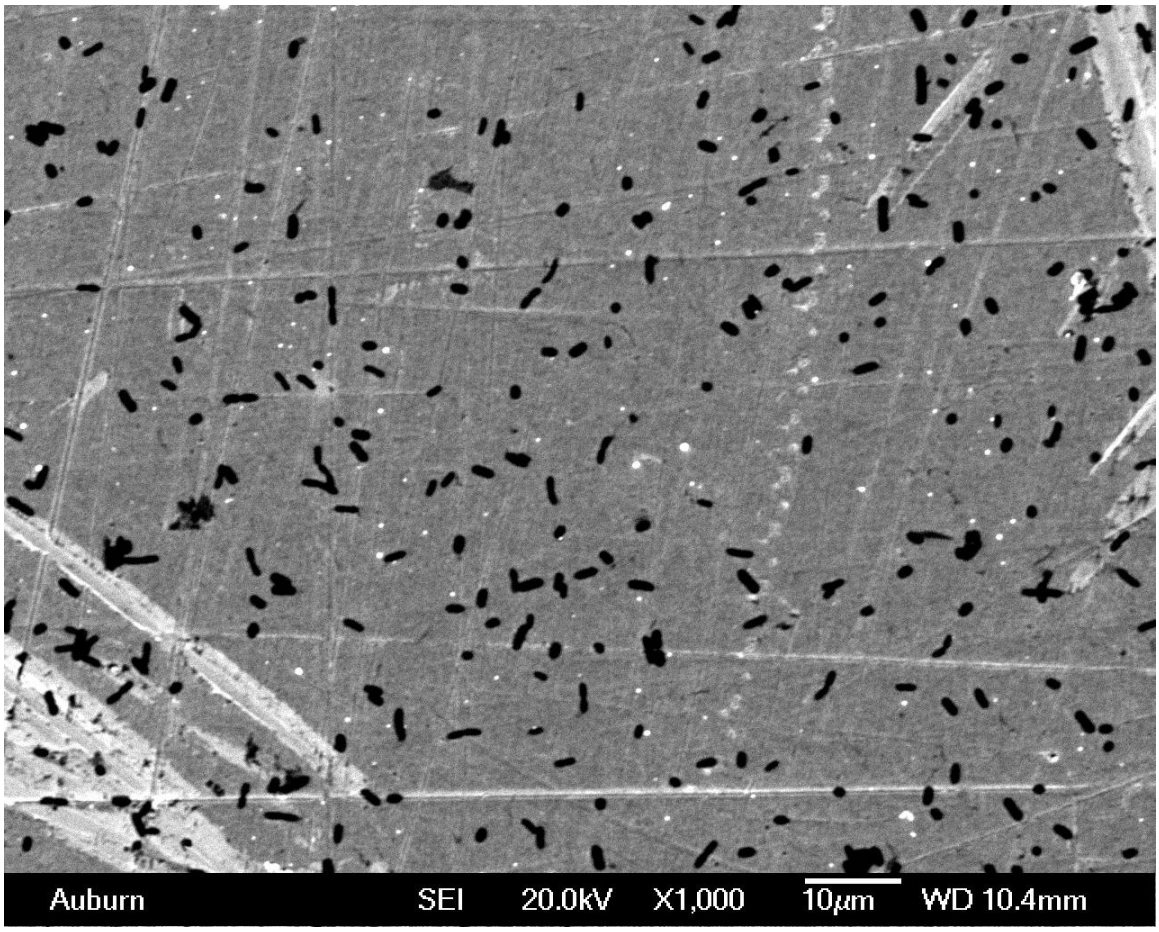

Figure 7.3: Typical SEM picture of the measurement sensor surface after exposure to 5×10^8 cfu/ml *S. typhimurium* suspension in distilled water.

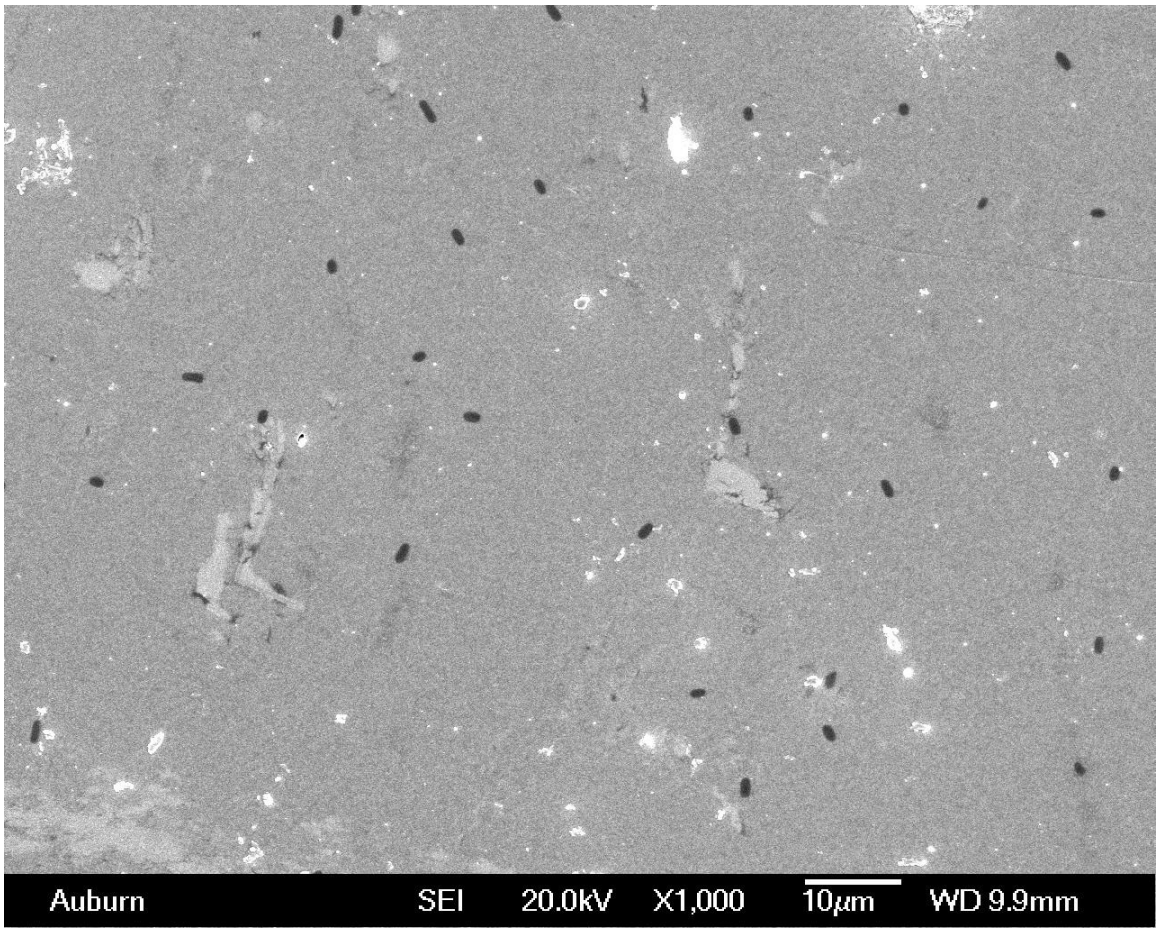

Figure 7.4: Typical SEM picture of the control sensor surface after exposure to 5×10^8 cfu/ml *S. typhimurium* suspension in distilled water.

7.2 Detection using Grouped Sensors

The group detection method was used for the detection of *S. typhimurium*. This detection was realized by using three magnetoelastic biosensors as a group to detect *S. typhimurium* sinultaneously. For each test, one sensor was put in one of the coils in pulse system for use as the reference sensor and three other sensors, each in a separate tube, were put in the other coil for use as the measurement sensors. The three measurement sensors were used for simultaneous detection of *S. typhimurium*. The resonant frequencies of the three measurement sensors were measured independently 5 times. Each measurement sensor was then coated with E2 phages as described in Chapter 3. The dynamic bindng as described in the beginning of this chapter was used for these tests. After binding with *S. typhimurium*, the sensors were washed one time with distilled water, dried in air and then exposed to OsO_4 for 45 minutes. After OsO_4 treatment, three measurement sensors in each group were put back into the tubes in the coil and tested for their resonant frequency independently again for 5 times.

Figure 7.5 is a typical result for the detection of 5×10^7 cfu/ml *S. typhimurium* suspension in distilled water using a group of three magnetoelastic biosensors. The resonant frequency of all the three sensors decreased after the detection of *S. typhimurium*. The frequency decreases of the three sensors are 3.04 kHz, 3.20 kHz and 2.92 kHz and the average frequency change of this group of sensors is 3.05 kHz. Figure 7.6 shows a result of using grouped sensors to detect 5×10^5 cfu/ml *S. typhimurium* suspension. All three sensors showed a decrease in their resonant frequencies after the detection of *S. typhimurium* in the suspensions. The frequency decreases of the three sensors are 2.353 kHz, 0.753 kHz and 0.941 kHz. Although Sensor 1 gives a relatively larger frequency shift than the other two sensors, by taking the average of all frequency shifts of the group of the sensors, we get a average frequency shift of 1.35 kHz. Notice that the amplitude at the resonant frequency changes for each measurement. This change in amplitude is assumed to be caused by the location differnece of the sensors in the transformer coils. Compared with using single sensors, group

sensor detection uses multiple sensors as a group and takes the average of the results from all sensors in the group. This will decrease the effect of individual erroneous results and thus give more reliable results.

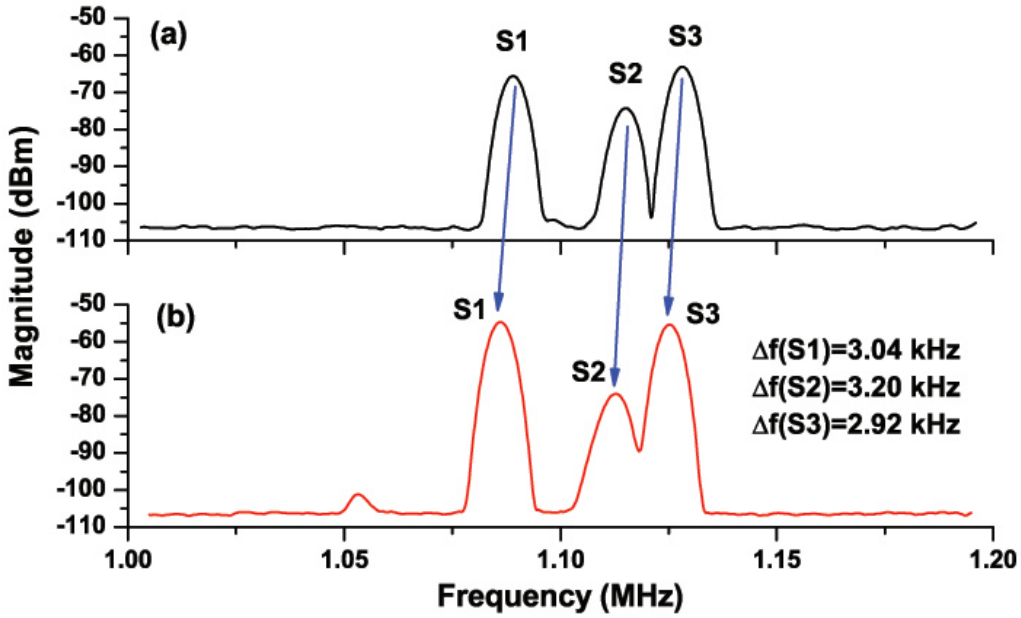

Figure 7.5: Typical response of a group of three magnetoelastic sensors (a) before and (b) after exposure to *S. typhimurium* suspension at a concentration of 5×10^7 cfu/ml.

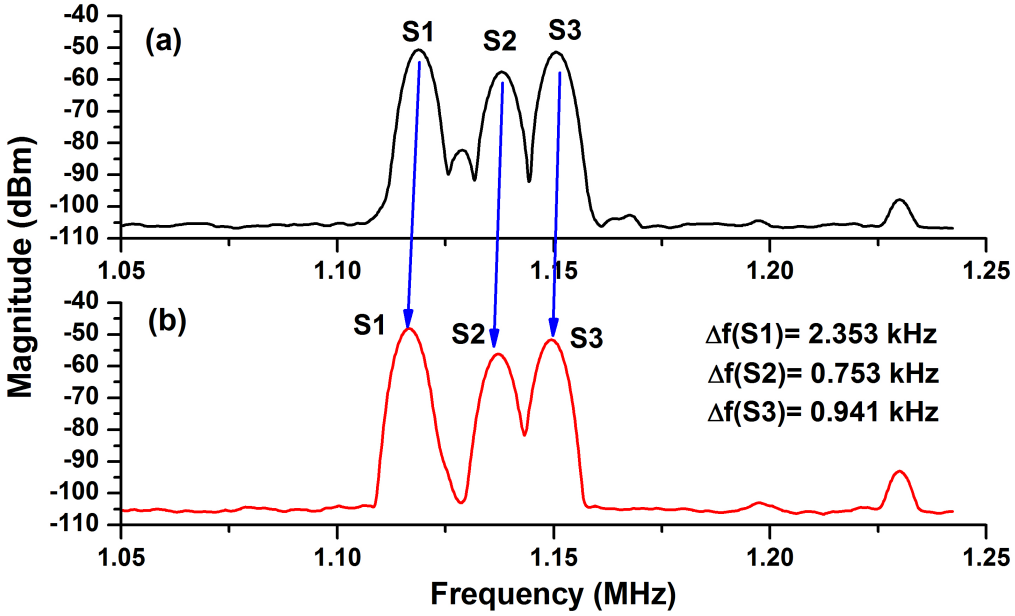

Figure 7.6: Typical response of a group of three magnetoelastic sensors (a) before and (b) after exposure to *S. typhimurium* suspension at a concentration of 5×10^5 cfu/ml.

The summary of the detection results are shown in Figure 7.7 and the Hill plot is shown in Figure 7.8. Table 7.1 is a summary of single and grouped sensor performance for the detection of *S. typhimurium*. The detection limit for *S. typhimurium* using grouped sensors is determined as 8×10^4 cfu/ml. The sensitivity of the detection is 567.48 Hz/decade. The K_d is determined to be 385 cfu/ml, the Hill coefficient is determined as 0.31 and N is 3.25. The deviation of the group sensor detection is larger than that of single sensor detection. This may be caused by the inclusion of the grouped sensors, including the ones that give erroneous results. However, as indicated previously in this paper, the grouped sensor detection has the advantage of providing more reliable results than using single sensors. Further research needs to be performed using smaller sensors for grouped sensor detection and to use hundreds of sensors simultaneously to detect target pathogens.

Table 7.1: Performance characteristics of 2 mm E2 phage coated magnetoelastic biosensors for the detection of *S. typhimurium*.

Characteristics	single biosensors	grouped biosensors
Detection Limit (cfu/ml)	1.8×10^4	8×10^4
Sensitivity (Hz/decade)	615.75	567.48
Kd (cfu/ml)	450	385
Hill coefficient	0.39	0.31
N	2.57	3.25

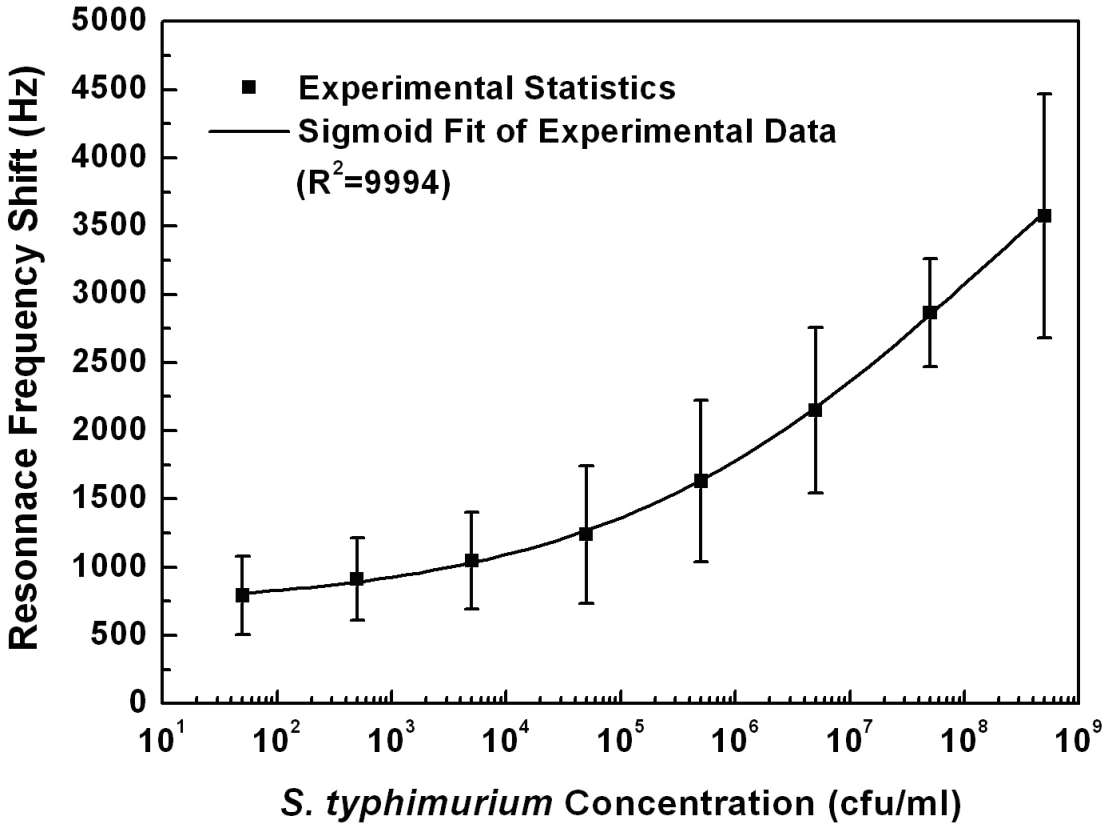

Figure 7.7: Multiple sensor response to concentrations of *S. typhimurium* suspensions (5×10^1 to 5×10^8 cfu/ml). The frequency shifts of control sensors are extracted from those of the measurement sensors. The smooth lines are the sigmoid fit for the experimental data ($R^2 = 0.9994$, $\chi^2 = 0.0043$;

Scanning electronic microscopy (SEM) was used to examine the sensor surface before and after the *S. typhimurium* detection to confirm the results obtained from frequency measurements. Figures 7.9 7.10 7.11 are typical SEM pictures of the sensor surface after detection of different concentrations of *S. typhimurium* suspensions. A large number of *S. typhimurium* cells were found on the sensor after the exposure to 5×10^8 cfu/ml *S. typhimurium* suspension, while fewer cells were bound to the sensor surface after exposing to *S. typhimurium* suspension at concentrations of 5×10^7, 5×10^6 and lower.

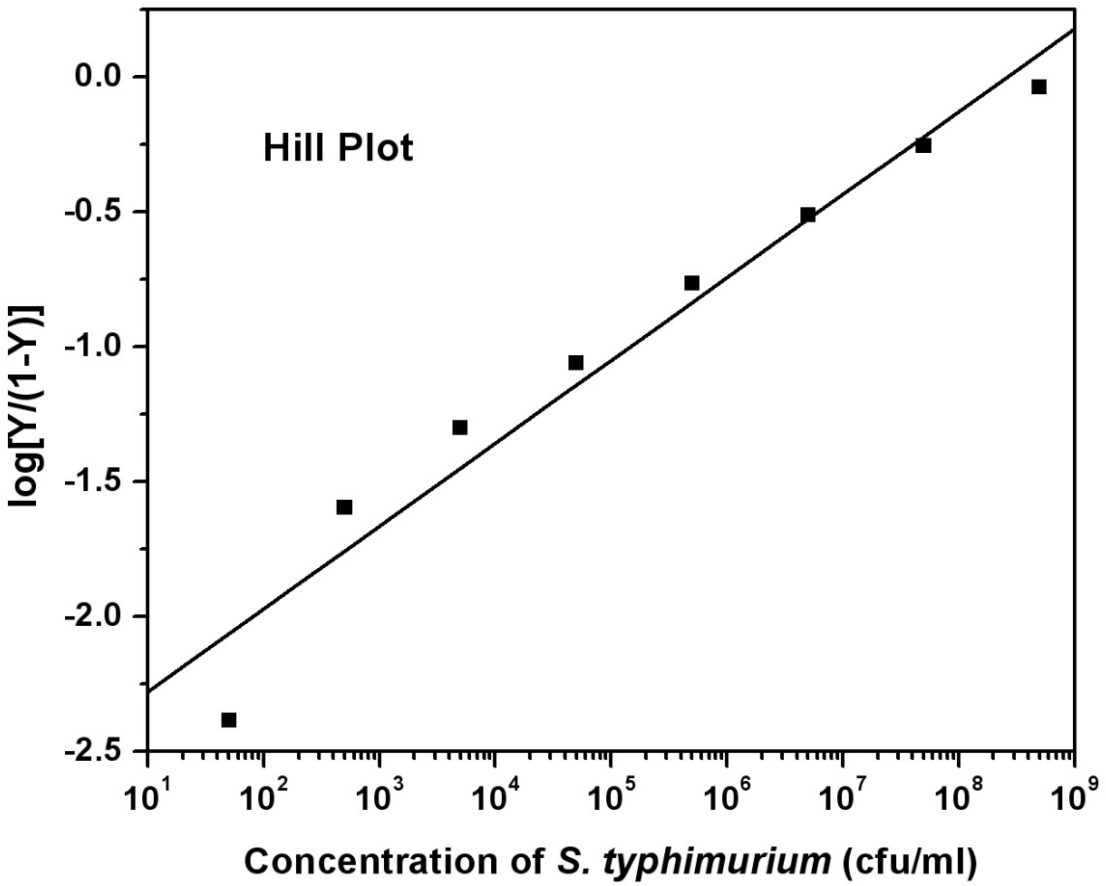

Figure 7.8: Hill plot showing the *S. typhimurium* binding to groups of 2 mm magnetoelastic biosensors. The frequency shifts of control sensors are extracted from those of the measurement sensors. The squares represent experimental data. The line represents the least square fit of the data ($R^2 = 0.9994$, $\chi^2 = 0.0043$).

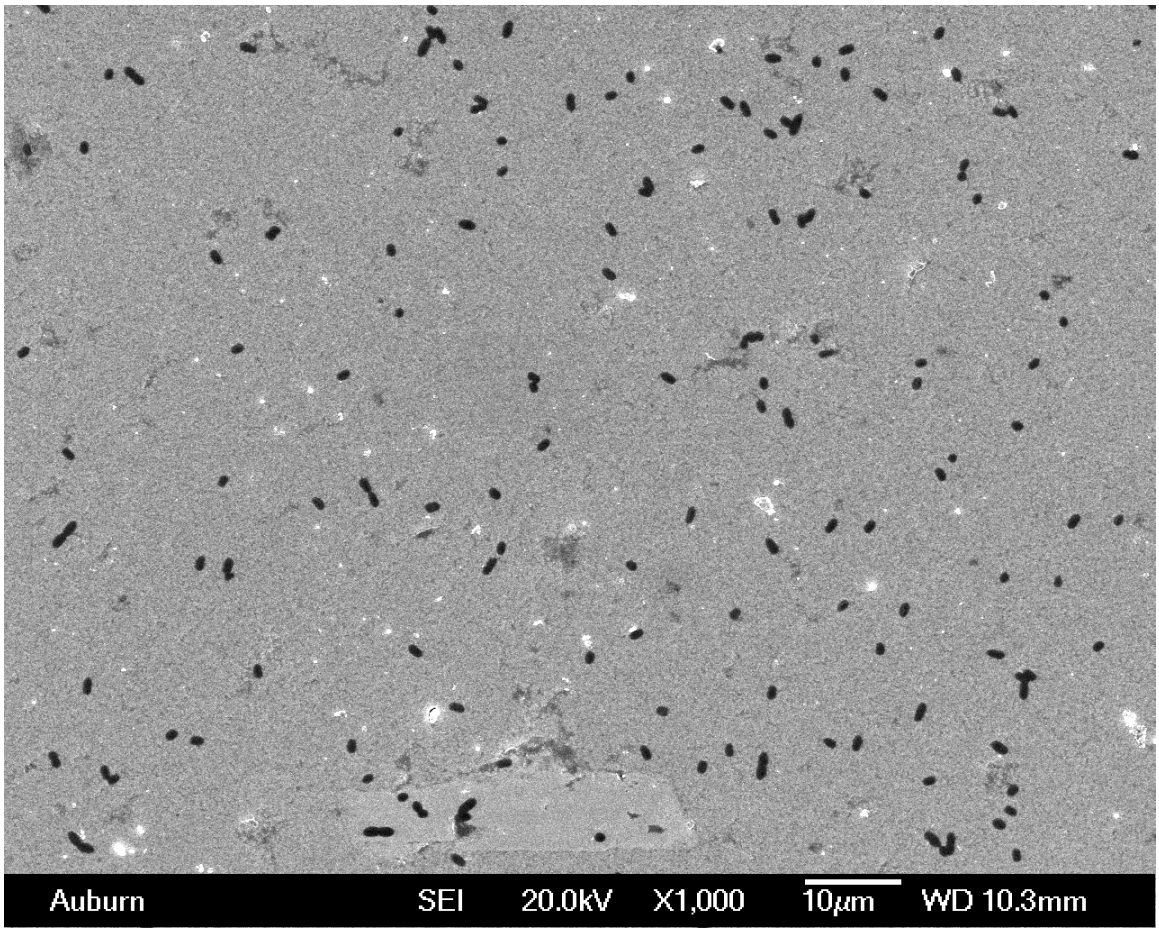

Figure 7.9: Typical SEM picture of the magnetoelastic biosensor surface after exposure to *S. typhimurium* suspension at a concentration of 5×10^6 cfu/ml.

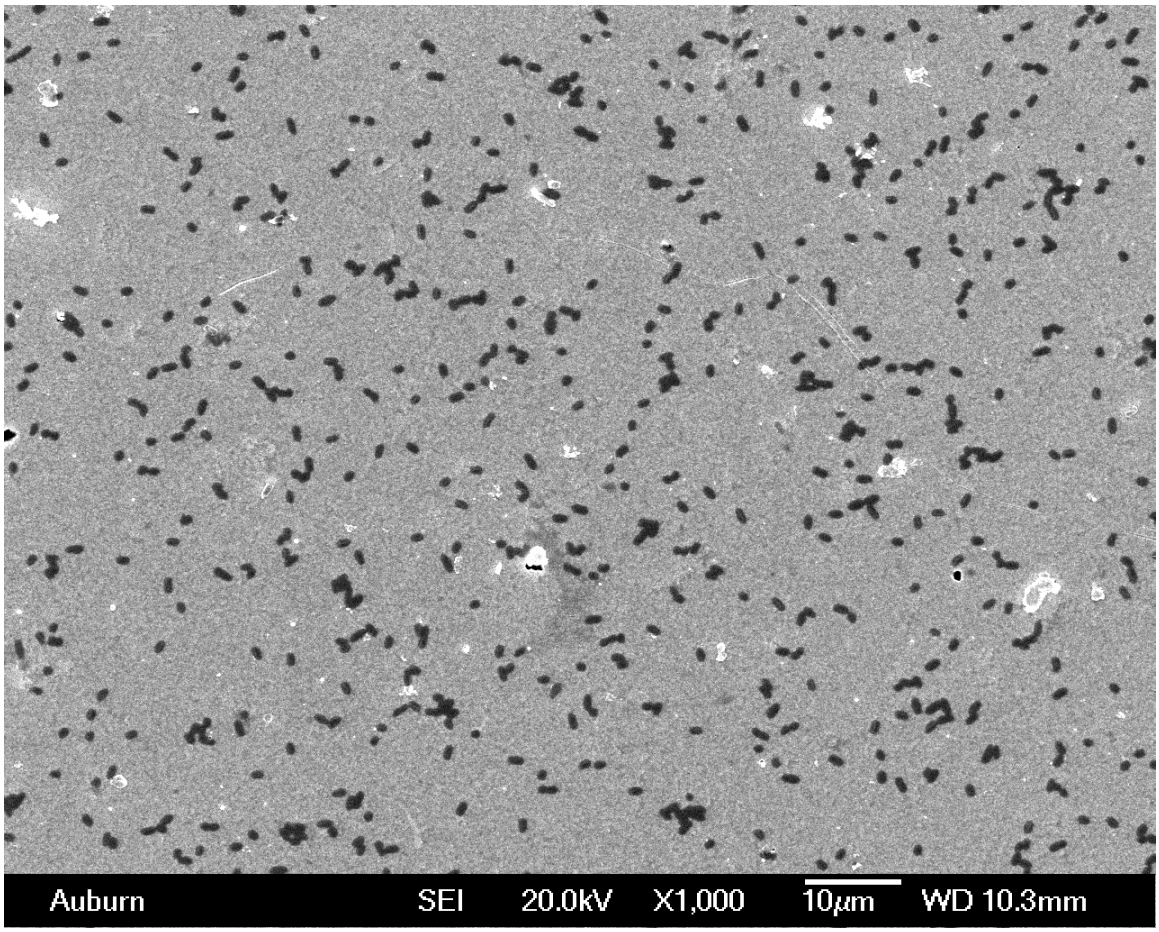

Figure 7.10: Typical SEM picture of the magnetoelastic biosensor surface after exposure to *S. typhimurium* suspension at a concentration of 5×10^7 cfu/ml.

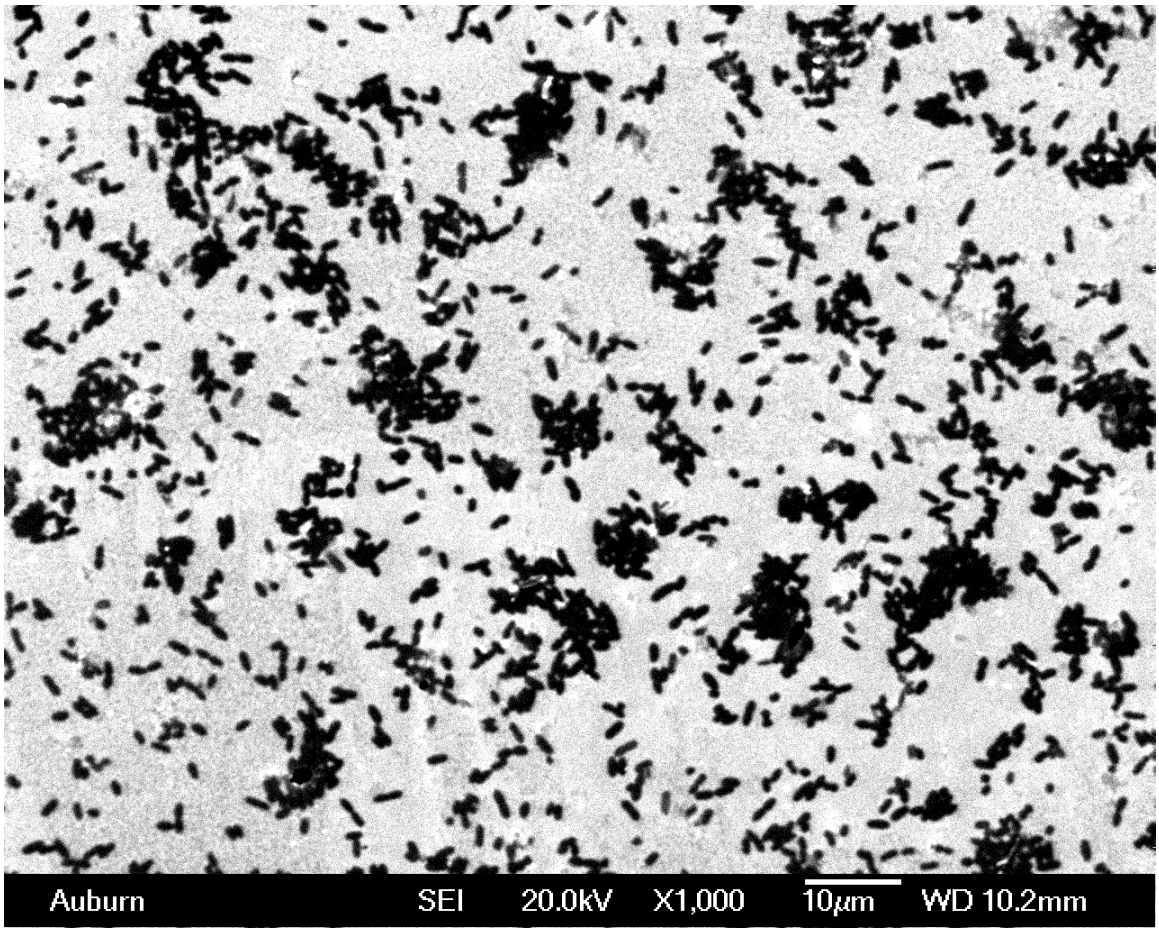

Figure 7.11: Typical SEM picture of the magnetoelastic biosensor surface after exposure to *S. typhimurium* suspension at a concentration of 5×10^8 cfu/ml.

7.3 Conclusions and Discussion

This study demonstrated the application of the pulse detection system for detecting *S. typhimurium* using magnetoelastic sensors coated with E2 phages. The detection of *S. typhimurium* utilized a dynamic binding procedure, and the frequency signals of the biosensors were measured in air. First, the detection was performed using a measurement biosensor and a control biosensor for each test. *S. typhimurium* suspensions at concentrations of 5×10^1 cfu/ml through 5×10^8 cfu/ml were tested and the detection limit was determined to be 1.8×10^4 cfu/ml. At a confidence level of 95%, we found the detection limit to be 5×10^3 cfu/ml. A linear response was found between concentrations of 5×10^4 cfu/ml and 5×10^7 cfu/ml and the sensitivity of the detection was found to be 615.75 Hz/decade. K_d was determined as 450 cfu/ml, the Hill coefficient was determined to be 0.39 and N was 2.57. Next, the detection was performed using grouped magnetoelastic sensors, where each test used 3 measurement sensors as a measurement sensor group and 3 control sensors as a control sensor group. With multiple sensors, the effect of a manufacturing defect is decreased and we get the benefit of averaging for more accurate and reliable results. The detection limit using grouped biosensors is 8×10^4 cfu/ml and a linear range was found between concentration of 5×10^5 cfu/ml to 5×10^8 cfu/ml. The sensitivity of the detection was found to be 567.48 Hz/decade and the K_d was determined to be 385 cfu/ml. The Hill coefficient was determined to be 0.31 and N was 3.25. SEM pictures and counts of bacteria were used to show that the actual frequency results closely correspond to the calculated values. It should be noted that nothing in the system would prohibit the use of multiple sensors in each transformer coil or a mixture of control sensors with measurement sensors in the transformer coils. In the future we expect to extend the testing to tens of sensors with a goal of simultaneous detection of up to 100 sensors. As sensors become very small (less than 1 mm long), they are difficult to handle, difficult to see, are easy to lose and the number of defective sensors may increase. However, a large number will still give a very reliable detection result.

Chapter 8

Optimization of Blocking on E2 Phage Based Magnetoelastic Biosensors

Blocking the non-specific binding is an essential part of biosensor development. A good blocking step should be able to block only the non-specific binding with minimum effect on the specific binding between biological recognition elements and target antigens. Specifically, for the detection of *S. typhimurium* using magnetoelastic biosensors, a good blocking step should provide maximum binding on measurement sensors that are coated with E2 phage and, at the same time, minimum binding on control sensors that are devoid of E2 phage.

One of the most common blocking reagents is Bovine Serum Albumin (BSA). It is usually used in traditional immunoassays [115], [116]. It has also been widely used in biosensors to block non-specific protein interactions [117] [118] [119] [120]. The concentration of BSA used in these applications ranges from 1mg/ml to 10 mg/ml. Optimizing the blocking step will require the optimization of the BSA concentration used in the blocking step. Besides BSA, in some immunoassays, milk and casein can also be used to block non-specific binding.

In this research, the effectiveness of blocking using different concentrations of blocking reagents, including BSA, milk and casein, for magnetoelastic biosensors was studied. Different concentrations of BSA, milk and casein were used and evaluated as blocking reagents for magnetoelastic biosensors. The BSA concentrations studied were 0.5 mg/ml, 1 mg/ml, 3 mg/ml and 5 mg/ml. The fat-free milk powder was purchased from a local grocery store and dissolved in distilled water. The concentrations of milk as a blocking reagent were 0.1 mg/ml, 0.5 mg/ml,3 mg/ml and 5 mg/ml. Casein powder was purchased from Across Organics and was dissolved in distilled water. Since the pH values of casein solutions were less than 7, NaOH solution was added to casein solutions to adjust the pH value to around 7.5

to allow best binding activity of E2 phages and also to help the casein power dissolve in the water. The concentrations of casein prepared were 0.5 mg/ml,3 mg/ml and 5 mg/ml.

The measurement biosensors were first immersed in 0.3 ml of 5×10^{11} vir/ml E2 phage and rotated on a motorized rotor at a speed of 10 RPM. After 1 hour, the phage coated sensors were washed with distilled water three times to remove the unbound or loosely bound phages. The rinsed sensors were then immersed in 0.3 ml of blocking reagent and rotated at a speed of 10 RPM for 1 hour. These sensors were then washed with distilled water twice and then dried in air. The control biosensors were prepared the same as the measurement biosensors except that the control sensors were not coated with phage. Two to three groups of measurement sensors (6 to 9 sensors) and two to three groups of control sensors (6 to 9 sensors) were used for each concentration of each blocking reagent. The measurement sensors and control sensors were exposed to 10 μl of 5×10^8 cfu/ml *S. typhimurium* suspension in 85% humidity for 1 hour. The sensors were then washed with distilled water 3 times. The resonance frequencies of the groups of sensors before and after the exposure of *S. typhimurium* were measured using the pulse detection system. After frequency measurements, the sensors were exposed to OsO_4 for 45 minutes, and then observed using the SEM.

The following figures are typical SEM pictures of sensor surfaces that were treated with different concentrations of BSA, milk and casein.

The area coverage of *Salmonella* on sensors were computed and the average *Salmonella* coverage on sensors were calculated for each blocking condition. Figure 8.12, 8.13 and 8.14 are the average area coverage of *Salmonella* on magnetoelastic sensor surfaces that were blocked with different concentrations of BSA, milk and casein. From these results, the control sensors that were blocked with BSA, milk and casein have similar *Salmonella* coverage, all of which are around 10%. The measurement sensors that were blocked with milk and casein give *Salmonella* coverage around 20%. However, the measurement sensors that were blocked with 1mg/ml BSA show *Salmonella* coverage up to about 35%. By using

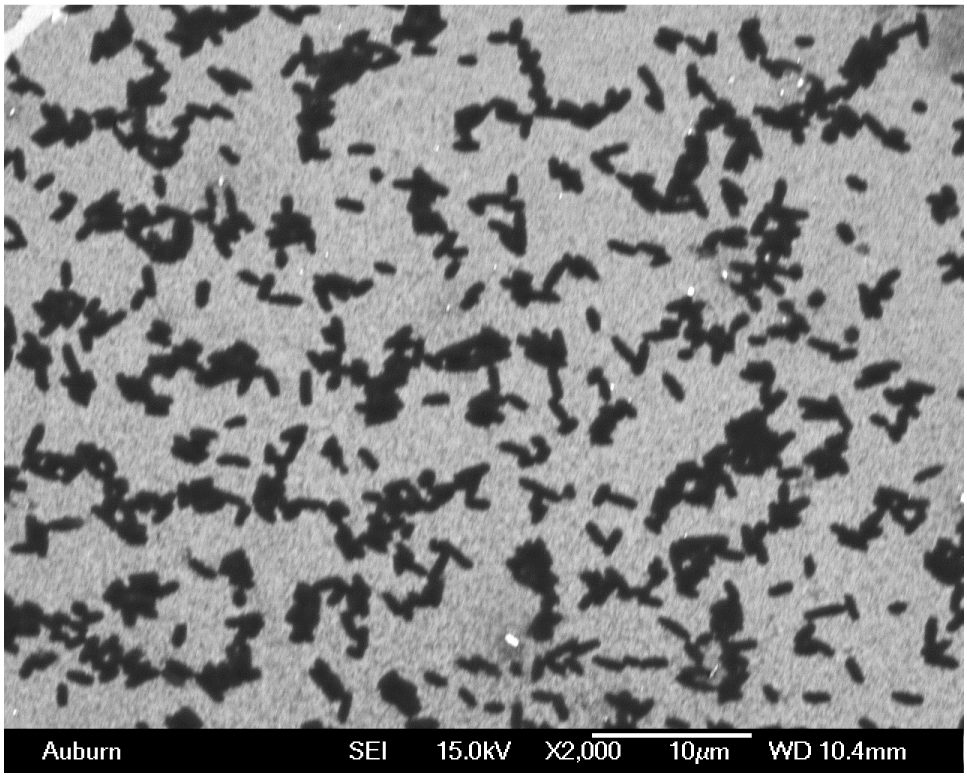

(a) Measurement sensor

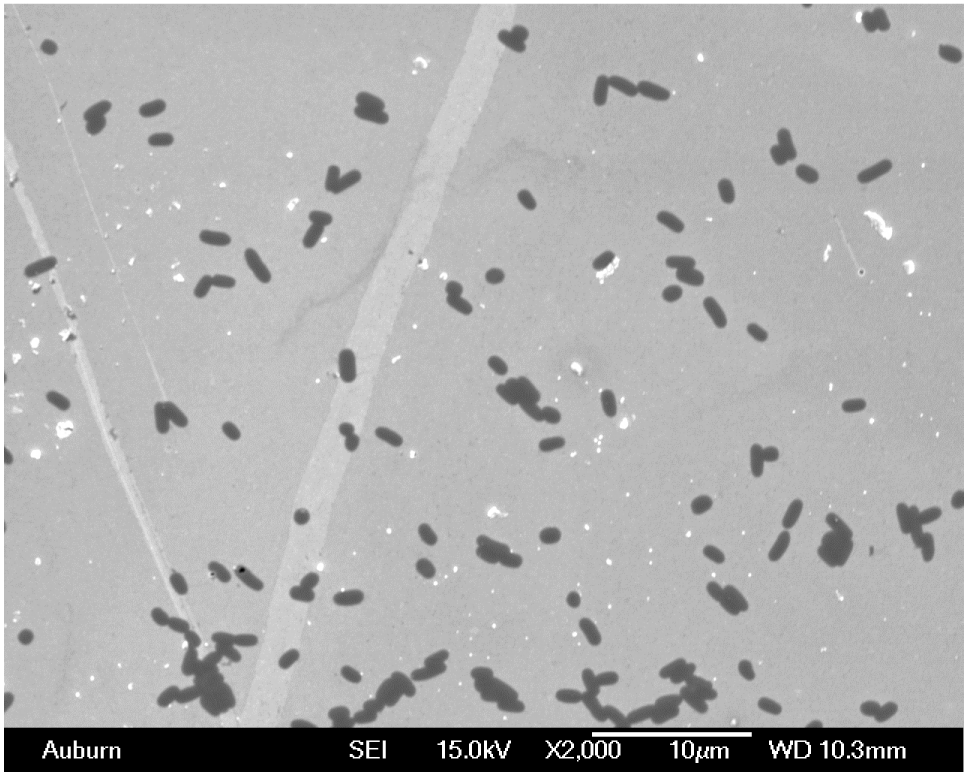

(b) Control sensor

Figure 8.1: Typical SEM picture of the magnetoelastic biosensors blocked with 0.5 mg/ml BSA after exposure to 5×10^8 cfu/ml *S. typhimurium* suspension.

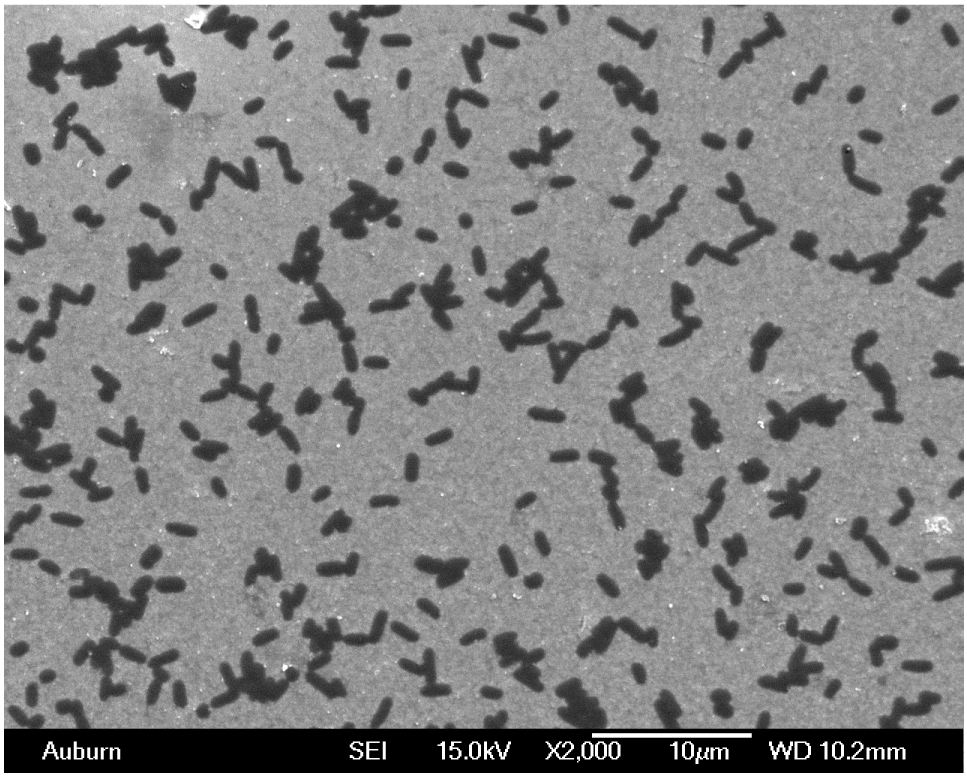

(a) Measurement sensor

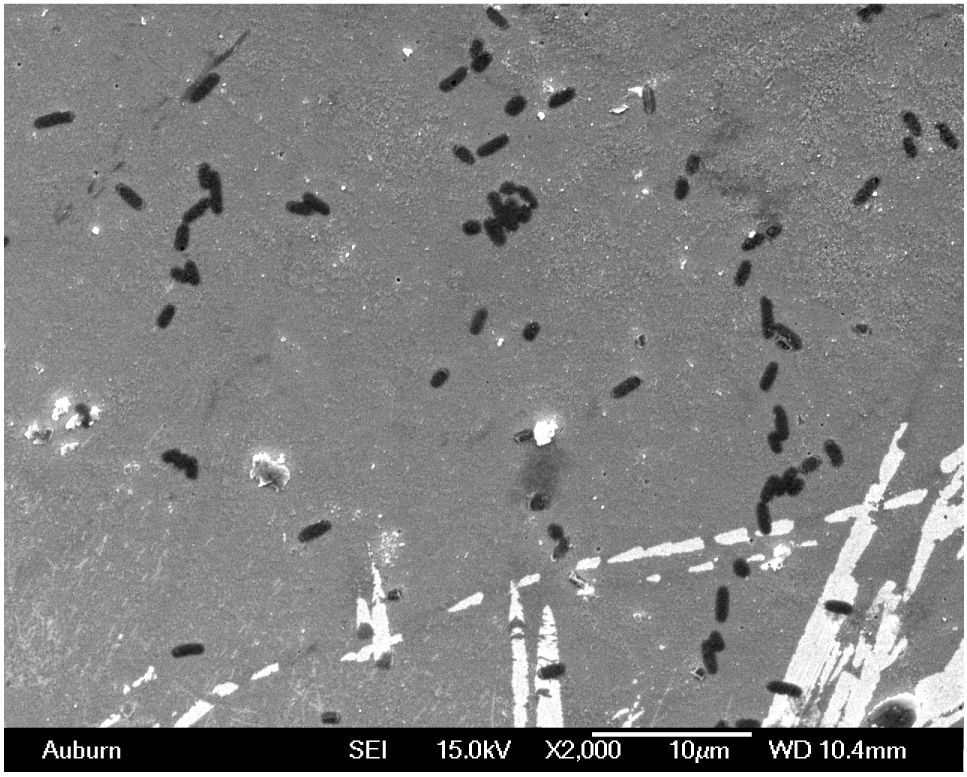

(b) Control sensor

Figure 8.2: Typical SEM picture of the magnetoelastic biosensors blocked with 1 mg/ml BSA after exposure to 5×10^8 cfu/ml *S. typhimurium* suspension.

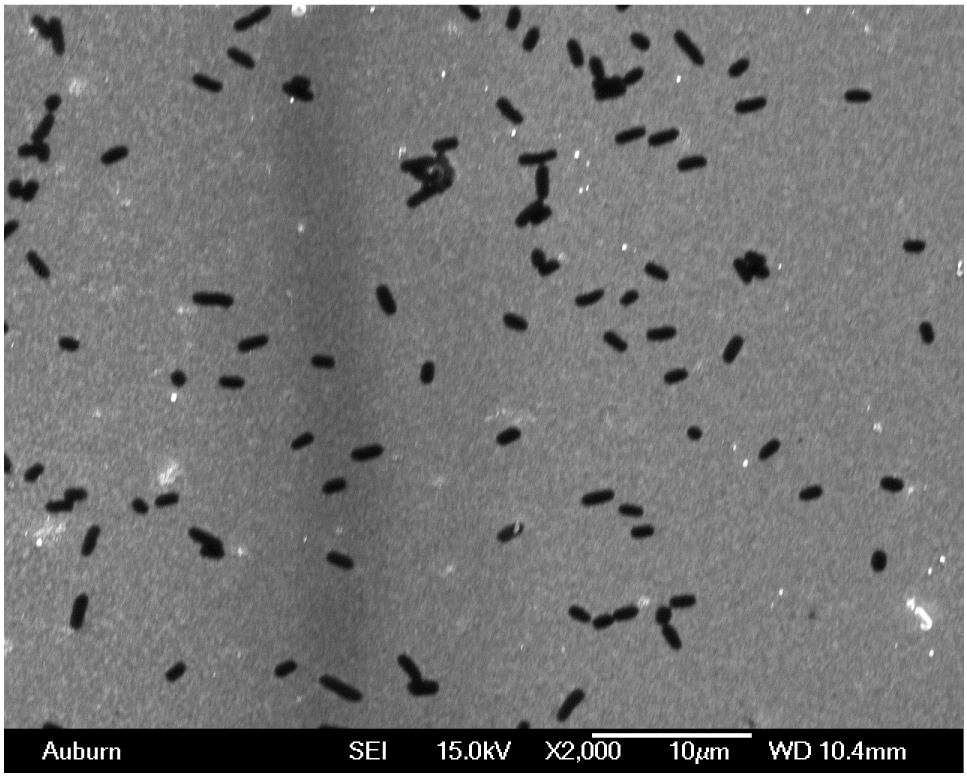

(a) Measurement sensor

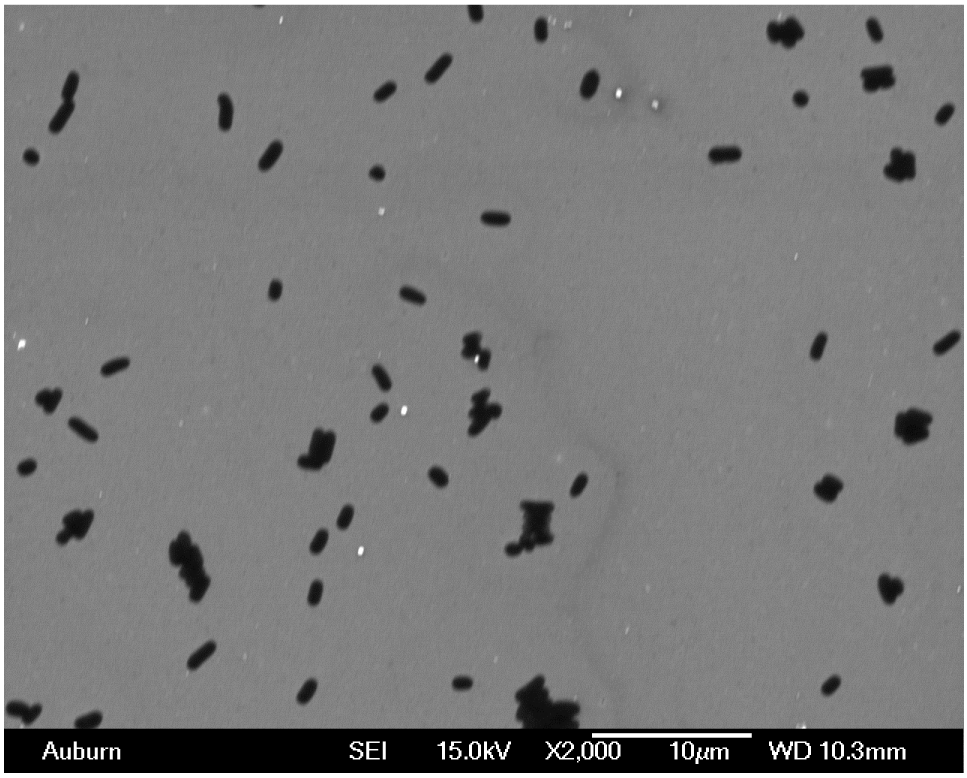

(b) Control sensor

Figure 8.3: Typical SEM picture of the magnetoelastic biosensors blocked with 3 mg/ml BSA after exposure to 5×10^8 cfu/ml *S. typhimurium* suspension.

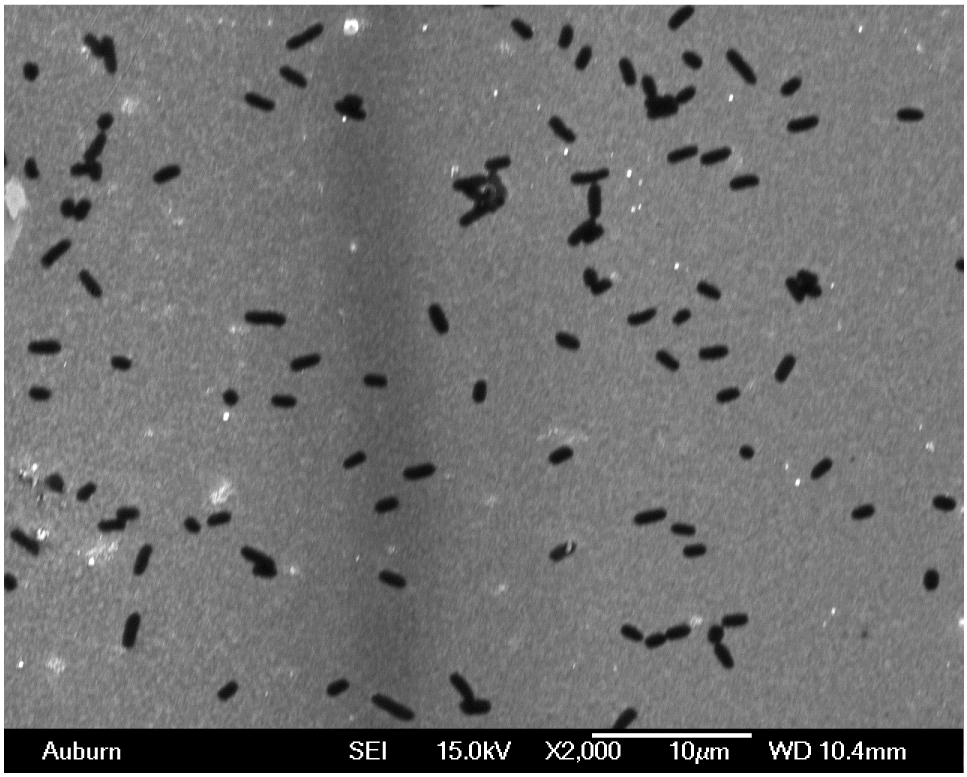

(a) Measurement sensor

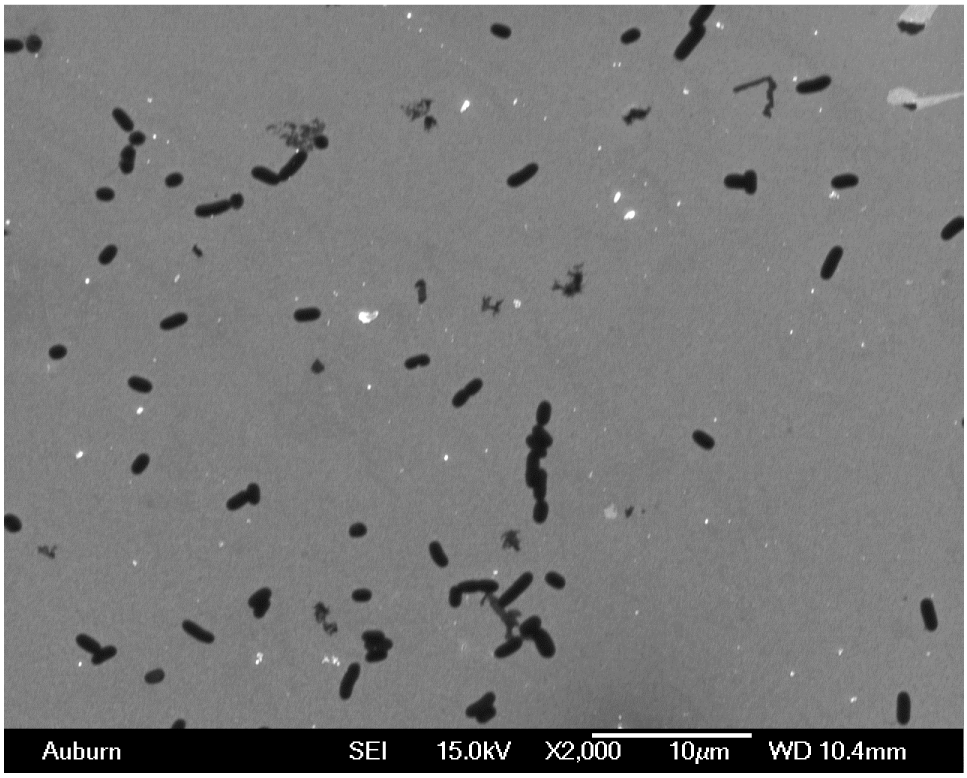

(b) Control sensor

Figure 8.4: Typical SEM picture of the magnetoelastic biosensors blocked with 5 mg/ml BSA after exposure to 5×10^8 cfu/ml *S. typhimurium* suspension.

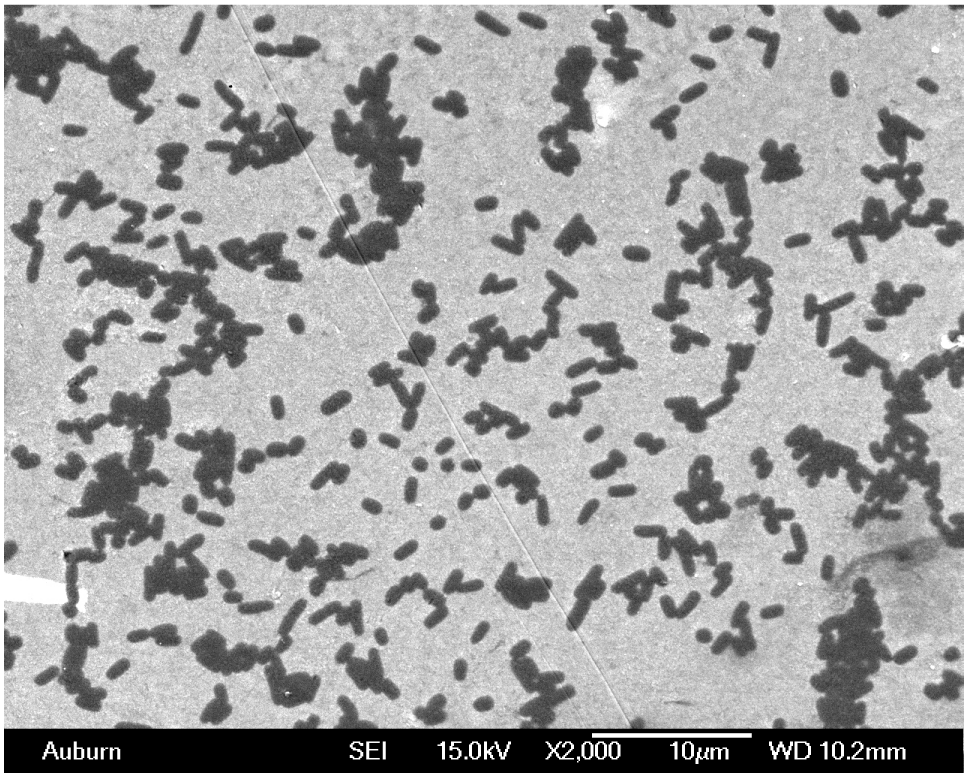

(a) Measurement sensor

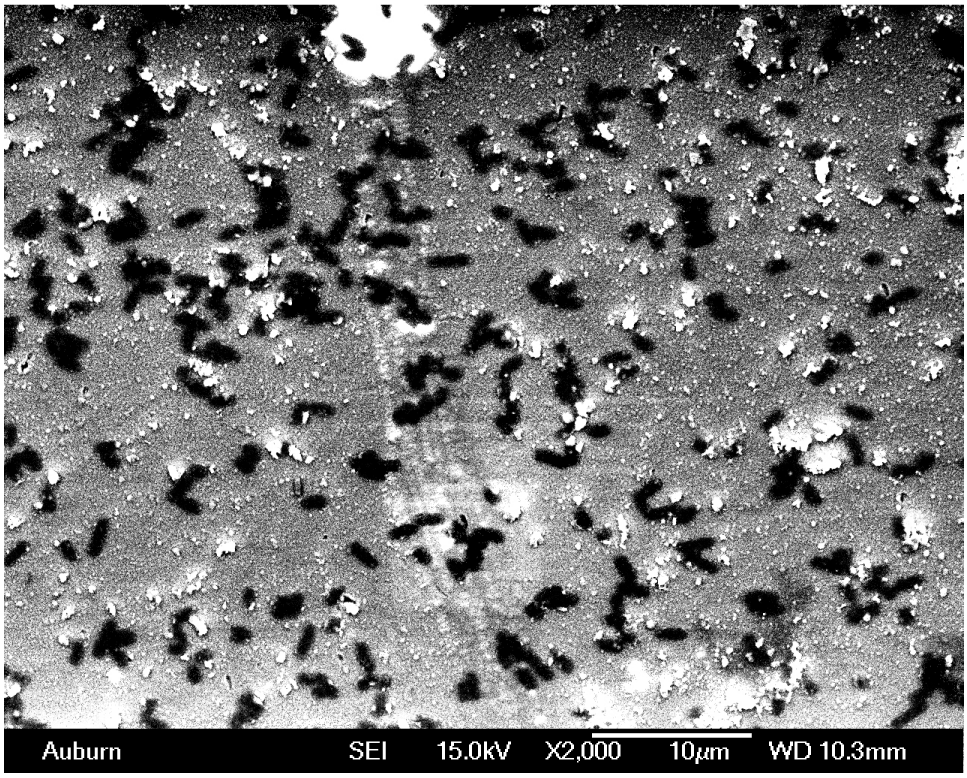

(b) Control sensor

Figure 8.5: Typical SEM picture of the magnetoelastic biosensors blocked with 0.1 mg/ml milk after exposure to 5×10^8 cfu/ml *S. typhimurium* suspension.

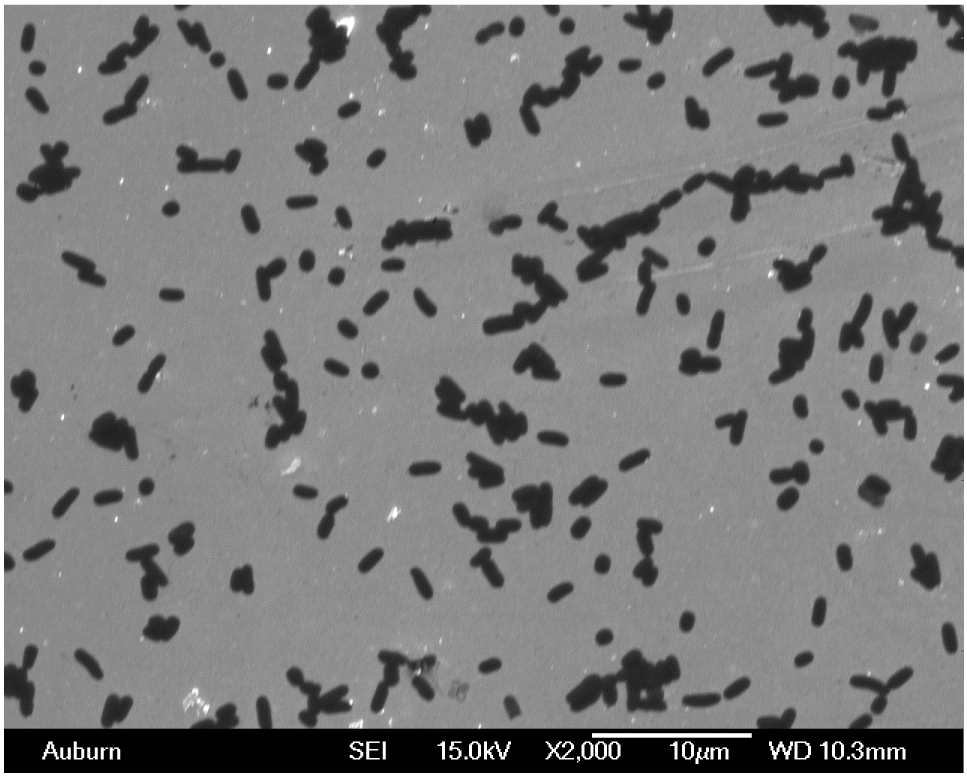

(a) Measurement sensor

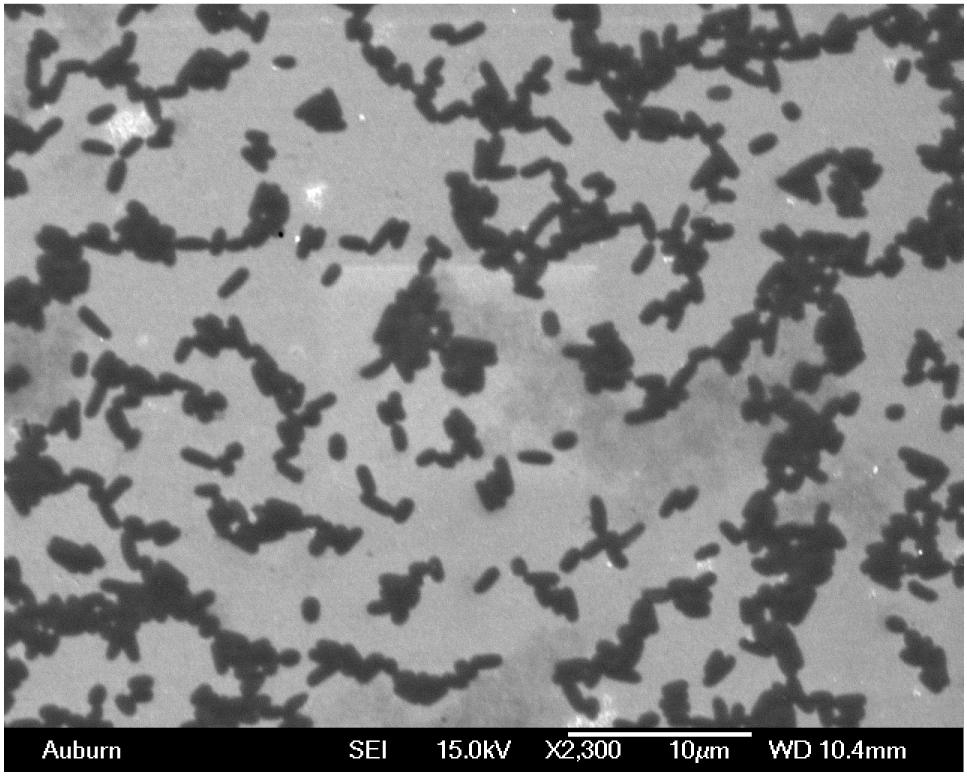

(b) Control sensor

Figure 8.6: Typical SEM picture of the magnetoelastic biosensors blocked with 0.5 mg/ml milk after exposure to 5×10^8 cfu/ml *S. typhimurium* suspension.

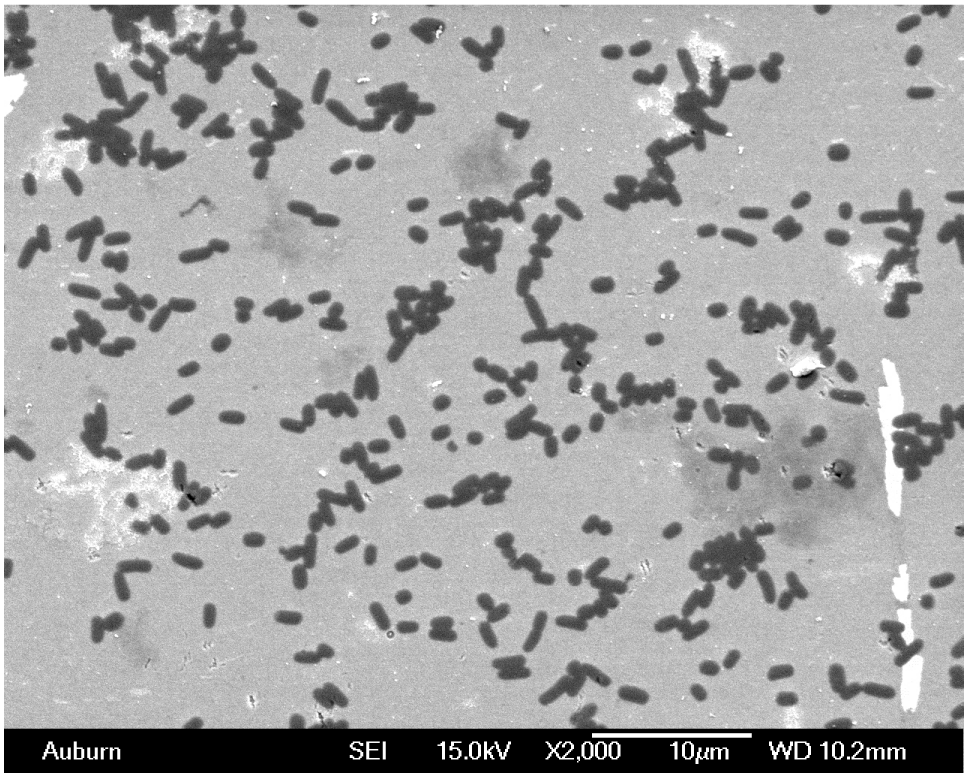

(a) Measurement sensor

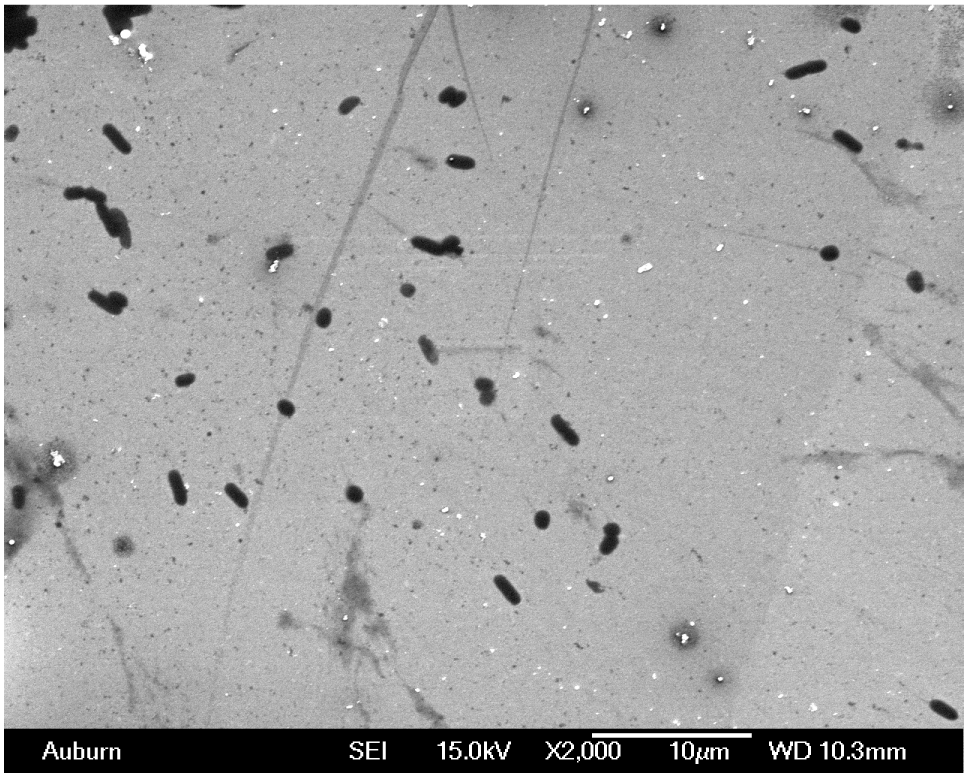

(b) Control sensor

Figure 8.7: Typical SEM picture of the magnetoelastic biosensors blocked with 3 mg/ml milk after exposure to 5×10^8 cfu/ml *S. typhimurium* suspension.

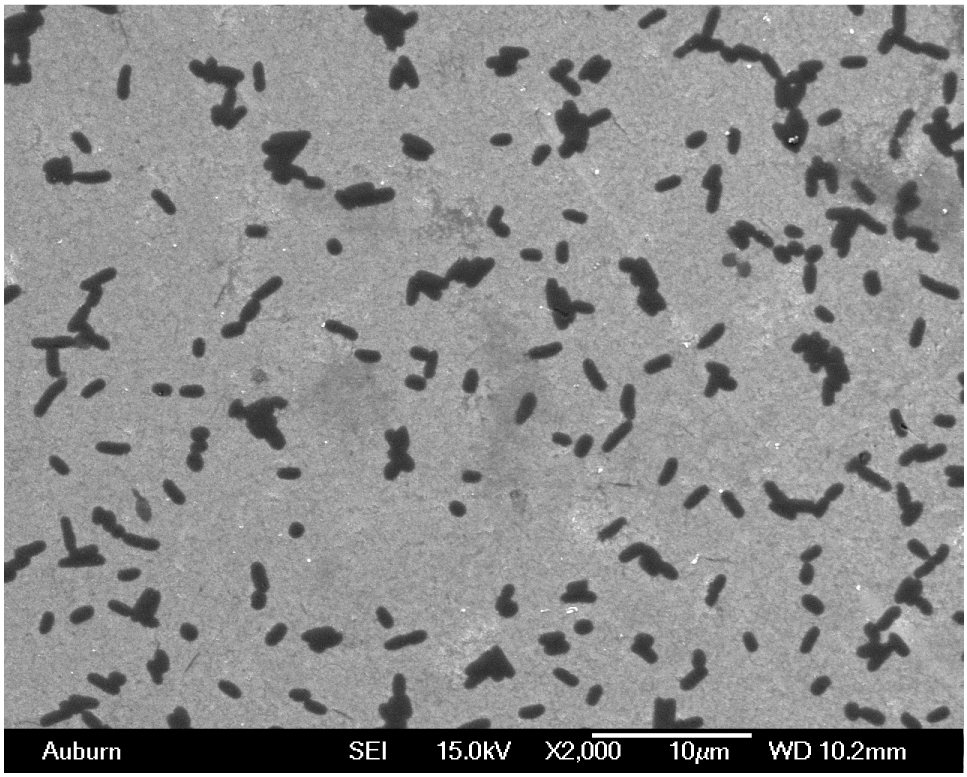

(a) Measurement sensor

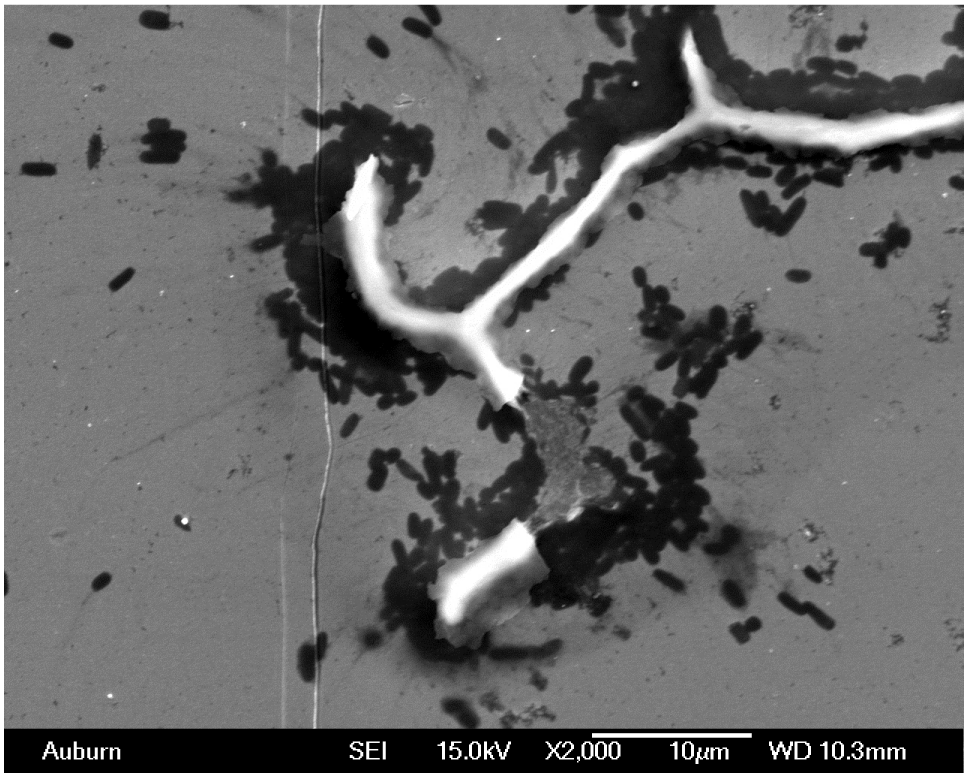

(b) Control sensor

Figure 8.8: Typical SEM picture of the magnetoelastic biosensors blocked with 5 mg/ml milk after exposure to 5×10^8 cfu/ml *S. typhimurium* suspension.

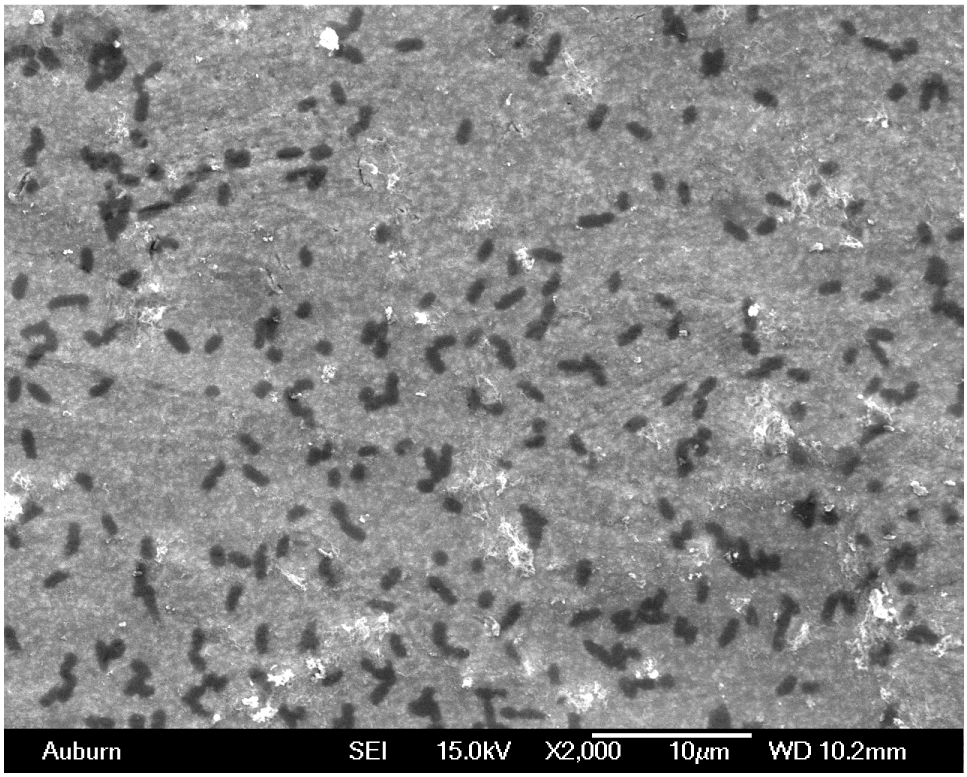

(a) Measurement sensor

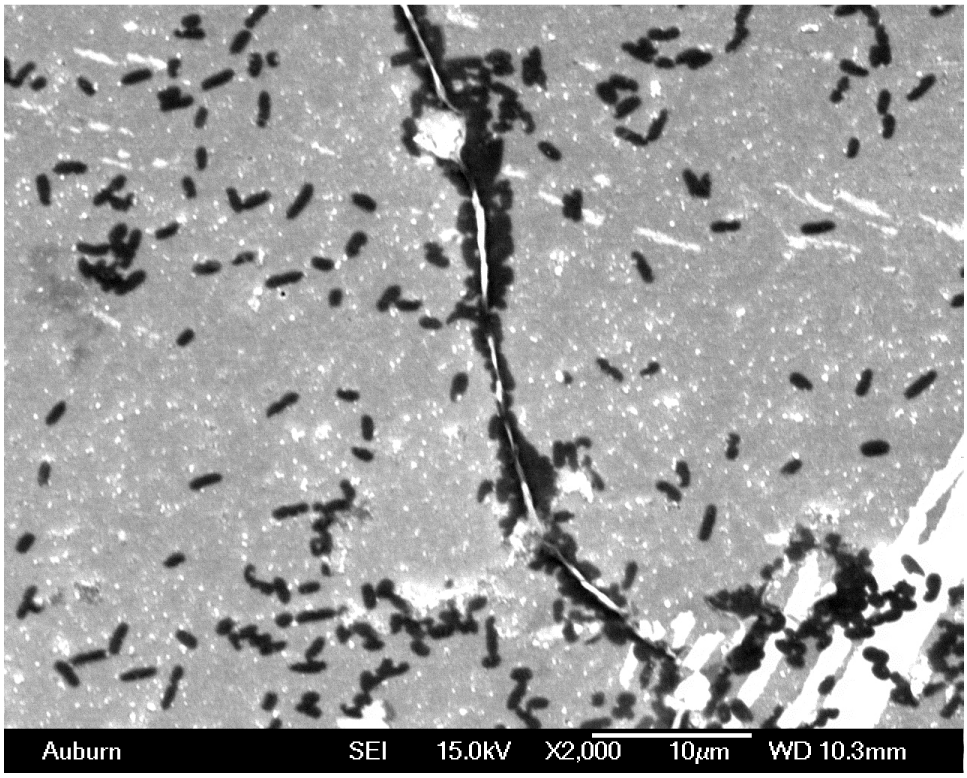

(b) Control sensor

Figure 8.9: Typical SEM picture of the magnetoelastic biosensors blocked with 0.5 mg/ml casein after exposure to 5×10^8 cfu/ml *S. typhimurium* suspension.

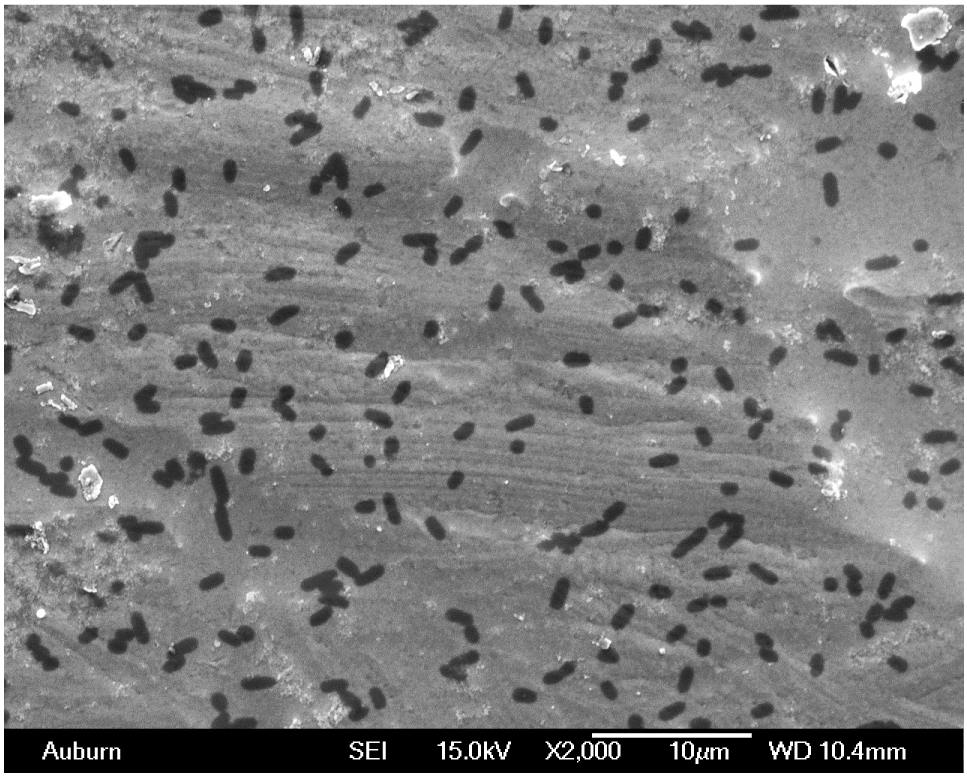

(a) Measurement sensor

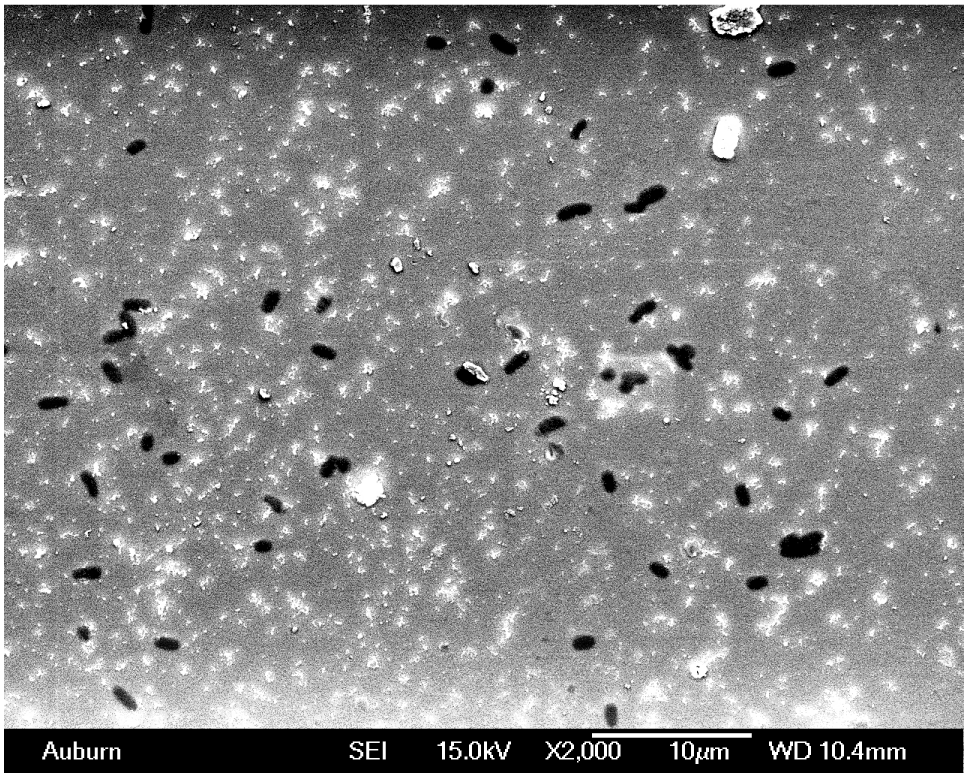

(b) Control sensor

Figure 8.10: Typical SEM picture of the magnetoelastic biosensors blocked with 1 mg/ml casein after exposure to 5×10^8 cfu/ml *S. typhimurium* suspension.

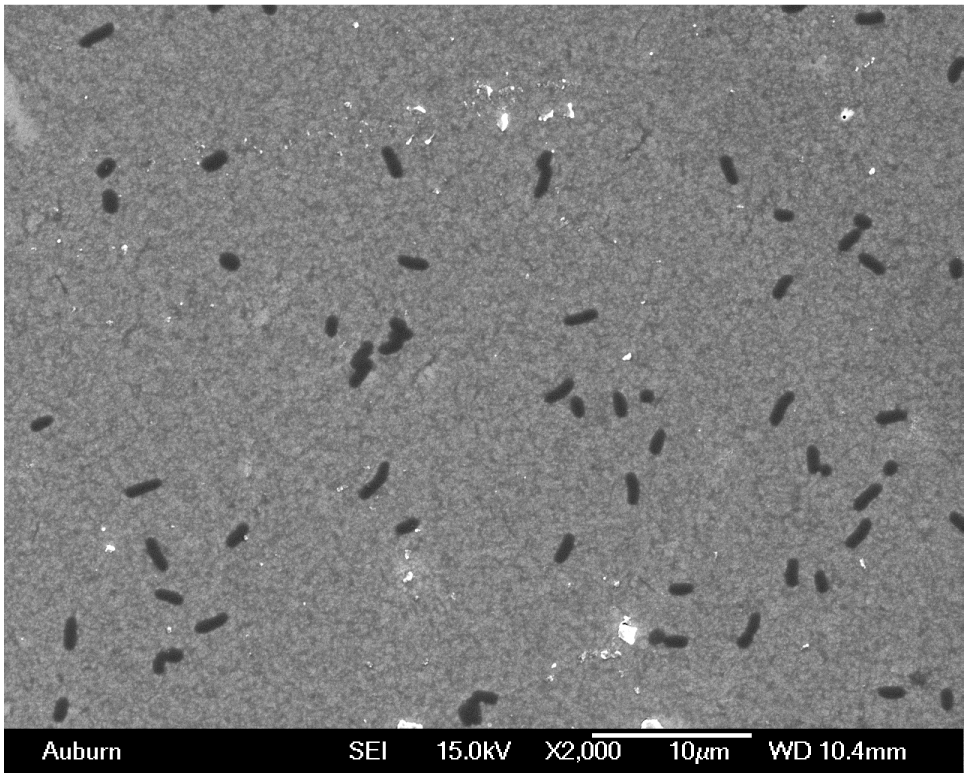

(a) Measurement sensor

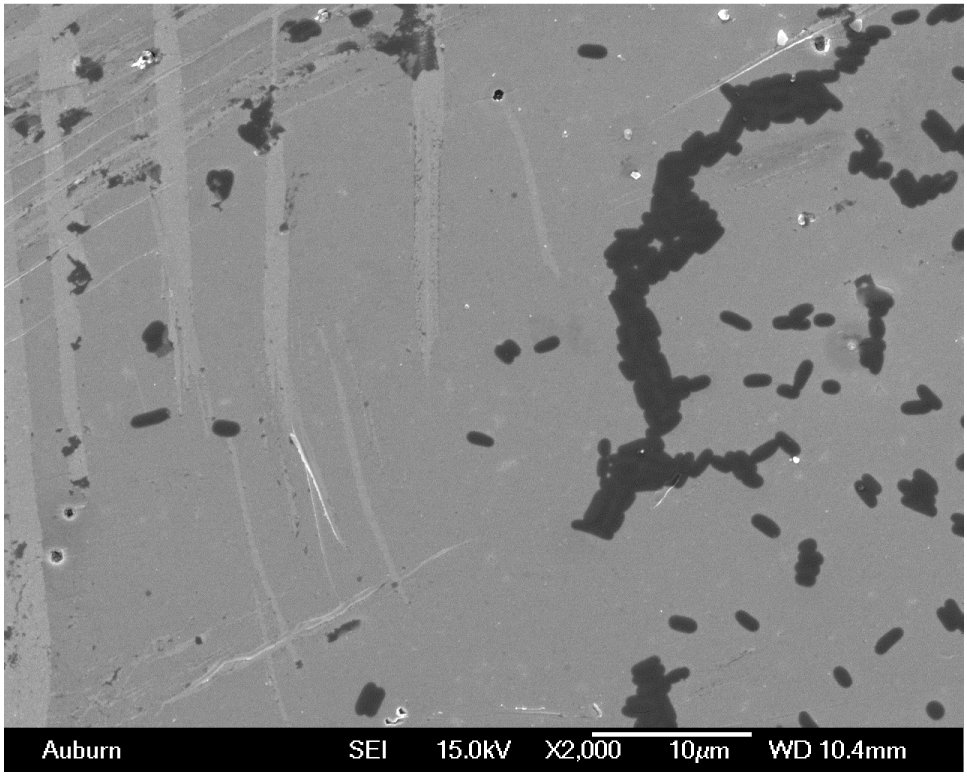

(b) Control sensor

Figure 8.11: Typical SEM picture of the magnetoelastic biosensors blocked with 5 mg/ml casein after exposure to 5×10^8 cfu/ml *S. typhimurium* suspension.

this blocking condition, the binding of *Salmonella* on control sensors is less then 15% of *Salmonella* binding on measurement sensors.

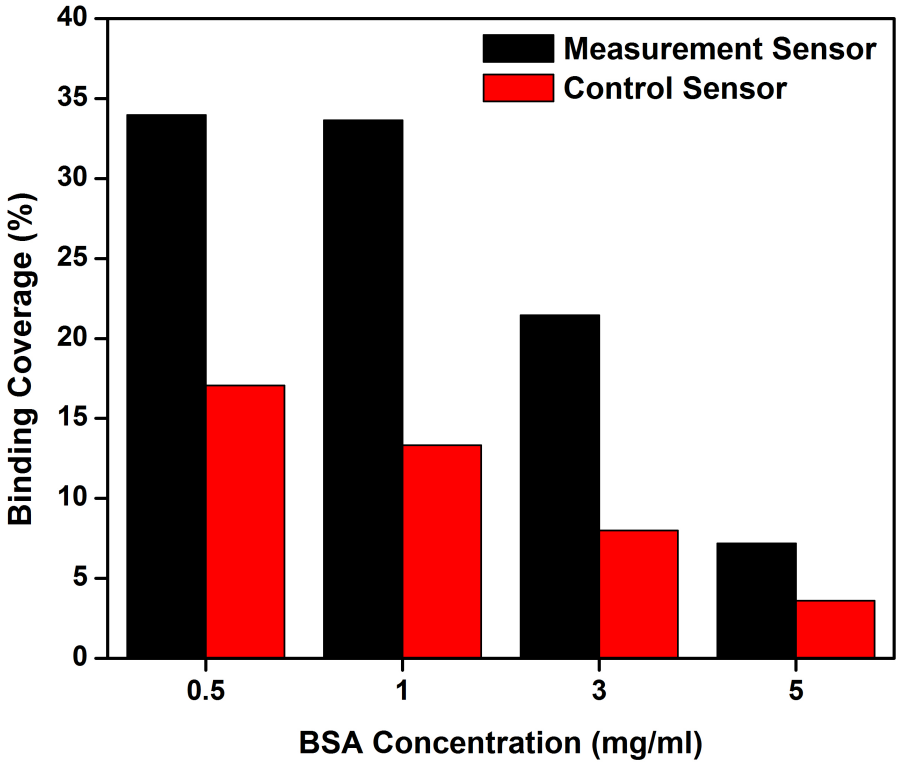

Figure 8.12: Average of bound *Salmonella* cell coverage on magnetoelastic biosensor surfaces that were blocked with different concentrations of BSA after exposure to 5×10^8 cfu/ml *S. typhimurium* suspension.

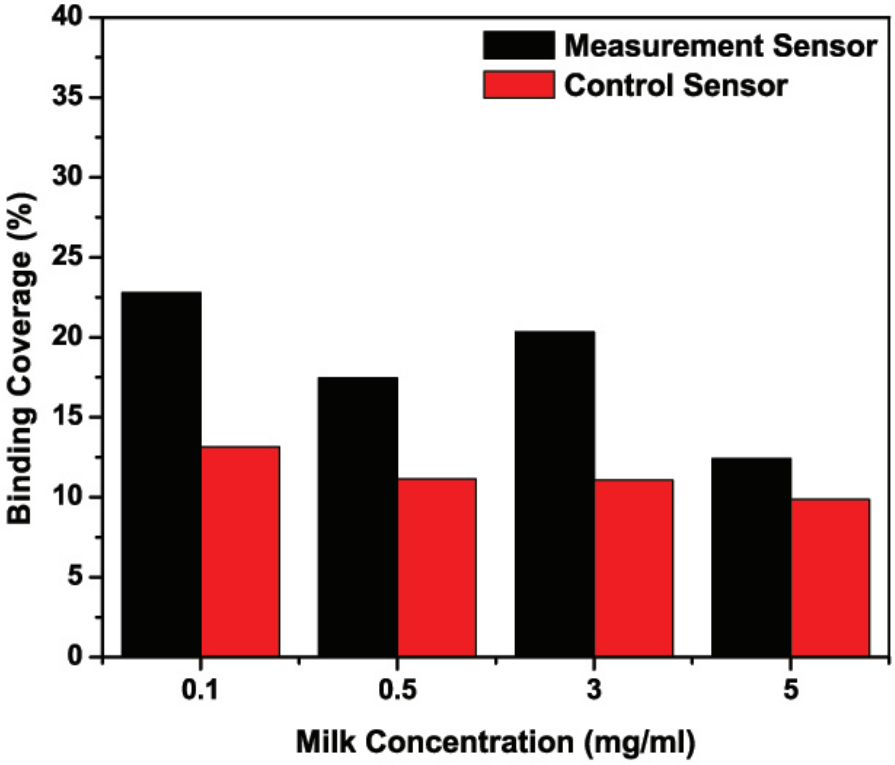

Figure 8.13: Average of bound *Salmonella* cell coverage on magnetoelastic biosensor surfaces that were blocked with different concentrations of milk after exposure to 5×10^8 cfu/ml *S. typhimurium* suspension.

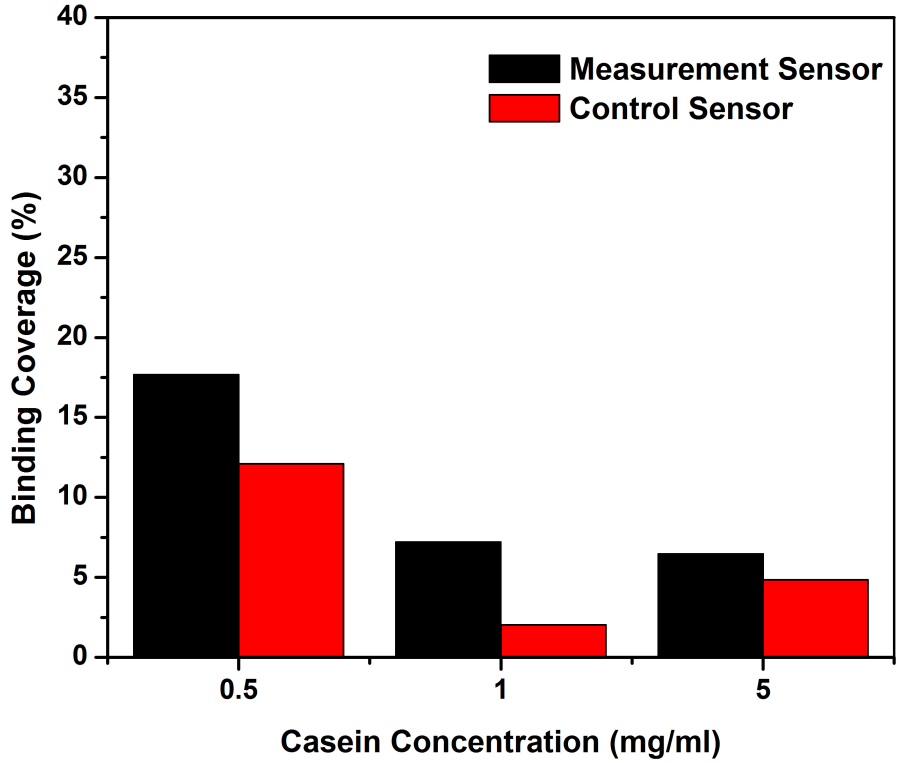

Figure 8.14: Average of bound *Salmonella* cell coverage on magnetoelastic biosensor surfaces that were blocked with different concentrations of casein after exposure to 5×10^8 cfu/ml *S. typhimurium* suspension.

Figure 8.15, 8.16 and 8.17 are the resonant frequency shifts of magnetoelastic sensors that were blocked with different concentrations of BSA, milk and casein. These frequency shifts results are consistent with the actual *S. typhimurium* coverage results.

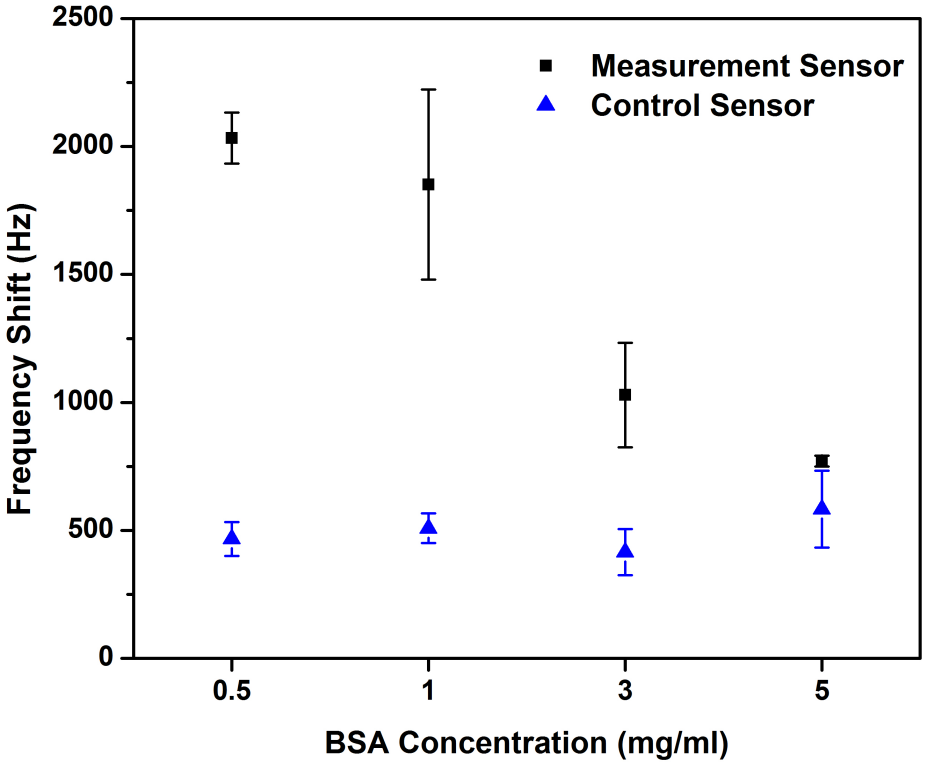

Figure 8.15: Frequency shifts of magnetoelastic biosensors that were blocked with different concentrations of BSA after exposure to 5×10^8 cfu/ml *S. typhimurium* suspension.

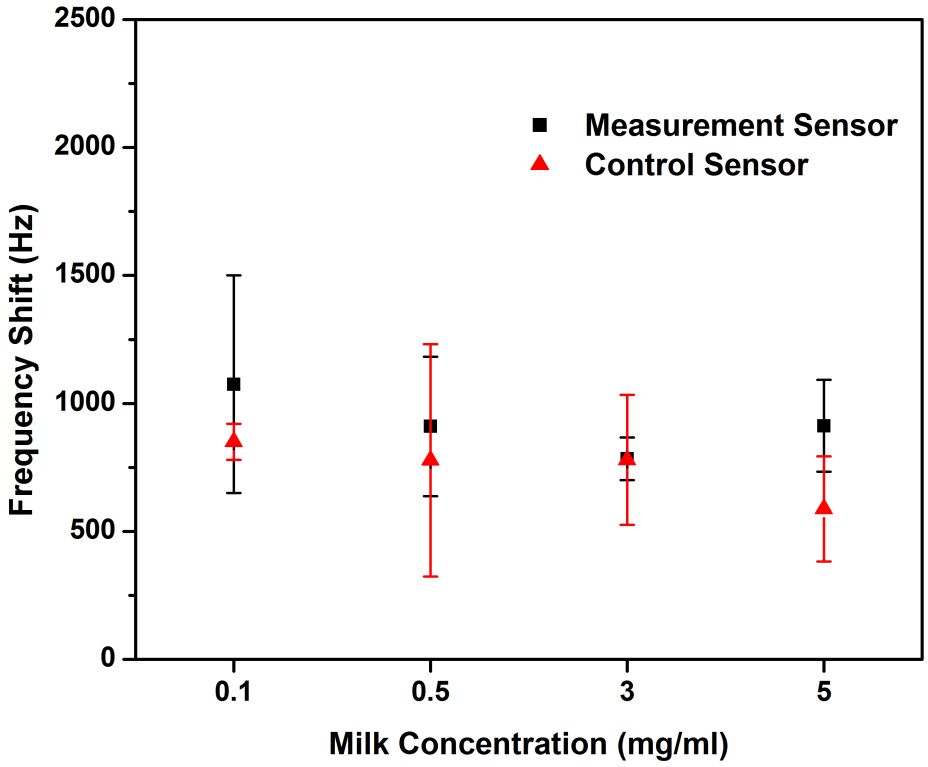

Figure 8.16: Frequency shifts of magnetoelastic biosensors that were blocked with different concentrations of milk after exposure to 5×10^8 cfu/ml *S. typhimurium* suspension.

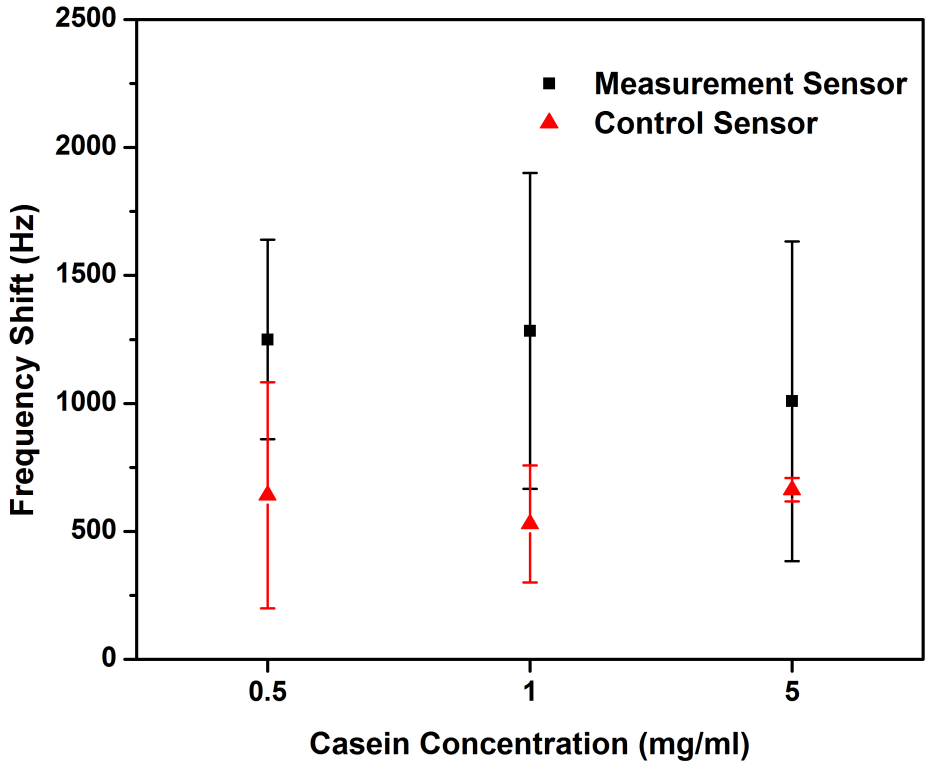

Figure 8.17: Frequency shifts of magnetoelastic biosensors that were blocked with different concentrations of casein after exposure to 5×10^8 cfu/ml *S. typhimurium* suspension.

In conclusion, this chapter studied the effectiveness of different concentrations of BSA, milk and casein as blocking reagents for magnetoelastic biosensors. The actual coverage of bound *S. typhimurium* were computed from SEM photographs of sensor surfaces, and the resonant frequency shifts of groups of sensors were measured using the pulse detection system. The results show that 1mg/ml BSA has the best blocking effect for E2 phage based magnetoelastic biosensors, while milk and casein have similar but less blocking effect on the magnetoelastic biosensors.

Chapter 9

Detection of *S. Typhimurium* on Cantaloupe Surface Using Multiple Magnetoelastic Sensors

9.1 Detection of *S. typhimurium* on Cantaloupe Surface

The detection of *S. typhimurium* was implemented directly on cantaloupe surfaces to duplicate a real situation of *Salmonella* contamination. The cantaloupes used in this experiment were purchased from local grocery stores and then washed and dried with a nitrogen flow. *S. typhimurium* 29631 AMES strain, a wild-type *Salmonella* strain, was used. A 20 μL *Salmonella* suspension was spiked onto the surface of cantaloupe using a pipette. The drop of *Salmonella* was then allowed to dry in room air at room temperature where the room air is controlled to a relative humidity of approximately 35 percent. After the *Salmonella* suspension dries for 3 to 5 minutes in air, three sensors were placed on each area occupied by the *Salmonella* as shown in Figure 9.1. Some areas had three measurement sensors and some had three control sensors. The measurement sensors to be used for measuring the *Salmonella* were coated with E2 phage. The control sensors were the same as the measurement sensors but had no phage. Next, the cantaloupe was placed in a humidity chamber of 85% relative humidity and remained there for 30 minutes, after which the sensors were removed for measurement. This procedure was performed for 8 different concentrations, ranging from 5×10^1 cfu/ml through 5×10^8 cfu/ml. Each concentration was tested with 5 sets of measurement sensors (15 sensors) and 5 sets of control sensors (15 control sensors).

Figure 9.1: Three magnetoelastic sensors for simultaneously detecting *S. typhimurium* directly on the cantaloupe surface. Sensor Dimensions: 2000 $\times$ 400 $\times$ 15 μm.

Figure 9.2 is a typical measurement sensor group response to 5×10^8 cfu/ml *S. typhimurium* suspension spiked on cantaloupe surface. A scaling factor of 0.8 was used for the after *S. typhimurium* exposure curve. All three sensors in the measurement group show decreases in their resonant frequencies after exposure to the contaminated cantaloupe surface. The frequency decreases of the three sensors are 3.67 kHz, 2.80 kHz and 2.23 kHz, respectively. The average frequency change of this group of sensors is 2.90 kHz. The variance in the frequency shifts is due to the non-uniform distribution of the *Salmonella* cells on the cantaloupe surface. The uneven distribution is due to the roughness of the cantaloupe surface and also to the uneven drying of the solution spiked onto the cantaloupe surface. As the solution dries, the *Salmonella* will congregate to the last areas of moisture and form clumps of *Salmonella*. Figure 9.4(b) shows quite dramatically the uneven distribution of *Salmonella* attached to the sensor where a black area contains a high concentration of *Salmonella* and the area on either side containing almost no *Salmonella*.

The control sensors that are devoid of E2 phage are designed to be not able to bind with *S. typhimurium*and only provide a reference signal caused by environmental changes or system errors. Figure 9.3 shows a typical result of detection using a group of control sensors. A scaling factor of 0.8 was used for the after *S. typhimurium* exposure curve. All of the three sensors show small frequency shifts as compared to the much larger frequency shift of the measurement sensors. In the test shown in Figure 9.3, after exposure to cantaloupe surfaces spiked with 5×10^8 cfu/ml *S. typhimurium* suspension, the frequency shifts of the three control sensors are only 120 Hz, 425 Hz and 130 Hz, respectively. The average frequency change of this group of sensors is 225 Hz. This number is dramatically different from the average frequency shift of measurement sensors obtained from Figure 9.2. The SEM photograph of the control sensor (Figure 9.5) shows only a few *Salmonella* cells. This confirms the results from the frequency shifts.

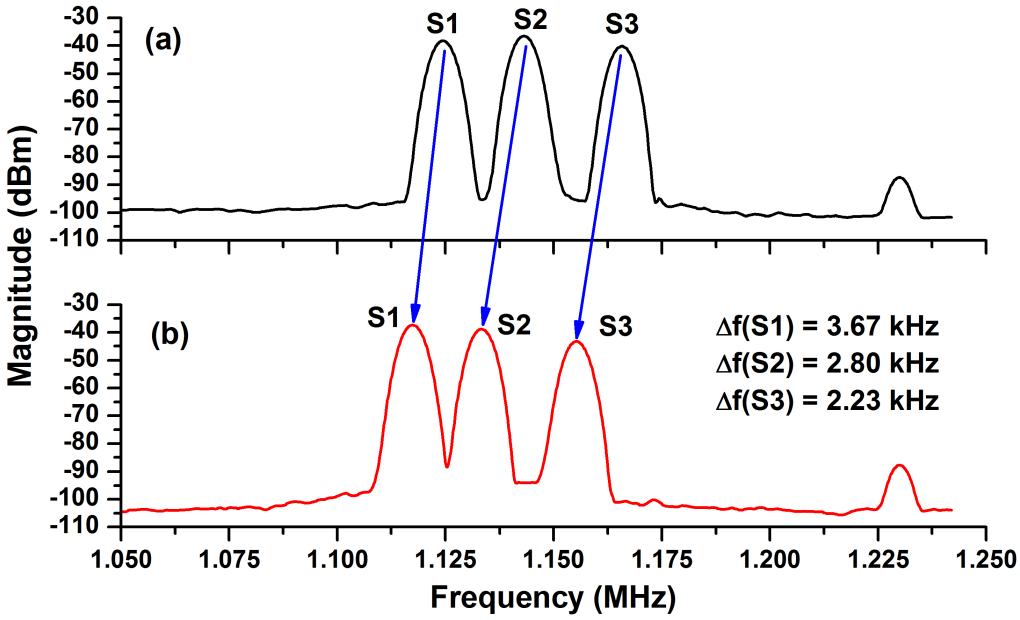

Figure 9.2: Typical response of a group of three measurement sensors before and after the detection of *S. typhimurium* suspensions (5×10^8 cfu/ml) on cantaloupe surface.

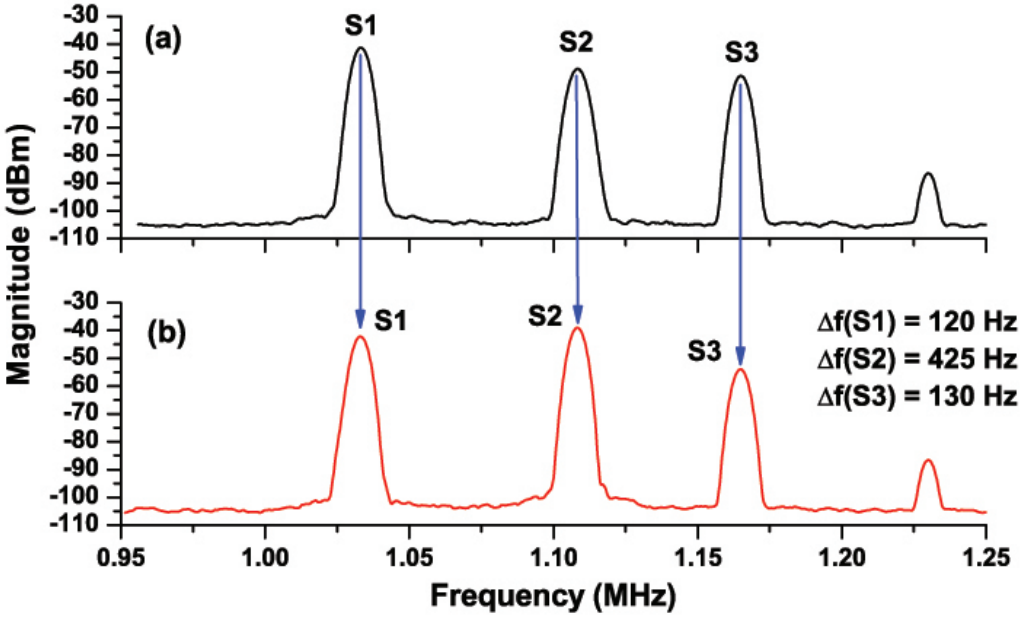

Figure 9.3: Typical response of a group of three control sensors before and after the detection of *S. typhimurium* suspensions (5×10^8 cfu/ml) on cantaloupe surface.

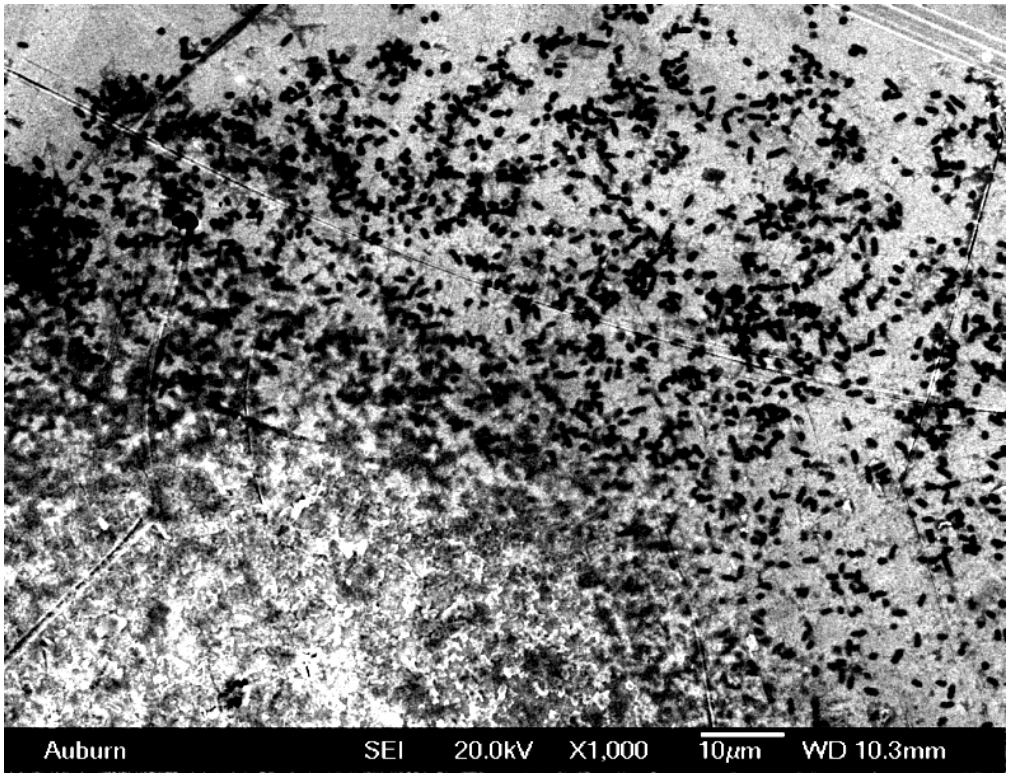

(a)

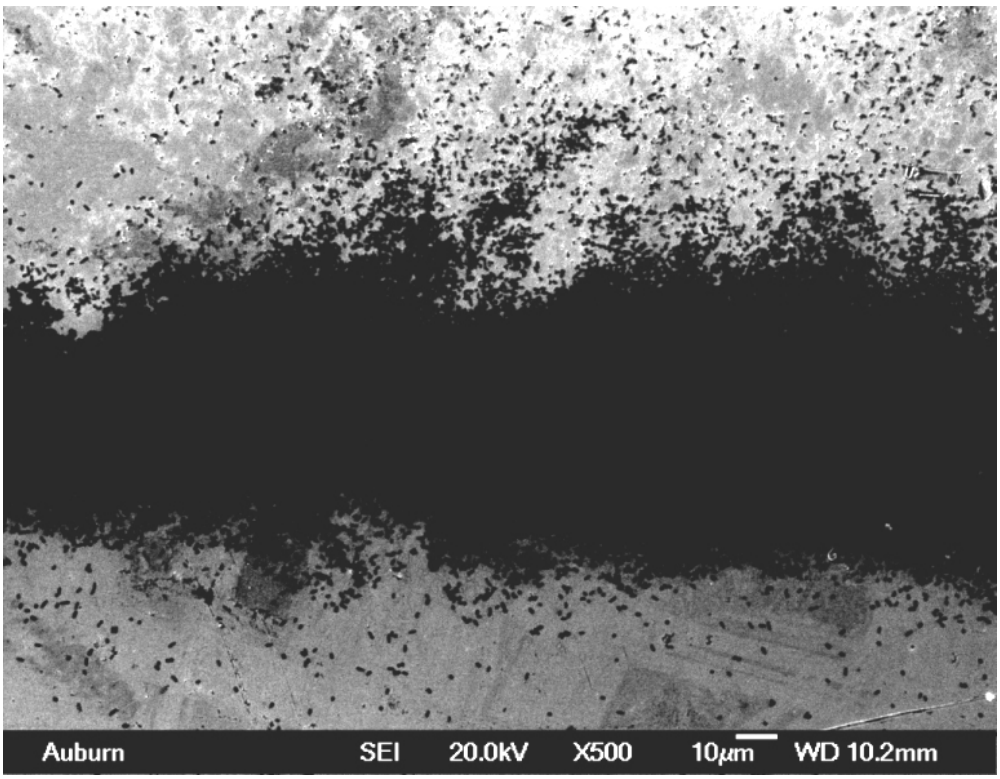

(b)

Figure 9.4: Typical SEM picture of the measurement biosensors after binding with *S. typhimurium* suspension at concentration of 5×10^8 cfu/ml spiked on cantaloupe surface.

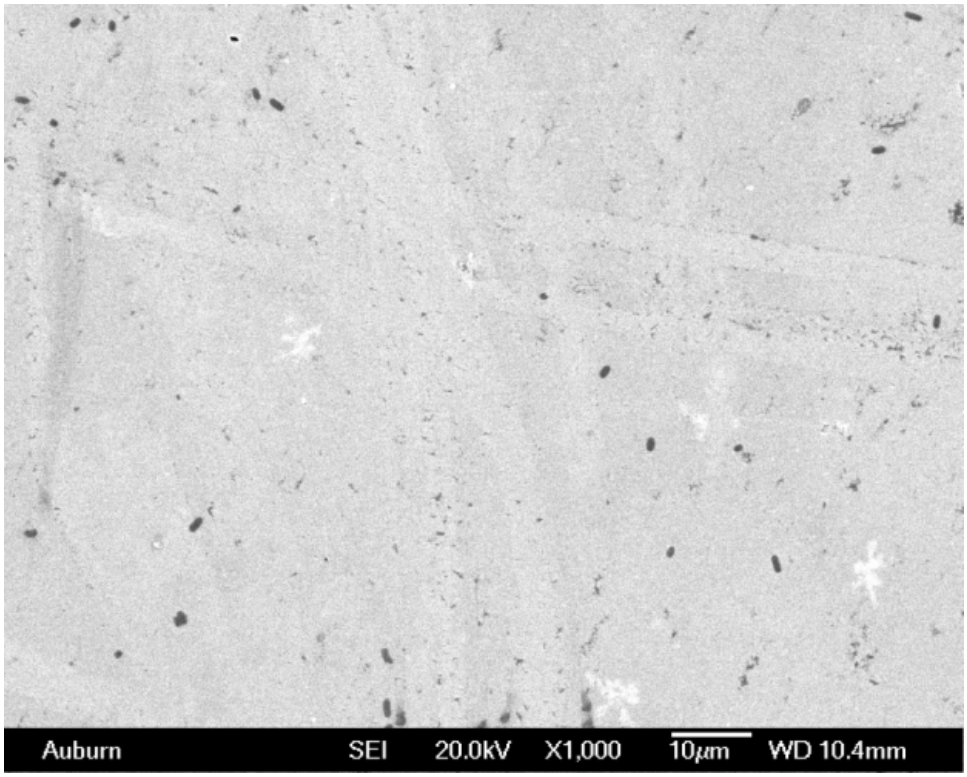

Figure 9.5: Typical SEM picture of the control biosensors after exposed to *S. typhimurium* suspension at concentration of 5×10^8 cfu/ml spiked on cantaloupe surface.

The cantaloupe was spiked with suspensions of *Salmonella* ranging from 5×10^8 cfu/ml to 5×10^1 cfu/ml. The areas on the cantaloupe surface spiked with different concentrations are shown in SEM photographs (Fig 9.6, Figure 9.7, Figure 9.8 and Figure 9.9). Figure 9.6 shows complete *Salmonella* coverage of an area of the cantaloupe surface, including both the higher ridges and the valleys. The following pictures (Figure 9.7 through Figure 9.9) show decreasing concentration levels of *Salmonella* and how most of *Salmonella* cells aggregate in the valleys. If the sensor falls onto the area where a large number of *Salmonella* cells exist, the sensor has a high probability of capturing more *Salmonella*, whereas if the sensor falls onto an area where few *Salmonella* cells exist, the probability of the sensor capturing *Salmonella* is low.

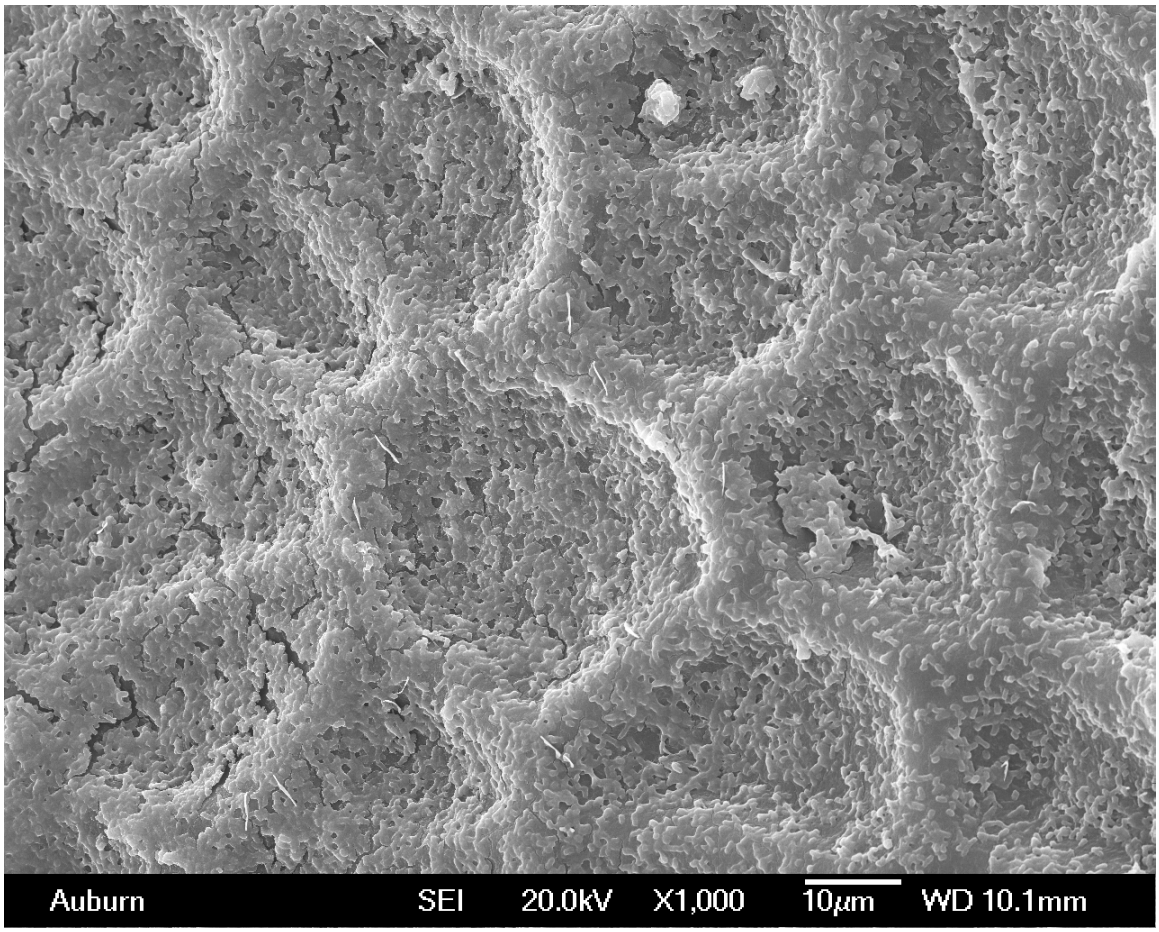

Figure 9.6: Typical SEM picture ($\times$1000) showing the cantaloupe surface spiked with 5×10^8 cfu/ml *S. typhimurium* suspension.

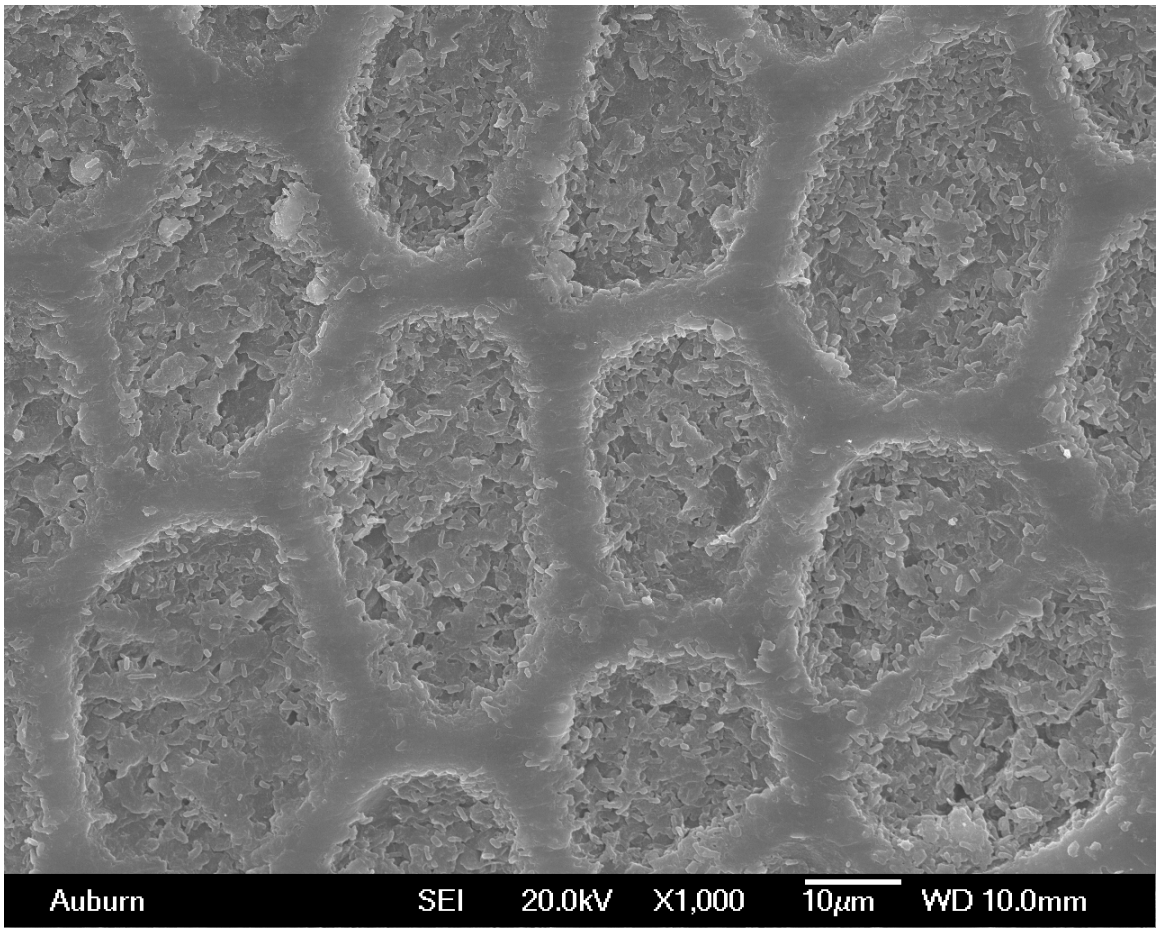

Figure 9.7: Typical SEM picture ($\times$1000) showing the cantaloupe surface spiked with 5×10^6 cfu/ml *S. typhimurium* suspension.

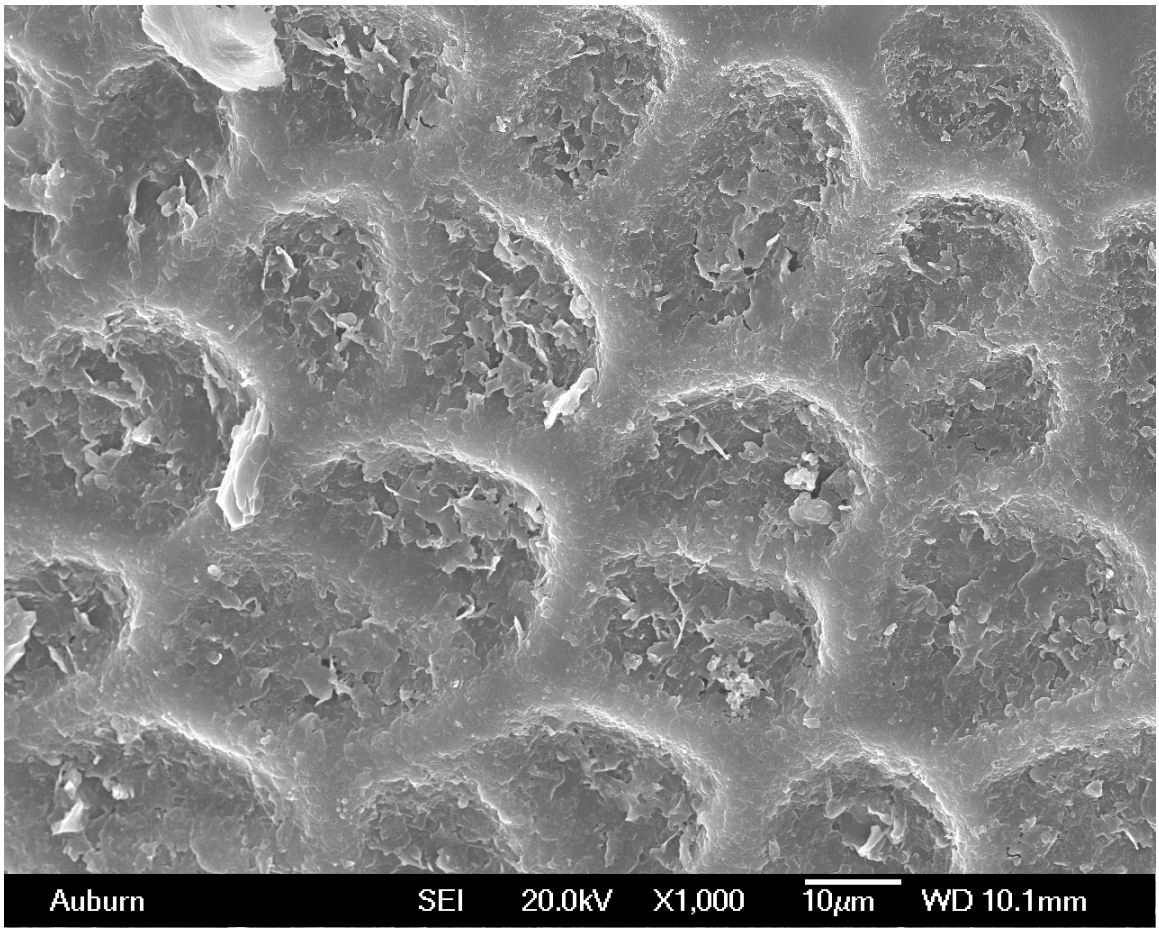

Figure 9.8: Typical SEM picture ($\times$1000) showing the cantaloupe surface spiked with 5×10^4 cfu/ml *S. typhimurium* suspension.

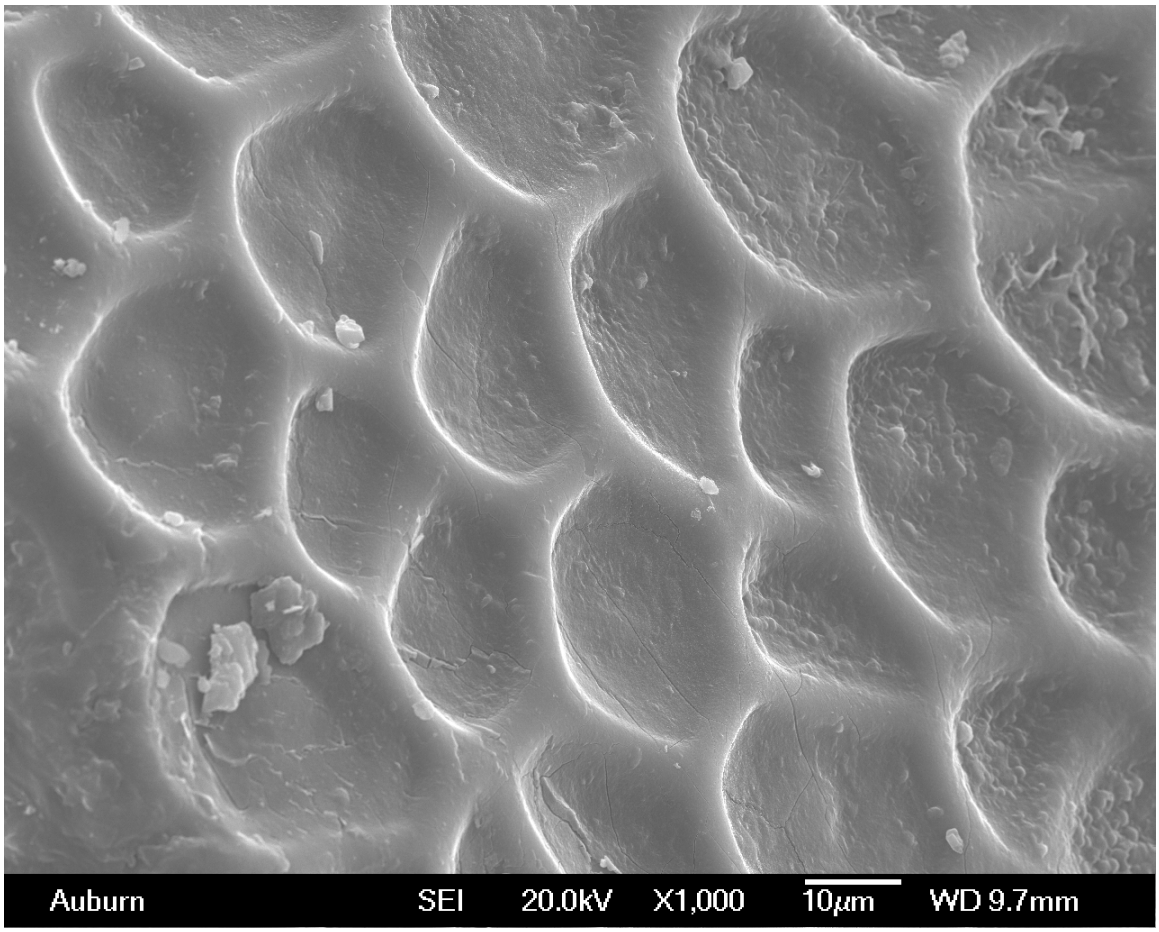

Figure 9.9: Typical SEM picture ($\times$1000) showing the cantaloupe surface spiked with 5×10^1 cfu/ml *S. typhimurium* suspension.

Figure 9.10 is a summary of the frequency shifts from the measurement sensor groups and control sensors groups. Unlike the previous detection results obtained in solution where *Salmonella* cells are uniformly suspended thus the frequency shifts are close for each concentration, this detection result on cantaloupe surfaces shows a scattered distribution of the frequency shifts for each concentration, ranging from 0 Hz to the maximum. However, it is obvious that the maximum frequency shifts of the measurement sensors increases with increasing spiked *Salmonella* concentration, whereas the maximum frequency shifts of the control sensors are similar for all *Salmonella* concentrations.

The detection on cantaloupe surfaces spiked with various concentrations of *S. typhimurium* suspensions (5×10^1 cfu/ml to 5×10^8 cfu/ml) using measurement sensors and control sensors are compared using a one-sided student's t-test. The results are shown in Table 9.1. Based on this result, with 85% confidence level, the responses of the measurement sensors are significantly different from the the responses of control sensors when spiked with *S. typhimurium* concentration of 5×10^3 cfu/ml or higher. This means that with 85% confidence level, *S. typhimurium* is detected directly on cantaloupe surface when spiked with *S. typhimurium* concentration of 5×10^3 cfu/ml or higher.

The detection results of measurement sensors (clear area) and control sensors (shaded area) at various *S. typhimurium* concentrations ranging from 5×10^1 cfu/ml to 5×10^8 cfu/ml were compared using two-sided student's t-test. The results are shown in Table 9.2. Based on this result, the responses of control sensors are similar for all *S. typhimurium* concentrations, whereas the responses of measurement sensors are significantly greater among most of the concentrations. For example, with 85% confidence level, the response at a concentration of 5×10^5 cfu/ml is significantly different from the response at a concentration of 5×10^3 cfu/ml.

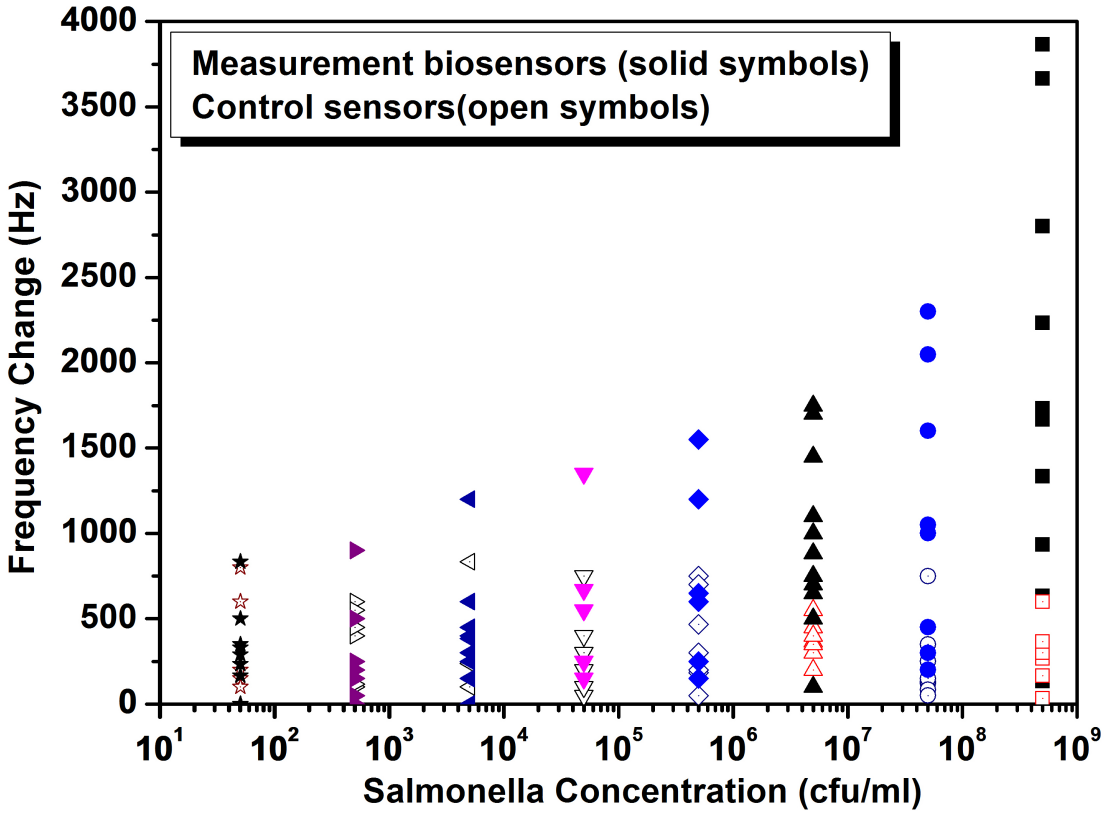

Figure 9.10: Multiple sensor response to concentrations of *S. typhimurium* suspensions (5×10^1 to 5×10^8 cfu/ml) on cantaloupe surfaces.

Table 9.1: P values associated with one-sided student's t-test for detection of *Salmonella* for all concentrations (5×10^1 cfu/ml to 5×10^8 cfu/ml) after comparing measurement sensors and control sensors.

Magnetoelastic Sensor Measurement Vs Control	P value associated with Student's t-test (Unequal Variance) Concentration of *S. typhimurium*							
	5×10^1 cfu/ml	5×10^2 cfu/ml	5×10^3 cfu/ml	5×10^4 cfu/ml	5×10^5 cfu/ml	5×10^6 cfu/ml	5×10^7 cfu/ml	5×10^8 cfu/ml
p	0.34	0.29	**0.13**	**0.03**	**0.01**	< 0.0001	**0.01**	< 0.0001

Table 9.2: P values associated with two-sided student's t-test for measurement sensors (clear area) and control sensors (shaded area) after comparing detection of *Salmonella* for all concentrations (5×10^1 cfu/ml to 5×10^8 cfu/ml).

Magnetoelastic Sensor Measurement Vs Control	P value associated with Student's t-test (Unequal Variance) Concentration of *S. typhimurium*							
	5×10^1 cfu/ml	5×10^2 cfu/ml	5×10^3 cfu/ml	5×10^4 cfu/ml	5×10^5 cfu/ml	5×10^6 cfu/ml	5×10^7 cfu/ml	5×10^8 cfu/ml
5×10^1 cfu/ml	-	1	0.57	0.14	0.05	0.01	0.03	< 0.0001
5×10^2 cfu/ml	0.94	-	0.6	0.17	0.06	0.01	0.03	< 0.0001
5×10^3 cfu/ml	0.87	0.9	-	0.36	0.13	0.02	0.04	< 0.0001
5×10^4 cfu/ml	0.92	0.97	0.94	-	0.5	0.08	0.1	0.01
5×10^5 cfu/ml	0.91	0.95	0.96	0.98	-	0.25	0.2	0.02
5×10^6 cfu/ml	0.96	0.82	0.76	0.84	0.81	-	0.61	0.08
5×10^7 cfu/ml	0.82	0.84	0.94	0.89	0.9	0.69	-	0.23
5×10^8 cfu/ml	0.9	0.95	0.96	0.98	1	0.81	0.91	-

To confirm the results of detecting *Salmonella* on cantaloupe skin, the aforementioned experiment was repeated for the same 8 concentrations, ranging from 5×10^1 cfu/ml through 5×10^8 cfu/ml. Each concentration was tested with 2 to 3 groups of measurement sensors (6 to 9 sensors) and 2 groups of control sensors(6 sensors).

Figure 9.11 is a summary of the frequency results of the this second set of experiments. The distribution and the range of the frequency responses are similar to the ones shown in Figure 9.10. All frequency responses for each concentration are scattered from around 0 Hz to maximum. The maximum frequency shifts of the measurement sensors increases with increasing spiked *Salmonella* concentration, whereas the maximum frequency shifts of the control sensors are similar for all *Salmonella* concentrations. For spiked *Salmonella*

concentration of 5×10^8 cfu/ml, the maximum frequency response of the measurement sensors are close to 4 kHz for both sets of experiments.

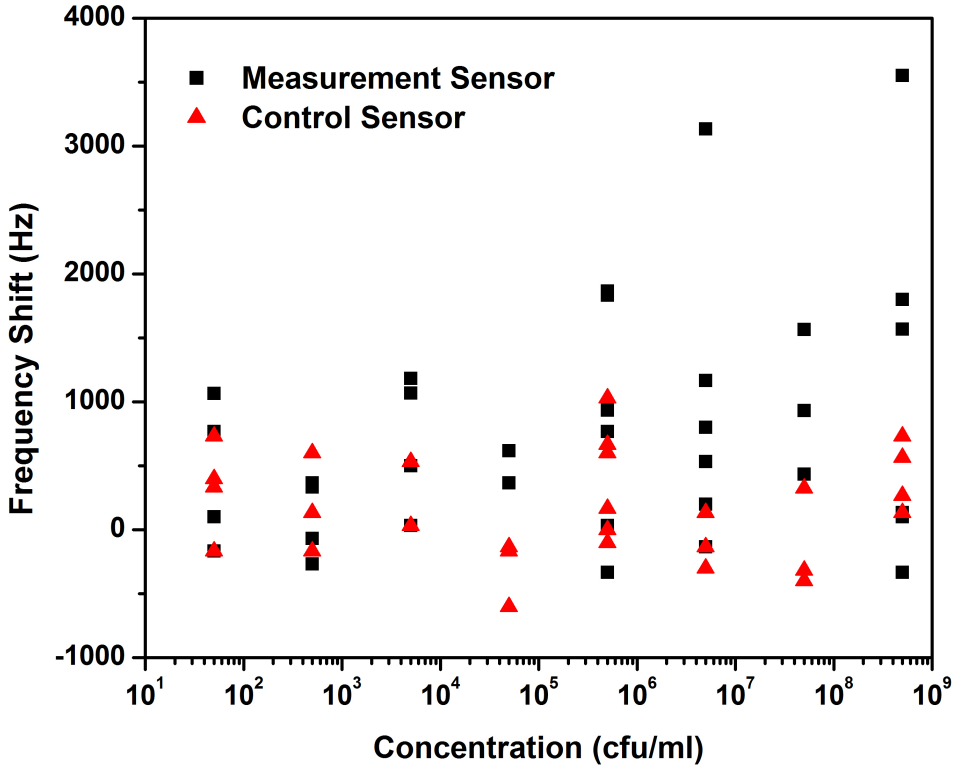

Figure 9.11: Result of second test using multiple sensor to detect concentrations of *S. typhimurium* suspensions (5×10^1 to 5×10^8 cfu/ml) spiked on cantaloupe surfaces.

SEM pictures of the sensor surface were taken to compare with the frequency results. Figure 9.12, Figure 9.13, Figure 9.14 and Figure 9.15 are typical SEM pictures of measurement sensor surfaces after exposure on cantaloupe skins that are spiked with different concentrations of *Salmonella*. The number of *Salmonella* cells captured on the sensor decreases with decrease of spiked *Salmonella* concentration. Figure 9.16 is a typical SEM picture of the control sensor surface after exposure to cantaloupe skins that are spiked with 5×10^4 cfu/ml *Salmonella*. No *Salmonella* cells were captured on the sensor surface. This result is consistent with the frequency responses shown in Figure 9.10.

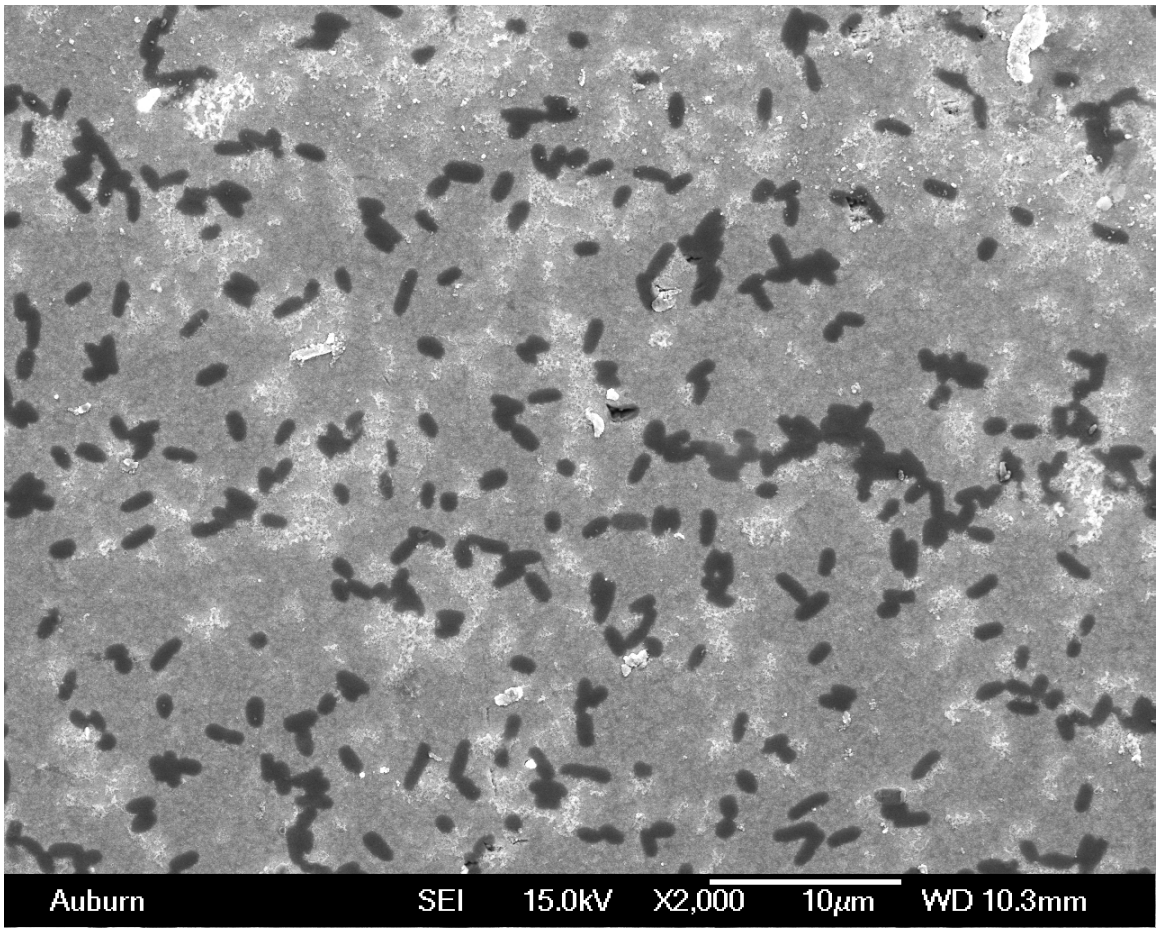

Figure 9.12: Typical SEM picture of the measurement biosensors after binding with *S. typhimurium* suspension at a concentration of 5×10^8 cfu/ml spiked on cantaloupe surface.

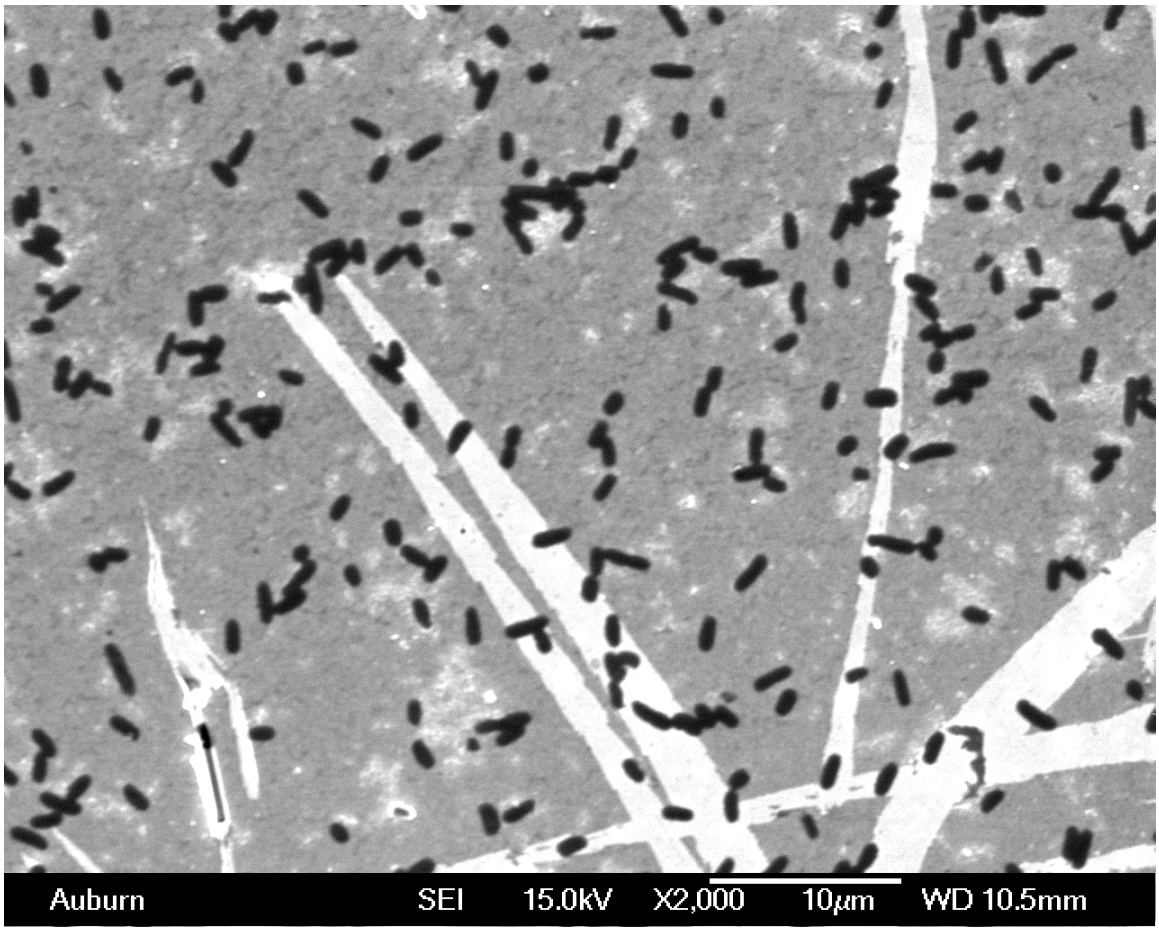

Figure 9.13: Typical SEM picture of the measurement biosensors after binding with *S. typhimurium* suspension at a concentration of 5×10^7 cfu/ml spiked on the cantaloupe surface.

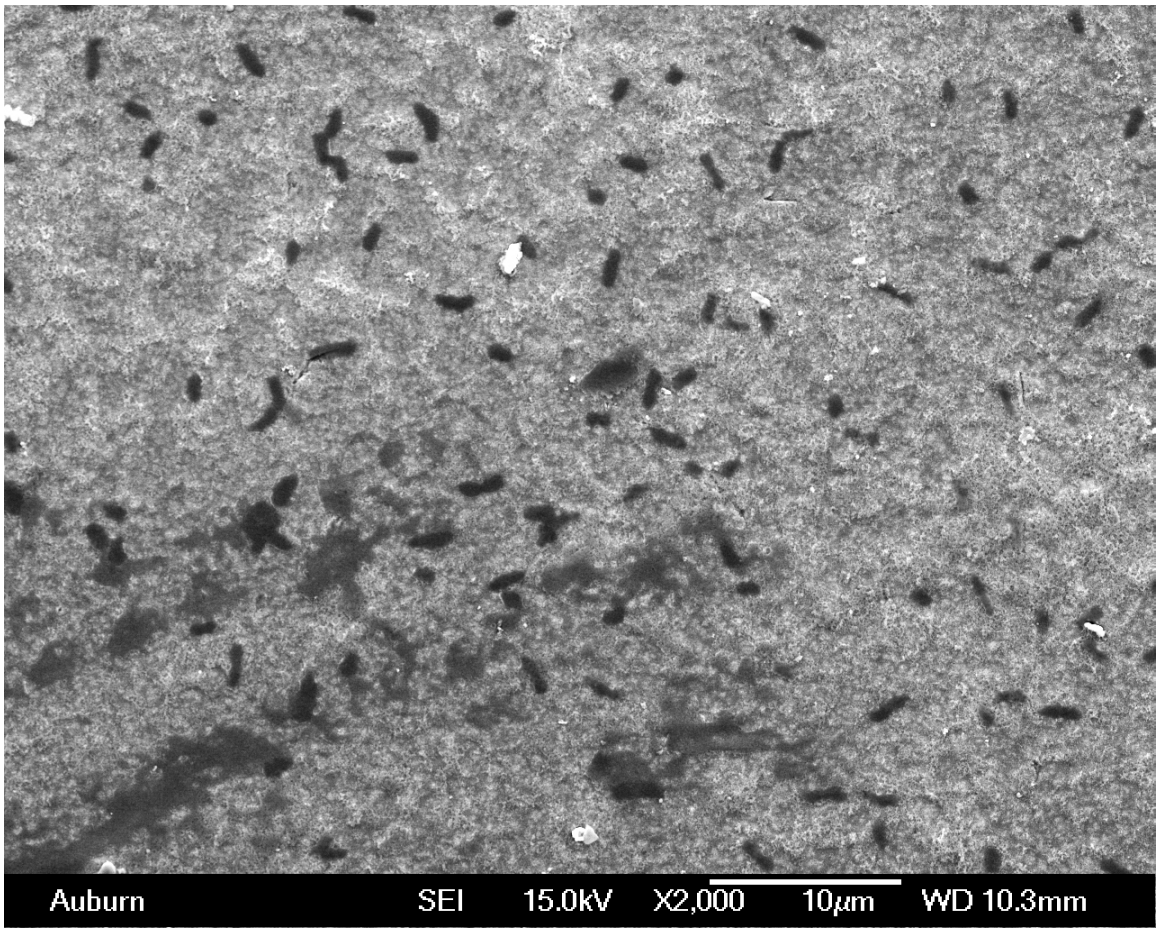

Figure 9.14: Typical SEM picture of the measurement biosensors after binding with *S. typhimurium* suspension at concentration of 5×10^6 cfu/ml spiked on the cantaloupe surface.

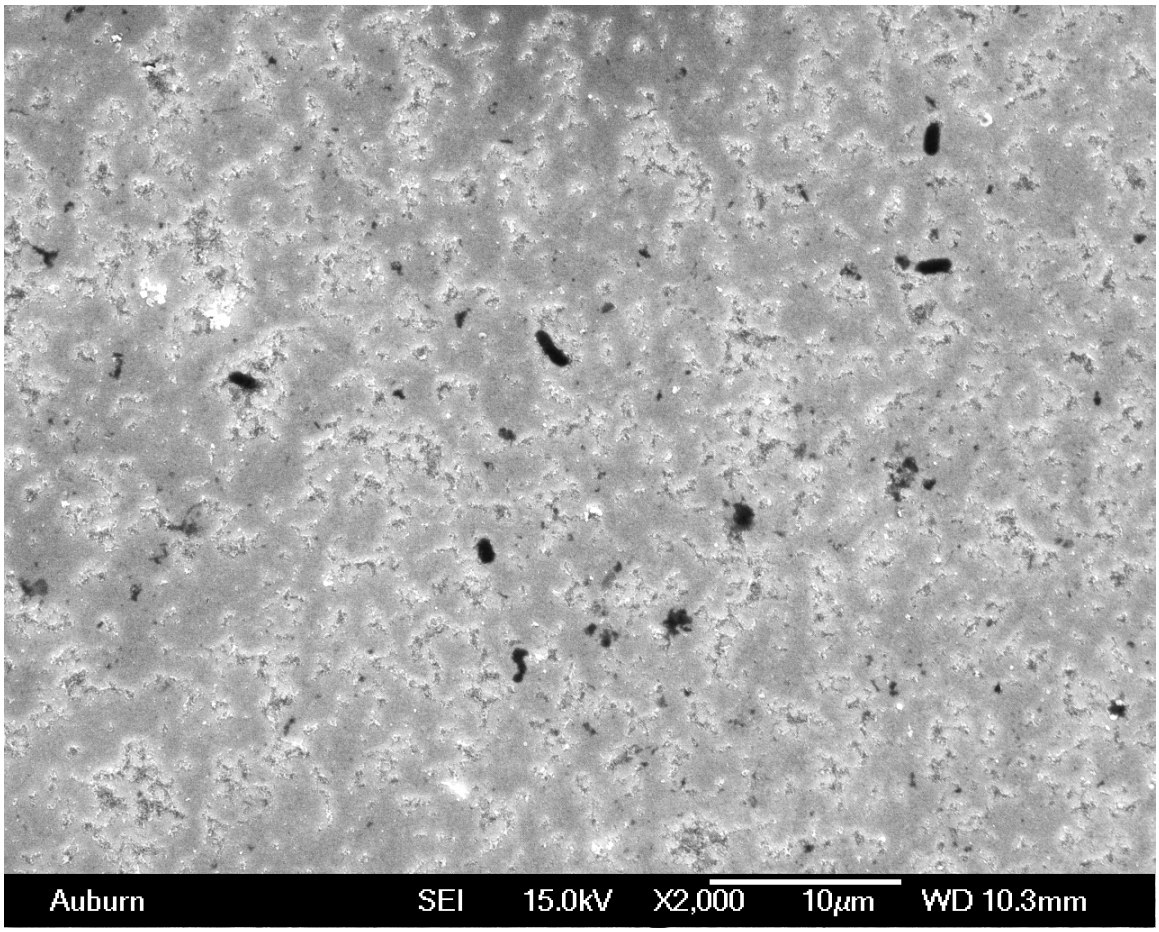

Figure 9.15: Typical SEM picture of the measurement biosensors after binding with *S. typhimurium* suspension at concentration of 5×10^4 cfu/ml spiked on the cantaloupe surface.

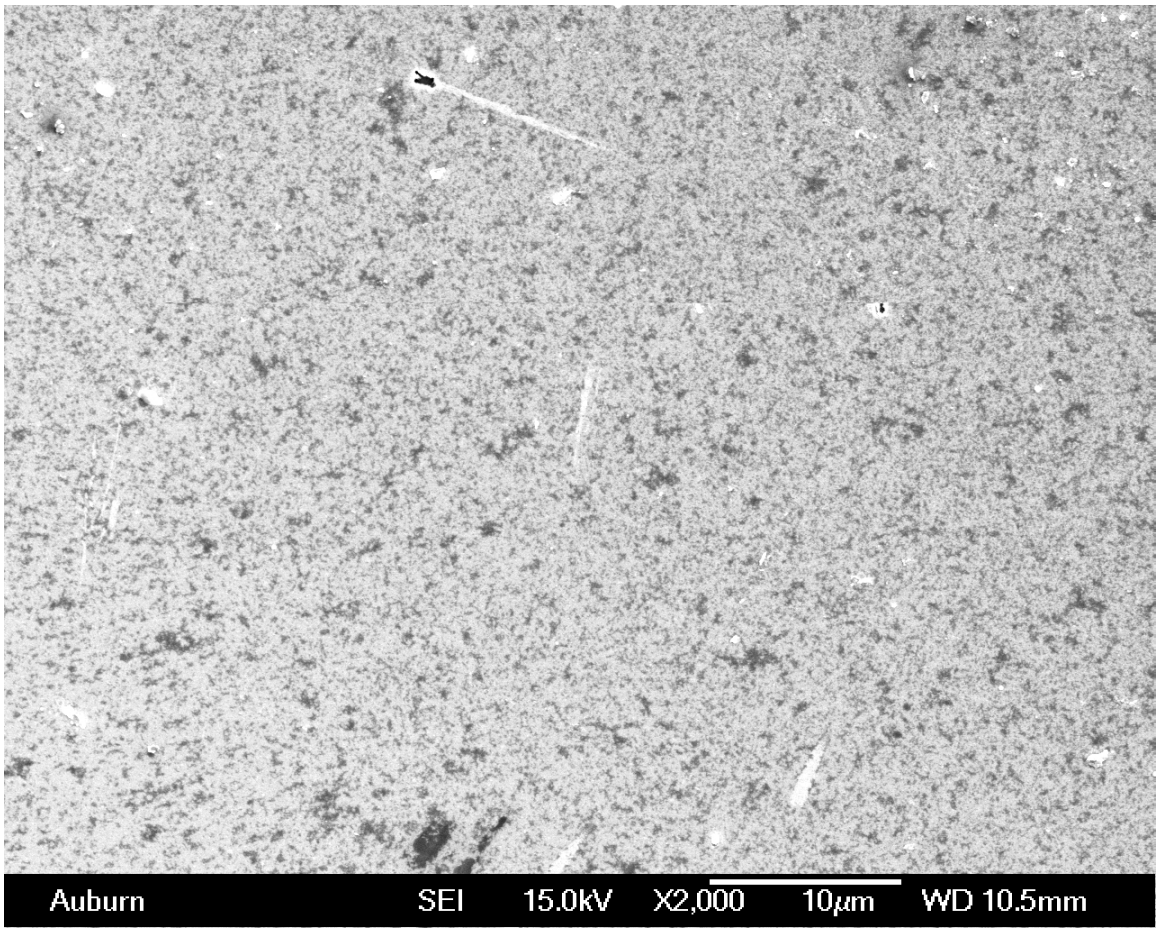

Figure 9.16: Typical SEM picture of the control biosensors after exposure to *S. typhimurium* suspension at concentration of 5×10^4 cfu/ml spiked on the cantaloupe surface.

9.2 Conclusions and Discussion

This research was conducted to study the detection of *Salmonella* directly on fresh cantaloupe surfaces using multiple magnetoelastic biosensors. Different concentrations of *S. typhimurium* suspensions were spiked onto cantaloupe surfaces and dried in air. The magnetoelastic biosensors were directly placed on the cantaloupe surface and the detection took place in a controlled humidly environment for 30 minutes. A multiple sensor detection design was used for this test where 3 measurement sensors and 3 control sensors were used for each test. Due to the roughness of the cantaloupe surface and also to the uneven drying of the solution spiked onto the cantaloupe surface, the sensor responses were scattered from 0 Hz to the maximum for each spiked *Salmonella* concentration. The results from a student's t-tests showed that the control sensors had similar responses among all concentrations whereas the responses of measurement sensors are significantly different for most concentrations. The results also showed that with 85% confidence level, *S. typhimurium* was detected directly on a cantaloupe surface when the spiked *S. typhimurium* concentration was 5×10^3 cfu/ml or higher. SEM photographs of the sensor surfaces verified that the frequency shifts of the measurement sensors were due to the specific binding of *S. typhimurium* onto the biosensors. This detection result on cantaloupe skin was confirmed by performing a second set of independent experiments.

Chapter 10

Conclusions

This work uses both frequency domain method and pulse method to characterize free-sanding magnetoelastic biosensors. By using the frequency domain method, the influence of the external magnetic field on the resonance behavior of the sensor was studied for 1 mm and 2 mm sensors. The real-time detection of *B. anthracis* spores was conducted in a flowing system using a frequency domain method. The results showed that the detection limit for the 1 mm and 2 mm sensors were 10^5 spores/ml and 3.3×10^4 spores/ml respectively. The sensitivity of the detection using the 1 mm and 2 mm sensors were found to be 138.17 Hz/decade and 333.11 Hz/decade respectively. K_d was 366.70 spore/ml and 132.59 spore/ml for the 1 mm and 2 mm lengths respectively.

A pulse detection system was developed for characterizing the magnetoelastic sensors. This system eliminates the bias magnetic field, uses FFT to separate the signal from the noise, can provide good signal to noise ratio, has provisions for a control sensor and has the capability to work with multiple sensors simultaneously. An equation has been derived to describe the operation of one and two sensors in the transformer coils and used to plot data that closely simulates the data plots from the test system. We have shown that the system provides signals that are well above the noise floor by more than 40 dBm, and that by keeping pulse power constant the signal amplitude, resonant frequency and Q-value are kept constant. The effect of pulse power on the resonance behavior of the sensor was studied. The stability study of the system showed an average standard deviation of 129 Hz and an average drift of -10.4 Hz per hour.

The study of sensor position in the pulse system showed that the resonant frequencies of the sensor when placed in the middle of the coil and when half out of the coil are different,

with no significant difference between either end. However, when two sensors are placed in the center of the coil, whether they are placed end by end or side by side, the two sensors have a significant effect on the resonant frequencies as compared to the individual resonance frequencies.

Multiple sensor approach was demonstrated and studied using the pulse method. It was found that when using multiple sensors simultaneously, sensor interference is one of the most significant problems. By adding a multi-access channel structure in the pulse system, the interference between two adjacent sensors was minimized. Testing with two sensors showed that when using this structure, adding a second sensor does not affect the resonant frequency of the first sensor. The repeatability of multiple sensor detection in air was also studied and the results showed that the standard deviation when measuring three 1 mm magnetoelastic sensors simultaneously is around 500 Hz, which is less than the minimum requirement for the actual detection.

The detection of *S. typhimurium* in air has been performed using the pulse system. The detection using a single magnetoelastic sensor showed a detection limit of 5×10^3 cfu/ml and K_d of 450 cfu/ml. Grouped sensor detection using multiple magnetoelastic biosensors simultaneously has been demonstrated. With multiple sensors, the effect of a manufacturing defect can be decreased and we get the benefit of averaging for more accurate and reliable results. The detection limit using grouped biosensors is 8×10^4 cfu/ml and K_d is 385 cfu/ml.

The effectiveness of different concentrations of BSA, milk and casein as blocking reagents for magnetoelastic biosensors, and the blocking of E2 phage based magnetoelastic biosensors can be optimized by using 1mg/ml BSA. Milk and casein have similar but less blocking effect on the magnetoelastic biosensors.

Direct detection of *S. typhimurium* on real food produce was performed using multiple phage-coated magnetoelastic biosensors and multiple control sensors. Due to the roughness of the cantaloupe surface and also to the uneven drying of the solution spiked onto the cantaloupe surface, the sensor responses were scattered from 0 Hz to the maximum for each

spiked *Salmonella* concentration. The results from student's t-tests showed that the control sensors had small but similar responses among all concentrations whereas the responses of measurement sensors were significantly different from the control sensor response. This study demonstrated that multiple magneoelastic biosensors are capable of detecting *Salmonella* directly on cantaloupes skin.

Chapter 11

Recommendations for Future Works

Based on the result that smaller sensors provide higher mass sensitivity, it would be beneficial to use smaller sensors for further investigation of the magnetoelastic sensors. Moreover, it should be noted that nothing in the pulse detection system would prohibit the use of multiple sensors in each transformer coil. As sensors become very small, it is easy to lose them or have a few defective sensors. Future research could extend the testing to tens of sensors with a goal of simultaneous detection of hundreds of sensors. This research has demonstrated that magnetoelastic biosensors may be used to directly detect pathogenic bacteria on fresh produce using groups of sensors. Further investigations should be performed to study and calibrate the detection results under different environmental conditions and also to further improve the sensitivity and reliability of the detection.

Bibliography

[1] J. Wan, *Development and Study of Phage-Coated Magnetoelastic Biosensors for the Detection of Bacillus Anthracis Sterne Spores*. PhD thesis, Auburn University, 2008.

[2] R. S. Lakshmanan, *Phage-Based Magnetoelastic Sensor for the Detection of Salmonella Typhimurium*. PhD thesis, Auburn University, 2008.

[3] "http://www.honeywell.com," retreived 2010.

[4] P. S. Mead, L. Slutsker, V. Dietz, L. F. McCaig, J. S. Bresee, C. S. Patricia, M. Griffin, and R. V. Tauxe, "Food-related illness and death in the united states," *Emerging Infectious Diseases*, vol. 5, pp. 607–625, 1999.

[5] "Investigation update: Outbreak of salmonella typhimurium infections, 2008-2009," tech. rep., Centers for Disease Control and Prevention, Update for April 29, 2009.

[6] "Investigation update: Multistate outbreak of human salmonella enteritidis infections associated with shell eggs," tech. rep., Centers for Disease Control and Prevention, September 9, 2010.

[7] E. V. Olsen, S. T. Pathirana, A. M. Samoylov, J. M. Barbaree, B. A. Chin, W. C. Neely, and V. Vodyanoy, "Specific and selective biosensor for salmonella and its detection in the environment," *Journal of Microbiological Methods*, vol. 53, no. 2, pp. 273–285, 2003.

[8] J. C. Pyun, H. Beutel, J. U. Meyer, and H. H. Ruf, "Development of a biosensor for e. coli based on a flexural plate wave (fpw) transducer," *Biosensors and Bioelectronics*, vol. 13, no. 2-3, pp. 839–845, 1998.

[9] B. Cunningham, M. Weinberg, J. Pepper, C. Clapp, R. Bousquet, B. Hugh, R. Kant, C. Daly, and E. Hauser, "Design, fabrication and vapor characterization of a micro-fabricated flexural plate resonator sensor and application to integrated sensor arrays," *Sensors and Actuators B: Chemical*, vol. 73, no. 2-3, pp. 112–123, 2001.

[10] E. Howe and G. Harding, "A comparison of protocols for the optimisation of detection of bacteria using a surface acoustic wave (saw) biosensor," *Biosensors and Bioelectronics*, vol. 15, no. 11-12, pp. 641–649, 2000.

[11] E. Berkenpas, P. Millard, and M. Pereira da Cunha, "Detection of escherichia coli o157:h7 with langasite pure shear horizontal surface acoustic wave sensors," *Biosensors and Bioelectronics*, vol. 21, no. 12, pp. 2255–2262, 2006.

[12] S. Li, L. Fu, J. M. Barbaree, and Z. Y. Cheng, "Resonance behavior of magnetostrictive micro/milli-cantilever and its application as a biosensor," *Sensors and Actuators B: Chemical*, vol. 137, no. 2, pp. 692–699, 2009.

[13] P. J. Conroy, S. Hearty, P. Leonard, and R. J. O'Kennedy, "Antibody production, design and use for biosensor-based applications," *Seminars in Cell & Developmental Biology*, vol. 20, no. 1, pp. 10–26, 2009.

[14] R. Guntupalli, J. Hu, R. S. Lakshmanan, T. S. Huang, J. M. Barbaree, and B. A. Chin, "A magnetoelastic resonance biosensor immobilized with polyclonal antibody for the detection of salmonella typhimurium," *Biosensors and Bioelectronics*, vol. 22, no. 7, pp. 1474–1479, 2007.

[15] J. Thodorids, "Casimir davaine (1812-1882): a precursor of pasteur," *Medical history*, vol. 10, no. 2, pp. 155–165, 1966.

[16] R. Koch, "Investigations into bacteria: V. the etiology of anthrax, based on the ontogenesis of bacillus anthracis," *Cohns Beitrage zur Biologie der Pflanzen*, vol. 2, no. 2, pp. 277–310, 1876.

[17] J. G. Holt, N. R. Krieg, P. H. A. Sneath, J. T. Staley, and S. T. Williams, *Bergey's manual of determinative bacteriology*, ch. Group 17: gram-positive cocci, pp. 527–558. Williams and Wilkins, Baltimore, Md., 9th ed., 1994.

[18] L. Baillie and T. Read, "Bacillus anthracis: a bug with attitude," *Curr Opin Microbiol*, vol. 4, pp. 78–81, 2001.

[19] P. Sneath, N. Mair, M. Sharpe, and H. J.G., *Bergey's Manual of Systematic Bacteriology*. Maryland, USA: Williams & Wilkins, Baltimore, Maryland, USA, 1986.

[20] T. Dixon, M. Meselson, J. Guillemin, and P. C. Hanna, "Anthrax," *N Engl J Med*, vol. 341, pp. 815–826, 1999.

[21] J. Guillemin. University of California Press, 1999.

[22] "Update: Investigation of bioterrorism-related anthrax and interim guidelines for exposure management and antimicrobial therapy, october 2001," vol. 50, no. 42, pp. 909–919, 2001.

[23] B. Tindall, P. Grimont, G. Garrity, and J. P. Euzeby, "Nomenclature and taxonomy of the genus salmonella," *Int. J. Syst. Evol. Microbiol*, vol. 55, pp. 521–524, 2005.

[24] M. T. Madigan and J. M. Martinko. Perason, 2006.

[25] J. C. of the International Committee on Systematics of Prokaryotes, "The type species of the genus salmonella lignieres 1900 is salmonella enterica (ex kauffmann and edwards 1952) le minor and popoff 1987, with the type strain lt2t, and conservation of the epithet enterica in salmonella enterica over all earlier epithets that may be applied to this species. opinion 80," *Int J Syst Evol Microbiol*, vol. 55, pp. 519–520, Jan. 2005.

[26] C. C. Ginocchio, S. B. Olmsted, C. L. Wells, and J. E. Galn, "Contact with epithelial cells induces the formation of surface appendages on salmonella typhimurium," *Cell*, vol. 76, no. 4, pp. 717–724, 1994.

[27] K. J. Ryan and C. G. Ray. McGraw Hill, 4th ed., 2004.

[28] "Salmonellosis - outbreak investigation, october 2006," tech. rep., Centers for Disease Control and Prevention, November 3, 2006.

[29] "Investigation of outbreak of infections caused by salmonella litchfield," tech. rep., Centers for Disease Control and Prevention, April 2, 2008.

[30] K. M. Sorrells, M. L. Speck, and J. A. Warren, "Pathogenicity of salmonella gallinarum after metabolic injury by freezing," *Appl. Environ. Microbiol.*, vol. 19, no. 1, pp. 39–43, 1970.

[31] L. R. Beuchat and E. K. Heaton, "Salmonella survival on pecans as influenced by processing and storage conditions," *Appl. Environ. Microbiol.*, vol. 29, no. 6, pp. 795–801, 1975.

[32] A. B. Hunter-Cevera, J. C. Academic Press, San Diego, 1996.

[33] R. M. Lequin, "Enzyme immunoassay (eia)/enzyme-linked immunosorbent assay (elisa)," *Clin Chem*, vol. 51, no. 12, pp. 2415–2418, 2005.

[34] "Food allergen partnership," tech. rep., U. S. Food and Drug Administration, 2001.

[35] R. K. Saiki, D. H. Gelfand, S. Stoffel, S. J. Scharf, R. Higuchi, G. T. Horn, K. B. Mullis, and H. A. Erlich, "Primer-directed enzymatic amplification of dna with a thermostable dna polymerase," *Science*, vol. 239, no. 4839, pp. 487–491, 1988.

[36] S. Cheng, C. Fockler, W. Barnes, and H. R., "Effective amplification of long targets from cloned inserts and human genomic dna," *Proc Natl Acad Sci*, vol. 91, no. 12, pp. 5695–5699, 1994.

[37] R. Saiki, S. Scharf, F. Faloona, K. Mullis, G. Horn, H. Erlich, and N. Arnheim, "Enzymatic amplification of beta-globin genomic sequences and restriction site analysis for diagnosis of sickle cell anemia," *Science*, vol. 230, pp. 1350–1354, Dec. 1985.

[38] J. M. Bartlett and D. Stirling, "A short history of the polymerase chain reaction," *Methods Mol Biol*, vol. 226, pp. 3–6, 2003.

[39] A. Cavalcanti, B. Shirinzadeh, M. Zhang, and L. Kretly, "Nanorobot hardware architecture for medical defense," *Sensors*, vol. 8, no. 5, pp. 2932–2958, 2008.

[40] G. W. Litman, J. P. Rast, and M. J. Shamblott, "Phylogenetic diversification of immunoglobulin genes and the antibody repertoire," *Mol. Biol. Evol.*, vol. 10, no. 1, pp. 60–72, 1993.

[41] G. B. Pier, J. B. Lyczak, and L. M. Wetzler. ASM Press, 2004.

[42] R. A. Rhoades and R. G. Pflanzer. Thomson Learning, 4th ed., 2002.

[43] J. Woof and D. Burton, "Human antibody-fc receptor interactions illuminated by crystal structures," *Nat Rev Immunol*, vol. 4, no. 2, pp. 89–99, 2004.

[44] J. Janeway, C. A., P. Travers, M. Walport, and M. J. Shlomchik. Garland Publishing, 5th ed., 2001.

[45] L. Borghesi and C. Milcarek, "From b cell to plasma cell: regulation of v(d)j recombination and antibody secretion," *Immunol Res*, vol. 36, no. 1-3, pp. 27–32, 2006.

[46] S. Jayasena, "Aptamers: An emerging class ofmolecules that rival antibodies in diagnostics," *Clinical Chemistry*, vol. 45, no. 45, pp. 1628–1650, 1999.

[47] G. P. Anderson and N. L. Nerurkar, "Improved fluoroimmunoassays using the dye alexa fluor 647 with the raptor, a fiber optic biosensor," *Journal of Immunological Methods*, vol. 271, no. 1-2, pp. 17–24, 2002.

[48] L. R. Hirsch, J. B. Jackson, A. Lee, N. J. Halas, and J. L. West, "A whole blood immunoassay using gold nanoshells," *Analytical Chemistry*, vol. 75, no. 10, pp. 2377–2381, 2003.

[49] K. M. Hansen, H.-F. Ji, G. Wu, R. Datar, R. Cote, A. Majumdar, and T. Thundat, "Cantilever-based optical deflection assay for discrimination of dna single-nucleotide mismatches," *Analytical Chemistry*, vol. 73, no. 7, pp. 1567–1571, 2001.

[50] T. Sano, C. L. Smith, and C. R. Cantor, "Immuno-pcr: very sensitive antigen detection by means of specific antibody-dna conjugates," *Science*, vol. 258, no. 5079, pp. 120–122, 1992.

[51] C. M. Niemeyer, M. Adler, and R. Wacker, "Immuno-pcr: high sensitivity detection of proteins by nucleic acid amplification," *Trends in Biotechnology*, vol. 23, no. 4, pp. 208–216, 2005.

[52] V. A. Petrenko, "Landscape phage as a molecular recognition interface for detection devices," *Microelectronics Journal*, vol. 39, no. 2, pp. 202–207, 2008.

[53] D. A. Marvin, L. C. Welsh, M. F. Symmons, W. R. P. Scott, and S. K. Straus, "Molecular structure of fd (f1, m13) filamentous bacteriophage refined with respect to x-ray fibre diffraction and solid-state nmr data supports specific models of phage assembly at the bacterial membrane," *Journal of Molecular Biology*, vol. 355, no. 2, pp. 294–309, 2006.

[54] D. A. Marvin, "Filamentous phage structure, infection and assembly," *Current Opinion in Structural Biology*, vol. 8, no. 2, pp. 150–158, 1998.

[55] L. Olofsson, J. Ankarloo, and I. A. Nicholls, "Phage viability in organic media: insights into phage stability," *Journal of Molecular Recognition*, vol. 11, no. 1-6, pp. 91–93, 1998.

[56] B. P. Pal, *Fundamentals of Fibre Optics in Telecommunication and Sensor Systems*. New Delhi: New Age International, 1992.

[57] G. H. Cross, A. A. Reeves, S. Brand, J. F. Popplewell, L. L. Peel, M. J. Swann, and N. J. Freeman, "A new quantitative optical biosensor for protein characterisation," *Biosensors and Bioelectronics*, vol. 19, no. 4, pp. 383 – 390, 2003.

[58] N. C. G. Swann, M.J. Freeman, *Handbook of Biosensors and Biochips*, ch. Dual Polarization Interferometry: A Real-Time Optical Technique for Measuring (Bio)Molecular Orientation, Structure and Function at the Solid/Liquid Interface, pp. 549–568. Wiley, 2007.

[59] A. Boudjemline, D. T. Clarke, N. J. Freeman, J. M. Nicholson, and G. R. Jones, "Early stages of protein crystallization as revealed by emerging optical waveguide technology," *Journal of Applied Crystallography*, vol. 41, pp. 523–530, Jun 2008.

[60] A. Mashaghi, M. Swann, J. Popplewell, M. Textor, and E. Reimhult, "Optical anisotropy of supported lipid structures probed by waveguide spectroscopy and its application to study of supported lipid bilayer formation kinetics," *Analytical Chemistry*, vol. 80, no. 10, pp. 3666–3676, 2008. PMID: 18422336.

[61] N. Sanghera, M. J. Swann, G. Ronan, and T. J. Pinheiro, "Insight into early events in the aggregation of the prion protein on lipid membranes," *Biochimica et Biophysica Acta (BBA) - Biomembranes*, vol. 1788, no. 10, pp. 2245 – 2251, 2009. Includes Special Section: Cardiolipin.

[62] T.-H. Lee, C. Heng, M. J. Swann, J. D. Gehman, F. Separovic, and M.-I. Aguilar, "Real-time quantitative analysis of lipid disordering by aurein 1.2 during membrane adsorption, destabilisation and lysis," *Biochimica et Biophysica Acta (BBA) - Biomembranes*, vol. 1798, no. 10, pp. 1977 – 1986, 2010.

[63] F. Prieto, B. Seplveda, A. Calle, A. Llobera, C. Domnguez, and L. M. Lechuga, "Integrated mach-zehnder interferometer based on arrow structures for biosensor applications," *Sensors and Actuators B: Chemical*, vol. 92, no. 1-2, pp. 151 – 158, 2003.

[64] P. Hariharan and P. Hariharan, "The mach-zehnder interferometer: Initial adjustment," in *Basics of Interferometry (Second edition)*, pp. 191 – 192, Burlington: Academic Press, second edition ed., 2007.

[65] M. Jiang and E. Gerhard, "A simple strain sensor using a thin film as a low-finesse fiber-optic fabry-perot interferometer," *Sensors and Actuators A: Physical*, vol. 88, no. 1, pp. 41 – 46, 2001.

[66] M. G. Cottam, *Introduction to Surface and Superlattice Excitations*. New York: Cambridge University Press, 1989.

[67] J. Homola, *Springer Series on Chemical Sensors and Biosensors*, ch. Surface Plasmon Resonance Based Sensors. Berlin: Springer-Verlag, 2006.

[68] M. A. Cooper, "Optical biosensors in drug discovery," *Nat Rev Drug Discov*, vol. 1, pp. 515–528, July 2002.

[69] Z. Salamon and G. Tollin, "Surface plasmon resonance, theory," in *Encyclopedia of Spectroscopy and Spectrometry* (J. Lindon, ed.), pp. 2804 – 2812, Oxford: Academic Press, 1999.

[70] R. Cush, J. Cronin, W. Stewart, C. Maule, J. Molloy, and N. Goddard, "The resonant mirror: a novel optical biosensor for direct sensing of biomolecular interactions part i: Principle of operation and associated instrumentation," *Biosensors and Bioelectronics*, vol. 8, no. 7-8, pp. 347 – 354, 1993.

[71] L. Wang, Y. Sun, J. Wang, X. Zhu, F. Jia, Y. Cao, X. Wang, H. Zhang, and D. Song, "Sensitivity enhancement of spr biosensor with silver mirror reaction on the ag/au film," *Talanta*, vol. 78, no. 1, pp. 265 – 269, 2009.

[72] M. Marrakchi, S. V. Dzyadevych, F. Lagarde, C. Martelet, and N. Jaffrezic-Renault, "Conductometric biosensor based on glucose oxidase and beta-galactosidase for specific lactose determination in milk," *Materials Science and Engineering: C*, vol. 28, no. 5-6, pp. 872 – 875, 2008. MADICA 2006 Conference, Fifth Maghreb-Europe Meeting on Materials and their Applicatons for Devices and Physical, Chemical and Biological Sensors, MADICA 2006 Conference, Fifth Maghreb-Europe Meeting on Materials and their Applicatons for Devices and Physical, Chemical and Biological Sensors.

[73] Z. Zhang, S. Xia, D. Leonard, N. Jaffrezic-Renault, J. Zhang, F. Bessueille, Y. Goepfert, X. Wang, L. Chen, Z. Zhu, J. Zhao, M. G. Almeida, and C. M. Silveira, "A novel nitrite biosensor based on conductometric electrode modified with cytochrome c nitrite reductase composite membrane," *Biosensors and Bioelectronics*, vol. 24, no. 6, pp. 1574 – 1579, 2009.

[74] S. Q. Lud, M. G. Nikolaides, I. Haase, M. Fischer, and A. R. Bausch, "Field effect of screened charges: Electrical detection of peptides and proteins by a thin-film resistor," *Chem. Eur. J. of Chem. Phys.*, vol. 7, no. 2, pp. 379–384, 2006.

[75] R. A. Villamizar, A. Maroto, F. X. Rius, I. Inza, and M. J. Figueras, "Fast detection of salmonella infantis with carbon nanotube field effect transistors," *Biosensors and Bioelectronics*, vol. 24, no. 2, pp. 279 – 283, 2008.

[76] D. A. C. S. R. Holler, F. James; Skoog, *Principles of Instrumental Analysis (6th ed.)*, ch. "Chapter 1"., p. 9. Cengage Learning, 2007.

[77] W. Shen, L. C. Mathison, V. A. Petrenko, and B. A. Chin, "Design and characterization of a magnetoelastic sensor for the detection of biological agents," *Journal of Physics D: Applied Physics*, vol. 43, no. 1, p. 01500.

[78] G. Sauerbrey, "Verwendung von schwingquarzen zur wgung dnner schichten und zur mikrowgung," *Zeitschrift fr Physik A Hadrons and Nuclei*, vol. 155, pp. 206–222, 1959. 10.1007/BF01337937.

[79] L. D. L.L.Bao, W. Z. Wei, L. H. Nie, and S. Z. Yao, "Continuous measurement of bacterial populations on the surface of a solid medium with a thickness shear mode acoustic resonator in series," *Enzyme and Microbial Technology*, vol. 19, no. 7, pp. 525 – 528, 1996.

[80] E. V. Olsen, S. T. Pathirana, A. M. Samoylov, J. M. Barbaree, B. A. Chin, W. C. Neely, and V. Vodyanoy, "Specific and selective biosensor for salmonella and its detection in the environment," *Journal of Microbiological Methods*, vol. 53, no. 2, pp. 273 – 285, 2003. Detection of Microbial Pathogens using Molecular Methods.

[81] B. A. Cavic and M. Thompson, "Interfacial nucleic acid chemistry studied by acoustic shear wave propagation," *Analytica Chimica Acta*, vol. 469, no. 1, pp. 101 – 113, 2002.

[82] K. A. Marx, T. Zhou, A. Montrone, H. Schulze, and S. J. Braunhut, "A quartz crystal microbalance cell biosensor: detection of microtubule alterations in living cells at nm nocodazole concentrations," *Biosensors and Bioelectronics*, vol. 16, no. 9-12, pp. 773 – 782, 2001.

[83] F. Li, J. H.-C. Wang, and Q.-M. Wang, "Thickness shear mode acoustic wave sensors for characterizing the viscoelastic properties of cell monolayer," *Sensors and Actuators B: Chemical*, vol. 128, no. 2, pp. 399 – 406, 2008.

[84] L. Rayleigh, "On waves propagated along the plane surface of an elastic solid," *Proceedings of the London Mathematical Society*, vol. s1-17, pp. 4–11, Nov. 1885.

[85] L. Fu, K. Zhang, S. Li, Y. Wang, T.-S. Huang, A. Zhang, and Z.-Y. Cheng, "In situ real-time detection of e. coli in water using antibody-coated magnetostrictive microcantilever," *Sensors and Actuators B: Chemical*, vol. 150, no. 1, pp. 220 – 225, 2010.

[86] R. Guntupalli, R. S. Lakshmanan, J. Hu, T. S. Huang, J. M. Barbaree, V. Vodyanoy, and B. A. Chin, "Rapid and sensitive magnetoelastic biosensors for the detection of salmonella typhimurium in a mixed microbial population," *Journal of Microbiological Methods*, vol. 70, no. 1, pp. 112–118, 2007.

[87] R. S. Lakshmanan, R. Guntupalli, J. Hu, D.-J. Kim, V. A. Petrenko, J. M. Barbaree, and B. A. Chin, "Phage immobilized magnetoelastic sensor for the detection of salmonella typhimurium," *Journal of Microbiological Methods*, vol. 71, no. 1, pp. 55 – 60, 2007.

[88] M. L. Johnson, J. Wan, S. Huang, Z. Cheng, V. A. Petrenko, D.-J. Kim, I. H. Chen, J. M. Barbaree, J. W. Hong, and B. A. Chin, "A wireless biosensor using microfabricated phage-interfaced magnetoelastic particles," *Sensors and Actuators A: Physical*, vol. 144, no. 1, pp. 38–47, 2008.

[89] S. Huang, H. Yang, R. Lakshmanan, M. Johnson, J. Wan, I.-H. Chen, H. W. III, V. Petrenko, J. Barbaree, and B. Chin, "Sequential detection of salmonella typhimurium and bacillus anthracis spores using magnetoelastic biosensors," *Biosensors and Bioelectronics*, vol. 24, no. 6, pp. 1730 – 1736, 2009.

[90] F. Xie, H. Yang, S. Li, W. Shen, J. Wan, M. L. Johnson, H. C. Wikle, D.-J. Kim, and B. A. Chin, "Amorphous magnetoelastic sensors for the detection of biological agents," *Intermetallics*, vol. 17, no. 4, pp. 270 – 273, 2009. Sixth International Conference on Bulk Metallic Glasses (BMG VI).

[91] S. Huang, J. Hu, J. Wan, M. L. Johnson, H. Shu, and B. A. Chin, "The effect of annealing and gold deposition on the performance of magnetoelastic biosensors," *Materials Science and Engineering: C*, vol. 28, no. 3, pp. 380–386, 2008.

[92] J. Wan, H. Shu, S. Huang, B. Fiebor, I.-H. Chen, V. A. Petrenko, and B. A. Chin, "Phage-based magnetoelastic wireless biosensors for detecting bacillus anthracis spores," *Sensors Journal, IEEE*, vol. 7, pp. 470–477, 2007.

[93] K. Zeng, K. G. Ong, C. Mungle, and C. A. Grimes, "Time domain characterization of oscillating sensors: Application of frequency counting to resonance frequency determination.," *Review of Scientific Instruments*, vol. 73, no. 12, pp. 4375–4380, 2002.

[94] K. Zeng and C. A. Grimes, "Threshold-crossing counting technique for damping factor determination of resonator sensors," *Review of Scientific Instruments*, vol. 75, no. 12, pp. 5257–5261, 2004.

[95] K. Zeng, M. Paulose, K. G. Ong, and C. A. Grimes, "Frequency-domain characterization of magnetoelastic sensors: a microcontroller-based instrument for spectrum analysis using a threshold-crossing counting technique," *Sensors and Actuators A: Physical*, vol. 121, no. 1, pp. 66–71, 2005.

[96] W. Shen, R. S. Lakshmanan, L. C. Mathison, V. A. Petrenko, and B. A. Chin, "Phage coated magnetoelastic micro-biosensors for real-time detection of bacillus anthracis spores," *Sensors and Actuators B: Chemical*, vol. 137, no. 2, pp. 501–506, 2009.

[97] K. Zeng, K. G. Ong, X. Yang, and C. A. Grimes, "Board level integrated microsystern design and associated technique for impedance analysis of resonator sensors," *Sensor Letters*, vol. 4, no. 388-397, pp. 388–397, 2006.

[98] W. Shen, L. C. Mathison, V. A. Petrenko, and B. A. Chin, "A pulse system for spectrum analysis of magnetoelastic biosensors," *Applied Physics Letters*, vol. 96, p. 163502, 2010.

[99] W. Shen, Z. Zhang, S. Horikawa, A. Zhang, J. Teng, L. C. Mathison, and B. A. Chin, "Time domain characterization of magnetoelastic sensors: A pulse method for resonance frequency determination," *Review of Scientific Instruments*, vol. 81, no. 1, p. 084702, 2010.

[100] L. Meirovitch. Boston: McGraw-Hill.

[101] S. Li, *Development of Novel Acoustic Wave Biosensor Platforms Based on Magnetostriction and Fabrication of Magnetostrictive Nanowires*. PhD thesis, Auburn University, 2007.

[102] J. Wan and B. Chin, "Characterization and application of wireless magnetostrictive micro-sensors," in *Sensors, 2005 IEEE*, pp. 24 –27, 302005-nov.3 2005.

[103] C. Liang, S. Morshed, and B. C. Prorok, "Correction for longitudinal mode vibration in thin slender beams," *Applied Physics Letters*, vol. 90, no. 22, pp. 221912–3, 2007.

[104] E. du Trmolet de Lacheisserie, "Magnetoelastic properties of amorphous alloys," *Journal of Magnetism and Magnetic Materials*, vol. 25, no. 3, pp. 251–270, 1982.

[105] S. Timoshenko and D. H. Young. New York: Van Nostrand, 3rd ed., 1955.

[106] C. A. Grimes, K. G. Ong, K. Loiselle, P. G. Stoyanov, D. Kouzoudis, Y. Liu, C. Tong, and F. Tefiku, "Magnetoelastic sensors for remote query environmental monitoring," *Smart Materials and Structures*, vol. 8, no. 5, pp. 639–646, 1999.

[107] N. S. Perov, E. V. Pan'kova, G. S. Kuznetsov, V. V. Rodionov, and M. Inoue, "Magnetoelastic waves in amorphous ribbons excited by local ac magnetic fields: Effect of stresses and dc magnetic field," *Journal of Magnetism and Magnetic Materials*, vol. 310, no. 2, Part 3, pp. 2633–2635, 2007.

[108] C. Mungle, C. A. Grimes, and W. R. Dreschel, "Magnetic field tuning of the frequency-temperature response of a magnetoelastic sensor," *Sensors and Actuators A: Physical*, vol. 101, pp. 143–149, Sept. 2002.

[109] J. D. Livingston, "Magnetomechanical properties of amorphous metals," *physica status solidi (a)*, vol. 70, no. 2, pp. 591–596, 1982.

[110] S. Chikazumi and S. H. Charap, *Physics of Magnetism*. New York: John Wiley & Sons, Inc., 1964.

[111] W. T. Thomson, *Theory of vibration with applications*. New Jersey: Prentice Hall, 3rd ed., 1988.

[112] S. Huang, *Simultaneous Detection of Salmonella Typhimurium and Bacillus Anthracis Spores Using Remote Phage Based Magnetoelastic Microbiosensors*. PhD thesis, Auburn University, 2010.

[113] M. R. Campbell, G.A., "Detection of pathogen escherichia coli o157:h7 using self-excited pzt-glass microcantilevers," *Biosensors and Bioelectronics*, vol. 21, pp. 462–473, 2005.

[114] J. Wan, M. L. Johnson, R. Guntupalli, V. A. Petrenko, and B. A. Chin, "Detection of bacillus anthracis spores in liquid using phage-based magnetoelastic micro-resonators," *Sensors and Actuators B: Chemical*, vol. 127, no. 2, pp. 559 – 566, 2007.

[115] V. Kandimalla, N. Kandimalla, K. Hruska, and M. Franek, "Detection of sulfamethazine in water, milk and pig manure by dipstick immunoassay," *Veterinarni Medicina*, vol. 52, p. 445450, 2007.

[116] J. Cao, P. ZHAO, X. H. MIAO, L. J. ZHAO, L. J. XUE, and Z. T. QI, "Phage display selection on whole cells yields a small peptide specific for hcv receptor human cd81," *Cell research*, vol. 13, pp. 473–479, 2003.

[117] K. A. Davis and T. R. Leary, "Continuous liquid-phase piezoelectric biosensor for kinetic immunoassays," *Analytical Chemistry*, vol. 61, no. 11, pp. 1227–1230, 1989.

[118] S. Mao, G. Lu, K. Yu, and J. Chen, "Specific biosensing using carbon nanotubes functionalized with gold nanoparticle-antibody conjugates," *Carbon*, vol. 48, no. 2, pp. 479 – 486, 2010.

[119] E. Moore, M. Pravda, and G. G. Guilbault, "Development of a biosensor for the quantitative detection of 2,4,6-trichloroanisole using screen printed electrodes," *Analytica Chimica Acta*, vol. 484, no. 1, pp. 15 – 24, 2003.

[120] V. Nanduri, I. B. Sorokulova, A. M. Samoylov, A. L. Simonian, V. A. Petrenko, and V. Vodyanoy, "Phage as a molecular recognition element in biosensors immobilized by physical adsorption," *Biosensors and Bioelectronics*, vol. 22, no. 6, pp. 986 – 992, 2007.